THE UNIVERSITY OF QUEENSLAND

AUSTRALIA

The cardioprotective effects of growth hormone secretagogues in mouse models of myocardial ischemia reperfusion and infarction

Hayley McDonald

BVSc (Distinction), Dip. ECVIM-CA (Cardiology), MRCVS

A thesis submitted for the degree of Doctor of Philosophy at

The University of Queensland in 2019

School of Biomedical Sciences

Abstract

Introduction: Ischemic heart disease (IHD) is a leading cause of death and disability worldwide. With the optimisation of treatment for patients with acute myocardial infarction (AMI), there has been a parallel increase in the survival of patients with severely compromised cardiac function. Pathological ventricular remodelling and myocardial dysfunction are key events in the progression of AMI, with heart failure remaining to be one of the most challenging conditions to prevent and manage in AMI patients. Therefore, the preservation of left ventricular (LV) function and prevention and reversal of cardiac fibrosis is essential for the management of these patients. However, to date, there remains a lack of effective therapeutic agents available for targeting these adverse processes post-AMI. Furthermore, the research field of cardio-protection has been plagued by numerous failed attempts to translate promising therapeutic strategies for preventing myocardial ischemic injury discovered in the basic science laboratory into the clinical setting. A major factor underlying this failure entails the inappropriate use of experimental animal models.

Growth hormone secretagogues (GHS) have been demonstrated to improve cardiac function, attenuate inflammation, remodeling and modulate the autonomic nervous system (ANS) in models of cardiovascular disease (CVD). This work aimed to determine whether hexarelin (HEX), a synthetic GHS, could preserve LV function and attenuate inflammation and remodeling in mouse models of myocardial ischemia reperfusion and infarction.

Methods: Myocardial ischemia was induced by either transient or permanent ligation of the left descending coronary artery in male C57BL/6J mice followed by chronic vehicle or HEX administration throughout the recovery period. High field magnetic resonance imaging (MRI) was employed to assess LV function and tissue characteristics. More specifically ischemia-injured and sham mice were subjected to MRI using a T_1-weighted late gadolinium enhancement sequence (LGE) at 9.4 Tesla (T) to measure LV function, mass and infarct size.

The development of novel techniques to assess area at risk at 16 T were also explored in this work.

Results: In response to the ischemic insult, HEX-treated mice demonstrated a significant improvement in LV function compared with the VEH-treated group. A significant decrease in interstitial collagen, TGF-β1 expression and myofibroblast differentiation was also seen in the HEX-treated mice. HEX treatment shifted the balance of ANS towards a parasympathetic predominance, evidenced by a smaller low/high-frequency power ratio (LF/HF) and increased normalized high frequency power (nHF) measured by heart rate variability analysis. This was combined with a significant decrease in cardiac troponin-I and inflammatory cytokines, suggestive of a HEX-mediated anti-inflammatory effect and amelioration of cardiomyocyte injury based on a reduction in cardiac troponins.

Conclusion: These results demonstrate that GHS may preserve LV function and prevent adverse remodeling in mouse models of myocardial ischemia, reperfusion and infarction by attenuating cardiac fibrosis and cardiomyocyte injury, reducing inflammatory cytokine profiles and modulating the ANS. This work provides novel insight into the anti-fibrotic effects of HEX and is suggestive of a potential translational application of this synthetic peptide for AMI patients. Importantly, in this work we were able to clearly demonstrate the cardioprotective effect of HEX therapy using clinically-relevant models, where HEX was administered prior to myocardial reperfusion, representing a protocol that could be employed in the reperfusion unit. Therefore, this work signifies a noteworthy contribution to the field of cardio- protection.

Declaration by author

This thesis is composed of my original work, and contains no material previously published or written by another person except where due reference has been made in the text. I have clearly stated the contribution by others to jointly-authored works that I have included in my thesis.

I have clearly stated the contribution of others to my thesis as a whole, including statistical assistance, survey design, data analysis, significant technical procedures, professional editorial advice, financial support and any other original research work used or reported in my thesis. The content of my thesis is the result of work I have carried out since the commencement of my higher degree by research candidature and does not include a substantial part of work that has been submitted to qualify for the award of any other degree or diploma in any university or other tertiary institution. I have clearly stated which parts of my thesis, if any, have been submitted to qualify for another award.

I acknowledge that an electronic copy of my thesis must be lodged with the University Library and, subject to the policy and procedures of The University of Queensland, the thesis be made available for research and study in accordance with the Copyright Act 1968 unless a period of embargo has been approved by the Dean of the Graduate School.

I acknowledge that copyright of all material contained in my thesis resides with the copyright holder(s) of that material. Where appropriate I have obtained copyright permission from the copyright holder to reproduce material in this thesis and have sought permission from co-authors for any jointly authored works included in the thesis.

Publications included in this thesis

1. (McDonald, H., et al. Physiological Reports, 2018) – incorporated into Chapter 5, subsection 5.2.

Contributor	Statement of contribution
Author Hayley McDonald	Conception and design (55%) Analysis and interpretation (60%) Drafting and production (60%)
Author Chen Chen	Conception and design (10%) Analysis and interpretation (5%) Drafting and production (10%)
Author Nyoman Kurniawan	Conception and design (10%) Analysis and interpretation (10%) Drafting and production (10%)
Author Jason Peart	Conception and design (10%) Analysis and interpretation (5%) Drafting and production (10%)
Author Graham Galloway	Conception and design (5%) Analysis and interpretation (5%) Drafting and production (2%)
Author Chrishan Samuel	Conception and design (5%) Analysis and interpretation (10%) Drafting and production (4%)
Author Simon Royce	Conception and design (5%) Analysis and interpretation (5%) Drafting and production (4%)

2. (McDonald, H., et al. Biomedicine and Pharmacotherapy, 2020) – incorporated into Chapter 5, subsection 5.3.

Contributor	Statement of contribution
Author Hayley McDonald	Conception and design (53%) Analysis and interpretation (60%) Drafting and production (60%)
Author Chen Chen	Conception and design (10%) Analysis and interpretation (5%) Drafting and production (10%)
Author Nyoman Kurniawan	Conception and design (15%) Analysis and interpretation (10%) Drafting and production (12%)
Author Jason Peart	Conception and design (10%) Analysis and interpretation (5%) Drafting and production (10%)
Author Graham Galloway	Conception and design (2%) Analysis and interpretation (5%) Drafting and production (2%)
Author Chrishan Samuel	Conception and design (5%) Analysis and interpretation (10%) Drafting and production (4%)
Author Simon Royce	Conception and design (5%) Analysis and interpretation (5%) Drafting and production (2%)

Other publications during candidature

Publications:

- **McDonald, H**., Peart, J., Kurniawan, N., Galloway, G., Royce, S., Samuel, C. S., & Chen, C. (2018). Hexarelin treatment preserves myocardial function and reduces cardiac fibrosis in a mouse model of acute myocardial infarction. *Physiological reports*, *6*(9), e13699.

- **McDonald, H**., Peart, J., Kurniawan, N.D., Galloway, G., Royce, S.G., Samuel, C.S. and Chen, C. (2020). Hexarelin targets neuroinflammatory pathways to preserve cardiac morphology and function in a mouse model of myocardial ischemia-reperfusion. *Biomedicine & Pharmacotherapy*, *127*, p.110165.

Conference abstracts:

- **British Society for Cardiovascular Research: Translation of Cardiovascular Science to the Clinic,** Kelvin Gallery, University of Glasgow, Glasgow, UK: September 2015. Protective role of growth hormone secretagogues against myocardial dysfunction in mouse models of myocardial ischemia, reperfusion and infarction. Mcdonald H., Kurniawan N.D., Peart, J. Chen, C.

- **Ischaemic conditioning and targeting reperfusion injury: a 30 year voyage of discovery,** Barcelona, Hospital Universitari Vall d'Hebron: May 2016. Cardioprotective role of growth hormone secretagogues in mouse models of myocardial ischemia, reperfusion and infarction. Mcdonald H, Peart J, Kurniawan N.D, Galloway G, Samuel C, Chen, C.

- **British Cardiovascular Society/British Society for Cardiovascular Research,** Manchester, UK: June 2016. Cardioprotective role of growth hormone secretagogues in mouse models of myocardial ischemia, reperfusion and infarction. Mcdonald H, Peart, J, Kurniawan N.D, Galloway G, Samuel S, Chen C.

- **European Society of Hypertension: Hypertension and Cardiovascular Protection.** Milan, Italy: June 2017. Hexarelin preserves myocardial function and reduces inflammation and fibrosis in a mouse model of myocardial ischemia reperfusion. Mcdonald H, Peart, J, Kurniawan N.D, Galloway G, Royce S.G, Samuel S, Chen C.

Contributions by others to the thesis

Prof. Chen and Dr. Peart were integral to conceiving and designing this project. Dr. Kurniawan contributed significantly to all aspects of the advanced magnetic resonance imaging, particularly the technical aspects of image acquisition. Dr. Samuel contributed to the design and technical aspects of the histology and morphometric analysis. Dr Huang contributed to the cytokine and troponin-I analysis.

The work of this thesis was funded by NHMRC grant to C. Chen and The University of Queensland. The author would also like to acknowledge the facilities, scientific and technical assistance of the National Imaging Facility, a National Collaborative Research Infrastructure Strategy (NCRIS) capability, at the University of Queensland.

Statement of parts of the thesis submitted to qualify for the award of another degree

None.

Research Involving Human or Animal Subjects

All experiments were approved by the Animal Ethics Committee of the University of Queensland and were performed in accordance to national guidelines (Ethics number SBMS/200/13/NHMRC). See Appendix (Chapter 9.1)

Acknowledgements

I would like to acknowledge those that have been instrumental in the completion of this project. Firstly, I would like to express my sincere gratitude to my primary supervisor Professor Chen Chen for his continuous support of my PhD studies with his patience, motivation and immense knowledge. Prof. Chen encouraged me to pursue a cardio-endocrine PhD project at the University of Queensland and supported me in securing an Australian Postgraduate Award, allowing me to undertake this doctoral research within his laboratory. I feel incredibly privileged to have Prof. Chen as my principal supervisor.

To Dr. Jason Peart who helped with the establishment of surgical models, experimental design and conceptualisation and revision of the manuscript. Dr Nyoman Kurniawan who spent countless hours with me in the MRI suite establishing successful cardiac imaging protocols. To Prof. Graham Galloway, without whose support the MRI component of this research would not be possible.

A large, heartfelt thanks to Kym French, who took the absolute best care of my mice and put up with my "all-nighters" in the Otto laboratory. Dr Cora Lau who also supported me and provided guidance throughout the completion of this thesis.

To Dr. Nick Cave who inspired me to pursue a PhD during my BVSc undergraduate years at Massey University. A big thanks to my residency supervisor, Professor Anne French at the University of Glasgow for allowing me extended periods of time off-clinics to be back in Australia completing my writing.

Lastly, to my family for always providing me with unrelenting support and helping me get through the toughest of times. To David McColl, for keeping me motivated (and awake) by putting up with my constant late-night international phone calls and supporting me no matter what.

Financial support

This research was supported by an Australian Postgraduate Award, Australian NHMRC, and The University of Queensland.

Keywords

Myocardial infarction, myocardial ischemia-reperfusion, hexarelin, growth hormone secretagogue, remodelling, fibrosis, inflammation, autonomic nervous system.

Australian and New Zealand Standard Research Classifications (ANZSRC)

ANZSRC code: 110201, Cardiology (incl. cardiovascular diseases), 50%
ANZSRC code: 111699, Medical physiology not elsewhere classified, 20%
ANZSRC code: 111502, Clinical pharmacology and therapeutics, 30%

Fields of Research (FoR) Classification

FoR code: 1102, Cardiorespiratory Medicine and Haematology, 50%
FoR code: 1116, Medical Physiology, 20%
FoR code: 1115, Pharmacology and Pharmaceutical Sciences, 30%

Table of Contents

FIGURES:

TABLES:

Abbreviations

α7nAChR	α-7 nicotinic acetylcholine receptor
3DMSME	3D multi-slice multi-echo sequence
ACH	Acetylcholine
AMI	Acute myocardial infarction
ANS	Autonomic nervous system
ANTHEM-HF	Autonomic Neural regulation Therapy to Enhance Myocardial function in Heart Failure
AT	Angiotensin
ATP	Adenosine triphosphate
CAP	Cholinergic anti-inflammatory pathway
CARDIA	Coronary Artery Risk Development in young Adults
CMRI	Cardiac magnetic resonance imaging
CNS	Central nervous system
CRP	C-reactive protein
CSNA	Cardiac sympathetic nerve activation
CTnI	Cardiac troponin I
CVD	Cardiovascular disease
Cx	Connexin
ECG	Electrocardiograph
ECM	Extracellular matrix
EDV	End diastolic volume
EEC	Enteroendocrine cells
EF	Ejection fraction
ESV	End systolic volume
ET	Endothelin
FLASH	Fast low angle shot
FOV	Field-of-view
FS	Fractional shortening
Gd	Gadolinium
Gd-DTPA	Gadopententate dimeglumine

GE	Gradient echo
GH	Growth hormone
GHS	Growth hormone secretagogue
GHS-R	Growth hormone secretagogue receptor
HEX	Hexarelin
HFpEF	Heart failure with preserved ejection fraction
HFr	High-frequency
HR	Heart rate
HRV	Heart rate variability
HW	Heart weight
IBD	Inflammatory bowel disease
IC	Interstitial collagen
IHD	Ischemic heart disease
IL	Interleukin
INOVATE-HF	Increase of Vagal Tone in Heart Failure
IP	Intraperitoneal
IR	Ischemia reperfusion
IRI	Ischemia reperfusion injury
IV	Intravenous
KO	Knock out
LAD	Left anterior descending coronary artery
LF	Low-frequency
LGE	Late gadolinium enhancement
LPS	Lipopolysaccharide
LV	Left ventricle
LVIDd	Left ventricular internal dimension in diastole
LVIDs	Left ventricular internal dimension in systole
LVAWd	Left ventricular anterior wall thickness in diastole
LVPWd	Left ventricular posterior wall thickness in diastole
LVAWs	Left ventricular anterior wall thickness in systole
LVPWs	Left ventricular posterior wall thickness in systole
MI	Myocardial infarction
MMP	Matrix metalloproteinase
MPIO	Microparticles of iron oxide

NE	Norepinephrine
NECTAR-HF	NEural Cardiac TherApy foR Heart Failure)
NGF	Nerve growth factor
nHFr	Normalized high frequency power
nLF	Normalized low frequency power
NTS	Nucleus tractus solitaries
NYHA	New York Heart Association
PNA	Parasympathetic nervous activity
PPCI	Percuraneous coronary intervention
PSNA	Parasympathetic nerve activity
ROI	Region of interest
RR	Respiratory rate
SC	Subcutaneous
SMA	Smooth muscle actin
SNA	Sympathetic nervous activity
SNR	Signal to noise ratio
SNS	Sympathetic nervous system
STZ	Streptozotocin
SV	Stroke volume
T2DM	Type 2 diabetes mellitus
T_2w	T_2-weighted
T	Tesla
TE	Echo time
TGF	Transforming growth factor
TI	Inversion time
TL	Tibial length
tLAD	Transient ligation of the left descending coronary artery
TNF	Tumour necrosis factor
TR	Repetition time
TTC	Triphenyl tetrazolium chloride
VEH	Vehicle
VLF	Very-low-frequency
VN	Vagus nerve
VNS	Vagal nerve stimulation

1. Introduction

1.1 Ischemic Heart Disease

Ischemic heart disease (IHD) is a leading cause of morbidity and mortality worldwide and is associated with considerable health care costs (1-3). The introduction of reperfusion therapies have substantially reduced mortality and morbidity amongst acute myocardial infarction (AMI) patients, however, there are limited therapies designed for targeting the prevention of myocardial ischemia-reperfusion injury (IRI) and the chronic sequelae of AMI (3) Thus, despite improvement in treatment protocols, concern for the development of chronic cardiac morbidities and sudden cardiac death continue to negatively influence prognosis and result in substantial health care costs (1, 2).

Myocardial ischemia occurs when coronary blood flow and oxygen availability are insufficient to meet the oxygen requirements of the heart (4). The consequences of myocardial ischemia are dependent on the nature and severity of the ischemic episode and elapsed time to subsequent re-establishment of coronary blood flow (4). If the coronary artery is occluded for more than 20 minutes irreversible damage can occur, with lesser periods causing myocardial tissue dysfunction and loss (3, 5). Deprivation of oxygen and nutrient supply results in a series of abrupt biochemical and metabolic changes within the myocardium (3). The absence of oxygen halts oxidative phosphorylation, leading to mitochondrial membrane depolarization, adenosine triphosphate (ATP) depletion and inhibition of myocardial contractile function (3). During an acute myocardial infarction (AMI), occlusion of a coronary artery territory leads to necrosis of the myocytes, following a 'wavefront' pattern, spreading from the subendocardial layers to the subepicardium (6). Without collateral blood supply or

reperfusion, complete necrosis can occur in the territory devoid of perfusion. 'Area-at-risk' is the term given to the total amount of myocardium at risk of necrosis (7). In the absence of reperfusion, very few interventions are able to limit infarct development (3, 8).

The treatment of IHD has entered a new era in which mortality can approximately be halved by procedures that allow the rapid reperfusion of blood flow to the ischemic zone of the myocardium (3, 9). Reperfusion allows the return of blood flow to the ischemic area, re-admission of oxygen and metabolic substrates with washout of ischemic metabolites (8). Timely myocardial reperfusion via primary percutaneous coronary intervention or thrombolytic therapy is essential to salvage viable myocardium, limit infarct size, preserve left ventricular systolic function, and prevent the onset of heart failure (3, 9).

Although essential, the process of myocardial reperfusion can *itself* induce further cardiomyocyte death in a phenomenon known as myocardial reperfusion injury (10). Reperfusion may lead to further complications such as diminished cardiac contractile function (stunning), arrhythmias and irreversible cell injury leading to necrosis and apoptosis (3, 9). Early reperfusion therapy and other recent advances in the treatment of AMI have substantially reduced mortality and morbidity amongst these patients, however, there remains no effective therapy for the prevention of myocardial reperfusion injury and its sequelae (3). Early arrhythmias can often prove fatal and chronic left ventricular (LV) remodelling and heart failure continue to be major determinants of prognosis after AMI (11, 12). A key event in the progression to heart failure is the pathological remodelling of the LV secondary to cardiac fibrosis (12). To date, there remains no effective therapy able to successfully target and alleviate

excessive fibrosis post-AMI (12-14).

The development of cardioprotective agents to improve myocardial function, decrease the incidence of arrhythmias, delay the onset of necrosis, limit the total extent of infarction and prevent adverse LV remodelling are of significant clinical importance in the AMI patient. There are limited pharmacological agents capable of targeting these adverse processes both acutely, ie, in the catheter laboratory, as well as after discharge of the patient. Furthermore, quantifying critical zones such as the area-at-risk and irreversible myocardial injury can allow determination of myocardial salvage and therapeutic efficacy but these are challenging to accurately assess non-invasively in both pre-clinical and clinical studies.

1.2 Assessment of myocardial injury in situ

The most critical determinant of prognosis in patients with AMI is infarct size. Infarct size is a predictor of chronic LV function and clinical outcome in patients after AMI, and is inversely related to prognosis (15). An important goal in cardiovascular drug development is to achieve infarct size-limiting agents, to aid this; animal models of infarct size are of great clinical importance in preclinical drug development (8). Accurate determination of the extent of infarction is necessary to evaluate interventions that may delay the onset of necrosis and limit the extent of infarct size during ischemia-reperfusion (IR) (8).

Historically, two-dimensional echocardiography has been the most commonly used non-invasive method for measuring cardiac function in *in vivo* experimental animal models (16), however, magnetic resonance imaging (MRI) allows more accurate three-dimensional characterization of cardiac structure and function (17). MRI has

thus emerged as a powerful and reliable tool to non-invasively study the cardiovascular system in clinical practice (18, 19).

Cardiac MRI (cMRI) is considered one of the most important imaging tools in assessment of the heart after AMI (19, 20). Pathological changes in the injured myocardium, such as in the presence of fibrosis, haemorrhage and oedema, influence the signal intensity on T_1- and T_2- weighted imaging (21, 22). Early identification of patients with sub-optimal cardiac recovery after AMI is of great importance to improve clinical management. Therefore, both functional and structural characterization of the infarcted myocardium is important for risk stratification of patients after AMI (19, 20). cMRI has the key unique strength of allowing myocardial tissue characterization in addition to cardiac volume and function quantification. This strength permits better diagnosis, prognostication and tracking of therapy and holds advantages over the traditional echocardiographic approach in AMI assessment (7, 8).

Murine cMRI is very challenging due to the small size of the mouse heart and rapid heart rate (400-600 beats/min). High field strengths (>7 Tesla (T)) are generally required to obtain sufficient signal-to-noise ratio to perform murine cMRI studies (16, 23), compared to human clinical MRI, which is commonly in the range of 1-3T. It has been shown that murine LV function can be reliably measured using cMRI. Studies in mice measuring global LV function have demonstrated that the global ejection fraction in healthy adult mice (60-75%) is similar to that reported in humans (23).

Accurate quantitative assessment of LV function and structural abnormalities of myocardial tissue are of key importance in both the clinical AMI patient and in

disease models. Accurate determination of the extent of infarction is necessary to evaluate interventions that may delay the onset of necrosis and limit the extent of infarct size during IR. These are important concepts in developing preclinical AMI models (8).

1.3 Growth Hormone Secretagogues

1.3.1 Ghrelin

Growth hormone secretagogues (GHS) have recently been identified as synthetic compounds (mostly peptides) that stimulate growth hormone (GH) release from the pituitary gland through the G-protein-coupled receptor (GHS-R) expressed mainly in the pituitary and hypothalamus (24, 25). The endogenous ligand, ghrelin, was originally isolated from the stomach wall in 1999 (26). Ghrelin is a peptide of 28 amino acids, in which the serine 3 residue is *n*-octanoylated (26). There are two distinct circulating forms of ghrelin: acylated ghrelin and des-acyl ghrelin. Acylated ghrelin binds to the growth hormone secretagogue receptor 1a (GHS-R) and features a post-translational modification of *O*-*n*-octanoylation at serine 3 which is required for its multifaceted endocrine functions (26). Des-acyl ghrelin is the major molecular form secreted into the circulation and lacks this post-translational modification. Des-acyl ghrelin is speculated to bind to an unidentified receptor distinct from GHS-R (27-29).

Ghrelin is a pleiotropic peptide and has many functions other than the control of GH release (30). The wide distribution of the ghrelin receptor indicates multiple paracrine, autocrine and endocrine roles for ghrelin (31). The GHS-R receptor is expressed in many peripheral organs including the stomach, intestine (32), pancreas (33), kidney (34), heart and aorta (35).

Ghrelin plays a major role in the regulation of systemic metabolism and has been shown to exert a number of central and peripheral actions such as regulation of food intake, control of energy balance, glucose metabolism and insulin release, and stimulation of gastric acid secretion and motility (25, 36-39). The presence of GHS-R within blood vessels and cardiac tissue suggests that ghrelin also has cardiovascular effects (35, 40, 41).

1.3.2 Hexarelin

Hexarelin (HEX) is a synthetic hexapeptide belonging to the GHS family that has been reported to feature cardiovascular activity (42, 43). HEX is recognized to be both chemically more stable and functionally more potent than ghrelin (26, 42-44). Specifically, HEX has been demonstrated to be more potent in improving heart function after myocardial infarction (MI) when compared with ghrelin (45). HEX has also been shown to significantly prevent damage induced by myocardial ischemia-reperfusion injury (IRI) (46, 47). Ghrelin has been demonstrated to be far less effective in preventing increases in LV end diastolic pressure, coronary perfusion pressure and release of creatine kinase in the heart perfusate of isolated working hearts (48).

GHS-R appears to mediate the action of HEX, however some studies report that in addition, the CD36 receptor may at least be partly responsible for the actions of HEX within the heart and cardiomyocytes (44). The half-maximal effective concentration for the GHS-R of HEX (1.7nM) is comparable to that of ghrelin (1.0nM), therefore, the additional beneficial effects of HEX are speculated to be the result of CD36 activation (42, 49). Other studies report identical effects of HEX and ghrelin on

cardiomyocytes via activation of GHS-R, although the molar dosages of ghrelin were demonstrated to be 10 times that of HEX (50-52). It has therefore been speculated that ghrelin plays a minor role in the control of heart function and actions of HEX are mediated in part by GHS-R and largely by interactions with CD36 (44, 48).

1.3.3 Growth Hormone Secretagogues in Clinical Trials

There are accumulating reports describing the application of GHS in clinical trials (53-56). Ghrelin has been demonstrated to improve LV function, remodelling and cardiac cachexia in rats with chronic heart failure (57). The same group proceeded to show that in human patients with chronic heart failure, repeated ghrelin administration over 3 weeks improved LV function, exercise capacity and muscle wastage (53). Chronic heart failure patients treated with an intravenous (IV) ghrelin infusion showed a significant decrease in mean arterial blood pressure with no significant effect on heart rate. Ghrelin treatment was seen to markedly increase cardiac index and stroke volume index in the absence of renal effects in these patients (54).

The cardiovascular effect of a constant rate infusion of ghrelin was studied in healthy young men and demonstrated that persistent supraphysiological ghrelin levels stimulated LV function without changing endothelium-dependent vasodilation (55). In healthy volunteers, IV administration of human ghrelin reduced cardiac afterload and increase cardiac output without increasing heart rate (56). Furthermore, infusion of HEX has been shown to exert an inotropic effect in healthy male patients without significant effects on mean arterial blood pressure or heart rate (41). These effects suggest that HEX may influence the baroreceptor reflex.

In a randomized, controlled trial investigating the effect of exercise training on ghrelin levels in the setting of heart failure with preserved ejection fraction (HFpEF), exercise training had a significant impact on endogenous ghrelin levels (58). Exercise training was found to increase ghrelin levels. Patients with lower ghrelin levels at baseline were found to experience a more pronounced increase in ghrelin under the training intervention (58).

Ghrelin has been proposed as a potential biomarker and prognostic indicator in patients with chronic heart failure (57, 59). Recent data suggests that the GHS-R/ghrelin axis shows potential as a marker of cardiac dysfunction (60). In this study, tissue ghrelin was found to be a more sensitive indicator than b-type natriuretic peptide in detecting the biochemical processes characteristic of heart failure. Thus, eluding to the potential of ghrelin as a cardiac-specific biomarker in pre-clinical stages of heart failure (60). At the preclinical-level, researchers have also shown decreased levels of GHS-R in rodent models of diabetic cardiomyopathy (61).

HEX has already been utilized in human studies of cardiovascular disease (CVD), demonstrating that it is a both safe and efficacious peptide. However, the potential therapeutic effects of HEX remain largely unexplored, particularly in the setting of myocardial IR. Ghrelin is an unstable natural peptide that can easily be transformed and degraded and limits clinical use. Hexarelin is a more potent and stable alternative to ghrelin. Studies conducted to date warrant further investigation and clarification of underlying mechanisms leading to cardioprotection.

1.4 Growth Hormone Secretagogues: influence on myocardial remodeling and function

1.4.1 Cardiac Fibrosis

It is well known that a major determinant of survival after recovery from AMI is LV remodelling (62). Myocardial infarction can lead to progressive ventricular remodelling, increased myocardial wall stress and can ultimately result in heart failure (14).

Following AMI, cardiac fibroblasts are key effector cells in inflammation, repair and remodelling of the heart (63). Phenotypically transformed fibroblasts, termed myofibroblasts, are instrumental in all fibrotic conditions and are activated in response to myocardial injury and chronically increased mechanical load (64). Myofibroblasts are central to fibrogenesis at the site of remodelling following infarction (65, 66). These transformed fibroblasts are not residents of normal cardiac tissue and appear at the site of an infarct with a hallmark expression of α- smooth muscle actin (SMA) (67, 68).

Timely activation of the endogenous pathways that inhibit inflammation is important to prevent the catastrophic consequences of uncontrolled inflammation on cardiac geometry and function post-MI (63). Induction of pro-inflammatory cytokines, such as interleukin (IL)-1 and tumour necrosis factor (TNF)-α play an important role in acquisition of a pro-inflammatory phenotype by cardiac fibroblasts during the early stages following AMI and have been demonstrated to play a role in cardiac remodelling and progression of heart failure (69-72). Sustained presence of

inflammatory cytokines leads to activation of matrix metalloproteinases (MMPs), resulting in ventricular dilation through slippage of collagen (73, 74). Myocyte hypertrophy and progressive fibrosis lead to dysfunction of the LV, eventually resulting in heart failure and potentially, sudden cardiac death (63). HEX has been demonstrated to reduce the presence of proinflammatory cytokines and transforming growth factor (TGF)-β1, a major pro-fibrotic cytokine (75) (Fig. 1).

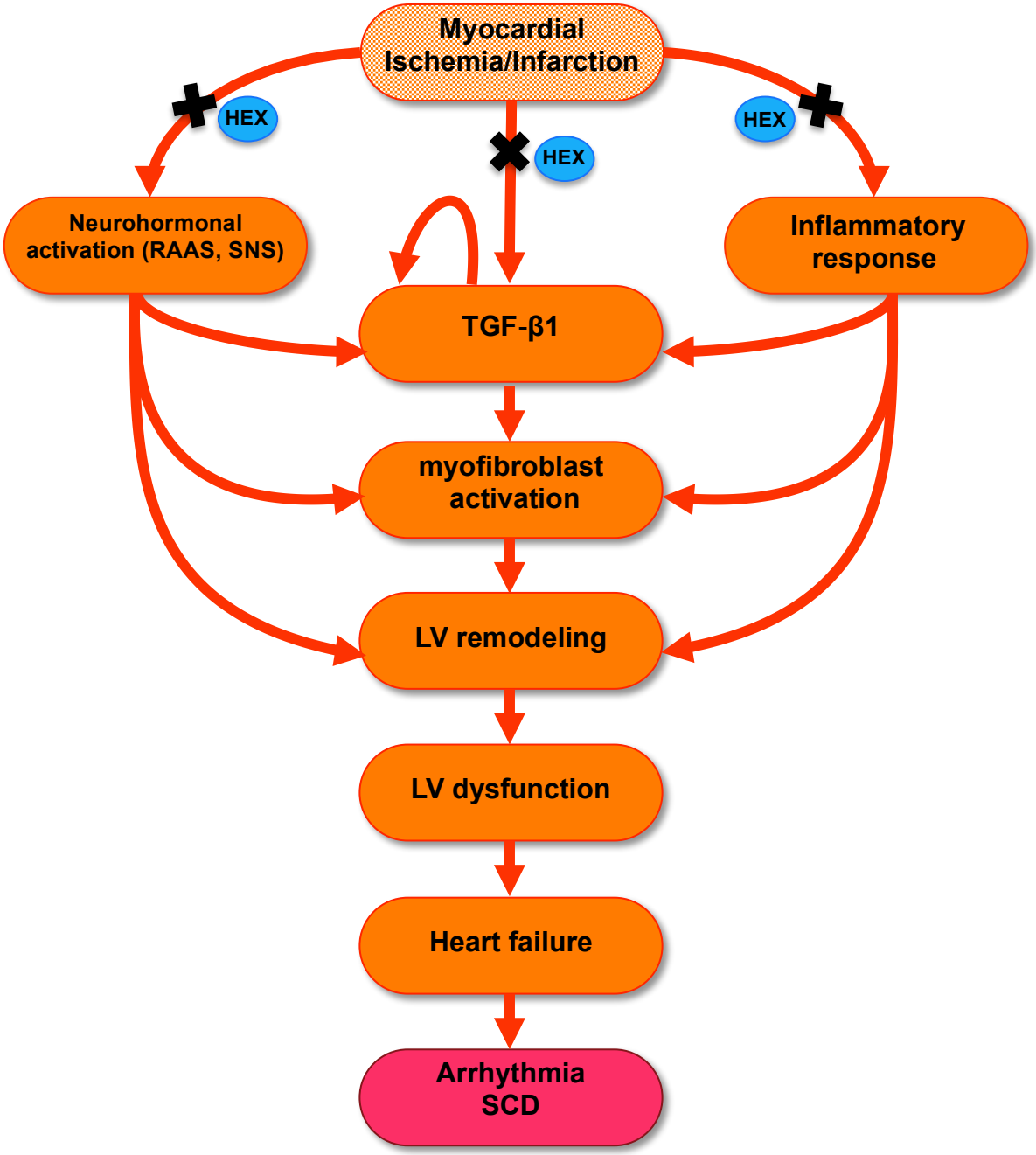

Figure 1 (from (75)): AMI induces dynamic alterations in fibroblast phenotype, initiates an inflammatory response and activates neurohormonal pathways. These alterations collectively result in cardiac remodelling, mechanical dysfunction and electrical disturbances in the failing heart, increasing the risk of sudden cardiac death (12). TFG-β1 is markedly augmented following AMI and is the most potent profibrotic cytokine known, causing excessive extracellular matrix production, inducing its own secretion and driving myofibroblast activation (12). Inflammatory cytokines exert potent pro-inflammatory actions on cardiac fibroblasts and can negatively affect LV function. Similarly, the renin-angiotensin-aldosterone system and sympathetic nervous system activation play a critical role in activation of myofibroblasts and influence LV remodelling & dysfunction (12, 67). HEX may attenuate and actively reverse cardiac remodelling and myocardial fibrosis by targeting these pathways (indicated by "x") and thus holds promise in returning the failing heart to a functional state. Figure from (75)

1.4.2 Remodelling and Sequelae

Adverse sequalae of cardiac remodelling and fibrosis includes the development of arrhythmias and risk of sudden death (63). Ventricular tachycardia and fibrillation are major causes of morbidity and mortality in patients with AMI. Sympathetic hyperinnervation and heterogenous cardiac nerve sprouting have been demonstrated to contribute to ventricular arrhythmogenesis and sudden cardiac death in human and animal MI models (76-80). The autonomic nervous system (ANS) plays an intricate role in the pathophysiology of arrhythmias leading to sudden cardiac death and a bulk of evidence describes the potent protective effect of vagal activation on the ischemic heart resulting in a lower risk of lethal arrhythmias (81, 82). As such, neuraxial modulation has emerged as an important avenue of scientific inquiry and therapeutic intervention (83-85). Ghrelin has been clearly demonstrated to attenuate sympathetic re-innervation and modulate the ANS (11, 86-93). These effects may contribute to the prevention of ventricular arrhythmias and sudden cardiac death in GHS-treated models of MI and may hold relevance for clinical translation.

Cardiac remodeling has been associated with gap junction heterogeneities after AMI

(94, 95). A growing body of evidence suggests that fibroblasts and cardiomyocytes may contribute to cardiac homeostasis by intracellular communications known as connexins (63). Connexin (Cx)-43, a principal component of ventricular gap-junction proteins, contributes to intercellular communication and electrical coupling of cardiomyocytes. During ischemia, uncoupling can occur, leading to pro-arrhythmic effects that contribute to the genesis of ventricular arrhythmias (96-99). Cx43-deficient mice have been reported to be markedly susceptible to ischemia-induced ventricular arrhythmias and sudden death (98, 100).

A loss of phosphorylated Cx43 has been associated with sympathetic nervous system activation in AMI and leads to increased ventricular arrhythmias (100). Vagal nerve stimulation during AMI has been shown to modify ANS activity and exert an antiarrhythmic effect that is accompanied by a preservation of phosphorylated Cx43 (101, 102). Soeki et al. demonstrated a reduction in ventricular arrhythmias and preservation of phosphorylated Cx43 in rats administered ghrelin during AMI in comparison with sham-operated rats. Co-administration with atropine or blockade of vagal afferent nerves diminished these effects (103). Additional studies also indicate that cardiomyocyte coupling may be improved through neural modulation mediated via GHS (45, 104).

In the setting of MI, myocyte death is accompanied by a neural remodeling process beginning acutely after coronary occlusion. This process may lead to denervation, nerve sprouting and hyperinnervation and can lead to a higher risk of life-threatening arrhythmias (80). Nerve growth factor (NGF) is a neurotropin regulating differentiation, survival and synaptic activity of the peripheral nervous system; expression of NGF rises after AMI and drives the regeneration process of the

sympathetic nerves. The level of NGF synthesized is correlated with innervation density (105, 106). Post-MI, inflammatory cells express large amounts of NFG which is temporo-spatially linked with nerve sprouting and sympathetic hyperinnervation density (107, 108). AMI is associated with a cytokine-driven inflammatory reaction where cytokine activation of the nuclear transcription factor (NF)-κβ mediates the tissue inflammatory response and neurotrophin-regulated signaling pathways (109, 110). NF-κβ activity is linked with endothelin (ET)-1 expression, which induces NFG production (111). Yuan et al demonstrated that ghrelin treatment in rats after MI inhibited neural remodelling, attenuated the inflammatory response through suppression of IL-1β, and TNFα and decreased NGF levels. Furthermore, NF-κβ activation was inhibited and decreased ET-1 mRNA expression was observed in the infarcted heart (112).

ET-1 is a highly pro-fibrotic agent, enhancing collagen expression in myocardial fibroblasts and inducing myofibroblast phenoconversion. Increased levels of ET are seen in response to tissue damage, hypoxia and induction of TGF-β1 and angiotensin (AT)-II (113-123). IL-1 and TNFα can stimulate ET-1 and ET-1-mediated electrical remodeling has been shown to correlate with reduced Cx43 expression and function (124, 125). GHS have been demonstrated to inhibit myocardial and neural remodelling through an anti-inflammatory effect, this has been shown to be mediated (at least in part) via inhibition of ET-1 expression in the infarcted heart (112, 126). Chronic treatment with ghrelin has been recently demonstrated to attenuate acute MI-induced arrhythmogenic properties via modulation of Cx43, likely through increased expression of Cx43 via inhibition of ET-1 (94).

Pharmacological modulation of NGF expression may represent a novel strategy to

prevent the nerve-sprouting phenomenon occurring just after AMI, which appears to be involved in the genesis of arrhythmias. Given the biological effects of IL-1β, TNFα, NF-κβ, the anti-inflammatory effect of HEX could be linked to decreased NFG, ET-1 and sympathetic nerve sprouting, and likely to be associated with a preservation of phosphorylated Cx43 (Fig. 2).

Furthermore, it has been suggested that modulation of the myofibroblast cytoskeleton may also have anti-arrhythmic effects (127). Experimental evidence suggests that α-SMA-containing stress fibres contribute to the arrhythmogenic potential of myofibroblasts and thus targeting the fibroblast may hold promise in treatment of infarct-related arrhythmias (127). Myofibroblast modulation may represent a strategy explaining HEX's anti-arrhythmic properties and is likely to link to cardiac fibroblasts, Cx43 regulation and electrical remodelling (68, 94).

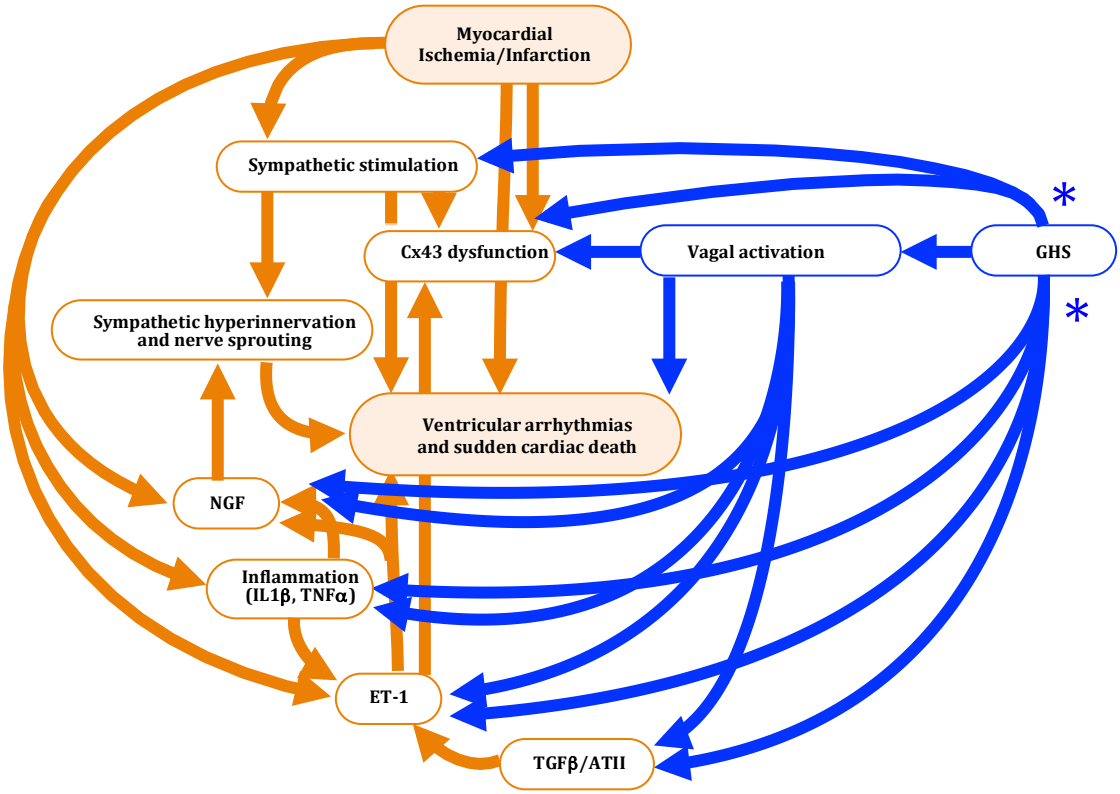

Figure 2: GHS have clear effects on preservation of Cx43 and modulation of the myofibrocyte phenotype in addition to reductions in ET-1, NGF and sympathetic hyperinnervation. These effects appear to ultimately cumulate in a reduction in cardiac fibrosis and preservation of myocardial function. It is unclear as to whether these effects are directly associated with GHS treatment or are indirect via autonomic modulation and the anti-inflammatory actions of GHS. See text for further details. Key: orange arrows represent enhancement; blue arrows represent a protective modulation. *It is unclear whether these effects are direct or indirect via autonomic modulation. Abbreviations: ANS, autonomic nervous system; Cx, connexin; ET, endothelin; GHS, growth hormone secretagogues; MI, myocardial infarction; NGF nerve growth factor.

Adverse ventricular remodelling is key factor underlying the deterioration in cardiac function ultimately leading to increased morbidity and mortality. The discovery of novel approaches to halt these detrimental remodelling pathways prior to the establishment of chronic cardiac disease is critical. Recent evidence suggests that the autonomic nervous system can have profound effects on CV function, remodelling, inflammation, IRI and mortality. In the following section we will introduce the novel and largely undiscovered link between GHS, cardiovascular disease and the autonomic nervous system.

1.5 The Autonomic nervous system, cardiovascular disease & GHS: A novel approach to cardioprotection?

1.5.1. Sympathetic Activity in cardiovascular disease:

Activation of the sympathetic nervous system (SNS) in heart failure patients has been studied in detail and shown to contribute significantly to disease progression (128-

131). The extent of elevation of norepinephrine concentration in patients with heart failure has been demonstrated to correlate directly with the severity of LV dysfunction and inversely with prognosis. Plasma norepinephrine has been shown to be elevated even in patients with asymptomatic LV dysfunction and increases with progression to overt heart failure (128-132). Ghrelin has recently been proposed as a similarly useful biomarker and prognosticator in chronic heart failure (133).

The high mortality in MI has been strongly associated with an adverse and sustained increase in cardiac sympathetic nervous system activity (CSNA), initiated within the first hour of infarction (11, 88, 134). By providing inotropic support to the heart after MI an increase in sympathetic nervous activity appears to have an initial benefit. However, long-term, sympathetic overstimulation is detrimental to the myocardium and is associated with an increased risk of potentially fatal ventricular arrhythmias, LV remodelling and heart failure (135, 136).

Through the suppression of CSNA activity, beta-adrenergic blockade has been shown to reduce the incidence of ventricular arrhythmias, attenuate adverse ventricular remodelling and decrease mortality after MI (135, 137, 138). Beta-adrenergic blockers have been shown to improve many important outcomes, including hospitalization and total mortality in chronic heart failure patients, amelioration of LV remodelling and improvement in functional class (137-140).

The mechanisms underlying the increase in CSNA after MI remain to be fully elucidated (11, 134). Despite the fact that sympathetic activity has long been implicated in morbidity and mortality associated with MI, limited information is available on the time course and degree of sympathetic activation post-MI. Furthermore, the mechanisms that trigger the initial increase in sympathetic activation

(SNA) after acute MI may not be the same as those that sustain the increase in SNA in chronic heart failure (11). Studies indicate that the increase in CNSA follows an unpredictable time course post-MI (134). In a conscious sheep model, direct continuous recordings taken from the post-ganglionic cardiac thoracic nerves pre- and post-MI, showed a transient increase in CSNA, significant by the second hour after MI. The increase in CSNA was sustained for at least seven days (134).

Accumulating evidence indicates that inhibition of CSNA improves survival post-MI and mitigates LV remodelling and dysfunction (11, 134, 141). The initial increase within the few first hours after MI contributes significantly to ventricular arrhythmias and consequently, a high mortality. *This may represent an important time-point for therapeutic intervention in AMI patients* (11, 90, 134). There is an intricate causal relationship between early and chronic changes in the neural control of cardiac function in heart failure (134). *Although chronic therapeutic interventions are developing for chronic heart failure patients, it is the period immediately after MI, before autonomic modulation of cardiac function becomes irreversibly activated, that may appears critical for optimizing short and long-term outcome by therapeutic intervention* (11).

1.5.2 GHS and cardiac sympathetic nerve activation

Therapeutic administration of GHS in experimental animal models undergoing iatrogenically- induced MI has been promising. The efficacy relating to the temporal-relationship of dose administration requires further description and, specific investigation in IR models.

In a rat model of MI, early ghrelin treatment was shown to prevent the increase in CNSA after MI, reduce the incidence of arrhythmias and improve early survival

prognosis (90). Schwenke et al, demonstrated that a single bolus of ghrelin, with a plasma half-life of < 60 minutes, given within 30 minutes of left anterior descending coronary artery (LAD) ligation, prevented an increase in CSNA (90). This inhibition was sustained for at least 2 weeks and attenuated the magnitude of ventricular remodelling and dysfunction and reduced mortality (11). When administration of ghrelin was delayed (>24hrs) to a point where SNA was maximally increased, daily ghrelin administration was seen to only transiently reduce sympathetic tone after MI (11). In conscious rats after MI, acute administration of ghrelin also decreased CSNA when assessed by heart rate variability analysis (91).

Similarly, mice that received one oral dose of HEX within 30 minutes of MI had a higher ejection fraction and fractional shortening measured 14 days post-MI with lowered plasma epinephrine and dopamine levels. The authors concluded that early HEX treatment protected against chronic cardiac dysfunction after AMI (104).

Therapeutic doses of ghrelin have been demonstrated to have little influence on arterial blood pressure, heart rate and CSNA at baseline and it has been speculated that ghrelin may have a stronger effect on the activated SNS compared with the non-activated system (88, 91). Ghrelin has also been shown to decrease arterial blood pressure without altering heart rate, suggesting that the normal compensatory responses to lowering of blood pressure (i.e. SNS-mediated increase in heart rate) are inhibited by ghrelin-mediated inhibition of SNA (142-144). In healthy human subjects, ghrelin has been shown to suppress CNSA and stimulate cardiac parasympathetic nerve activity (PSNA) (92). Furthermore, the sympathoinhibitory effects of ghrelin are not evident in vagotomised humans and the response is diminished in obese individuals (86).

Studies employing ghrelin knock-out mice have demonstrated that endogenous ghrelin plays a crucial role in preventing CSNA, arrhythmias and improving survival prognosis post-MI (88). Catecholamine concentrations are dramatically increased after MI in Ghrelin knock-out mice, reflecting stronger sympathetic nerve activation. These findings imply that endogenous ghrelin may have important effects on balancing the dysregulated ANS (88). The beneficial effects of ghrelin were seen to be abolished after blockade of the vagal nerves by administration of methylatropine bromide or perineural treatment of both cervical vagal trunks with the afferent neurotoxin, capsaicin. Thus suggesting that these effects may be mediated through the action of ghrelin on the vagal afferent nerves (88).

Endogenous ghrelin also plays a crucial role in improving ventricular remodelling and protecting myocardial function after MI (145). Telemetric assessment in conscious animals showed that deteriorated ventricular function in ghrelin knock-out mice was accompanied by excessive CSNA and decreased PSNA. Treatment with metoprolol or ghrelin was shown to suppress CSNA activation, decrease circulating catecholamines and prevent ventricular remodelling and dysfunction (145). Thus, evidence is accumulating to support an indirect cardioprotective effect of ghrelin via central and peripheral modulation of the autonomic nervous system potentially via cardiac vagal activation (11, 88).

The GHS-R is located within the main cardiovascular control centre in the nucleus tractus solitarius (NTS) where baroreceptor and chemoreceptor afferents terminate (87). Studies have also demonstrated the existence of GHS-R in the infarcted myocardium (91, 146). Co-staining with acetylcholine-esterase suggests that the GHS-R is localized in the vagal nerve (VN) terminals of the heart, with afferent

projections to the NTS (147). The location and signalling pathway of ghrelin and the GHS-R in the heart shows a striking resemblance with that of the gastrointestinal system (148). Within the mouse heart, the GHS-R has been detected in very close proximity to the choline actyltransferease positive nervous terminals (90, 91, 147). It is possible that peripheral ghrelin modulates the cardiac vagal afferent nerve and NTS signalling, resulting in a decrease in sympathetic activity and enhancement of PSNA (90). This has been suggested in a rat model of MI (91).

A number of studies demonstrate that ghrelin may also act centrally to modulate the sympathetic nervous system (149). The NTS is an important regulator of blood pressure and the SNS. Ghrelin has been shown to induce c-fos expression within the NTS (150) and central administration of ghrelin has been demonstrated to act directly on the NTS to suppress SNA and decrease arterial blood pressure (87, 89). Intracerebroventricular injection of ghrelin has been seen to decrease SNA in conscious rabbits and suppress SNA in brown adipose tissue in rats (89, 93).

The intertwined effects of GHS, the ANS and cardiac function are intriguing and may represent a novel therapetutic approach to cardioprotection. HEX remains unexplored in this setting, specifically as a therapeutic agent in reperfused ischemic heart disease.

1.5.3 Vagal activity in cardiovascular disease

Autonomic imbalance, characterized by vagal withdrawal and sympathetic predominance has been linked to impaired cardiovascular function and elevated mortality in various cardiovascular diseases including heart failure, arrhythmias, IRI, and hypertension (151-154). Traditionally, the cardiovascular function of the VN has entailed regulating sinus rhythm and atrioventricular node conduction. However,

recent evidence indicates that the VN can have profound effects on LV remodelling, cardiovascular function, IRI, arrhythmias and mortality (155).

Congestive heart failure and AMI are diseases associated with essential perturbations in the ANS (139). Reduced vagal tone, characterized by depressed heart rate variability and blunted baroreflex sensitivity is closely related to disease progression and poor clinical outcome in these patients (156, 157). Defective parasympathetic cardiac control may occur before, or in parallel with, elevation in sympathetic tone in the development of heart failure (139). Both experimental and clinical studies have demonstrated the close association between reduced vagal reflexes and increased cardiovascular mortality (158).

Conventionally, pharmacological interventions, such as beta-blocker treatment has primarily targeted suppressing sympathetic over-activation, while vagal modulation has been neglected (159). Parasympathetic tone restoration/augmentation has recently emerged as a promising therapeutic approach for normalising autonomic imbalance and preventing the progression of heart failure (160). The mechanisms and causal relationship between the withdrawal of parasympathetic tone and chronic heart failure progression remain uncertain (139).

1.5.4 GHS and the Vagus Nerve

The VN has been shown to have an important role in signalling between peripheral ghrelin and central appetite centres (142). Intravenous administration of ghrelin has stimulatory effects on gastric motility and gastric acid secretion with these effects abolished by atropine pre-treatment or bilateral cervical vagotomy (161-163).

Centrally administered ghrelin has been demonstrated to activate efferent cardiac vagal nerves in anaesthetized rabbits resulting in increased acetylcholine (ACH) release into the sinoatrial node and a subsequent reduction in heart rate. ACH was seen to recover to baseline level after vagotomy (147). Interestingly, the maximum dialysate ACH concentration after intracerebroventricular injection of ghrelin has been shown to reach a concentration almost equivalent to that induced by electrical stimulation of the right cervical VN at 10-20Hz (164). Thus, ghrelin may act as an important mediator in the central nervous system (CNS) to activate the cardiac VN (147). In this study, ghrelin did not change norepinephrine release (147), thus, it has been speculated that ghrelin has a stronger inhibitory effect on the activated sympathetic nervous system (90, 91).

1.5.5 Inflammation and the Vagus nerve

Balanced inflammatory responses are essential elements of a successful host response after injury. However, excessive and sustained inflammatory responses can lead to severe tissue damage (165). The VN has been suggested as an important link between the involuntary nervous system and proinflammation for over 70 years (166). The afferent sensory fibres and efferent motor fibres suggest that the VN can sense continuing inflammation and can act rapidly and efficiently to suppress it. Thus, the vagus can act as an endogenous mechanism to regulate the magnitude of innate immune responses and subsequently attenuate inflammation (165).

It is well known that activation of efferent VN fibres can modulate local and systemic inflammatory responses (165, 167-169). This motor arc of this inflammatory reflex is termed the ‘cholinergic anti-inflammatory pathway’ (CAP) and was first described by Tracey et al (165). Cytokines produced by immunoactive cells secondary to

exogenous or endogenous stimuli are registered by afferent vagus neurons (170, 171). Information travels centrally to the NTS to communicate with the brainstem, hypothalamus and forebrain, affecting glucocorticoid release, inhibiting proinflammatory cytokines and reflexively activating efferent vagal pathways (171-173). The CAP consists of VN signaling leading to an ACH-dependant interaction with the α-7 nicotinic acetylcholine receptor (α7nAChR) subunit on macrophages and monocytes and the subsequent reduction of inflammatory cytokines (170, 174, 175). The CAP is considered a mechanism by which the CNS may regulate excessive inflammation and limit self damage (176). The precise mechanism of how VN activation exerts its protective effects is highly complex and further mechanistic studies need to be conducted in this field.

Activation of the CAP is possible via vagal nerve stimulation (VNS) or pharmacologically via administration of selective α7nAChR agonists or inhibitors of acetylcholinersetase (177, 178)**.** Cholinergic agonists have been shown to produce the same effects as VNS (179). Cholinergic stimulation has been demonstrated to reduce pro-inflammatory cytokine production and prevent lethal tissue injury in multiple models of local and systemic inflammation and sepsis (180), including acute lung injury (181, 182), arthritis (183), burns (184, 185), cerebral ischemia (186), colitis (187), encephalomyelitis (188), haemorrhagic shock (189, 190), intracerebral haemorrhage (191), myocardial (192), renal (193) and splanchnic IRI (194), pancreatitis (195), polymicrobial abdominal sepsis (196-198) and post-operative ileus (199).

Pharmacological activation of the CAP is intriguing concept requiring exploration as a therapeutic strategy for IRI in IHD

1.5.6 The cholinergic anti-inflammatory pathway: Mechanism of action

Inflammation has been demonstrated to play a major role in IRI (200, 201). The anti-inflammatory function of the VN is mediated through several pathways, some of which remain controversial (202). Briefly, these pathways are proposed as: the hypothalamic-pituitary-adrenal axis whereby stimulation of vagal afferent fibres ultimately results in release of cortisol from the adrenal glands. Secondly, in the splenic sympathetic anti-inflammatory pathway, the VN stimulates the splenic nerve to release norepinephrine which interacts with the β2 adrenergic receptor of splenic lymphocytes to release ACH & ultimately inhibit the release of TNFα from splenic macrophages via the α7nAChR (202). Lastly, the CAP is mediated through vagal efferent fibres that synapse onto enteric neurons and release ACH. ACH binds to the α7nAChR on macrophages and inhibits release of TNFα and pro-inflammatory cytokines (202) (Fig. 3).

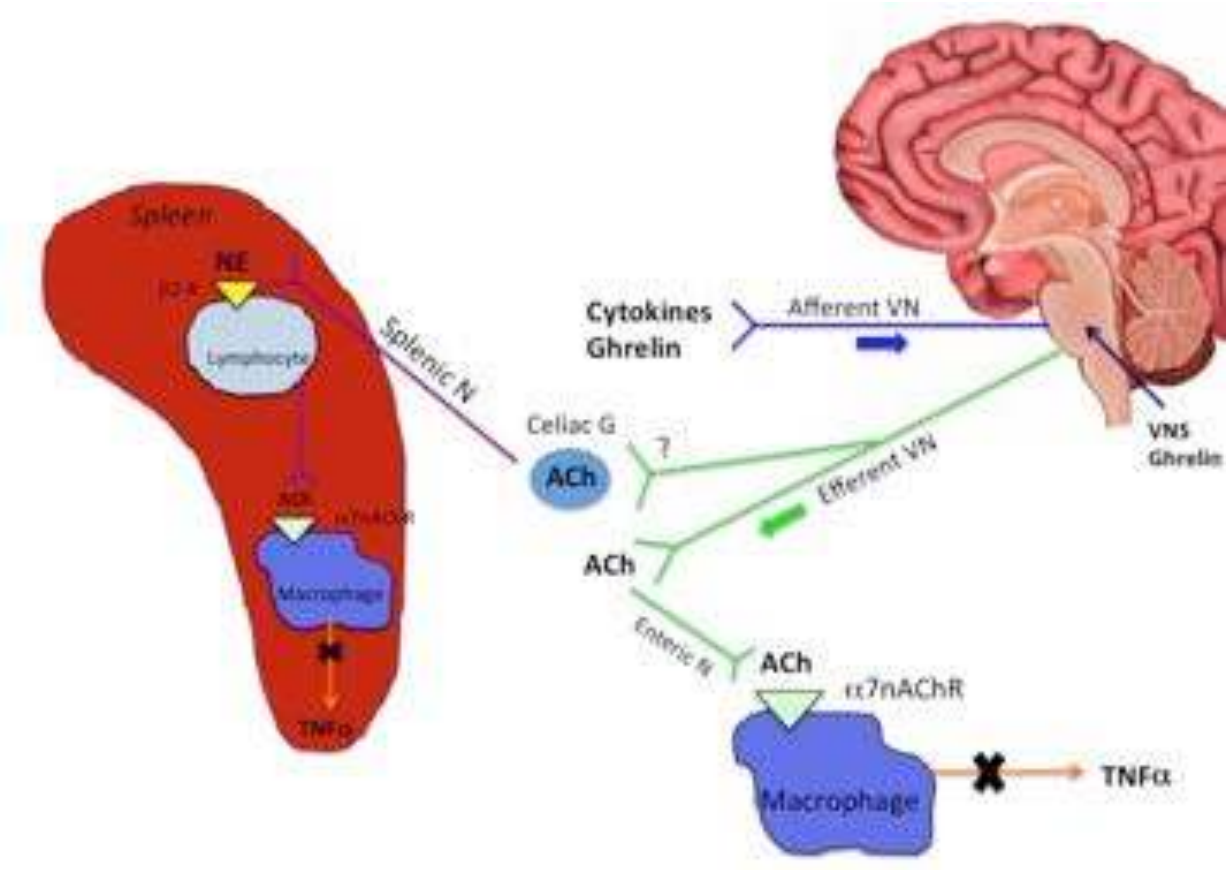

Figure 3: Pathways of vagal function, figure modified from (202). Inflammatory cytokines can activate the afferent VN, which projects to the NTS. Ghrelin binds to the GHS-R and can also modulate this reflex. Ghrelin and VNS can result in central modulation of inflammation via influencing the efferent VN and the CAP (see text). Activation of the splenic pathway is controversial. Abbreviations: Ach, acetylcholine; α7nAChR, α–7–nicotinic acetylcholine receptor; β2-R, beta 2 adrenergic receptor; CAP, cholinergic anti-inflammatory pathway; celiac G, celiac ganglion; NTS, nucleus tractus solitaries; TNFα, tumour necrosis factor α; VN, vagal nerve; VNS, vagal nerve stimulation.

Several studies indicate that action potentials transmitted in the VN traverse the subdiaphragmatic VN, the celiac ganglion and the splenic nerve. Vagal innervation of the spleen is controversial, some report it to be under the control of the VN terminating on macrophages expressing α7nAchR and inhibiting TNFα release (203-207) (see Fig. 3). The spleen is a major source of circulating TNF α and interestingly, splenectomy has been shown to lower TNF α similarly to VNS (203, 208).

Furthermore, splenectomy has been shown to reverse cardiac remodelling and inflammation in heart failure animals. In a mouse model of MI-induced heart failure, splenocytes transferred from these mice to normal mice were observed to migrate to the heart and induce LV dilation, dysfunction and fibrosis (142). These results suggest that the spleen may modulate cardiac inflammation. The metabolic activity of the spleen has also been shown to independently predict risk of subsequent cardiovascular disease events in humans (144). It remains unclear whether vagus activation has direct cardiac or indirect anti-inflammatory effects (or both), there does however, appear to be convincing evidence of a cardiosplenic axis (144)

Efferent vagal fibres release ACH in the reticulo-endothelial system (spleen, liver, gastrointestinal tract). The nicotinic subunit, α7nAchR, is present on macrophages, monocytes, dendritic cells, T-cells and endothelial and non-neuronal cells. Activation of α7nAchR present on macrophages stimulates JAK and STAT anti-inflammatory pathways, inhibits NFκB and prevents cytokine synthesis and release (206, 209, 210). Vagal stimulation has been demonstrated to inhibit TNFα synthesis in wild-type, but not α7-deficient mice, thus demonstrating the essential role of the α7-subunit modulating the CAP response (180, 204, 211). Nicotinic agonists for the α7nAchR have been suggested as therapeutic targets to treat sepsis (212). Efferent vagal activation inhibits TNFα in endotoxaemia without augmenting corticosteroid or IL-10 levels in animals with intact vagi (213).

α7nAChR-dependent cholinergic signalling is also implicated in suppressing production and release of HMGB1, a late cytokine mediator of the systemic inflammatory response (212). Administration of nicotine decreased serum levels of HMGB1 and improved survival in a rat model of sepsis (212). Transcutaneous VNS

has also been shown to reduce serum HMGB1 levels and improve survival of mice with sepsis (143).

1.5.7 Inflammation, Vagal Nerve Activation and Ghrelin

It has been well established that increasing parasympathetic tone, through VNS decreases inflammation in various models of physiologic insult, including myocardial IRI, cecal ligation and puncture, lipopolysaccharide injection, severe burn injury and traumatic brain injury (165, 174, 214-217).

Pharmacological stimulation of the VN may offer a novel approach to anti-inflammatory therapy, this is particularly exciting in the setting of IHD.. Beyond its anti-inflammatory effects, the VN aids as a conduct for neuro-enteric communication, whereby enhanced VN activity (of both central and peripheral divisions), leads to increased pancreatic exocrine function, gastrointestinal motility and changes in neuroendocrine profiles (218), this will be discussed further in the following chapters.

Ghrelin has been shown to have several anti-inflammatory properties involving vagus activation. Intravenous ghrelin administration in septic mice has been shown to decrease levels of the pro-inflammatory cytokines IL-1 and IL-6. Subdiaphragmatic vagotomy completely abolishes this inhibitory effect (196). Vagotomy also abrogated ghrelin's protective effect on sepsis-induced organ function parameters such as aspartate aminotransferase, alanine aminotransferase and lactate (196). Similar findings were also demonstrated after ghrelin treatment in a rat model of endotoxemia (219, 220). Intravenous administration of ghrelin decreased both circulating norepinephrine and TNFα levels in a model of sepsis. Administration of a specific ghrelin receptor antagonist increased the release of norepinephrine and TNFα in normal rats, demonstrating that ghrelin may modulate the overstimulated sympathetic

nerve in sepsis (221). Interestingly, the inhibitory effect of ghrelin on norepinephrine release was completely blocked by intracerebroventricular administration of a GHS-R receptor antagonist, whereas its down-regulatory effect on TNFα release was only partially diminished (221).

Circling levels of ghrelin were significantly decreased in a rat model of polymicrobial sepsis induced by caecal ligation and puncture; with the GHS-R being markedly elevated in early sepsis (222, 223). Down-regulation of ghrelin in sepsis appears to play a role in activating sympathostimulatory nuclei in the brain and increasing norepinephrine release from the sympathetic nerve fibres (221, 224). Furthermore, enterectomy prior to onset of sepsis has been demonstrated to markedly reduce circulating levels of norepinephrine, indicating that the gut is the major source of norepinephrine release during sepsis. It has been described that approximately 50% of the norepinephrine released in the body is produced by the sympathetic fibres in the gut (225-227).

Ghrelin has been demonstrated to have no direct effect on cytokine release from kupffer cells or peritoneal macrophages isolated from normal rats, suggesting an indirect anti-inflammatory mechanism (196). Ghrelin's beneficial effect in inhibiting cytokine release in sepsis is likely to be mediated by combined action of activation of the VN and the inhibition of SNA. *Ghrelin appears to have the potential to rebalance the dysregulated sympathetic/parasympathetic nervous system in sepsis (221). It also seems possible that ghrelin may be a major player in the enteric arm of the CAP. The neuroinflammatory-modulating properties of GHP may also hold true in CVD.*

Inflammation has been demonstrated to play a major role in IRI (228, 229). Ghrelin has been demonstrated to activate the CAP in various models of ischemia-reperfusion

(IR) (230). Administration of ghrelin after gut-IR attenuated excessive inflammation and reduced organ injury demonstrated through the rapid activation of the CAP (231). In a rat model of renal IR, ghrelin administration during reperfusion attenuated both the systemic and renal-specific inflammatory response and was mediated through the VN (232). Ghrelin was also demonstrated to have protective effects in cisplatin-induced nephrotoxicity through inhibition of inflammatory reactions (233). Ghrelin administered as a single dose immediately following sepsis was also found to protect the kidneys from injury by attenuating the pro-inflammatory markers, it was thought that was likely to be mediated through the VN (234)

Using a mouse model of pressure-overload cardiac hypertrophy it was demonstrated that the absence of endogenous ghrelin resulted in severe cardiac hypertrophy and diastolic dysfunction (235). This was accompanied by an increase in the proinflammatory cytokines IL-6 and IL-1β. Administration of ghrelin suppressed the increase in IL-6 and IL-1β and improved cardiac function; it was thought that this was mediated through the CAP (235). Huang et al recently demonstrated that HEX protected cardiomyocytes from IRI partly through modification of the IL-1 signaling pathway, including down-regulation of IL-1β expression and up-regulation of IL-1Rα expression in the IR myocardium. This was mediated via activation of the GHS-R (47).

1.5.8 Anti-inflammatory benefits of vagal nerve stimulation in the heart

A lack of progression in the development of new drug therapies has stimulated interest in new, non-pharmacological approaches for the management of heart failure secondary to LV systolic dysfunction (192, 214, 236, 237). VNS has been shown to address the imbalance between the sympathetic nervous system (SNS) and

parasympathetic nervous system (PNS) (158). GHS may also hold promise in influencing the ANS in heart failure patients (230).

An improvement in LV ejection fraction, ventricular arrhythmias and survival has been demonstrated secondary to VNS in heart failure models (132, 238-241). Vagal stimulation has been seen to improve cardiac autonomic control and significantly attenuate heart failure development in various animal models (242, 243).

An increase in the pro-inflammatory cytokines TNFα, IL-1β, IL-6, IL-18 have been observed in models of chronic heart failure (244, 245). Increased morbidity and mortality has also been associated with cytokine release in chronic heart failure patients (246). VNS has been demonstrated to reduce these markers to near normal (214, 247-249). Importantly, regulation of inflammation may improve cardiac performance and outcome (214, 247). VNS has been shown to reduce LV end-diastolic pressure, increase cardiac output and survival in a rat model of MI (238, 239). In rodents, increased infarct size has been associated with elevated levels of TNFα, with VNS shown to decrease levels of inflammatory markers and infarct size (250, 251). VNS appeared to ameliorate ischemia-induced cardiac dysfunction by inhibiting TNFα-mediated signalling in a number of similar studies (252-254).

Using a swine MI model, VN stimulation was seen to decrease episodes of ventricular fibrillation, reduce infarct size and improve ventricular function (255, 256). Similarly, in a canine model of coronary artery occlusion and myocardial infarction, VNS protected against ventricular fibrillation and improved systolic function (257, 258). Low-level VNS normalized C-reactive protein, IL-1-6, TNFα, pro-ANP, pro-BNP levels and improved LV function in a canine ventricular pacing-heart failure model

(132). Furthermore, VNS was seen to attenuate the reduction in baroreflex sensitivity, rise in plasma norepinephrine and angiotensin II (132, 257). Similar findings were demonstrated by Zhang who employed a canine myocardial IRI model (259). In a canine chronic heart failure model induced by multiple sequential coronary micro-embolism, VNS decreased LV end systolic volume, end diastolic volume and increased ejection fraction (257). Addition of VNS to beta blockade increased LV ejection fraction and decreased LV end systolic volume more than that obtained by B-blockade alone (238, 257).

A major determinant of survival after recovery from MI is LV remodeling (260). VNS has been demonstrated to improve LV remodeling by down-regulation of MMP-9 and TGF-β1 protein expression post-MI (239, 261, 262). MMP-9 and TGF-β1 both play key roles in the progression of post-MI remodeling (263, 264). Inflammatory cytokines such as IL-1 can regulate fibroblast phenotype, activity and the activation of MMPs/TIMPs and thus can influence changes in degradation of the extracellular matrix and collagen deposition (47, 74, 265). VNS has also been demonstrated to attenuate interstitial fibrosis and collagen degradation in the non-infarcted myocardium with concurrent improvement in cardiac function (266). Interestingly, it is possible to substitute low-level transcutaneous electrical stimulation of the auricular branch of the VN for VNS to reverse cardiac remodeling in a canine model of post-ischemic heart failure (266, 267).

1.5.9 Vagal nerve stimulation- Clinical trials

Animal data indicates that the VN regulates an anti-inflammatory reflex in the heart and VNS can affect cardiac remodelling and survival outcomes (214). To date, similar data has not yet translated to the clinic, however, there does appear to be a

relationship between VN activation and inflammation in humans (214, 268). Recently, the CARDIA study (coronary artery risk development in young adults) revealed an inverse relationship between heart rate variability and inflammatory markers, demonstrating that efferent vagus activity is inversely associated with inflammation and cytokines (268).

Implantable electric devices for stimulation of the cervical VN have been used in clinical practice for over 20 years and were initially designed for treatment of epilepsy and depression (269). Schwartz et al. conducted the first clinical approach of chronic VNS using an implantable neurostimulator system for the treatment of severe chronic heart failure and demonstrated a significant improvement in New York Heart Association (NYHA) class, quality of life, LV end systolic volume and trend towards a reduction in LV end diastolic volume after 6 months (270)**.** De Farrari et al. further demonstrated a significant improvement in NYHA quality of life, LV ejection fraction and systolic pressure after one year (243). Furthermore, the ANTHEM-HF (Autonomic Neural regulation Therapy to Enhance Myocardial function in Heart Failure) trial demonstrated that chronic VNS was safe in heart failure with reduced ejection fraction (HFrEF) patients and improved LV ejection fraction, end systolic volume, heart rate variability, exercise intolerance and NYHA functional class (271). Conversely, NECTAR-HF (NEural Cardiac TherApy foR Heart Failure), a double blinded, randomized study of 96 patients comparing VNS to medical therapy, failed to demonstrate a significant effect on measures of cardiac remodelling and functional capacity in symptomatic heart failure patients (160). However, there was a significant improvement in quality of life (272).

INOVATE-HF (Increase of Vagal Tone in Heart Failure) was the first large multi centre, randomized, phase III study of VNS for the treatment of symptomatic heart failure (273). The results of this study showed that VNS did not improve the risk of death or heart failure events among patients with reduced LV ejection fraction. However, VNS improved quality of life, functional status and 6-min walk time in chronic heart failure patients (274). *It is worthy to note, that the patients enrolled in this study did not have inflammatory markers present. Thus, we might postulate that those with chronic fibrotic cardiomyopathic diseases may not benefit from an anti-inflammatory approach to therapy. When there is the potential for remodeling, (ie, post- acute event) VNS may be more likely to have beneficial results (214, 272). This theory has been unexplored to date.*

In conclusion, the VN plays a vital role in maintaining normal cardiac function and reduced vagal tone is a hallmark of a variety of cardiovascular diseases (275). Given that traditional cardiovascular drugs have minimal influence on the inflammatory reflex or cytokines present in cardiovascular disorders, modulating the inflammatory response may represent a largely unexplored therapeutic strategy to reduce infarct size and improve recovery of cardiac function in the AMI patient. Identifying a means to physiologically modulate this inflammatory reaction might provide a rationale solution to protect against myocardial IRI and progression of heart failure. *GHS may represent a plausible answer.*

Ghrelin is likely to be one of the most important mediators in the CNS that activates the VN. GHS may regulate an endogenous pathway to reduce inflammation and protect cardiac function via restoration or augmentation of vagal tone. The therapeutic potential of GHS to modulate the ANS is clearly a feasible and promising

therapeutic target deserving further study and one of the overarching themes of this thesis.

1.6 The gut brain axis and metabolic actions of GHS

IHD in humans is a complex disorder caused by, or associated with other systemic diseases or conditions. IHD develops as a consequence of a number of etiological risk factors and coexists with other disease states that exert multiple biochemical effects on the heart and can potentially interfere with responses to cardioprotective interventions (9). These risk factors include systemic arterial hypertension and LV hypertrophy, hyperlipidemia, atherosclerosis, aging, diabetes and insulin resistance and heart failure (9).

1.6.1 Metabolic disease and Inflammation

Chronic diseases such as obesity, diabetes, cardiovascular and inflammatory bowel disease (IBD) share common features in their pathophysiology (276). It has been well described that inflammation is associated with metabolic alterations and, simultaneously, metabolic disorders often exhibit strong inflammatory underpinnings (276). Levels of acute phase-proteins such as C-reactive protein and proinflammatory cytokines are increased in individuals with obesity, indicative of chronic inflammation (277-279). Furthermore, chronic inflammation secondary to immune and metabolic dysregulation has been linked with hyperglycaemia, insulin resistance, dyslipidaemia and hypertension (277).

Obesity and the metabolic syndrome are closely associated with impaired cardiovascular regulation and atherosclerosis (277). The inflammatory responses associated with metabolic disease can cause cardiac injury and ventricular dysfunction. Elevated cytokine levels have been shown to relate directly to

deterioration of functional class and LV ejection fraction (244, 280). Cytokines can induce hypertrophy, influence myocardial contractility and promote apoptosis contributing to ventricular remodeling and dysfunction (281). Circulating inflammatory cytokines are independent predictors of mortality in patients with advanced heart failure (244, 280). Chronic inflammation has been linked to progression of heart failure, myocardial injury and cardiovascular death (214) (Fig. 4).

Given that traditional cardiovascular drugs have little influence on cytokines or the inflammatory reflex present in heart failure, recent evidence suggests that regulation of inflammation may improve cardiac performance and outcome (247, 282)

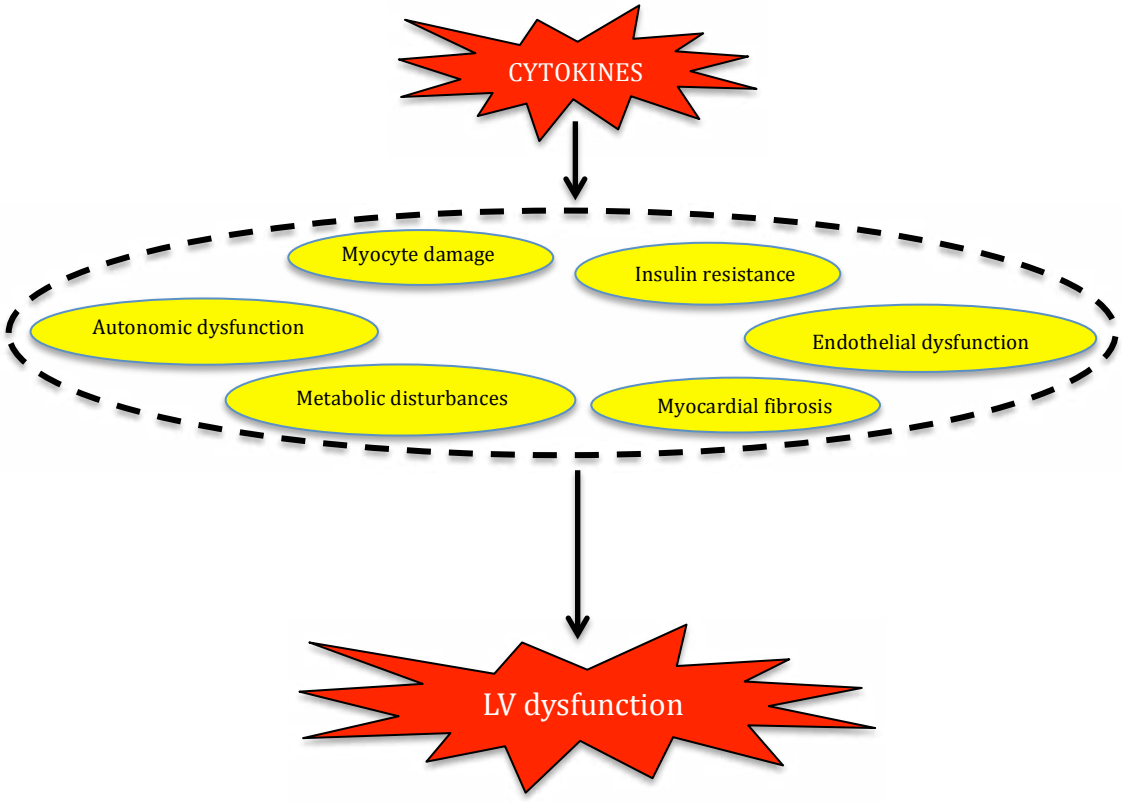

Figure 4: Proposed effects of cytokines. Ultimately, these effects can negatively influence left ventricular function.

1.6.2 Enteroendocrine cells and the immunoendocrine axis

Recently, the intestine and intestinal epithelial cells have been recognized as key players in maintaining both immune and metabolic homeostasis (283). Enteroendocrine cells (EEC) can regulate secretion, gastrointestinal motility and insulin release via the release of peptide hormones (276). These cells are also capable of sensing the lamina propria and luminal environment, including the microbiota, and can modulate signaling by the secretion of endocrine, metabolic, immune and neuronal mediators (276).

It has been increasingly recognized that gut-liberated mediators can influence brain function by acting as an interface between the gut enteric nervous system and CNS, thus effectively linking the CNS and immune system (283). The immune system has been shown to communicate with the brain via various pathways; the humoral route describes the transport of cytokines (or hormones) produced from the gut, immune cells or periphery to the brain via the circulation. Secondly, EEC and immune cells can communicate with afferent sensory nerve fibers through production of endocrine, metabolic, immune or neuronal mediators (284). Finally, circulating immune cells can be trafficked to the brain and influence the CNS via the liberation of inflammatory mediators (283).

During inflammation, both murine and human studies have demonstrated alterations in EEC cell number and secretions (285, 286). EEC cells can be considered integrators of inflammatory and metabolic signaling by acting as front-line pathogen-detectors releasing cytokines or peptide hormones that can directly influence immune

function (276, 286). Immune cells express an array of receptors for EEC-secreted peptides, suggesting the potential of bi-directional signaling in the immunoendocrine axis (286, 287). Importantly, mediators liberated by these cells can indirectly influence immune responses via the triggering of vagal afferents (286).

1.6.3 Vagus Nerve and Gut Peptides

The VN links the exchange signals between the periphery and CNS and is an essential pathway in the regulation of energy metabolism and food intake (148). Electrical stimulation, pharmacological and nutritional interventions have been reported to stimulate the anti-inflammatory actions of the VN. Subdiaphragmatic vagotomy prevents these actions (165, 288).

A number of appetite-regulating peptides are expressed in both the peripheral organs and CNS (148). The nodose ganglion is a constellation of vagal afferent neurons that synthesize receptors for gut peptides regulating feeding and energy homeostasis (289-291). These receptors are transported to afferent terminals in the gastrointestinal mucosa and are optimally positioned to monitor mediators released from gastrointestinal EEC (289). Gut peptides can modulate the activity of the VN by binding to receptors at the vagal afferent terminal that extend into the mucosal layer of the digestive tract (148, 284) (Fig. 5).

Ghrelin receptors are synthesized in the nodose ganglion and are transported to the vagal terminals on the digestive tract end (148). Once bound, information is conveyed to the NTS and the arcuate nucleus within the hypothalamus to modulate appetite-regulation (148, 289). Ghrelin is produced both centrally and in the periphery. A fasting state promotes an increase in plasma ghrelin levels (284), administration of exogenous ghrelin promotes food-seeking behaviour (288, 292). The reported

mechanisms by which ghrelin exerts its biological activities are complex. Ghrelin activates MAPKs, including ERK1/2 which are involved in the activation of nuclear transcription factors (293, 294).

1.6.4 Microbiota and GHS

The enteric nervous system has been described as an important signal transducer between the CNS and the gut (288). Interestingly, a number of disease states show a shift in the structure of the intestinal microbiota and this is thought to play an integral role in disease pathogenesis and clinical course (283, 295). Mice fed a high fat diet have been demonstrated to develop gastrointestinal inflammation; this is communicated to the hypothalamus through a vagal afferent pathway. It is thought that this may partly result from changes in the intestinal flora (289). Furthermore, the composition of the intestinal microbiota is thought to play an important role in altering host immune responses and influencing cytokine profiles, ultimately with the capacity to affect brain function (283). CNS pathologies such as autism, anxiety and depression are thought to be associated with dysbiosis of the intestinal microbiota (288). In mice, ischemic or traumatic brain injury has been demonstrated to drive changes in the intestinal microbiota (296). Components of the microbiota may be able to regulate intestinal motility and gut pain responses, indirectly via production of neuroactive mediators, such as ghrelin (297, 298). Circulating levels of ghrelin are increased by stress in human patients and rodent models (299, 300) and ghrelin administration has been demonstrated to have anxioloytic and anti-depressant effects in mice following calorie restriction (301). Furthermore, mice with elevated plasma ghrelin levels show less anxiety and depressive-like behaviours (301).

1.6.5 Metabolic disease, gut peptides, the vagus nerve and inflammation

Obesity has been shown to evoke a broad array of inflammatory and metabolic responses cumulating in low-grade local inflammation, disruption of metabolic homeostasis and defective insulin receptor signaling (302). A loss of glycemic control is seen in patients with sepsis and in animal models of endotoxin-induced inflammation (303, 304).

Decreased VN activity has been reported in obesity and metabolic derangements can alter the response of the VN to gut peptides (148, 277). An alteration in the VN response towards ghrelin has also been shown to occur in the obese state (289). Biosynthesis of ghrelin is downregulated in obesity, and fasting plasma ghrelin concentrations in humans are negatively correlated with body weight, percentage body fat, and fat mass (305, 306).

Studies suggest that ghrelin may play a crucial role in regulating the gastrointestinal inflammatory process and there is strong evidence supporting ghrelin's protective effect against intestinal inflammation (288, 307). High serum ghrelin levels have been reported in patients with IBD and experimental colitis with exogenous ghrelin shown to have an anti-inflammatory role (307, 308). Similarly, vagal alterations have also been implicated in the pathophysiology of Crohn's disease and inflammatory bowel syndrome (309). In patients with active ulcerative colitis and Crohn's disease, ghrelin is positively correlated with TNFα and C-reactive protein and negatively correlated with bodyweight (310). Ghrelin administration has a potent anti-inflammatory effect through the regulation of both pro-inflammatory and anti-inflammatory cytokines produced by LPS-stimulated macrophages (311). Furthermore, in sepsis, down-regulation of ghrelin appears to play a role in activation of sympathostimulatory

nuclei in the brain and increased norepinephrine release from sympathetic nerve fibers. Ghrelin treatment has also been seen to attenuate intestinal IRI in mice through the inhibition of pro-inflammatory cytokine release and a decrease in neutrophil infiltration via regulation of the NF-κβ pathway (312). Within the immune system, human mononuclear cells, monocytes, neutrophils, and B and T cells express GHS-R and T lymphocytes, B lymphocytes, and neutrophils express ghrelin and its receptor (313, 314). Through the modulation of the T-cell immune response, the protective effects of ghrelin have been demonstrated in an experimental model of chronic intestinal inflammation (315).

It is thought that the increased ghrelin levels could result as a consequence of tissue injury whereby intestinal inflammation and damage stimulate endogenous ghrelin production (316). It is possible that enhanced ghrelin expression could be interpreted as a response that results in increased anti-inflammatory mediators in order to counteract pro-inflammatory responses from activation of the NF-κβ pathway (317). Studies have suggested that the anti-inflammatory mechanisms of ghrelin are mediated through both the vagal pathway and directly through immune cells (307).

The exact anatomical interaction between the VN and the intestinal immune system is still controversial as the VN does not directly interact with the gut resident macrophages (202). The VN preferentially interacts with enteric neurons located within the intestinal muscularis layer. The nerve endings of these enteric neurons are located close to resident macrophages (202). Vagal modulation of intestinal resident macrophages is indirect, likely through these enteric neurons (202, 318). It seems likely that appetite-regulating peptides, such as ghrelin, may be a crucial factor in the anatomical link mediating this pathway. It is highly likely that our intestinal microbiome is able to influence our entire immune system via regulation of the

production of immunomodulatory enteroendocrine hormone peptides (286). This may represent an important component of the enteric limb of the CAP, and a pathway directly influenced by ghrelin.

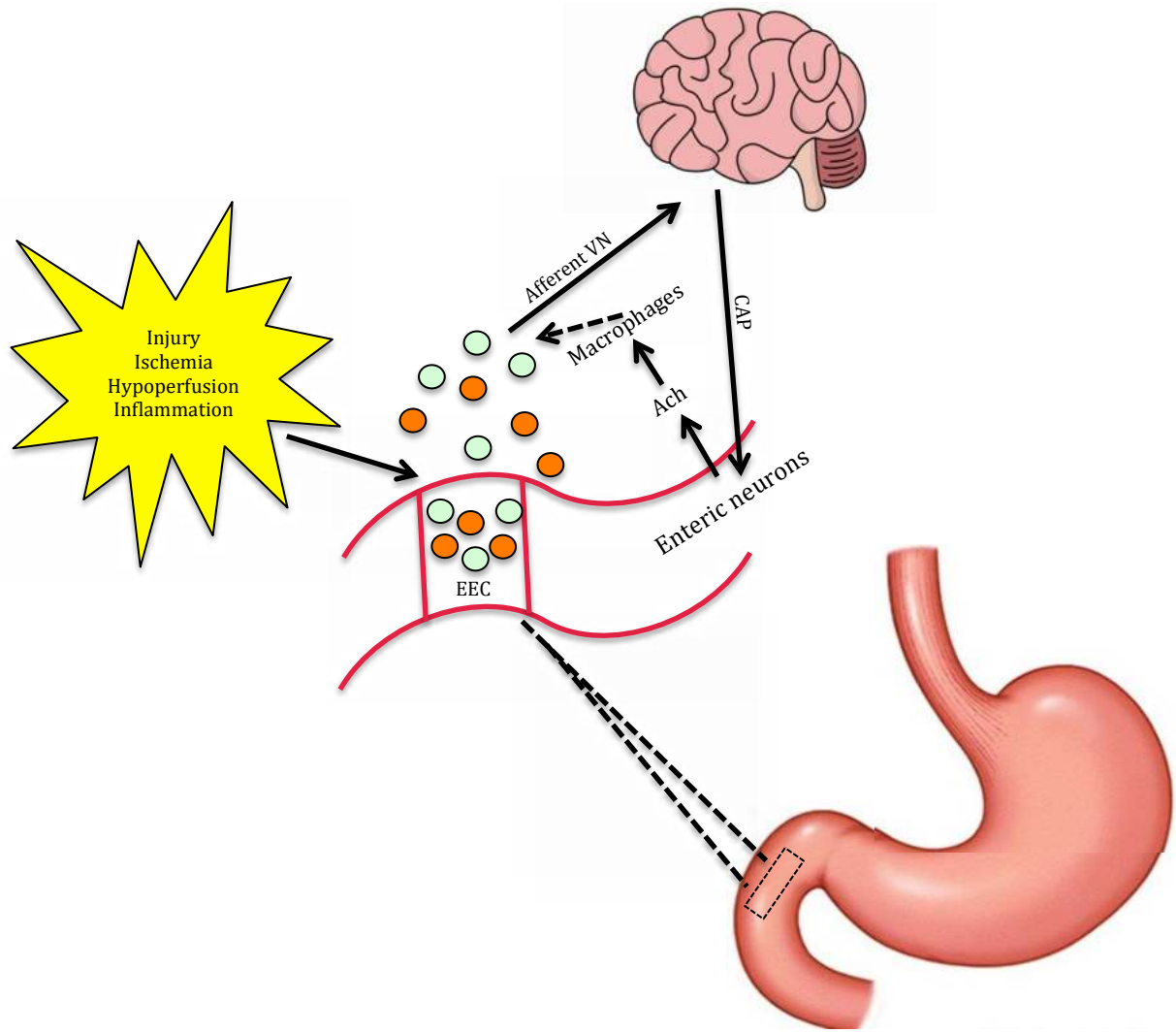

Figure 5: The enteric anti-inflammatory pathway: an *insult* results in induction of inflammatory cytokines and liberation of neuroendocrine mediators from enteroendocrine cells which activate the afferent vagus nerve. The CAP is mediated through vagal efferent fibres that synapse onto enteric neurons and release ACH. ACH binds to the α7nAChR of macrophages and inhibits release of TNFα and pro-inflammatory cytokines. Key: ACH, acetyl choline; CAP, cholinergic anti-inflammatory pathway. Green circles represent ghrelin, orange circles represent inflammatory cytokines.

1.6.6 Cholinergic anti-inflammatory pathway

As previously outlined, the inflammatory reflex is a centrally integrated physiological mechanism in which afferent VN signaling is activated by cytokines or EEC derived peptides (277). This signaling is functionally associated with efferent VN-mediated output to regulate proinflammatory cytokine production and inflammation (277) (Fig. 5). The inflammatory reflex has been exploited as a therapeutic mechanism in preclinical models of diseases etiologically characterized by excessive inflammation and inflammatory responses (277). The safety profile of VN stimulation has been well described given the historical use of surgically implanted devices for epilepsy and depression (319, 320).

VN efferents provide brain-derived output to the liver, gastrointestinal tract and pancreas (321). Metabolic molecules such as ghrelin can act directly within the brain to trigger efferent output that can influence and regulate metabolic homeostasis (277). In obesity, insufficient efferent VN cholinergic output may provide a causative role in the dysfunctional immune and metabolic regulation, especially given that activation of the efferent arm of the cholinergic inflammatory reflex is seen to attenuate both inflammation and metabolic derangements (277, 322-324). Similarly, activation of both arms of the inflammatory reflex by ghrelin appears to reverse metabolic complications (325, 326).

Cholinergic inhibition of cytokine production is mediated via activation of α7nAChR and suppression of NF-κβ nuclear translocation (277). There appears to be a critical role for α7nAChR in maintaining metabolic homeostasis; this has been specifically linked to suppression of inflammation thereby, controlling obesity-associated metabolic complications (277). Immune cells express α7nAchR and GHS-R;

therefore it is possible ghrelin may either attenuate the inflammatory activity of immune cells directly or via vagal stimulation (215, 327).

The chronic inflammatory state in metabolic disease has been shown to activate the SNS and dysregulate the VN, ghrelin has been shown to simultaneously modulate both. Evidence indicates that VN activity is impaired in obesity. By enhancing cholinergic signaling, this has can help suppress obesity-associated inflammation and the associated negative implications (277). Obesity, type 2 diabetes mellitus and CVD are directly linked. In obesity and type 2 diabetes mellitus, the VN activities regulating cardiac function and hepatic glucose metabolism are both impaired (277). Activation of pancreatic insulin secretion by efferent VN-derived cholinergic activation is also well documented. These findings suggest that augmentation of efferent VN activity could be beneficial in patients with insulin resistance, hyperglycaemia, and CVD (277).

Thus, VN dysregulation might contribute to the pathogenesis of obesity and its plethora of comorbidities. Ghrelin is an endogenous peptide that may be an effective cholinergic modulator for the alleviation of inflammation, metabolic complications and CVD (277, 328). Exogenous HEX appears to also activate these pathways.

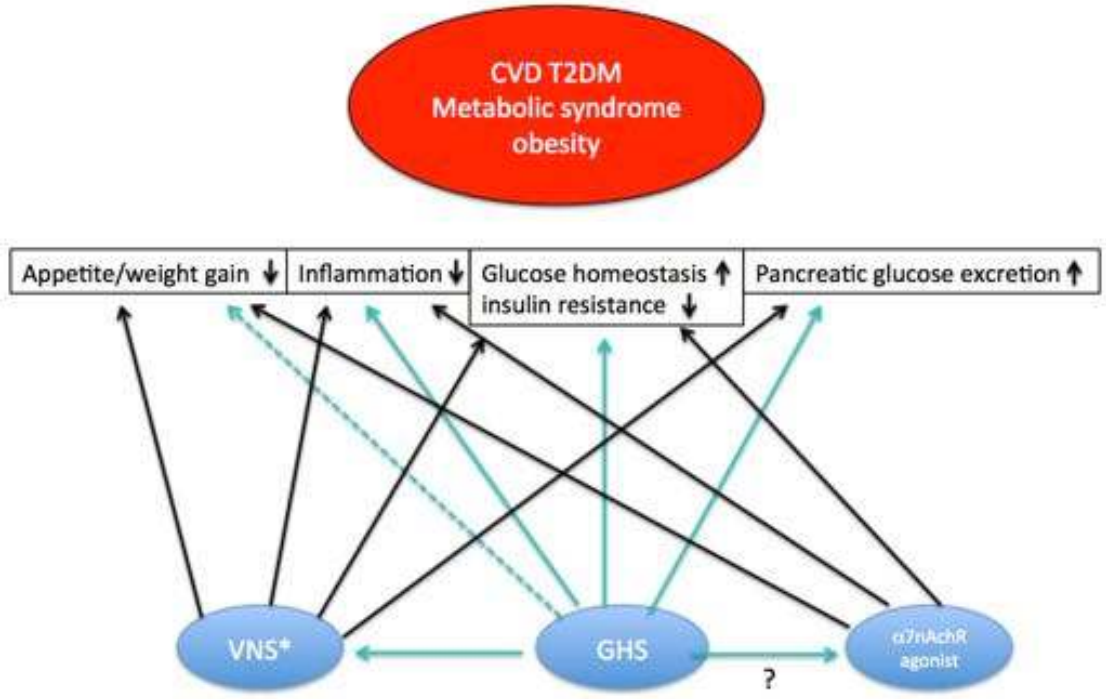

Figure 6: The influence of VNS and α7nAchR agonists on metabolic parameters. GHS modulate these parameters and are thought to have a protective effect similar to VNS and α7nAchR agonists. At this time it is unclear whether GHS themselves are direct α7nAchR agonists. Abbreviations: CVD, cardiovascular disease; GHS, growth hormone secretagogue; T2DM, type 2 diabetes mellitus; VNS, vagal nerve stimulation. *Pharmacological or device-induced VNS. Dotted line – negative influence.

1.6.7 Gut-brain axis conclusion

The gut–brain – (heart) axis presents an opportunity for the development of novel pharmacological (and nutritional) strategies that may be favorable in disorders where CVD and gastrointestinal diseases coexist (288). Anti-cytokine therapy and/or manipulation of the intestinal microbiota may simultaneously influence and uncouple pathological brain-gut signaling (297). *Through its influence on the VN, ghrelin may target and disrupt proximal drivers of aberrant disease processes in both metabolic and cardiac disease. The likelihood of these comorbidities to occur concurrently in the western world means that ghrelin holds the potential to fulfill a unique therapeutic*

niche. To the authors knowledge, GHS therapy in the obese, cardiac patient, remains completely unexplored.

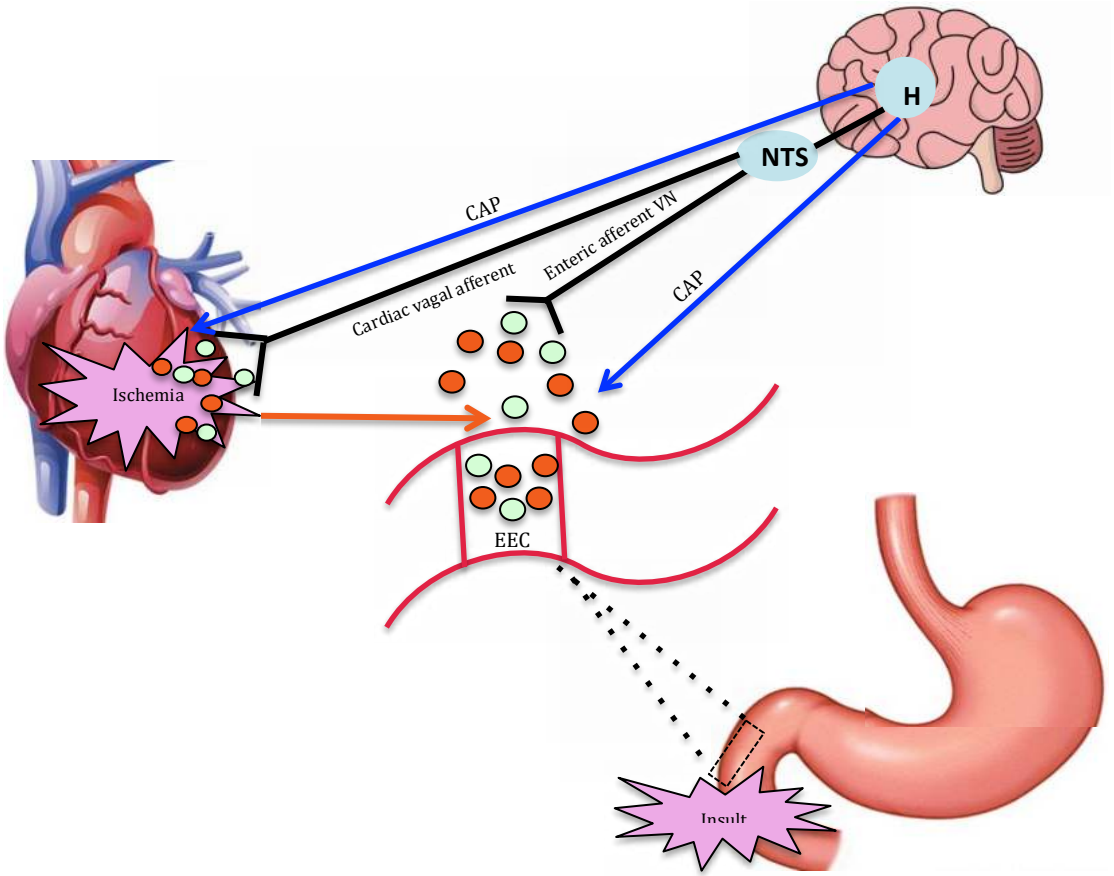

Figure 7: The Gut-brain-Heart Axis. In the enteric system, an *insult* results in the induction of inflammatory cytokines and liberation of neuroendocrine mediators from enteroendocrine cells that subsequently activate the afferent enteric vagus nerve. Similarly, an ischemic insult in the heart induces inflammatory cytokine release; it is possible that this insult also stimulates release of endogenous ghrelin. GHS can bind to the GHS-R localized in the vagal nerve terminals of the heart and activate the cardiac vagal afferent nerve. Furthermore, IHD, through mechanisms that reduce cardiac output (ie, systolic dysfunction, arrhythmias) can result in hypoperfusion of the gastrointestinal tract, this secondary "insult" will further liberate inflammatory cytokines and neuroendocrine mediators from the EEC to activate the vagal afferent nerve (orange arrow). This may explain how mediators from the gut can influence cardiac inflammation. The efferent arm of the vagus – the CAP – is activated to blunt inflammation (blue arrows). Key: CAP, cholinergic anti-inflammatory pathway; EEC, enteroendocrine cells; H, hypothalamus; NTS, nucleus tractus solitarius. Green circles represent ghrelin, orange circles represent inflammatory cytokines.

2. Aims and hypotheses

The research field of cardio-protection has been plagued by numerous failed attempts to translate promising therapeutic strategies for preventing myocardial ischemic injury discovered in the basic science laboratory into the clinical setting.

A major factor underlying this failure results from the inappropriate use of experimental animal models. Most preclinical studies in this field consist of experimental protocols that fail to clearly assess the critical interaction of ischemia, reperfusion injury and the subsequent therapeutic intervention. Early reperfusion therapy is paramount to improving outcome in AMI, thus, there is a clear need for studies employing reperfusion techniques at the preclinical level to allow for more seamless translational application.

In this thesis we aim to **develop and utilise an experimental animal model that closely simulates the critical "door-to-PPCI time"** and thus, represents a model more readily applicable to the human clinical setting by emulating the interaction of the ischemia and reperfusion.

The most critical determinant of prognosis in patients with AMI is infarct size. Infarct size is a predictor of chronic LV function, clinical outcome and is inversely related to prognosis. Accurate assessment of myocardial function and structural abnormalities are of key importance in the clinical environment and in disease models.

It is important to quantifying critical zones such as the area-at-risk and irreversible myocardial injury to allow determination of myocardial salvage and therapeutic efficacy. Here we aimed to **develop non-invasive imaging techniques to allow accurate quantitative assessment of LV function and the extent of infarction**.

Accurate determination of these factors are necessary in order **to critically evaluate interventions** that may delay the onset of necrosis and limit the extent of infarct size during myocardial IR.

The development of cardioprotective agents to improve myocardial function, delay the onset of necrosis, limit the total extent of infarction and prevent adverse LV remodelling are of significant clinical importance in the AMI patient. There are limited pharmacological agents capable of targeting these adverse processes. HEX, despite having similar actions to ghrelin, is chemically more stable and can be easily administered by the parenteral route, making it a potentially superior therapeutic alternative to ghrelin. Furthermore, HEX has already been utilized in human trials, demonstrating that it is a both safe and efficacious peptide. However, the **potential therapeutic effects of HEX remain largely unexplored, particularly in the setting of myocardial IR**. Studies conducted to date involving HEX are mostly in the context of non-reperfused experimental models, these studies warrant further **clarification of underlying mechanisms leading to cardioprotection, specifically in reperfused disease models.**

A lack of progression in the development of new drug therapies has stimulated interest in novel approaches for the prevention of myocardial ischemia- reperfusion injury and the chronic sequelae of AMI, such as heart failure. Traditional cardiovascular drugs have little influence on cytokines or the inflammatory reflex present in heart failure and evidence suggests that **regulation of inflammation** may improve cardiac performance and outcome. Restoration and **augmentation of parasympathetic** tone has also emerged as a promising therapeutic approach in

CVD. More recently, **pharmacological activation of the CAP** has become an intriguing concept requiring exploration as a **therapeutic strategy for IRI** in IHD.

Ghrelin appears to have the potential to rebalance the dysregulated autonomic nervous system in various disease states. Ghrelin may be a major player in the enteric arm of the CAP. It is possible that the **neuroinflammatory-modulating properties of GHS** may also similarly influence the diseased CV system. The **intertwined effects of GHS, the ANS, inflammation and cardiac function** are intriguing and may represent a **novel therapeutic approach to cardioprotection. HEX remains unexplored in this setting, particularly as a therapeutic agent for reperfused IHD**. These hypotheses will be addressed throughout this thesis.

3. Materials and Methods (part 1)

3.1 Ethical declaration

All experiments were approved by the Animal Ethics Committee of the University of Queensland (see Appendix) and were performed in accordance to national guidelines (Ethics number SBMS/200/13/NHMRC).

3.2 Surgical Methods

3.2.1 Myocardial ischemia reperfusion and infarction model

a. Anaesthesia and Intubation

Mice were anaesthetized using a combination of medetomidine and ketamine (Table 1) administered by intraperitoneal (IP) injection. Subsequently, mice were intubated using a self-made instrumentation kit described as follows: a plastic mount was used to suspend the mouse at approximately 45° by using a loop of suture to secure the upper incisors. A flexible fiber-optic light arm was positioned to allow trans-illumination of the larynx. The mouse was positioned on the mount and the tongue displaced laterally to maximize oropharyngeal exposure (Fig. 8).

Table 1: Anaesthesia and analgesia protocols

Drug	Ketamine	Medetomidine	Atipamezole	Carprofen
Dose (mg/kg)	75	1	1	5
Concentration (mg/ml)	100	1	0.05	0.5
Route	IP	IP	SC	SC

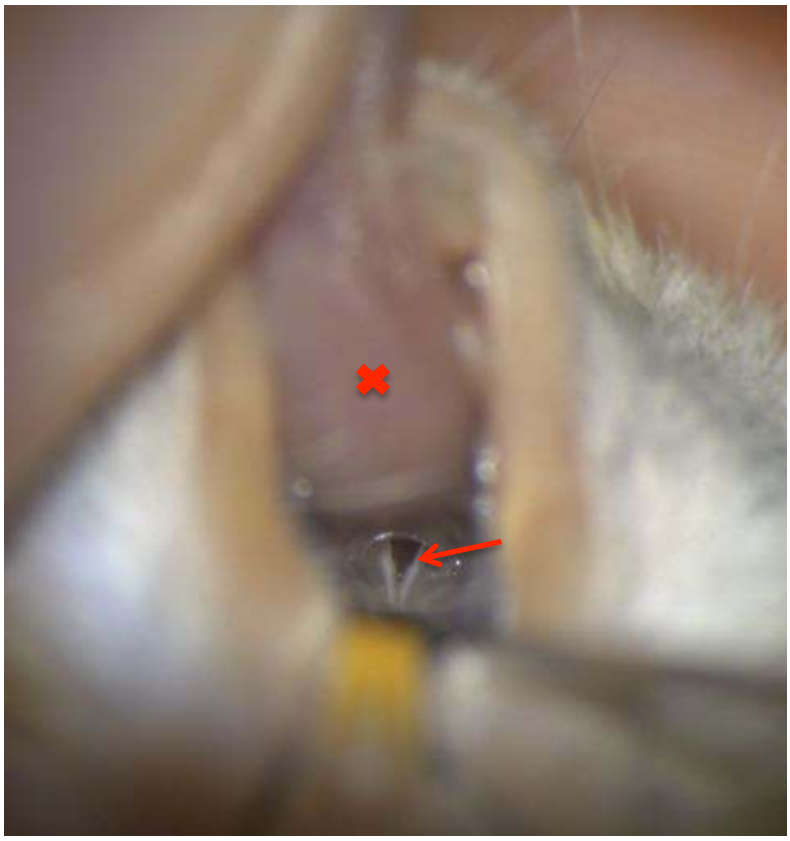

Figure 8: Visualisation of the oropharynx for endotracheal intubation, X delineates the tongue and the arrow points to the glottis.

Using a dissecting microscope, the glottis was identified by observing abduction of the vocal folds & a 20g over-the-needle intravenous catheter was inserted ~3mm into the trachea replacing the needle with a handmade guide wire. After successful intubation, the mouse was removed from the mounting and attached to a mouse ventilator (Harvard Apparatus) using a modified Y-shaped connector to minimize mechanical dead space. The tidal volume and ventilation rate were calculated based on body weight (i.e., 30g mouse: 135bpm, 0.2ml) as described by Tarnavski et al (329). Successful intubation was confirmed by visualizing the rhythmic movements of the chest synchronized with the ventilator. 100% oxygen (~0.5l/min) was loosely connected to the inflow inlet of the ventilator to provide oxygen-enrichment to room

air. Positive-end-expiratory pressure was set at ~1-3cm H_2O. During the procedure the anaesthetic plane was monitored constantly by assessing mucous membrane colour, respiratory pattern, HR and pedal reflex.

Figure 9: Rodent ventilator (Harvard Apparatus)

b. Optimization of endotracheal intubation

This method has been highly efficient, generally resulting in successful intubation within 30 seconds of positioning the animal. This method is non-invasive and negates employment of invasive methods such as a tracheotomy, thus decreasing the chance of postoperative complications. Faster and consistent placement of the endotracheal tube was achieved with surgical-microscope guidance, as the glottis could be more easily visualised. This approach appears to be novel as most papers describe a direct visualization approach for intubation without microscopic guidance (329, 330).

Figure 10: Surgical set up – the mouse is intubated with a 22g IV catheter (red arrow), positioned in right lateral recumbency and connected to the small animal ventilator (not shown). ECG leads are attached. Abbreviations: ECG, electrocardiography; IV, intravenous.

3.2.2 Surgical Model

a. Permanent coronary artery occlusion: myocardial infarction model

The chest of the mouse was shaved before endotracheal intubation. After intubation the mouse was placed on a heated pad (warmed to approximately 36-37°) and positioned in right lateral recumbency with the left forelimb extended cranially. The mouse was secured using surgical tape to extend the left foreleg cranially and the tail caudally. A suture was placed around the maxillary incisors to stabilize the head and prevent the endotracheal tube kinking and becoming obstructed. The surgical site was aseptically prepared using a chlorhexidine scrub with a final ethanol scrub. Lubricating tears were dispensed into both eyes to protect against corneal ulceration.

The surgical procedure was performed with the aid of a surgical microscope as follows:

A dorsoventral cutaneous incision was made at approximately the 4th intercostal space (caudal to the axillary region). The subcutaneous (SC) tissue and musculature was bluntly dissected using curved blunt forceps. A thoracotomy was performed at the ~4th intercostal space and expanded bluntly using the curved forceps. A magnetic retractor system with multi-positional retractors was positioned to allow visualization of the pleural cavity and expose the heart.

Figure 11: Thoracotomy site and positioning for exposure of the LAD. The red arrow points to the retractor. Abbreviations: LAD left anterior descending coronary artery.

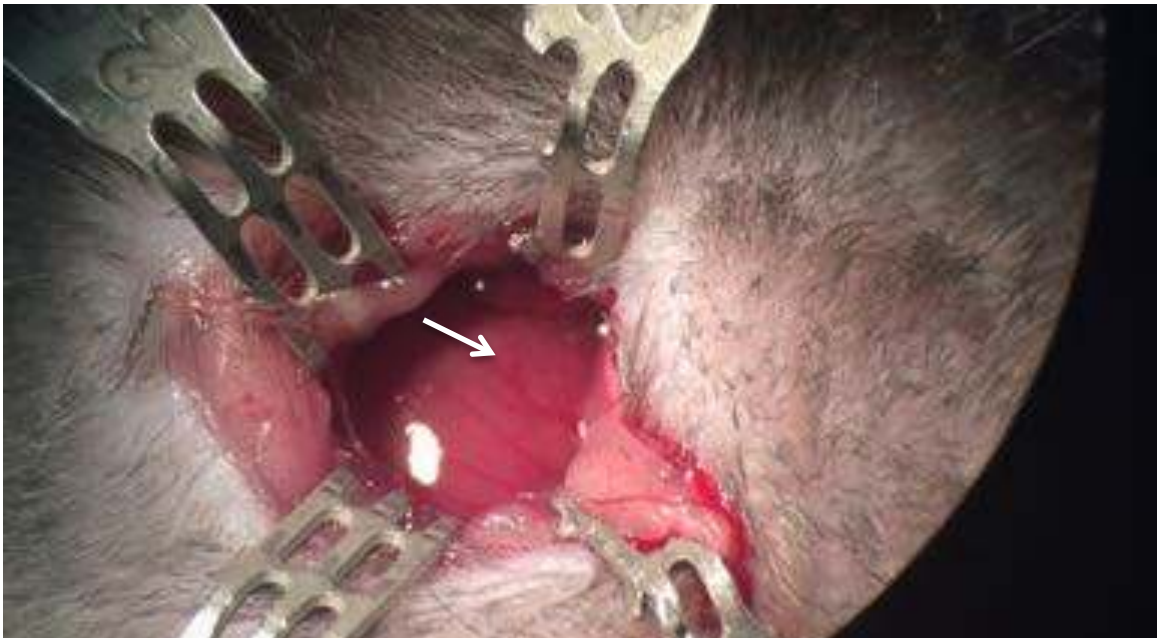

Figure 12: Visualisation of the LAD. The thoracotomy site is pictured and the heart is exposed with the LAD coursing over the surface (white arrow).

The pericardium was gently removed using blunt forceps and the LAD visualized coursing beneath the left auricular appendage as a "bright" vessel (Fig. 12). The location for ligation was identified (Fig. 13A/B) and selected to induce ~30-40% ischemia of the LV (~3mm below the auricular appendage). A 7-0 prolene suture with BV-1 tapered needle was placed beneath the LAD with a portion of surrounding myocardium (Fig. 13C). The LAD was ligated and successful occlusion confirmed by observing a change in colour (pallor) distal to level of LAD occlusion (Fig. 14A) and characteristic electrocardiographic (ECG) changes (Fig. 14B/C).

The multi-positional retractors were removed and the lungs reinflated by applying pressure to occlude the outflow circuit of the ventilator for 1-2 seconds. This helps to prevent atelectasis and poor recovery after surgery. Simultaneously, the thoracotomy site was closed as the lungs were reinflated and pressure applied to the thorax to minimize the occurrence of a pneumothorax. The chest wall was closed using 6-0

polydioxanone in a cruciate pattern. The musculature and cutaneous tissue were closed using a 5-0 non-absorbable suture in a simple continuous pattern.

Sham-operated mice underwent the above procedure excluding ligation of the LAD.

After completion of the surgery the mice were administered atipamezole and carprofen SC to help with anaesthetic recovery and a 0.5ml saline bolus SC (Table 1).

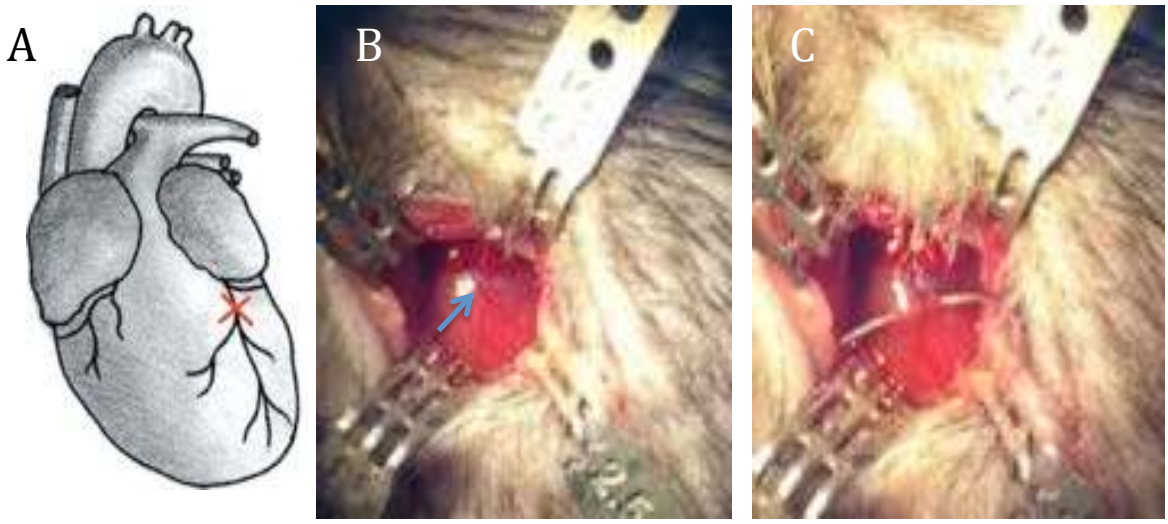

Figure 13: A - Schematic representation of the LAD and position of ligature placement. B - microscopic visualisation of LAD (arrow), C - placement of ligature at the correct location along the LAD ~3mm distal to the left auricular appendage.

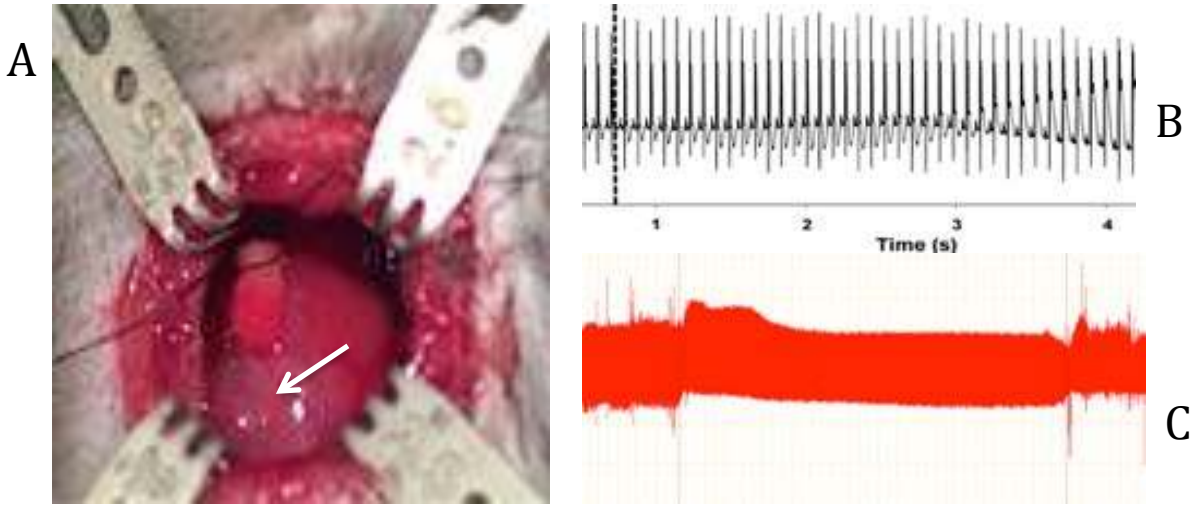

Figure 14: A - pale region (white arror) is visualized in the coronary territory distal to the level of LAD occlusion; B - characteristic ECG changes – onset of occlusion (dotted line) results in a peaking of the T wave and ST segment elevation. C: Real time ECG changes throughout the 40 minute IR period. Note the distinct ECG changes at onset of ischemia and reperfusion (first and second dotted lines respectively). Abbreviations: ECG, electrocardiogram; IR, ischemia reperfusion; LAD, left anterior descending coronary artery.

b. Transient Coronary Artery Occlusion: Ischemia-Reperfusion model

This model was utilized in attempt to simulate AMI and reestablishment of blood supply (reperfusion) to the ischemic myocardium. Thus representing a more clinically relevant model.

The "permanent ligation" procedure was followed as outlined above with the following modifications:

1. A 1mm piece of sterile 2-0 suture was placed over the LAD, following the natural course of the artery.
2. After placing the 7-0 sutures, the two ends were threaded through a 1-2mm piece of sterile PE10 tubing. The tubing was heat flared to create a blunt end thereby preventing the guide tubing from causing damage to the tissue where it contacts the heart.
3. For induction of ischemia, tension was applied to the ends of the 7-0 suture, effectively creating a "noose" around the LAD & occluding the artery. The suture was then secured by tying a knot at the distal end of the of PE10 tubing (Fig. 15).
4. During ischemia the retractors were removed to allow the chest wall to be reopposed and a saline-soaked swab was placed over the thoracotomy site.

5. Reperfusion was initiated after a period of 40 minutes by cutting the knot at the end of the PE tubing. The tubing, 7-0 & 2-0 sutures were subsequently removed.
6. Ventricular hyperaemia was observed, confirming reestablishment of blood flow to the myocardium.

Chest wall closure was performed as previously described.

Figure 15: Transient LAD ligation model. Note PE tubing and suture encompassing LAD.

c. Post-operative care

During the immediate post-operative period, ventilation was continued until spontaneous breathing was regained, at which point the mouse was removed from the ventilator with the endotracheal tube in place. The mouse was extubated once a

normal breathing pattern was reestablished, determined by the presence of a swallow reflex and the beginnings of voluntary motor function.

Once mobile, mice were placed in a clean cage with easy access to food and water. Gel pack and crushed wet food were provided and the recovery cage was supplemented with oxygen to provide an oxygen-rich environment of ~40-50% FiO_2. One half of the cage was positioned on top of a heating pad (at ~35°C) allowing the animal access to either warmth or ambient temperature. Mice were observed for the next 3-4 hours to monitor recovery & those that were not very active after this time remained in a heat-supplemented environment overnight.

Mice were monitored twice daily using a score sheet to record changes in breathing character/pattern, movement, surgical site, body condition, weight loss and behavior.

d. Optimization of surgical technique

The IR model described in the methods section of this doctoral project is a novel LAD occlusion mechanism. This was developed for various reasons, which are discussed below:

The literature describes various techniques for inducing myocardial IR in the mouse. Commonly, a piece of suture is placed over the LAD and a knot is tied over the suture to occlude the LAD. The suture is then released at the end of the ischemic period to allow reperfusion (329, 331). Various challenges were found with this technique: 1. Tension created by tying the knot often caused trauma (tearing) of the ventricular wall. 2. Knot placement was very close to the ventricular wall and thus was difficult to release without also causing ventricular trauma.

A second, less commonly described technique involves threading the suture ends through a piece of PE tubing and subsequently tying a knot on top of the tubing to occlude the LAD (332). Using this model, ventricular trauma was still observed

secondary to tension transmitted through the PE tubing to the ventricular tissue and causing tearing.

Trialing a variation of the above using both PE tubing and suture placement on top LV overlying the path of the LAD I was able to apply sufficient tension to occlude the LAD without visualising any microscopic ventricular trauma.

An ischemic time of 40 minutes was employed for the IR model. The justification for this was related to post-operative survival. The 3-week survival rate in this project was consistently >90% in mice with a 40 min ischemic period. In a trial using 60 minute ischemic time, 50% mice died in the 24hrs following surgery. This was likely related to the anaesthetic time in a mouse undergoing thoracotomy and difficulty maintaining adequate thermoregulation.

3.3 Assessment of Myocardial Injury

3.3.1 Post mortem measurement of infarct size

a. TTC

At the completion of the experiment, the mice were euthanized by cervical dislocation. The hearts were rapidly excised, trimmed of extracardiac tissue and rinsed with saline to flush out any remaining blood. Hearts were placed in a Zivic Mouse Heart Slicer Matrix (Zivic Instruments) and fixed in OCT compound at -20°C for 15 minutes to facilitate slicing. The heart was then transected into 6-8 short axis slices of 1mm thickness. Slices were thawed and immersed in 1% triphenyl tetrazolium chloride (TTC) in PBS at 37°C for 20 minutes whilst being constantly agitated. The slices were fixed in 10% neutral-buffered formalin overnight with each slice then photographed on each side with a digital camera mounted on a dissecting

microscope. Manual planimetry of viable and non-viable tissue was performed using ImageJ. Specifically, the total LV area and MI region were manually traced for each image and MI size was determined as a percentage of LV mass.

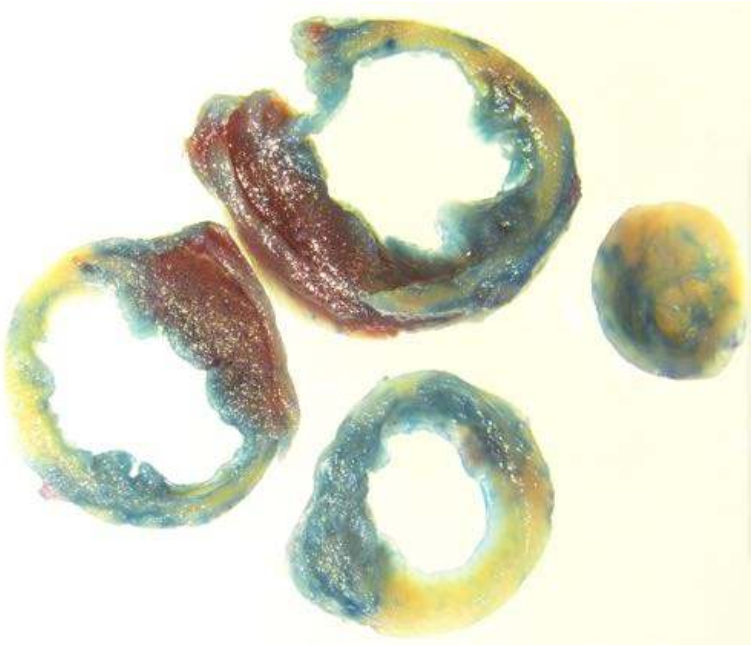

Figure 16: TTC staining to determine infarct size. White region: non-viable teissue, red: TTC stained (viable) tissue.

b. Evans Blue/TTC

The myocardial IR procedure was performed as described above. After reperfusion, the ligature was left in place while the mice recovered for 36 hours. To delineate the area-at-risk, the LAD was re-occluded (under repeat anaesthesia) and 3% Evans blue (mixed in saline), to a total volume of ~0.3ml, was infused via the tail vein. After approximately 2 minutes the mouse was euthanized by cervical dislocation. Hearts were then rapidly excised, trimmed of extracardiac tissue and rinsed with saline to flush out any remaining blood. Hearts were placed in a Zivic Mouse Heart Slicer Matrix (Zivic Instruments) and fixed in OCT compound at 20°C for 15 minutes. This provides the heart with enough rigidity to allow slicing. The heart was then cut into 6-8 short-axis slices of 1mm thickness using the matrix and immersed in 1% TTC at 37°C for 20 minutes whilst being constantly agitated. The slices were then fixed in

10% neutral-buffered formalin overnight to enhance contrast between viable and non-viable tissue. Each slice was photographed on both sides with a digital camera mounted on a dissecting microscope and manual planimetry of viable and non-viable tissue performed using ImageJ. Specifically, the total LV area, area-at-risk, and MI were manually traced for each image. Evans Blue-stained sections indicate the area-at-risk, TTC (red/pink) indicates viable tissue within the area-at-risk, and white indicates the necrotic MI. From these three regions of interest, area-at-risk as percentage of LV mass, MI as percentage of LV mass and MI as percentage of area-at-risk was determined (Fig. 16 & 17).

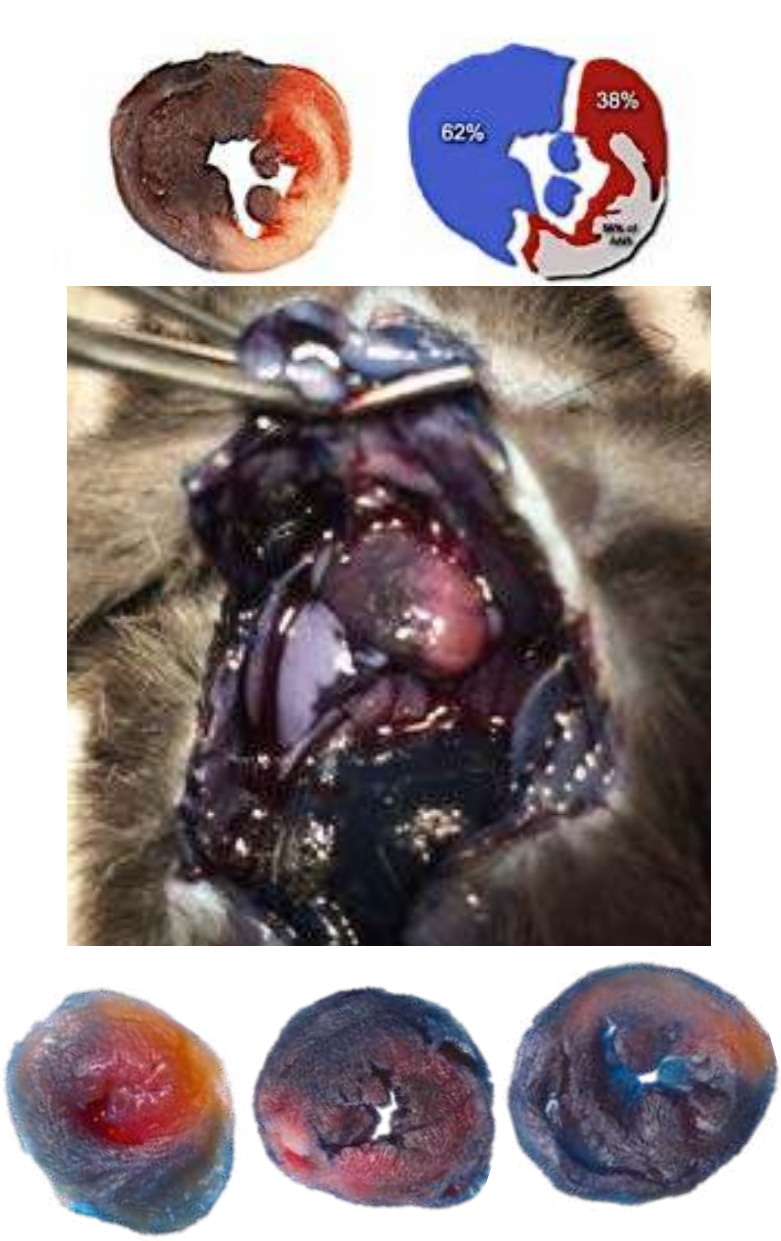

Figure 17: Histologic assessment of infarct size and area-at-risk – Schematic (top), in -situ (middle) and post sectioning (bottom). Evans blue - blue, TTC - red, infarct - white. Salvageable tissue (reversibly injured) = red.

3.3.2 Histology and morphometric analysis

Serial paraffin-embedded LV sections from each group of mice studied were stained with 0.1% picrosirius red to detect interstitial collagen deposition. Additional serial LV sections from each corresponding group of mice studied were immunohistochemically stained for selected markers associated with collagen

turnover; utilizing polyclonal antibodies to TGF-β1 (sc-146; 1:200 dilution; Santa Cruz Biotechnology Inc., Santa Cruz, CA, USA) and MMP-13 (the predominant collagenase in mice; ab75606; 1:100 dilution; Abcam; Redfern, NSW, Australia); or a monoclonal antibody to α-smooth muscle actin (α-SMA; a marker of myofibroblast differentiation; M0851; 1:250 dilution; DAKO Antibodies, Carpinteria, CA, USA). Detection of primary antibody staining was detected using DAKO Envision anti-rabbit or ARK biotinylation kits, respectively, and 3,3-diaminobenzidine. Morphometric analysis of picrosirius red- and immunohistochemically-stained sections was performed using Aperio software (Leica Biosystems, North Ryde, NSW, Australia) on whole tissue sections per mouse. In each case, the percentage staining of each marker analyzed per section was derived and expressed as the fold changes relative to the SHAM-VEH group, which was expressed as 1.

3.3.3 Hydroxyproline analysis

Equivalent frozen portions of LV tissue from each animal studied were lyophilized to dry weight measurements before being hydrolyzed in 6M hydrochloric acid for determination of their hydroxyproline content, as described previously (333). Hydroxyproline values were then converted to collagen content by multiplying by a factor of 6.94 (based on hydroxyproline representing approximately 14.4% of the amino acid composition of collagen in most mammalian tissues (334), further expressed as a percentage of the tissue dry weight (to yield collagen concentration), and finally expressed as the fold change relative to the SHAM-VEH group (which was expressed as 1).

3.3.4 Cytokine and Troponin-I determination

Blood samples were collected into plain tubes from mice after each respective procedure at specified time-points (see Chapter 5). The blood was allowed to clot appropriately and samples were centrifuged for serum removal and stored at -80^0 C until it was assayed. The serum concentrations of troponin-I (cTnI), IL-1β, IL-6 and TNF-α were measured at 24 hours and 21 days post operatively using a MILLIPLEX® map assay according to the manufacturer's instructions (Merck Millipore).

3.3.5 Heart rate variability analysis

HRV analysis is considered a sensitive and non-invasive, indirect measure of cardiac autonomic tone that has been extensively validated (335, 336).

HRV analysis was performed at specified time-points after each respective procedure (see Chapter 5). ECG signals were recorded using a physiological analyzing system (Bio Amp, AD Instruments, CA, USA). Mice were anaesthetized with isoflurane (induced at 4% and maintained at 1.5%). After the HR stabilized, ECG signals were recorded for a minimum of 20 minutes. Using a technique described by Thireau et al. (335) and recently by Mao et al. (88); ANS function was examined by power spectral analysis of HRV (LabChart Pro 7.0, ADInstruments, Australia). HR was used to generate a power spectral density curve using a fast Fourier transformation. The area under the curve was calculated for the very-low-frequency (VLF: 0-0.15Hz), low-frequency (LF: 0.15-1.5Hz), and high-frequency (HFr: 1.5-5Hz) band, based on previous studies (335). From these, the parameters: LF, HFr, normalized LF power (nLF), normalized HF power (nHFr), and ratio of LF to HFr power (LF/HF) were calculated as described in (88).

3.4 Basic template for experimental timeline

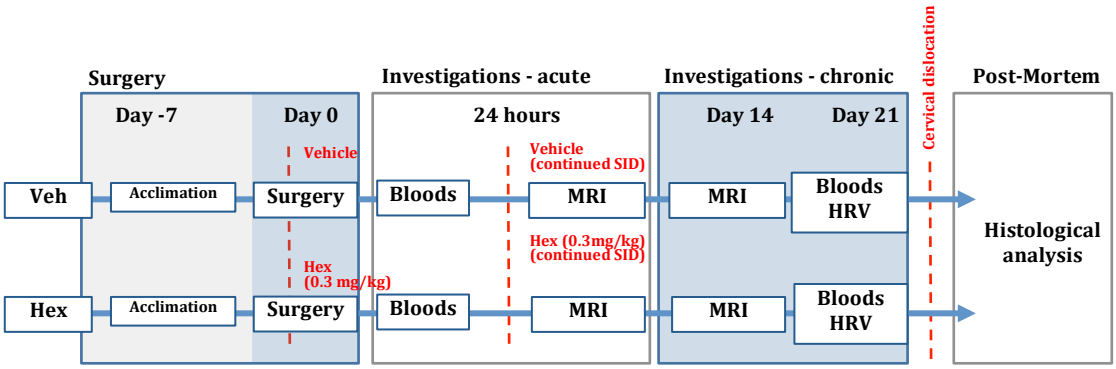

Figure 18: Basic experimental timeline, MI model

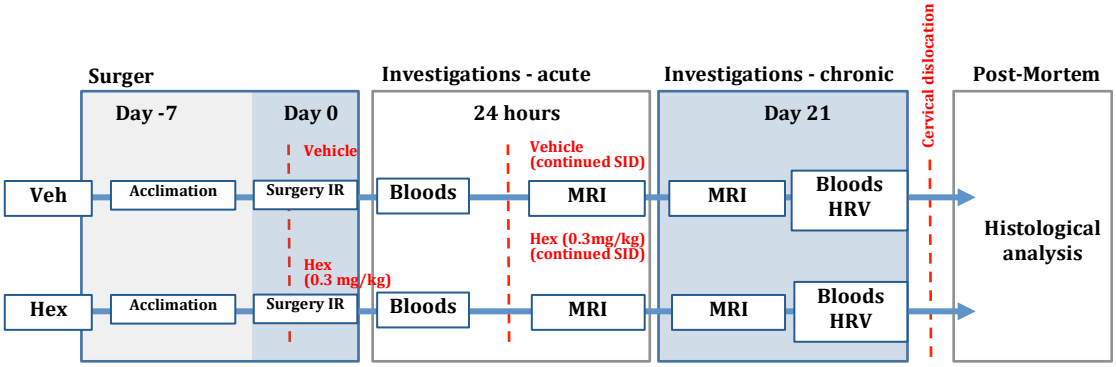

Figure 19: Basic experimental timeline, IR model

3.5 Statistical analysis

The statistical analysis methods have been described in the relevant sections of *Chapter 5: Results*.

4. Materials and Methods (part 2): Non invasive imaging

4.1 Echocardiography

4.1.1 Echocardiography Technique

a. Anaesthesia

Anesthesia was induced using 5% isoflurane in 100% medical grade oxygen with a flow rate of 1 L/minute into an induction chamber.

In rodents, the necessity of performing general anaesthesia to obtain echocardiographic measurements is a limitation on all cardiac function studies as there is the potential for anaesthesia-induced effects on cardiac function. To address this, efforts were directed towards anaesthetizing mice to the same anaesthetic plane, allowing the heart rate to stabilize and remain within a target range before recording echo loops. The echocardiographic studies were short, with the total time from induction to recovery (including image acquisition) limited to 10 minutes/mouse.

Once anaesthetized, the mouse was maintained with 1.5-2% isoflurane via a nose cone and body temperature was maintained with a warming pad. Transthoracic echocardiography was performed using a Philips iE33 ultrasound machine with a 15 MHz linear transducer (Philips, Amsterdam, Netherlands) interfaced with a layer of ultrasonic transmission gel.

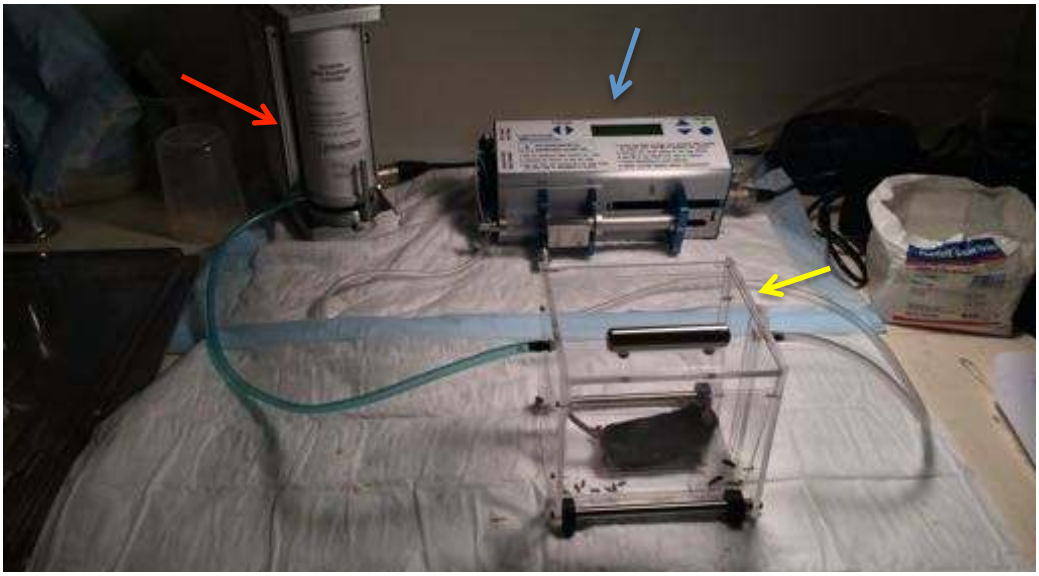

Figure 20: The general anaesthesia set up for echocardiographic studies, the blue arrow points to the vaporizer, yellow arrow: induction chamber, red arrow: scavenger system. A mouse is shown within the induction chamber.

Figure 21: Mouse with nose-cone and transthoracic echocardiography performed using a 15 MHz transducer.

b. Image acquisition

A 2D parasternal short-axis imaging plane was used to direct M-mode imaging at the level of the LV papillary muscles. The data was acquired and then calculated based on the average of three consecutive beats. End-diastolic left ventricular internal

dimension (LVIDd) and end-systolic left ventricular internal dimension (LVIDs) were determined. Left ventricular anterior and posterior wall thickness in diastole (LVAWd/LVPWd) and systole (LVAWs/LVPWs) was also measured.

Fractional shortening was calculated using the "leading edge method" by measuring the thickness from the leading edge of the upper echo interface to the leading edge of the lower echo interface (337). The following equation was used to calculate fractional shortening (FS):

$$FS\% = (LVEDd - LVESd)LVEDd * 100$$

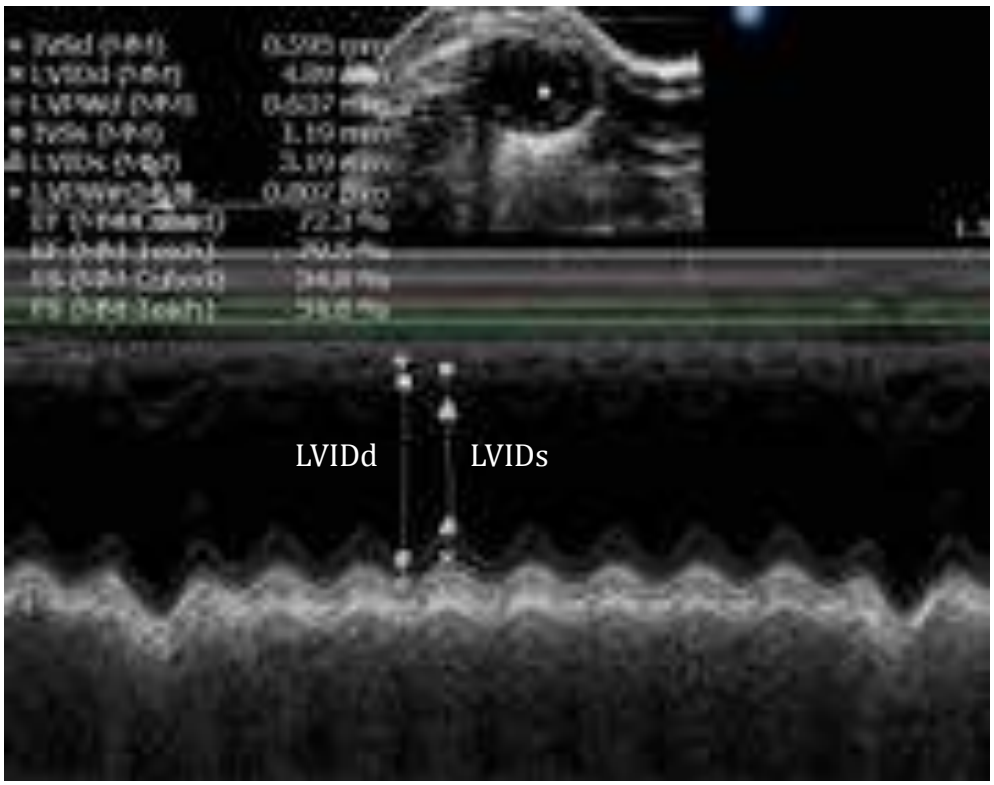

Figure 22: M-mode view of the LV at the level of the papillary muscles. The left ventricular end diastolic diameter and end systolic diameter are measured to calculate fractional shortening %.

4.2 MRI

4.2.1 MRI methods

a. In vivo MRI set-up

Anaesthesia was induced in a purpose-built chamber using 4-5% isoflurane (1 L/min) in 100% medical grade O_2. After induction, the mouse was transferred to a heat pad, placed in lateral recumbency and a nose-cone applied to maintain anaesthesia. The isoflurane concentration was reduced to ~2% for maintenance of anaesthesia.

Before contrast injection, supplemental heat (hot-water bottle) was applied to the tail of the mouse to allow vasodilation of the tail vein. Magnevist (Gadopentetate dimeglumine) was prepared (0.3 mmol/kg), warmed to body temperature and administered by IV injection into the lateral tail vein using a 30-gauge needle. The mouse was positioned in a purpose-built cradle (Bruker, Germany), secured in a supine position and maintained under anaesthesia with 1.5–2% isoflurane in 1-2 l/min O_2 via nose cone. Core temperature was maintained with a water-circulation system and lubricating ointment was applied to prevent ocular desiccation. An electrocardiographic (ECG) signal was derived using a 3-lead system obtained from surface electrodes attached to the palmar aspect of both forefeet and the plantar aspect of the left hind. A pressure-transducer for respiratory gating was attached to the animal's abdomen. Mice were imaged using a Bruker Biospec 9.4T small animal MRI scanner using a phase array coil and temperature-regulated small animal bed (Bruker Biospin, Ettlingen, Germany). Physiological monitoring (ECG and respiratory rate) was performed using a MRI-compatible SAII monitoring systems (Small Animal Instruments, NY, USA).

b. Materials

All experiments were carried out on a 40cm diameter horizontal bore 9.4 T scanner (Fig. 23), equipped with BGA 12S HP 660 mT/m gradients and interfaced with an 86mm quadrature transmit only coil and a phase array coil. MRI data was acquired using Paravision 5.1 (Bruker Biospin GmbH, Ettlingen, Germany). Imaging was initiated using a three-planer localizer scan and a gradient echo (Fast Low Angle Shot/FLASH) imaging sequence to ensure correct positioning. The probe was manually matched and tuned.

Figure 23: Bruker Biospec 9.4T small animal MRI scanner

c. Cardiac MRI protocol

After calibration using the Bruker standard adjustment protocol, which included shimming and RF pulse calibration, 2- and 4-chamber view scout scans were made to plan a single mid-cavity short-axis slice. Cine imaging was performed using a retrospectively-triggered (self-gated) INTRAGATE gradient-echo sequence (338), with the following parameters: TR = 5.6 ms, TE = 2.6 ms, number of movie frames = 20, slice thickness = 1 mm, matrix = 512 x 512, field-of-view (FOV) = 4 x 4 cm^2 Resulting in 78 x 78um in-plane resolution, with ~5mins acquisition per slice. Because of the slight difference in heart-size between mice, seven to nine short-axis slices with inter-slice distance of 1 mm and no slice gap were measured to cover the heart from apex to base. Late gadolinium enhancement (LGE) images in the slice locations were acquired 10-15 minutes after intravenous injection of Gd-DTPA (0.3mmol/kg BOW Magnevist; Bayer Germany).

d. Cardiac synchronization and gating techniques

To minimize motion artefacts, ECG and respiratory gating is mandatory to obtain high-quality time-resolved cardiac images. MRI images are formed from a number of sequence repetitions, each triggered during the same phase of the cardiac cycle to minimize motion artefacts (17).

In our studies, a retrospective gating sequence, INTRAGATE (338), was employed. This allows continuous cine-MRI data acquisition and simultaneous recordings of the synchronization source (ECG signal). The data is then re-ordered according to the sequential phase of the cardiac cycle using phase navigator echoes. In contrast, in prospective gating, a threshold ECG signal at each QRS complex triggers one data acquisition sequence at a time (339).

e. Determination of cardiac functional parameters

The MRI images were converted to DICOM format using Paravision 5.1 and processed with Osirix (340) software. The end-diastolic and end-systolic phases were identified on a slice-by-slice basis and the endocardial and epicardial borders were traced. The papillary muscles were excluded. LV end systolic volume (ESV), end diastolic volume (EDV), stroke volume (SV), and ejection fraction (EF) were computed from the traced borders. LV mass was obtained by multiplying the volume with the specific gravity of 1.05 g/cm^3 (341).

f. Determination of infarct volume

The contrast-enhanced MRI images in DICOM format were processed in Osirix. Image contrast windowing was adjusted to enhance the signal from the hyperintense region and null the signal from the nonenhanced region. Manual planimetry was performed on the images obtained and for each slice, the hyperintense region and total LV myocardial area was calculated. Slice hyperintense areas were then summated to generate infarct volume as a percentage of LV myocardial volume.

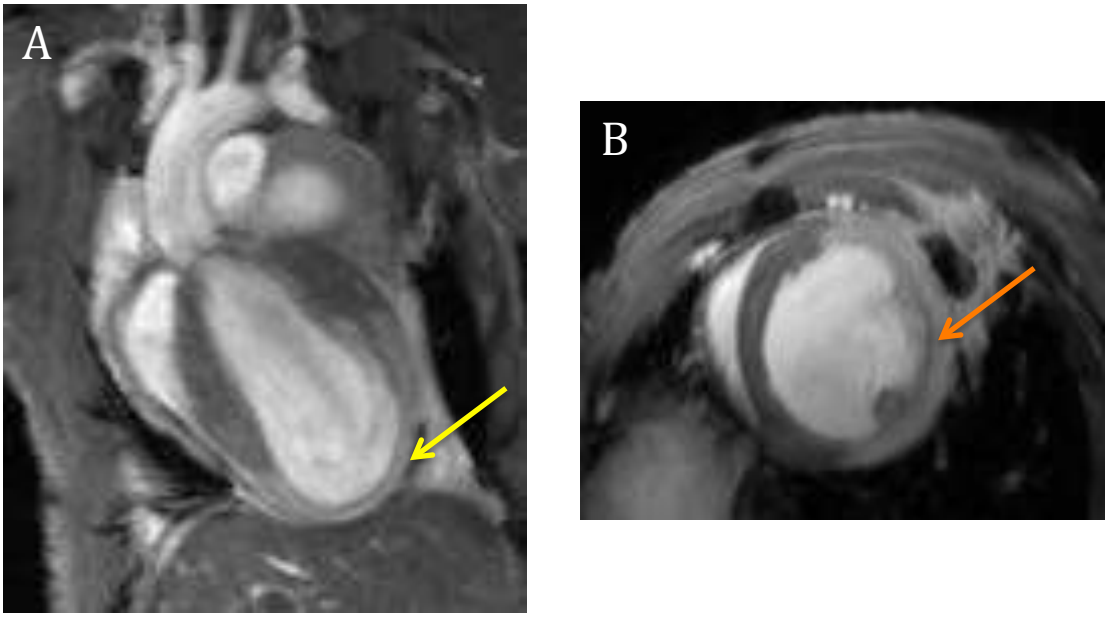

Figure 24: A/B demonstrates T_1w LGE imaging 24hrs post MI surgery, note the increased signal associated with the infarcted region (yellow and orange arrows). In addition, note the visible dyskinesia of the apex associated with the infarct in figure A ("ballooning" of the apex – yellow arrow). Images were acquired using T_1w INTRAGATE sequence at 9.4T. Abbreviations: LGE, late gadolinium enhancement; MI myocardial infarction.

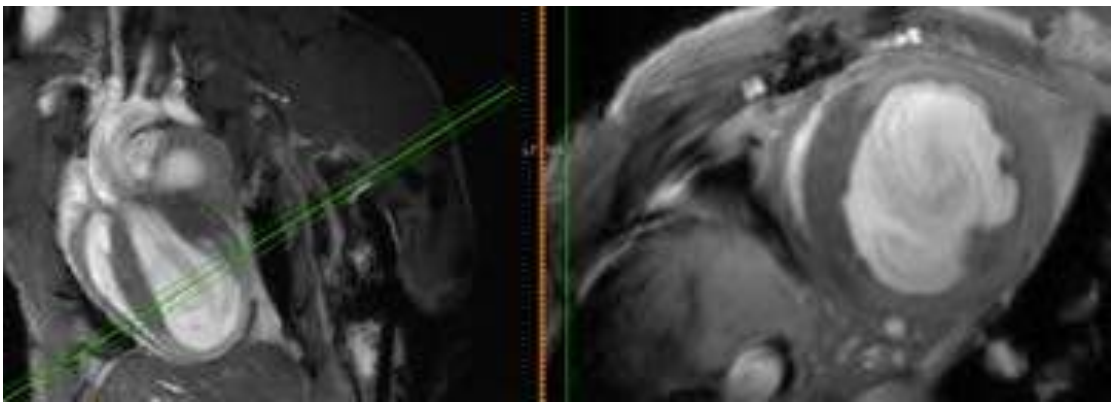

Figure 25: LV 2-chamber view (left) and the corresponding LV short axis image (right) through the transverse plane indicated by the green line.

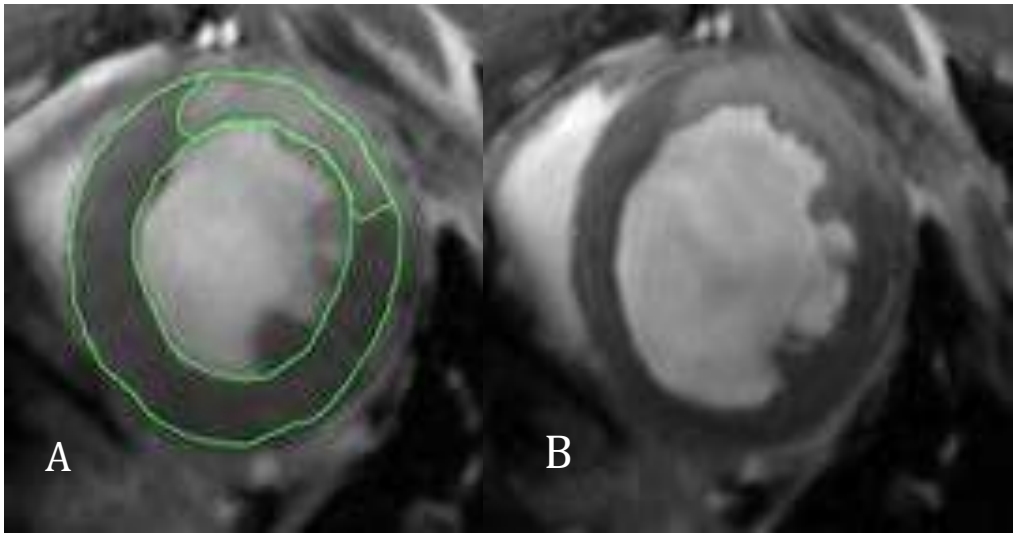

Figure 26: A- Tracing of endocardial, epicardial and infarct borders in systole. B- Untraced corresponding image in diastole.

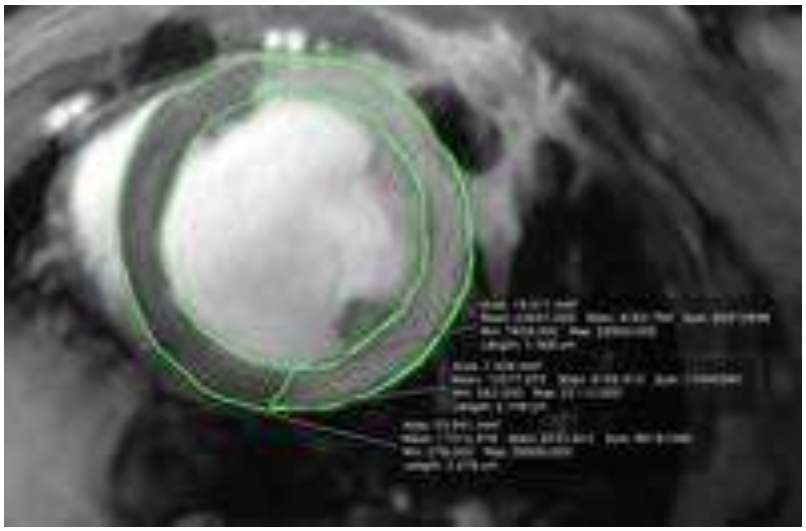
Figure 27: Osirix (340) software was used to perform manual planimetry on the images obtained for each slice. Here is an example of tracing of the endocardial, epicardial and infarct borders.

g. Measurement of the chronic infarct: midline length measurement

In addition to measuring infarct volume, the infarct was also measured using an alternative cMRI approach described as the "midline-length measurement". This was performed 14 days post-MI using a technique modified from Takagawa et al (342). Briefly, the *midline infarct length* was determined by measuring the midline length of the infarct that included 50% of the whole thickness of the myocardial wall. The LV

myocardial midline was measured as a *midline circumference*. All of the measurements were taken in diastole. Infarct size was calculated by dividing the sum of the midline infarct length from all sections by the sum of the midline circumference from all sections and multiplying by 100.

h. MRI optimization and considerations

Discussion of gadolinium administration and inhalational anaesthesia in cMRI:

IV administration is the optimal route of delivery of the contrast agent gadolinium (Gd) but is technically challenging in mice (341). A study by Bohl et al. determined characteristic pharmacokinetics for IV and intraperitoneal (IP) Gd injections. Both methods were found to retain sufficient T_1 contrast over a broad time frame with intravenous T_1 contrast peaking earlier and slightly higher than IP injection. It was concluded that IP injection could be employed as the method of choice in a routine, high-throughput setting due to the ease of administration (341).

We initially trialled administering IP Gd following the protocol described by Bohl et al. Unfortunately, we were unsuccessful with this method as we did not observe any contrast-enhancement post Gd injection, it was unclear why this was, it may have been dose-related (Bohl et al used a dose of 0.5mmol/kg), or our TI could have been suboptimal. Thus, in this project, IV administration of Gd was utilized & success rates consistently approached 100% for administration of Gd by the intravenous route. In this study, a gadolinium dose of 0.3mmol/kg was used, this dose lies within the range reported for previous animal studies (343).

Inhalational anaesthetic delivery in an ultra-high field magnetic resonance environment is challenging as long delivery lines are required to carry the gas from the vaporizer located outside the 5 gauss line to the to the cradle-system for delivery to the mouse. This system results in increased mechanical dead space and means that

the actual alveolar concentration of isoflurane is difficult to determine. Thus the plane of anaesthesia can be more challenging to control and the ability to monitor anaesthetic depth lies with the assessment of physiological parameters. The heart rate and respiratory rate were monitored using the SAII monitoring system (Small Animal Instruments, NY, USA) in order to maintain the depth of anaesthesia within an optimal plane (ie, respiratory rate: 40-60 bpm, heart rate: 300-400bpm).

5. Results

5.1 Part A: Method establishment: non-invasive imaging techniques

5.1.1 Preliminary Echocardiography

a. Introduction

Early identification of patients with sub-optimal cardiac recovery after MI is of great importance in order to improve clinical management of these patients (15). Both functional and structural characterization of the infarcted myocardium is important for risk stratification of patients after AMI (344).

Two-dimensional echocardiography is the most commonly used non-invasive method for measuring cardiac function *in vivo* in experimental animals (16) but has limitations, particularly in the assessment of AMI MI (16, 23). As a preliminary study, we sought to review the assessment of LV function in mice using echocardiography.

b. Method

Fractional shortening (FS) was assessed in 12 normal 10-12 week old male C57BL/6J mice by recording 3 serial M-mode-derived measurements taken over 7 days (day 1, 4 and 7). Anesthesia was induced using 5% isoflurane in 100% medical grade oxygen with a flow rate of 1 L/minute in an induction chamber then maintained with 1.5-2% isoflurane via a nose cone. Echocardiography was performed using a Philips iE33 ultrasound machine with a 15 MHz linear transducer (Philips, Amsterdam, Netherlands) interfaced with a layer of ultrasonic transmission gel. A 2D parasternal short-axis imaging plane was used to direct M-mode imaging at the level of the LV papillary muscles. The data was acquired and then calculated based on the average of

three consecutive beats. End-diastolic left ventricular internal dimension (LVIDd) and end-systolic left ventricular internal dimension (LVIDs) were determined and fractional shortening was calculated. Left ventricular anterior and posterior wall thickness in diastole and systole were also measured.

c. Results

Repeated echocardiography measurements (three times over 7 days, Table 2) of the average fractional shortening (FS) in 12 healthy mice showed that the average FS of healthy mice was 31.2 ± 1.61 % (mean ± SD). This preliminary study, however, also revealed that the echo-derived average FS measurements of each mouse could have a wide range of variance (0.6 to 54.3%).

Table 2: Fractional shortening (%) measured from 12 healthy mice over 7 days

	Average Fractional Shortening (%)				
Mouse#	Day 1	Day 4	Day7	Mean	Variance
1	32.0	31.2	28.6	30.6	3.2
2	-	32.0	30.0	31.0	2.0
3	32.4	29.6	32.6	31.5	2.8
4	32.6	35.2	29.2	32.3	9.1
5	25.3	30.3	30.7	28.8	9.1
6	29.7	31.4	27.2	29.4	4.5
7	31.7	32.0	33.2	32.3	0.6
8	29.3	39.8	25.6	31.6	54.3
9	31.3	36.8	32.0	33.4	9.0
10	34.1	38.3	29.5	34.0	19.4
11	34.6	28.8	29.0	30.8	10.8
12	32.9	26.0	28.6	29.2	12.1

Furthermore, side-by-side visualisation of data acquired by MRI (Fig. 28, top panel) and echocardiography (Fig. 28, bottom panel) illustrates the lack of clarity of the echocardiographic images for measuring the LV dimensions in diastole and systole compared to MRI. This is important, as accurate delineation of endocardial and epicardial borders in systole and diastole is crucial to allow calculation of measures of systolic function, wall thickness and LV mass measurements.

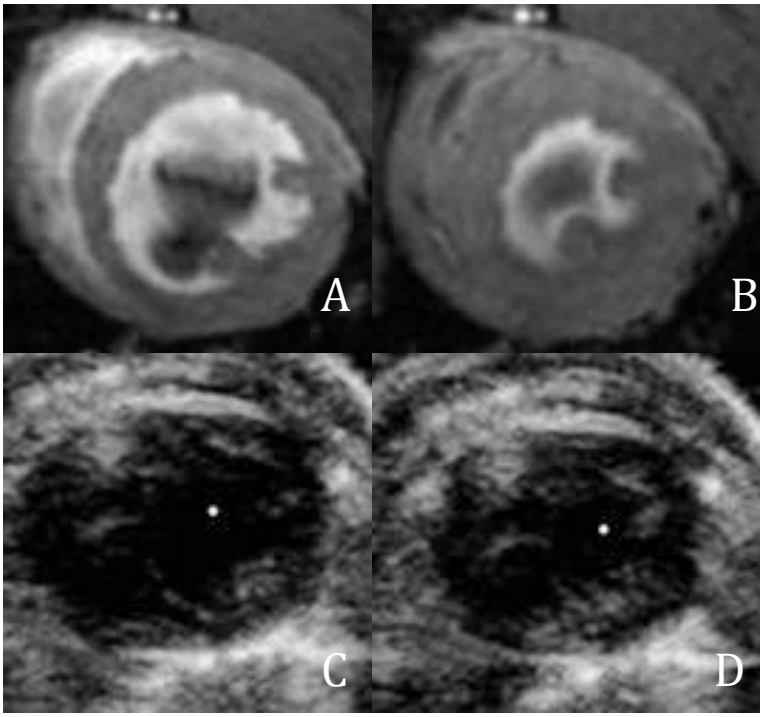

Figure 28: A/B: Example of a mid-cavity short axis view of LV in diastole (A) and systole (B) acquired using T1w INTRAGATE sequence at 9.4T. C/D: Corresponding 2D echo images of LV in diastole (C) and systole (D). Note the marked difference in resolution between the two imaging methods.

Furthermore, it was confirmed that infarct size determined using cardiac MRI matched that of TTC staining (Fig. 29), This finding is consistent with that reported in the literature and highlights the accuracy of infarct delineation when assessed by MRI (345).

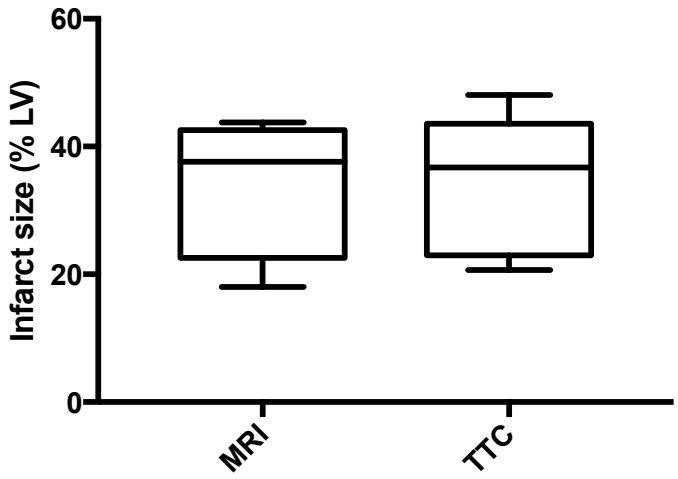

Figure 29: Infarct size in a group of mice were assessed by both cMRI (n=4) and TTC (n=5) 24 hours after permanent ligation of the LAD. A paired T test confirmed that there was no difference between the modalities, confirming that infarct size determined using cardiac MRI matched that measured by TTC staining.

d. Discussion

Although echocardiography is the most commonly used non-invasive method for measuring cardiac function *in vivo* in experimental animals (16), MRI allows more accurate three-dimensional characterization of cardiac structure and function within a single examination (17). MRI provides high spatial resolution, yielding detailed morphological information and allows the quantification of volumetric and functional changes in the heart (17). The resulting 3D image reconstruction means that analysis does not rely on geometrical assumptions for determination of LV volume, shape, or mass, which become problematic in the asymmetrical LV after MI (16, 23). MRI has emerged as a powerful and reliable tool to non-invasively study the cardiovascular system in clinical practice (23).

Assessment of LV systolic function using M-mode echocardiography is highly angle dependent and relies on geometrical assumptions for determination of LV volume,

shape and mass (23). While this technique can be effective in assessing non-infarcted hearts characterized by essentially homogenous LV contractile function, this situation no longer exists in the LV after a large MI. Thereafter, geometric assumptions may not hold true in mouse hearts rendered asymmetric by a large MI (23). A study by Stuckey et al compared short-axis 2D echo and cine-MRI measurements over several days in the same group of rats after chronic MI. Cine-MRI measurements of EF were 12 +/- 6% higher than those made using 2D-echo because of the higher spatial resolution of MRI. Repeated measurements showed cine-MRI was more reproducible than 2D-echocardiography, indicating that the accuracy of cine-MRI may allow identification of alterations in heart function which could be missed when using 2D-echocardiography (16).

Furthermore, cardiac MRI allows for accurate infarct size assessment. Late gadolinium enhancement (LGE) is considered the gold standard to assess infarct size after myocardial infarction and has been shown to predict functional recovery and mortality after myocardial infarction (19).

e. Conclusions

There are challenges regarding the accuracy and reproducibility of cardiac function measurements in mice using echocardiography, particularly in ischemic models. Although murine CMRI is challenging, murine LV function and tissue structure can be reliably measured using CMRI. CMRI is unique in its ability to integrate, in a single examination, structural abnormalities of myocardial tissue and accurate quantitative assessment of LV function (21, 23).

This doctoral project requires accurate assessment of LV function and tissue characteristics in mouse hearts rendered asymmetric by MI. Due to the superiority of

cMRI, it was agreed that this modality would be employed as the primary non-invasive imaging technique for this work.

5.1.2 MRI methods

a. Introduction

The area-at-risk describes the total amount of myocardium at risk of necrosis after AMI (Fig. 30). Early reopening of the occluded coronary artery interrupts this process by allowing reperfusion of this territory and salvage of (some) tissue within the area-at-risk (7). Thus, after AMI, the area-at-risk is generally smaller than the irreversibly injured myocardium (chronic infarct). Accurate quantification of the area-at-risk is important in studies aimed at determining the efficacy of infarct size-reduction therapies. Therefore, measurement of area-at-risk in addition to infarct size allows determination of myocardial salvage and thus therapeutic efficacy (346).

Furthermore, although researchers may ligate the LAD at what appears to be the same location in each mouse, the inherent variation in coronary artery anatomy and territory of the myocardium supplied by the coronary means that there is potentially considerable variation in the area-at-risk (347, 348). Measurement of the area-at-risk allows for MI size to be expressed relative to area-at-risk. Quantitating these values is important as this approach accounts for variability in coronary artery anatomical supply and the effect of therapy on the salvaged myocardium can be appreciated (347, 348).

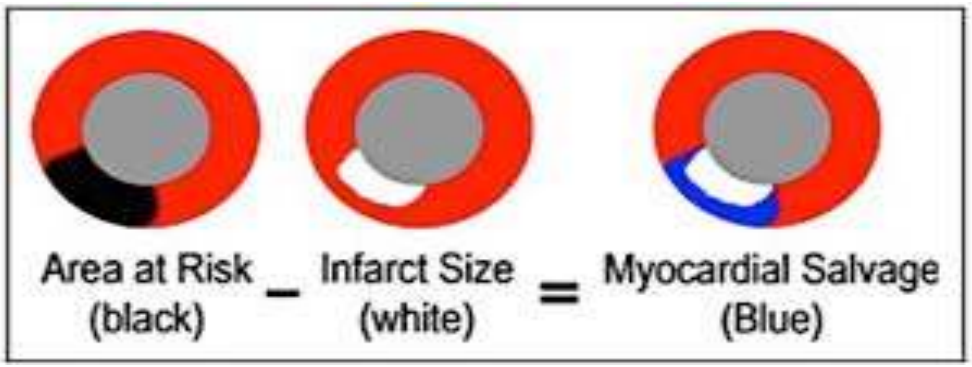

Figure 30: Schematic representation of infarct size, area at risk and myocardial salvage. Image from (349).

Iron oxide particles:

Microparticles of iron oxide (MPIO) provide excellent negative magnetic resonance contrast (hypointensity) and remain intravascular. A recent study by Grieve et al. compared histological methods of area-at-risk and infarct delineation to cMRI methods using a combination of T_2* contrast from MPIO to identify the area at risk, (by the absence of signal voids), together with Gd-based T_1-weighted enhancement to define the established infarct zone (identified by high intensity on the T_1 map) in a rat model of myocardial IR (347). This method was shown to improve the robustness in quantifying the salvageable myocardium.

Here, we aimed to delineate area-at-risk and infarct size by quantifying both the iron oxide- induced hypointense region combined with the Gd enhanced area in mice undergoing IR using a 16.4 T magnet. We hypothesised that by evaluating T_1, T_2 and iron oxide T_{2*} contrast-enhanced images we would be able to accurately distinguish the area-at-risk & infarct zones.

b. Materials and Methods

Paramagnetic iron microparticles

0.25 μm dextran covered microparticles of iron oxide particles (MPIO) (stock concentration of 25 mg/ml) were obtained from Kisker Biotech (Germany).

Pilot study for microparticle dose optimization

A 4.5mg/kg microparticle dose was initially tested as described by Grieve et al (347). However, in our model, this concentration was not was not found to provide sufficient negative contrast to accurately delineate between perfused and infarcted tissue. Therefore, a second trial was performed to test the following MPIO doses: 4.5mg/kg, 45mg/kg and 90mg/kg. Renal tissue was also harvested as a positive control to confirm perfusion of the iron particles (Fig. 31).

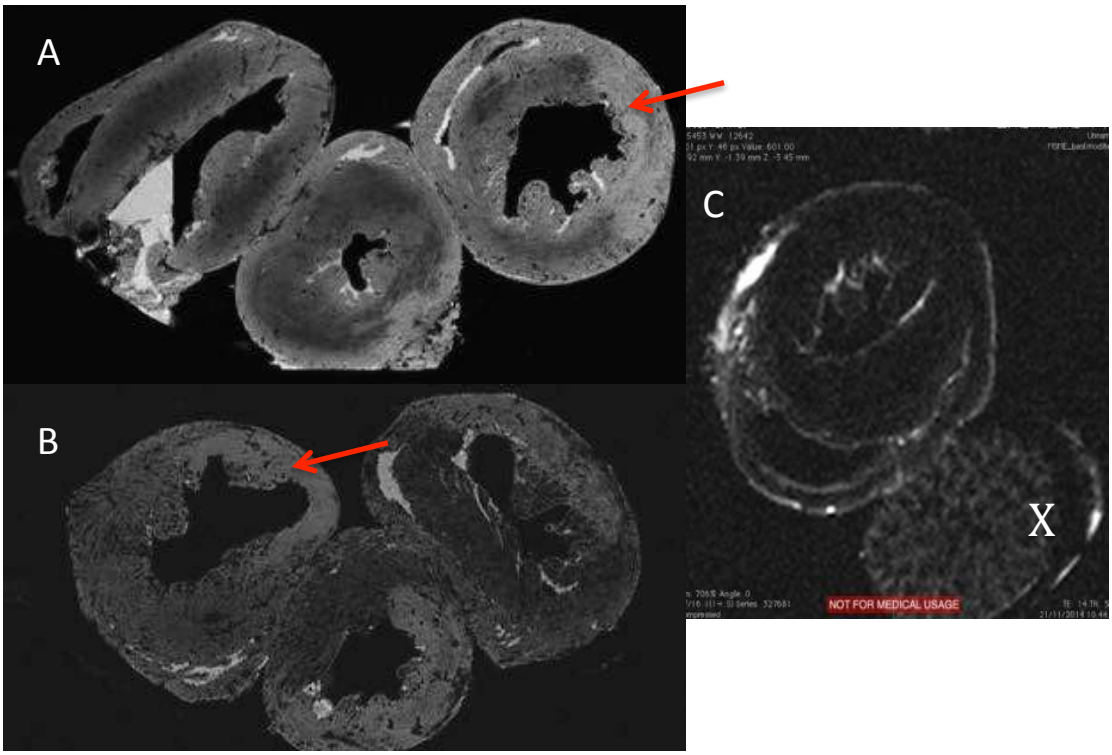

Figure 31: MPIO dose: A) 4.5mg/kg (n=3); B) 45mg/kg (n=3); C) 90mg/kg (n=3); showing increasing negative contrast within the perfused ventricular tissue as the microparticle dose increases. (A) Reveals low negative contrast, whereas (C) shows

excessive saturation of negative contrast associated with the high dose of microparticles. Note the hyperintense signal associated with the infarcted tissue in panels A & B (arrows). X denotes renal tissue with evidence of diffuse negative contrast signal consistent with MPIO uptake.

Quantification of the signal intensity within the perfused versus infarcted tissue was performed by analysis in Osirix (340). This was undertaken by drawing a circle within the representative region of interest (ROI) and recording the signal intensity within that tissue (see Fig. 32). The signal intensity was recorded from different positions and within different tissue slices, to allow calculation of the intensity ratio (perfused/infarcted). This was repeated for each MPIO dose (4.5 mg/kg (n=10), 45 mg/kg (n=10) and 90 mg/kg (n=10)).

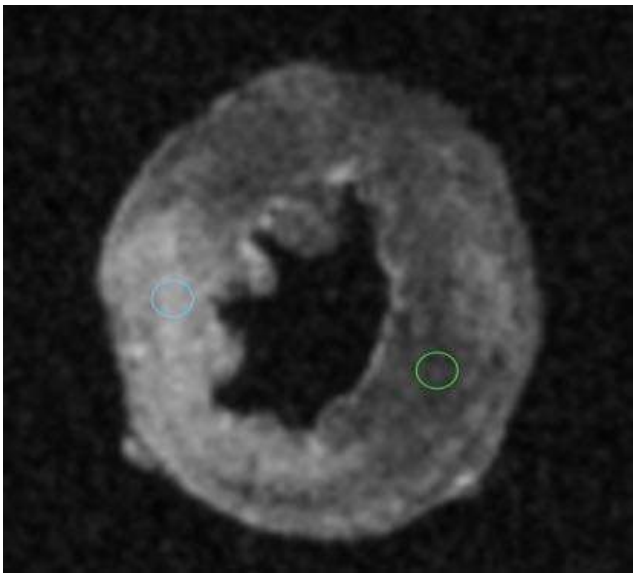

Figure 32: Optimisation of MPIO dosage: A circle was drawn and placed within the two regions of interest (ie, infarcted tissue (blue circle) and perfused tissue (green circle)). The signal intensity was compared between the two locations. This was repeated for each MPIO dose, using various tissue slices and locations. This figure represents a dose of 45mg/kg.

A paired t-test was performed to assess whether there was a difference in signal intensity between the infarcted and perfused tissue. For all doses (4.5 mg/kg, 45

mg/kg, 90 mg/kg) the t-valve was >> t-critical, therefore indicating there was a difference between the signal intensity between the ROIs (Fig. 33A). When using the dose of 45 mg/kg, the t-valve was much larger, indicating that this dose produced the largest difference in signal intensity between the ROIs (Fig. 33B/C), thus this dose was employed for all further studies.

A.

Dose (mg/kg)	Infarcted	Stdev	Perfused	Stdev	t-value	Tissue contrast enhancement	Stdev
4.5	3614	87	3312	118	8.73	1.90	0.04
45	8571	164	4627	228	97.21	1.86	.06
90	716	63	583	51	9.23	1.23	0.09

B.

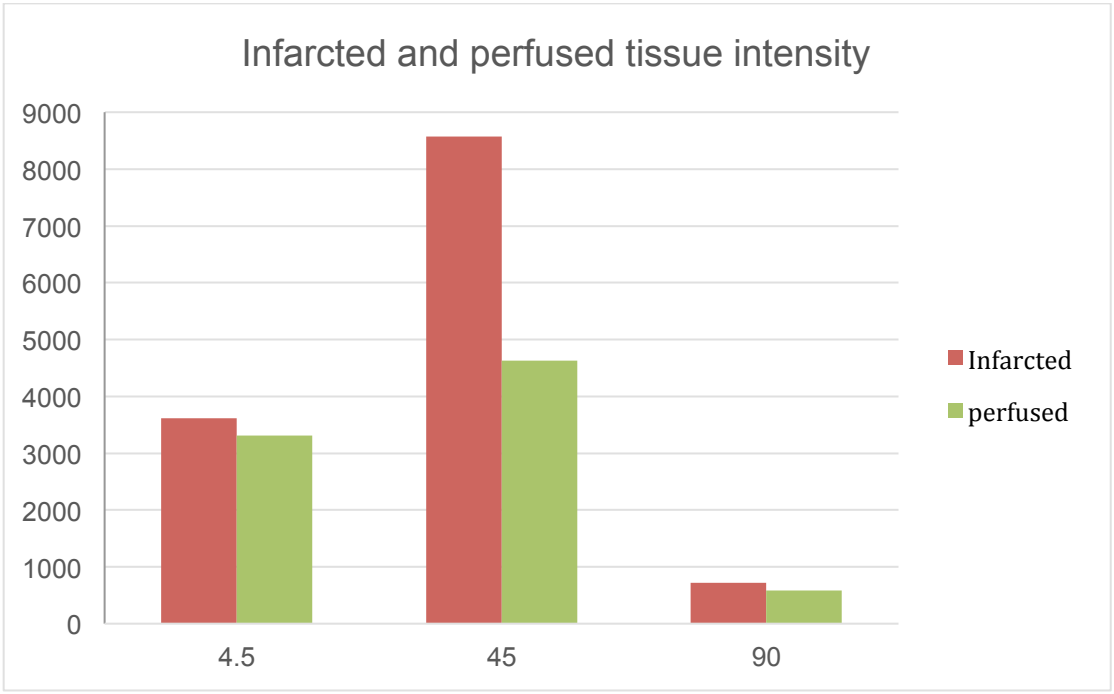

C.

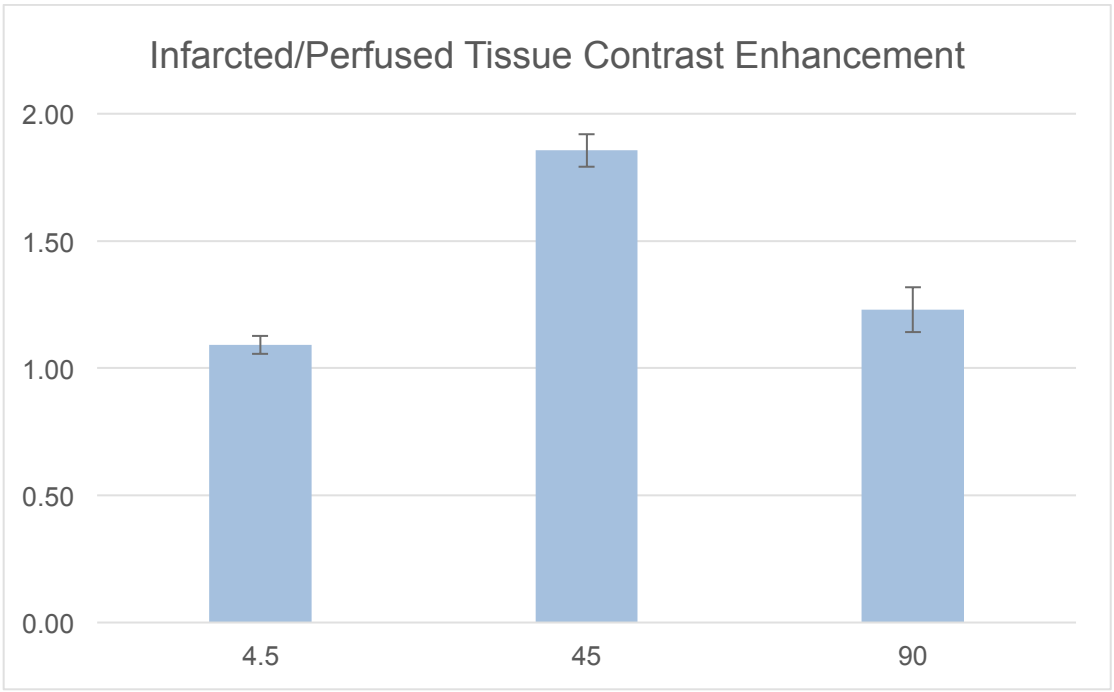

Figure 33: A) A paired t-test was performed to assess whether there was a difference in signal intensity between the infarcted (n=10) and perfused tissue (n=10) for each dose of MPIO. The t-critical for two tails paired measurements was 2.262, therefore all doses had a t-value >> t-critical, thus rejecting the null hypothesis that there was no difference between the signal intensity between the ROIs. The t-value for the 45 mg/kg dose was much larger than that of the other doses, indicating that this dose produced the greatest difference in signal intensity between the two tissue types.
B) Signal intensity (unit less) measured from the ROIs (infarcted (n=10), perfused (n=10)) in Osirix for all three doses.
C) The average signal intensity ratio (infarcted/perfused) calculated for each dose.

c. Animal Model

C57BL/6 mice (weight 25-35g) were acclimatized for a period of 1 week prior to surgery. The myocardial IR technique was approached as described in *Chapter 3.2.2 (b)* with ischemia induced for 40min. Following ischemia, the ligature surrounding the LAD was left in place while the mice recovered. After 36 hours, under repeat general anaesthesia, Gd (0.3mmol/kg) was infused via the tail vein. After a further 15 minutes the LAD was re-occluded employing the same open-chest approach. A solution containing 45mg/kg microparticles mixed with 3% Evans blue, in a total volume of ~0.3ml was infused into the tail vein. After approximately 2 minutes the

heart was excised and fixed in 10% neutral-buffered formalin for 2 hours then transferred to 0.2% Gd solution overnight. The hearts were then transferred into perfluoro-ether Fomblin solution (Y06/06, Solvay Solexis, Italy) 24 hours prior to MRI assessment. Fomblin was utilized to provide a black background to enhance visualisation of the tissue contrast (Fig. 34).

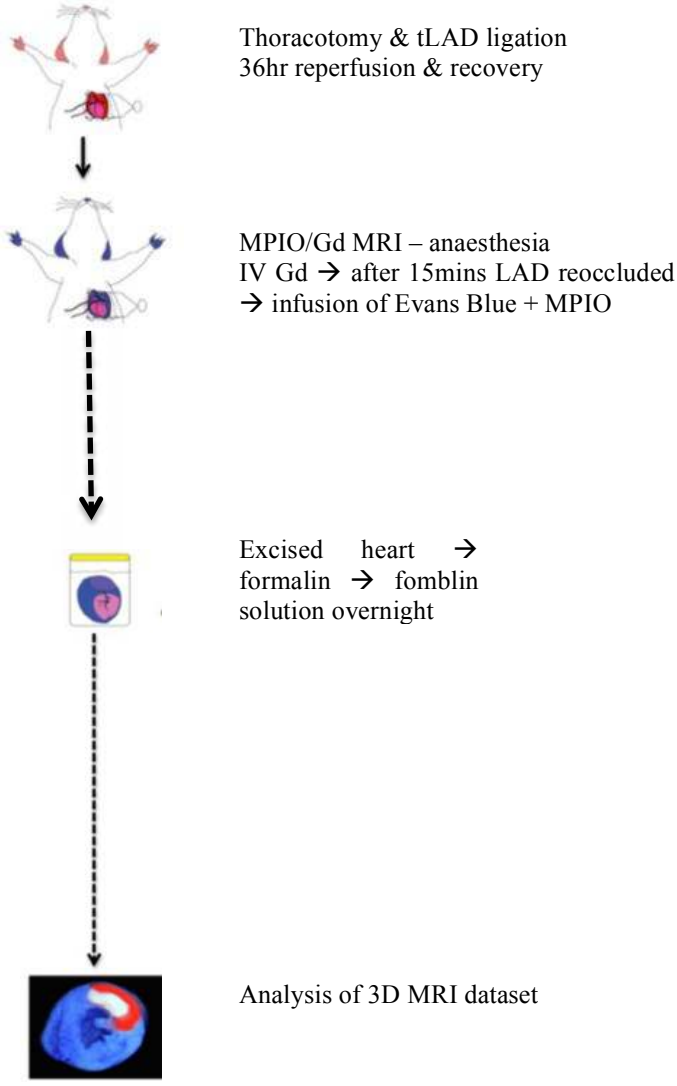

Figure 34: Illustration of MPIO/Gd 3D MRI technique. Modified from (347).

d. MRI Protocols

Sample preparation for imaging

A vertical 16.4 T magnet (Biospec, Bruker, Ettilingen, Germany) was employed for analysis of the cardiac samples. The samples were prepared into two groups for MRI analysis (Fig. 35).

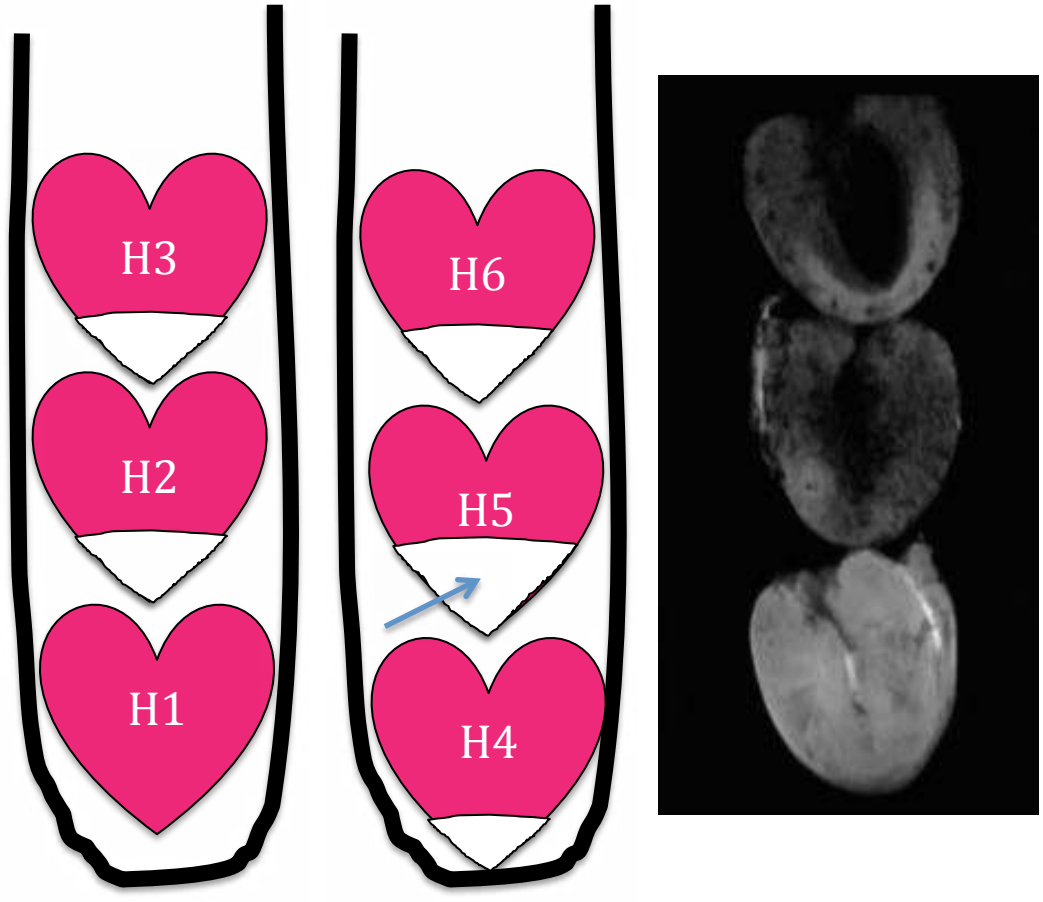

Figure 35: Three hearts were arranged into each test tube to allow for positioning within the bore of the 16.4 T magnet (right panel). The left panel shows the arrangement of the samples: Group 1: Heart 1 (H1), control- no infarct; H2/H3 hearts with an ischemic insult. Group 2: H4/H5/H6 -all hearts have an ischemic insult of a different size; this was due to purposeful LAD occlusion at different sites, thus rendering a different area-at-risk. The blue arrow indicates the ischemic region.

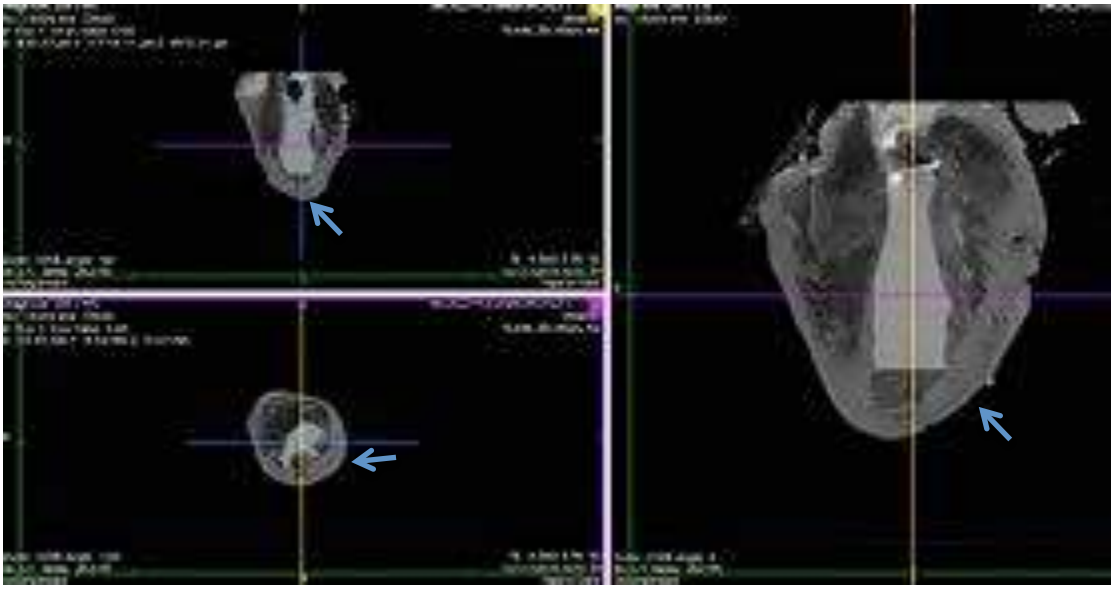

Figure 36: Preliminary "3D" view of gadolinium-enhanced infarct (arrows) (without microparticles) acquired using a T_1/T_2* weighted 3D FLASH sequence at 16.4T. 3D acquisition allows simultaneous axial, coronal and sagittal views of the heart (represented by the colour lines) that can be evaluated by "scrolling" through the tissue.

e. MRI Sequences

Three-dimensional gradient echo fast low angle shot – 3DGE (FLASH)

Three dimensional (3D) gradient echo (GE) fast low angle shot (FLASH) was acquired with the following parameters: echo time (TE) = 6.735 ms, repetition time (TR) = 40 ms, flip angle 30 ° . The spatial resolution was 0.040×0.039×0.039 mm/voxel with FOV of 25.60 mm ×10 mm × 10 mm and matrix size of 640 × 256 × 256. The number of averaging was 2 and the scan time was 40 minutes. In this sequence, the predominantly T2*-weighted image contrast is very useful to detect the perfused and non-perfused area delineated by the MPIO. The non-perfused region (area-at -risk) lacks the negative MPIO image contrast (Fig. 37).

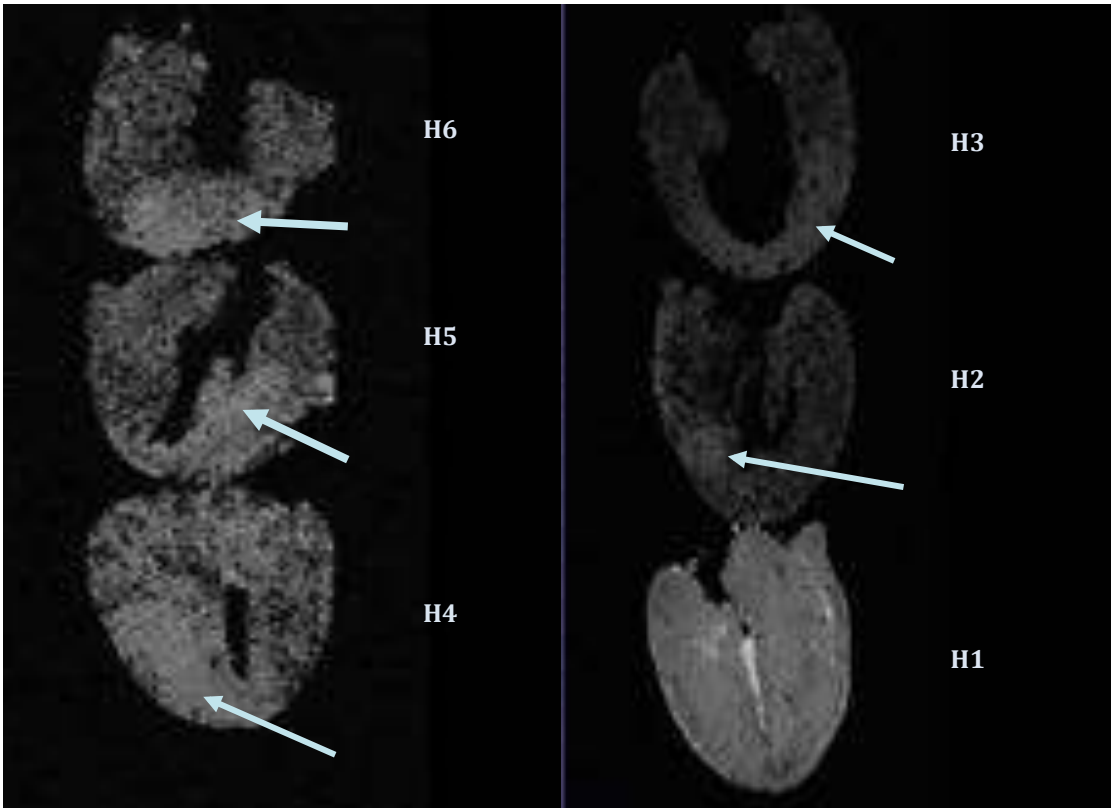

Figure 37: 3D FLASH sequence using the 6 heart samples: 5 samples show a non-perfused region (ie, lacking MPIO) representing the area-at-risk (grey arrows), H1 is the control.

Three-dimensional multi-slice multi-echo sequence – 3DMSME

The second sequence was a 3D multi-slice multi-echo sequence (3DMSME) acquired with multiple TE of 14, 28, 42 ms, TR = 400 ms. The spatial resolution was 0.078 × 0.078 × 0.078 mm/voxel, with a slice thickness of 10 mm and FOV of 25.600 × 10 × 10 mm, the matrix size was 328 × 128 × 128 with a number of averaging of 1. The scanning time was ~ 50 mins. This dataset has an increasing T_2 weighting, with the highest at 42ms. The different echo times had an impact on the signal to noise ratio, the longer echo times resulted in more signal decay. T_2 -weighting allowed assessment of the area-at-risk by delineating the oedematous region (350, 351).

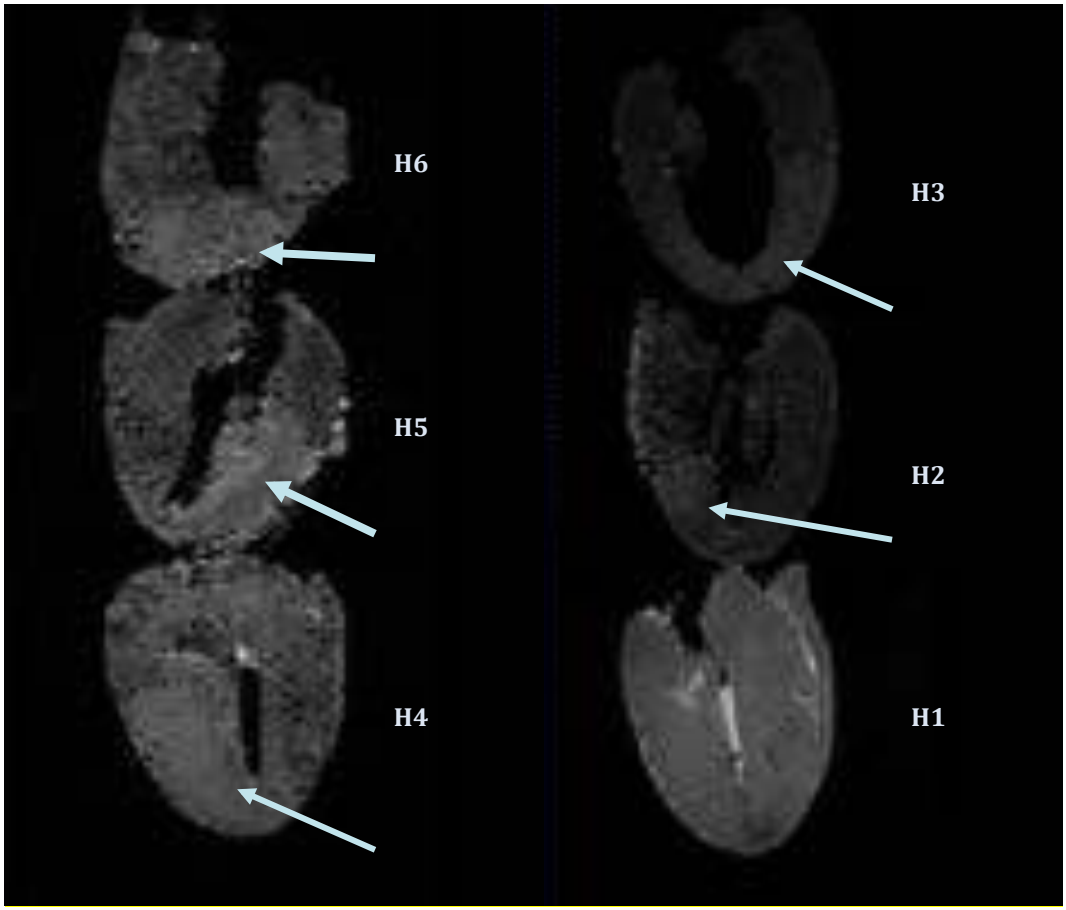

Figure 38: Images acquired with a 3DMSME sequence with TE of 42 ms. The arrow points to the odematous region (area-at-risk).

T_1 Map

A T_1 map was generated from the inversion recovery sequence with a TI of: 300, 500, 700, 800, 1000 and 1500ms. TR: 4000 ms, the number of averaging was 1 and the acquisition time was 7 mins 15 s. The spatial resolution was 0.078 × 0.078 mm/voxel, FOV: 10 × 10 mm. The matrix size: 128 × 128 and slice thickness: 0.5 mm. The infarcted and perfused region could be delineated from the T_1 map and the signal intensities were measured.

Equation [1] was used to fit the T_1 inversion recovery data:

$$M_z(t) = M_z, eq(1 - 2e^{\frac{-t}{T_1}}) \qquad [1]$$

T_2 Map

The T_2 map was acquired using a spin multi echo sequence with a TE of: 11, 22, 33, 44, 55, 66, 77, 88 ms), TR was 5000 ms,.The number of averaging was 1, FOV: 10 ×10 mm, matrix size: 128 × 128 mm, slice thickness: 0.5 mm and spatial resolution: 0.078 × 0.078 mm/pixel. The scan time was 11 mins. The infarct is visualized on the T_2 map as a hyperintense region (Fig. 39). As for the T_1 map, from the T_2 map the regions of interest (infarcted and perfused area) could be traced to measure the signal intensity in both.

Equation [2] was used to calculate the T_2 based on T_2 exponential decay:

$$M_{xy}(t) = M_{xy}(0)e^{\frac{-t}{T_2}}$$

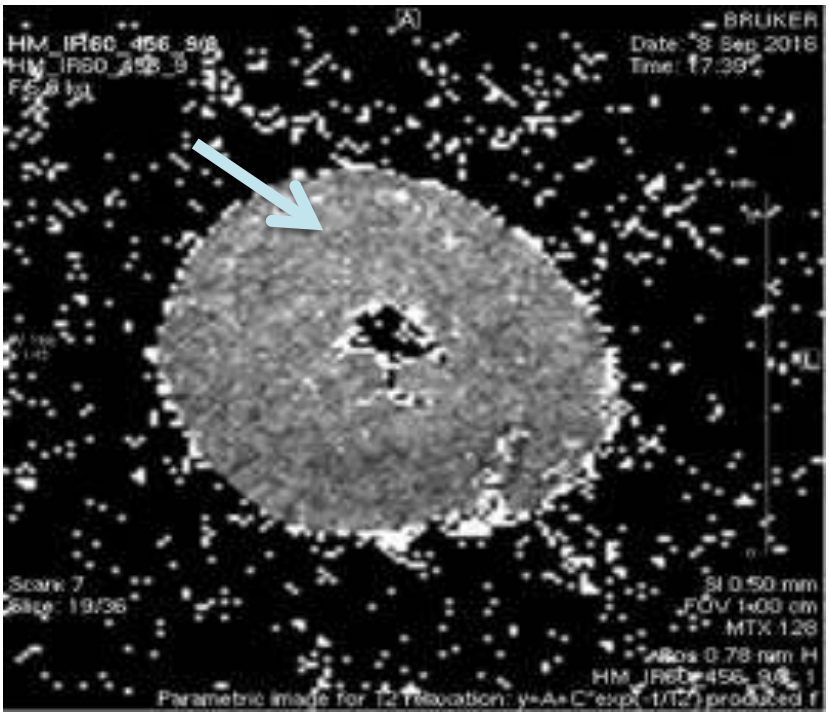

Figure 39: T_2 map, axial slice with the hyperintensity representing the infarct (arrow).

f. Image post processing

T_1 map and T_2 map evaluation

After generating the T_1 and T_2 map, the ROI was traced using Paravision 5.1 software. The image contrast and colour-threshold were adjusted in order to achieve optimal image contrast for visual assessment. The ischemic area on the T_2 map was seen as a hyperintense region with a high T_2 value. The T_2 value and standard deviation for each area was exported to Excel.

The same process was applied to the T_1 map. Visual assessment of the T_1 map proved challenging as it was hard to distinguish between the ischemic and perfused areas. Therefore, the ROI determined from the T_2 map was superimposed onto the same slice at the same location on the T_1 map. Figure 40 displays the T_1 and T_2 map images with the outlined ROI.

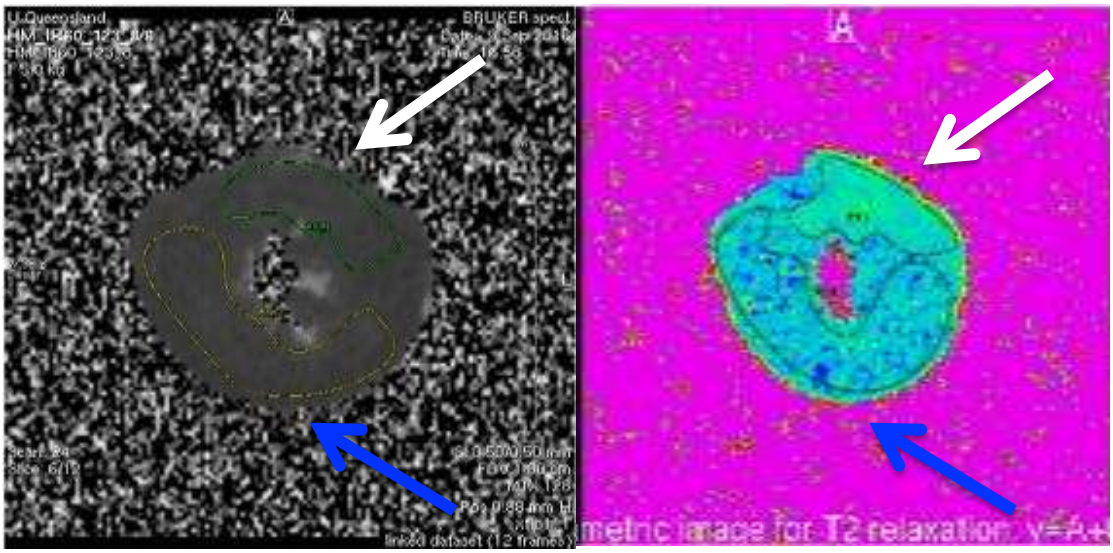

Figure 40: T1 map (left), T_2 map (right). ROI - white arrow: ischemic zone, blue arrow: perfused zone.

Image segmentation of 3DFLASH and 3DMSME sequences

The area-at-risk had a different appearance depending whether the 3DFLASH or 3DMSME sequences were employed. Segmentation was performed using ITK-SNAP

software to determine the normal and area-at-risk regions, and their volumes were shown using 3D rendering. By convention, the perfused area was coloured blue and the area-at-risk red. The segmentation was acquired manually, with the region of interest (ROI) coloured slice-by-slice in various orientations (axial-coronal and sagittal) to achieve the most accurate segmentation for the ROI. Delineation of the perfused area from the area-at-risk was based on visual assessment. The area-at-risk in the 3DFLASH sequence was seen as a non-perfused area, while in 3DMSME it was visualised as a hyperintense region. The size of the area-at-risk from the two sequences was compared, as each sequence had a different sensitivity for detection of these regions. After the segmentation was completed, the volumes were measured for both the perfused and area-at-risk regions using ITK-SNAP (Fig. 41). All measurements were exported into Excel to quantify the normally perfused region and area-at-risk in each sequence and determine the difference ("mismatch") between area-at-risk measured between each sequence.

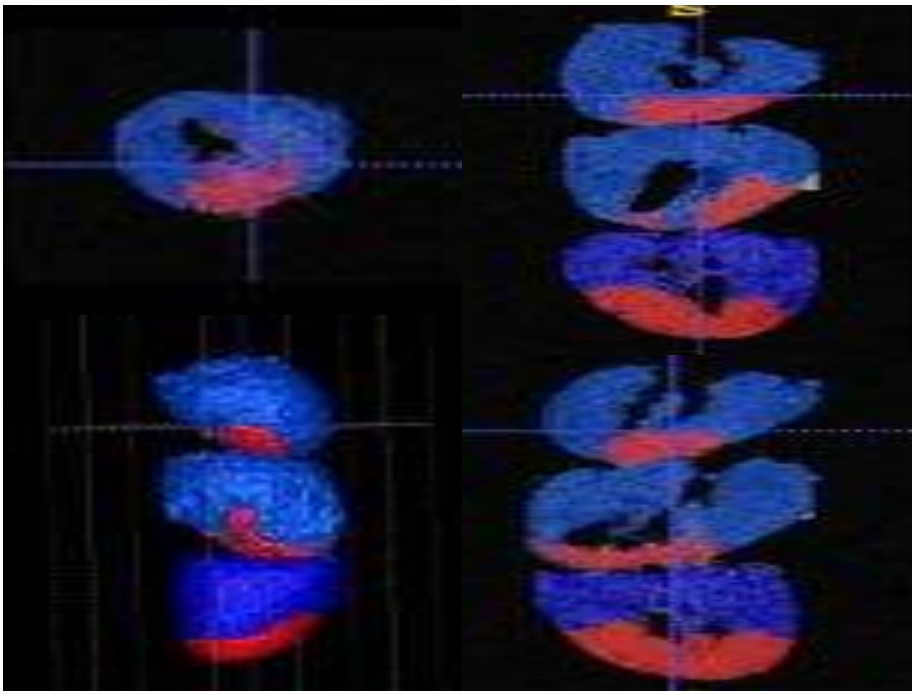

Figure 41: 3DFLASH sequence: An example of image segmentation of 3 hearts with an ischemic insult: area-at-risk coloured red and perfused tissue in blue.

Mismatch area measurement

Mismatch area: difference in the area-at-risk measured using the two sequences.

During the process of manual visual segmentation of 3DMSME, it became clear that different echo times (TE = 42.28, 28 and 14 ms) produced different image contrasts and thus a different size area-at-risk. Differences in the area-at-risk using each TE was calculated by volume subtractions of the segmented areas using this FSL fslmaths command:

(fslmaths 3DMSMETE42- sub 3DMSMETE28 mismatch42-28.nii).

To measure the area-at-risk mismatch between 3DMSME and 3DFLASH, they were co-registered using FSL linear registration software (FLIRT). Subsequently, the segmented areas between the two datasets were subtracted using fslmaths.

After the subtraction was completed, the image had three ROI: perfused, area-at-risk, mismatch. Figure 42 demonstrates delineation of the area-at-risk, perfused and mismatch zones in the 3D cross-sections, Using this approach, the ROIs can be visualised by the examiner when scrolling through the 3D reconstruction.

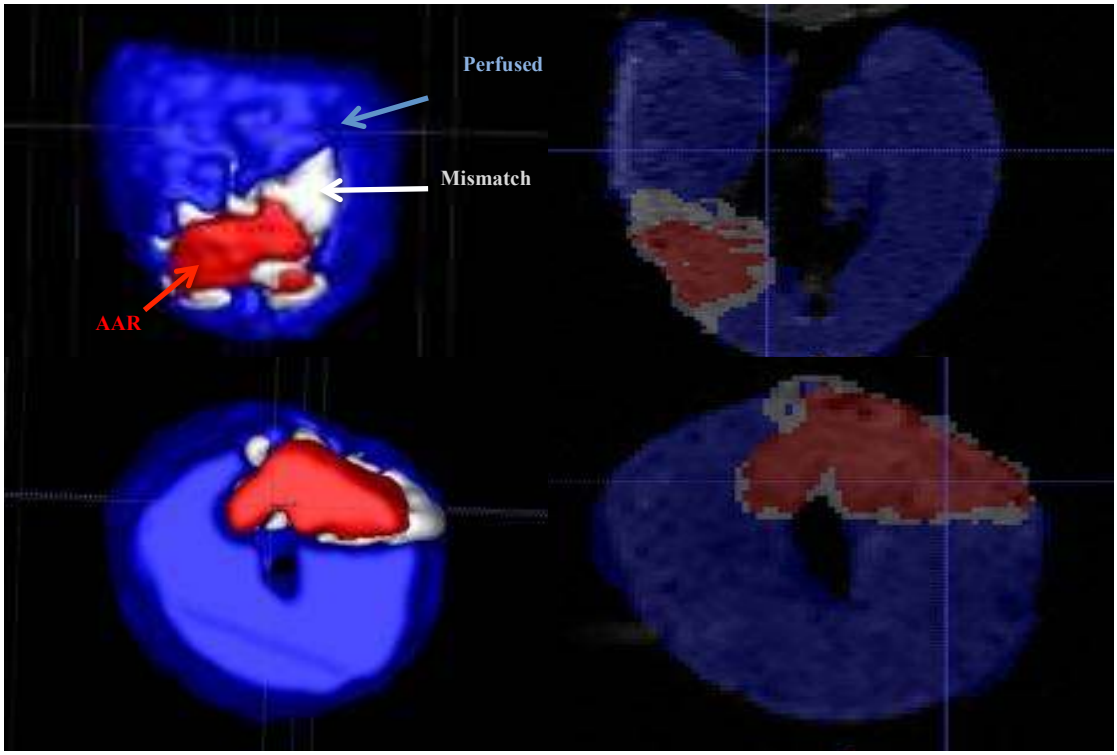

Figure 42: 3D reconstruction of a heart after subtraction of the 3DFLASH area-at-risk zone from that of the 3DMSME area-at-risk zone (using a TE 42ms). The perfused area is coloured blue, area-at-risk in red and the mismatch area between the two sequences is coloured in grey.

g. Results

Analysis of Regions of Interest

Figure 43 compares perfused, area-at-risk and mismatch area in the five ischemic hearts. Heart 1 (H1) was excluded, as there was no ischemic insult. The remaining five hearts, H2 (A), H3 (B), H4 (C), H5 (D) and H6 (E) each had a purposefully different area-at-risk based on level of LAD ligation. Assessment of the T_2* FLASH sequence demonstrated signal loss as a negative contrast (secondary to MPIO in the perfused tissue), while there was an absence of MPIO within the area-at-risk (non-perfused region). In contrast, with the MSME sequence, oedema within the tissue was visualised as a hyperintense signal, whereas there was a lower signal within perfused region.

Quantification of the ROI (area-at-risk) was different depending on which sequence was employed (FLASH vs MSME). The difference measured between the two sequences was described as the "mismatch". With the FLASH sequence, we identified an area-at-risk of 8.6% in H2 (A), H3 (B): 22.8%, H4 (C): 26.9 %,H5 (D): 7.5% and H6 (E) 10.3%. Using the MSME sequence the results were found to vary depending on the TE used, For example, in H2 the perfused tissue ranged from 90.3% to 95.1% and the oedema (area-at-risk) ranged from 4.9% to 9.7% of the area. In H3 area-at-risk: 22.9-34.3%, H4 area-at-risk: 30.6-33%, H5 area-at-risk: 17-27.7% and H6 area-at-risk: 9-16.5% (Fig. 43).

Comparison of the ROIs derived from the two different sequences showed that the area of oedema measured using MSME was typically larger than that of the non-MPIO perfused region measured with the FLASH sequence, ie, area-at-risk measurement: MSME > FLASH.

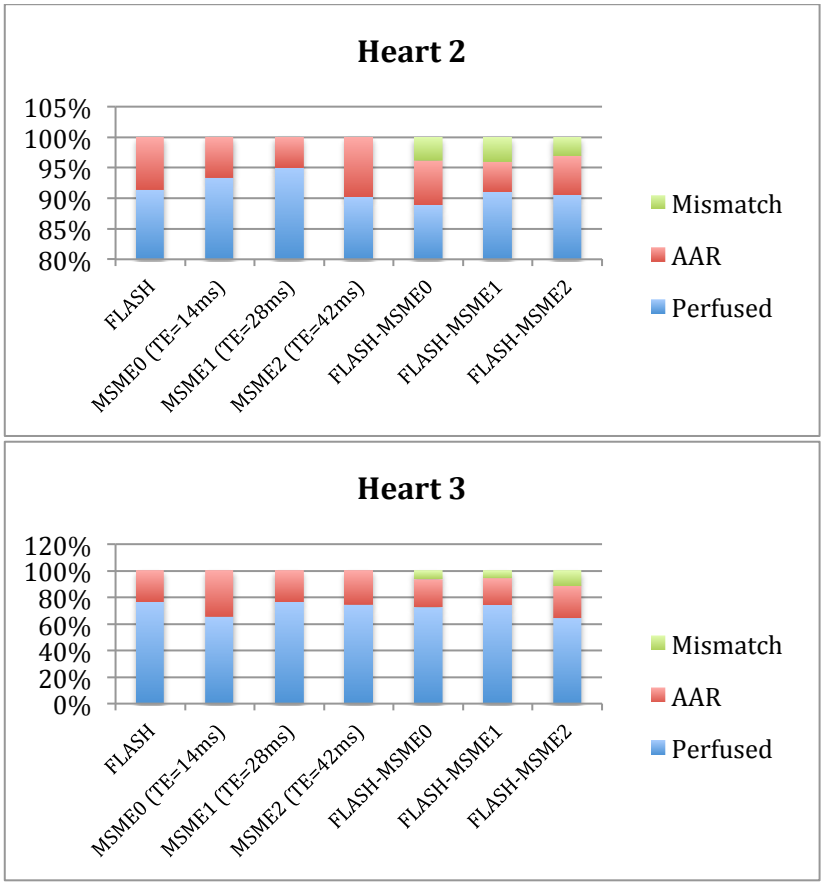

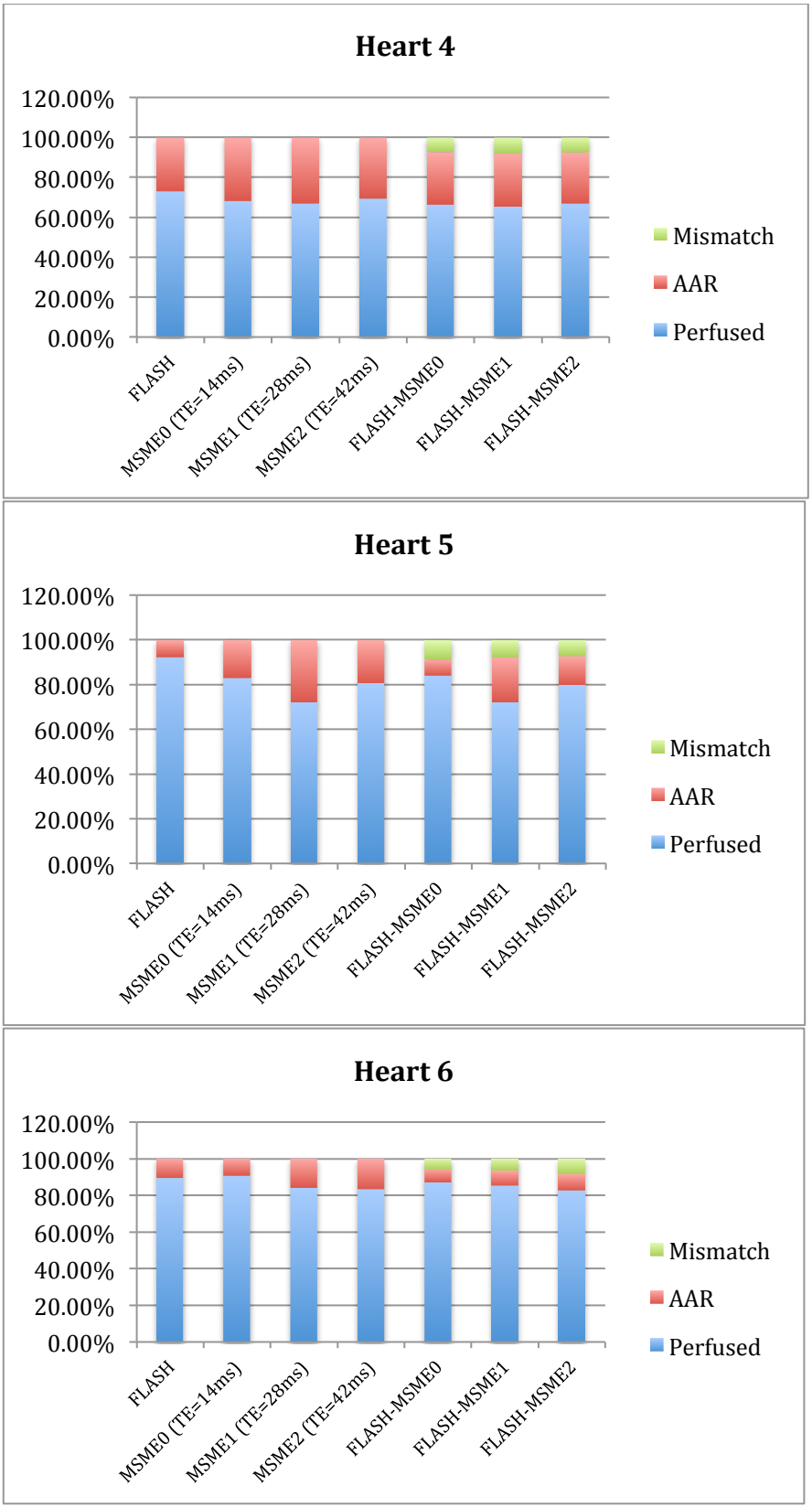

Figure 43: The sequences' (FLASH, MSME (TE 12, 28 and 42ms)) were all used to calculate the percentage of tissue that represented the area-at-risk (pink) and perfused tissue (blue) in each heart (n=5). Each sequence resulted in a slightly different area-at-risk. Thus, the mismatch area (green) between sequences was calculated by

subtracting the segmented area-at-risk and perfused volumes derived from the FLASH sequence from the MSME images at each TE (ie, FLASH-MSME0; FLASH-MSME1; FLASH-MSME2).

Effect of echo time in 3D-multi slice multi-echo

The different echo times employed in the 3DMSME sequence resulted in variable signal intensity, with a longer TE producing less signal-noise ratio. Figure 44 demonstrates the percentage area-at-risk volume of each heart at different echo times. Thus it is seen that each heart had a different area-at-risk based on the specific echo time. The results appear somewhat random as the area-at-risk volume in Heart 3 was greatest with an echo time of 14 ms, while for H5, it was greatest with an echo time 28 ms and H2 & H6 at 42ms. Therefore, it is difficult to accurately conclude how the volume of MSME-measured oedema (area-at-risk) was influenced by the echo time. Instead, this variability may relate to tissue fixation, which may alter the oedema content in the ex-vivo samples, or user-associated inaccuracies in manual analysis of the ROIs.

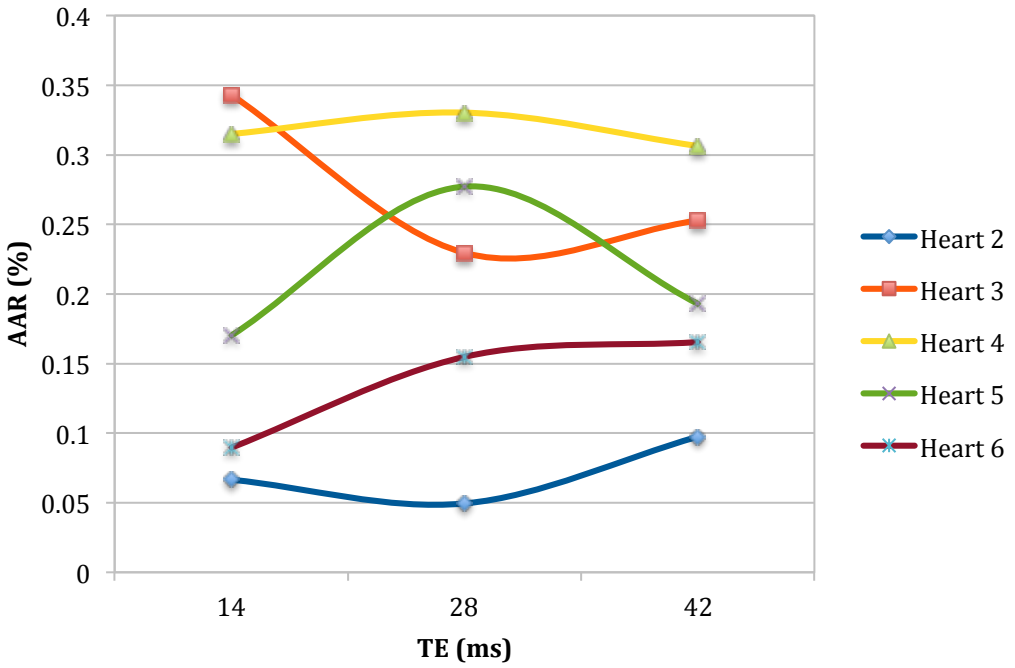

Figure 44: Based on the echo time employed (TE = 14, 28, 42 ms), there was a difference in the volume of area-at-risk measured in each heart (n=5) using the 3DMSME sequence.

Image analysis of the T1 and T2 map

The infarcted region was more clearly visible using the T_2 map compared to the T_1 map (Fig. 40, above). Using planimetry, the ROI was traced as the infarcted (irreversibly damaged) area and the non-infarcted area. In order to achieve accurate measurements, 2 slices were selected using each the T_1 and T_2 maps (T_1 (n=10); T_2 (n=10)). In both sequences, the signal intensity within the infarcted area was greater than the normal area. A paired T-test was used to determine whether there were any significant differences between the signal intensity of infarcted and non-infarcted tissue within the maps. T_1 and T_2 relaxations were both found to be longer in the infarcted tissue compared with the non-infarcted tissue (p = 0.04 and 0.001, respectively). This finding indicates that both the T_1 and T_2 maps were sensitive to detecting the differences between these two tissue populations (Fig. 46)

The direction of these changes in signal intensity was not as expected, as the T_1 relaxation time was expected to *decrease* within the infarcted region (due to Gd binding within the irreversibly injured tissue). We found that the T_1 relaxation time actually *increased* in this region (Fig. 45 B). This suggests that Gd did not successfully bind to the infarcted area. This unexpected changed may have been due to an inconsistent amount of irreversibly damaged tissue following a 40-minute ischemic time, or the Gd may have washed out during the heart fixation.

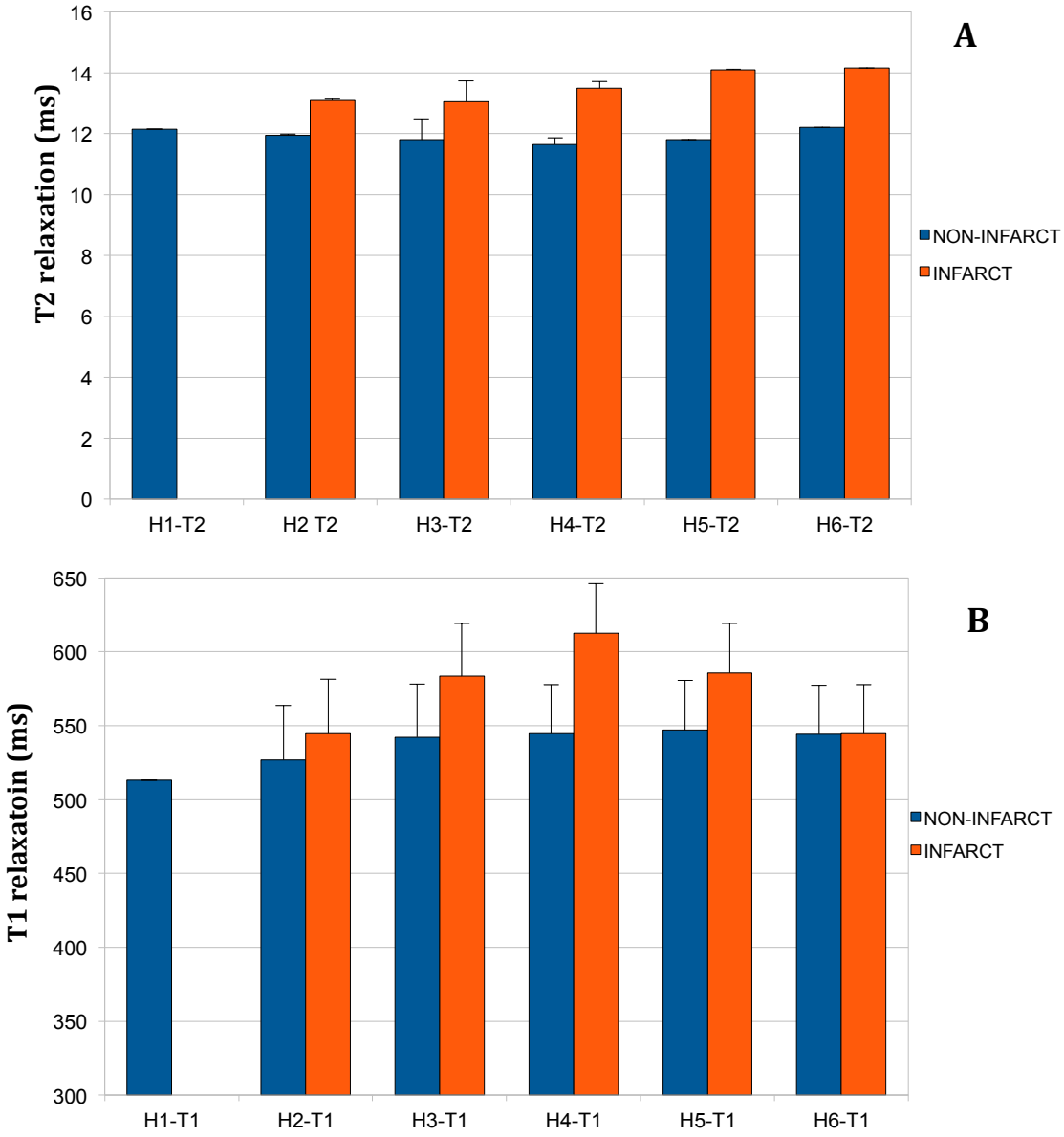

Figure 45: Difference in signal intensity between non-infarcted (blue) and infarcted tissue (red) seen using the T_2 (A) and T_1 (B) map in each heart (n=2 per heart)

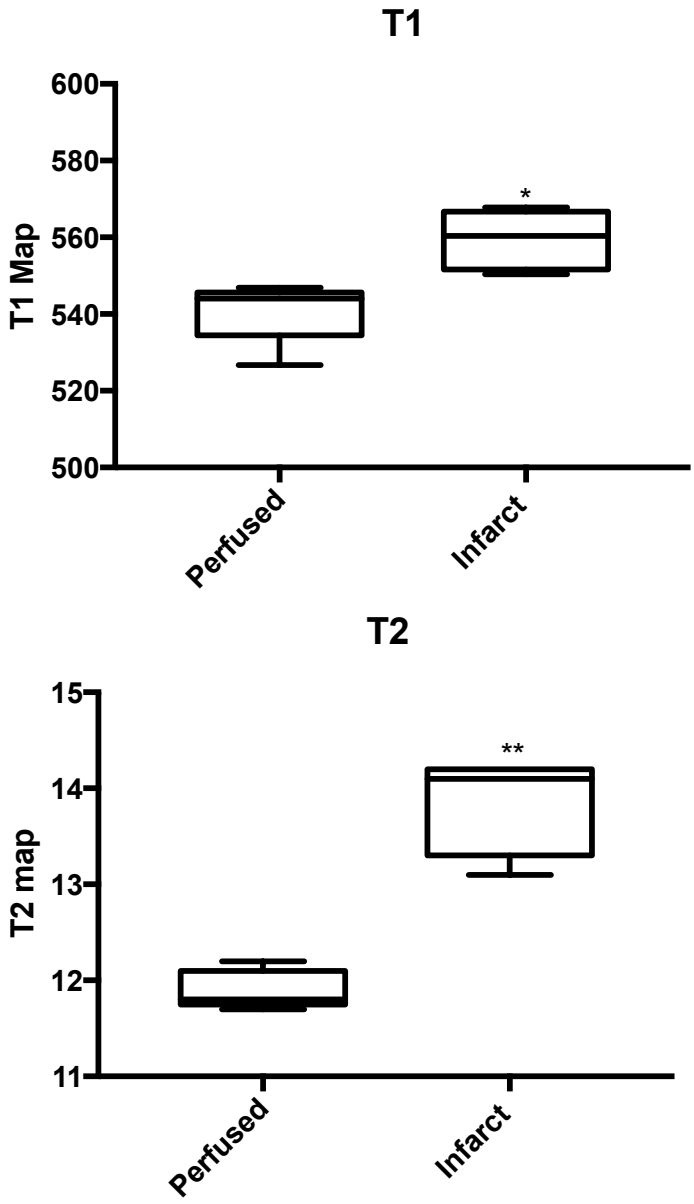

Figure 46: A paired T test analysis was used to determine the difference in signal intensity (Y axis) between perfused (n=10) and infarcted tissue (n=10). There was a significant difference in signal intensity seen between these regions using both the T_1 and T_2 map (p = 0.04 and 0.001 respectively).

h. Discussion

MRI assessment of myocardial tissue structure

Functional and structural characterization of the infarcted myocardium is important in the risk stratification of patients after MI (20). Pathological changes in the injured

myocardium, such as in the presence of fibrosis, haemorrhage and oedema, influence the signal intensity on T_1- and T_2- weighted imaging (21, 22, 352).

Myocardial fibrosis represents a hallmark of pathological remodelling within the myocardium (63). Fibrosis reduces cardiac function and plays a major role in cardiac arrhythmogenesis (63, 352). Recently within the clinical community, T_1 mapping in combination with contrast agent uptake has been utilized to characterize tissue structure not only after myocardial infarction but also in diffuse fibrosis (339, 353-355). T_1 mapping with contrast enhancement has limitations, such as the need for contrast injection and decreased contrast agent relaxivity at high field strength (356). *In vivo* T_2 measurements have been proposed as an alternative to assess diffuse interstitial fibrosis (357). A decrease in T_2 relaxation time has been measured *ex vivo* in the myocardium of diabetic rats and was associated with increased collagen content (358). *In vivo* T_2 measurements have also been used to noninvasively quantify myocardial fibrosis in diabetic mice at 11.75T and were shown to strongly correlate with myocardial fibrosis assessed by histological methods (18).

Recently, attention has also been directed towards the development of myocardial T_2 quantification and mapping techniques. T_2-weighted (T_2w) MRI is especially sensitive to water and can highlight oedematous areas (359, 360). The long T_2 relaxation times of water-bound protons are used to generate a water-specific contrast when applying T_2-weighted sequences, resulting in a high signal intensity of oedematous tissue (21).

T_2* mapping can also be used to obtain information on tissue structure (339, 361). T_2* contrast has been explored as a tool to diagnose the presence of haemorrhage and myocardial iron (348, 359, 362, 363). Reperfusion of severely ischemic myocardium

also leads to interstitial haemorrhage, which may be an important marker for irreversible microvascular damage (20, 364). Recently, it was demonstrated that T_2* has the potential to image fibrosis in the infarct zone (20, 365). The potential of T_2* mapping to image myocardial haemorrhage and fibrosis was evaluated in a recent study of IR-induced injury in mice and found to be a useful addition to late gadolinium enhancement (LGE) for follow up of myocardial remodelling and prediction of recovery from infarction (366). Interestingly in this study, a considerable infarct observed on day 1 (based on a large LGE positive area), was difficult to detect using LGE on day 7 and 28, suggesting considerable recovery of the area-at-risk. However, T_2* maps performed on day 7 and day 28 revealed low T_2* values in the infarct area, indicating that the infarct had not recovered (366). Changes in T_2* contrast in ischemic regions were associated with iron and collagen depositions and were found to correlate with reversibility of ischemic injury and infarct maturation (366). Thus, changes in T_2* can be associated with infarct age, reversibility of the injury, and can give an indication of the myocardial structural variability throughout infarct maturation (366).

MRI Imaging of infarct size and area at risk

Infarct size

LGE is considered the gold standard to assess infarct size after MI and has been shown to predict functional recovery and mortality (18, 19). In a LGE scan, T_1-weighted imaging is performed after injecting a gadolinium-based contrast agent to delineate injured myocardium (352).

LGE imaging exploits the substantially different acceleration of longitudinal magnetic relaxation (T_1 relaxation) in healthy tissue compared with infarcted tissue after the

administration of a T_1-shortening contrast agent (341). The extracellular contrast agent gadolinium-DPTA (Gd-DTPA) rapidly diffuses from the vascular space into most extracellular tissue fluid, but not the intracellular space (7). In the presence of Gd-DPTA the T_1 of tissues is potently shortened, resulting in increased signal on T_1w images (7). In acutely infarcted tissue, Gd tissue kinetics are altered, resulting in delayed washout secondary to decreased functional capillary density, permeability and coronary flow rates and increased volume of distribution secondary to loss of cell membrane integrity allowing Gd-DPTA to diffuse into the cellular compartment. Overall, this results in accumulation and lingering of Gd-DPTA in the infarcted tissue, resulting in a shorter T_1 (7, 352).

Practically, in order to perform LGE imaging, an inversion recovery sequence can be performed to manually set the inversion time (TI) in order to null "normal" remote myocardium, thus highlighting the greatest image intensity difference between normally perfused and infarcted tissue (367). This allows direct quantification of the spatial extent of the focal scar. At high field strength, there is an extremely high correlation between histological findings and LGE in ex-vivo rat hearts (345).

The time delay between injection of Gd-DPTA and image acquisition may affect the extent of LGE. In a rat model of MI, during the first 5 minutes after Gd-DPTA injection, delayed enhancement overestimated the size of histologically measured infarct by 20-40% (368, 369). When the TI was optimized, the extent of delayed enhancement was stable over time from 7-42 minutes after contrast injection in patients with reperfused AMI (370). Infarct volume measured with MRI was seen to remain consistent from 20-60 min after contrast administration (371).

Until recently, the assessment of infarct size in small animals in high magnetic fields

has been performed using a 'cine gradient echo pulse sequence' with a high dose of gadolinium chelates (369). This type of MRI protocol is limited in its ability to accurately delineate both the viable and non-viable myocardium post infarction (343, 372). The use of an inversion recovery T_1w approach has become an accepted modality for the clinical diagnosis of MI. (373, 374). Chapon et al. demonstrated that an inversion recovery pulse sequence could be used to discriminate infarct from non-infarcted myocardium in small rodents at 9.4T (343).

Area at Risk

Accurate quantification of area-at-risk is important in studies aimed at determining the efficacy of infarct size-reduction therapies. Measurement of area-at-risk in addition to infarct size allows determination of myocardial salvage and thus therapeutic efficacy (346, 375).

Despite being salvaged, the myocardium in this region is altered by ischemia. The development of oedema, secondary to inflammation, is one of the features of the area-at-risk, often occurring early, even after brief episodes of myocardial ischemia (351). In the setting of the acutely reperfused infarct, the relationship of myocardial oedema to irreversible myocardial injury provides information on the salvageable myocardium within the area-at-risk and is thus a guide to therapy (376). In a recent study, Gd-DTPA concentration was not seen to be significantly increased in reversibly injured ischemic myocardium (377).

T_2-weighted sequences are very sensitive to water-bound protons and have been shown to successfully visualize infarct-related oedema (355, 357). T_2-weighted images were first shown to represent area-at-risk in an ex-vivo canine model of both non-reperfused and reperfused MI, confirming a tight relationship between

myocardial T_2 and tissue-water content (378). Ugander et al. validated T_2-weighted and pre-contrast T_1-weighted images as measures of the area-at-risk against whole-heart microsphere reference standards (346). T_2-weighted images have been used to image salvageable myocardium in humans (376). Pulse sequences for T_2-weighted cMRI optimized for imaging humans do not directly apply to mice due to the use of higher magnetic field strengths and 10-fold greater heart rate in mice compared with humans (379). Beyers et al, recently developed a T_2-weighted protocol for mice, allowing *in vivo* imaging of area-at-risk, which showed a good correlation with histological measures of area-at-risk (379).

Histological assessment of Area-at-risk/Infarct size

Historically, histological sections have been used to visualise and measure the myocardial scar using stains specific for connective tissue in the extracellular space (380). Histology is widely utilized to quantify infarct size in mice, however this method is not ideal as it is a terminal measurement, resulting in the destruction of tissue preventing further functional or biochemical analysis (375).

Non-invasive imaging offers the advantage of allowing the comparison of infarct size before and after an intervention longitudinally, in the same animal (341). Importantly, this circumvents the need for euthanasia at each time point and minimizes animal numbers. A tight correlation between MRI and TTC infarct volumes has been observed in multiple studies (381, 382). In preclinical studies, post-mortem histological analysis is currently considered the gold standard for measuring infarct size. Current methods include perfusing the heart with Evans blue and TTC to quantitate the area-at-risk and infarct size (347).

TTC is a redox indicator used to differentiate between metabolically active and inactive cells and tissues (8). Tissue with dysfunctional mitochondria does not stain with TTC and results in a pale appearance (371). To delineate the area-at-risk, at the end of reperfusion period, the coronary arteries are re-occluded and hearts are perfused with Evans Blue to stain the perfused tissue dark blue, while the area-at-risk remains unstained (383).

The limitations of this method relate to the accuracy and reproducibility of this technique. Particularly with regards to accurate delineation of the infarct borders and area-at-risk zone. Manual slicing of fresh tissue results in thick tissue slices and thus there are assumptions made on how the tissue within the middle of the slice reflects that visualised on the surface of the slice (347). Visual interpretation and planimetry of heart sections can be subjective in cases with poor viable:nonviable contrast due to haemoglobin residues within the necrotic regions or TTC-induced geometric distortion of the sample. These issues are particularly significant when working with the small mouse heart (347).

TTC and LGE techniques have been demonstrated to be highly correlated (17). Grieve et al was the first to propose and describe the automated 3D MRI technique, resulting in an improved robustness in measuring salvageable tissue (347). This technique replaces the need for manual slicing of the heart and allows whole-heart analysis. The user can scroll through slices of the 3D dataset for segmentation and quantification of the ROI, removing many of the disadvantages associated with histological methods of assessment (Table 3)

Table 3: Advantages and disadvantages of Evans blue/TTC technique VS Ex vivo 3D MPIO/Gd MRI approach (modified from (347)). Blue panel: relevant to both techniques. Green coloured – considered as an advantage, red panel – considered less advantageous.

Evans Blue/TTC	**3D MPIO/Gd MRI**
Postmortem assessment, excluding serial measurements Requires religation of LAD under anaesthesia	
Requires manual cutting of fresh tissue into ~1mm slices. Results in approximately 6-8 slices/heart	High resolution, manual slicing not required.
Assumption that area-at-risk /MI is the same throughout the volume of the 1mm slice	No assumption required as large number of slices and high resolution. Able to "scroll" through slices
Evans blue can diffuse across the border zone of the area-at-risk and increases error. TTC staining can be variable and "dominate" Evans Blue making it difficult to determine the border zone	Border zones are seen clearly even >24hrs after fixing.
Requires manual tracing of borders and calculation of volumes for MI/ area-at-risk	Allows 3D digital analysis and automated segmentation
Requires tail vein injection	Requires two tail vein injections

In preclinical models it is important assure the accuracy of measurements when developing novel imaging techniques. In this study, we used a combination of T_1, T_2 and T_2* contrast acquired using 3DFLASH, 3DMSME and 2D spin echo sequences from six mouse hearts having undergone an ischemic insult and reperfusion.

We demonstrated that both the FLASH and 3DMSME sequences were able to detect the area-at-risk, however there was a mismatch in size noted between the sequences. The 3DMSME consistently measured a larger area-at-risk when compared with the FLASH sequence; possible explanations for this are discussed henceforth. T_2

sequences have been used clinically to delineate oedema (350, 351), however, there remains considerable controversy regarding the reliability and robustness of this as a measure of area-at-risk (384, 385). Given that MPIO provide excellent negative contrast and remain intravascular they may represent a more reliable method for quantifying area-at-risk. We propose that there may be less ambiguity by measuring regions delineated by MPIO accumulation compared to oedema quantification. Secondly, the FLASH sequence was of higher resolution than the 3DMSME sequence, thus potentially resulting in less partial volume error. Furthermore, T_2-weighted pulse sequences optimized for human imaging do not directly apply to mice due to the use of higher magnetic field strengths and 10-fold greater heart rate in mice compared with humans (379). Beyers et al, developed a T_2-weighted protocol for mice, allowing *in vivo* imaging of area-at-risk, which showed a good correlation with histological measures of area-at-risk (379). The study reported an echo time of 60 ms, which provided a high contrast between normal and oedematous tissue. Thus, this method could also be useful in evaluation area-at-risk *in vivo* however, technically this is very difficult and potentially less accurate compared to our high-resolution ex-vivo imaging techniques.

i. Conclusion

In this study, we describe a high-resolution 3D MRI technique to identify the area-at-risk using MPIO in place of the well-described Evans blue/TTC approach. This method is likely to reduce the potential for measurement error and allow access to high-resolution 3D images of the entire LV. In this study we demonstrated that high-resolution cMRI can provide a quantitative measurement of area-at-risk. This technique has the potential to allow improved robustness and accuracy in quantifying salvageable tissue in models of myocardial IR and may eventually have translational

application. The 3DFLASH sequence with MPIO may represent a more accurate and robust technique when determining the area-at-risk compared to the 3DMSME sequence. Moreover, both T_1 and T_2 maps were able to distinguishing between the non- and infarcted regions.

Limitations

This study had some limitations these are described below:

- The assessment of area-at-risk, infarct size and perfused ROI were based on visual assessment, which has the potential to result in inter-operator and intra-operator variability, this error was not assessed.
- The image segmentation was performed manually with the potential for error in accurately demarking the border zone for the ROI.
- The fixation protocol may have affected the kinetics of Gd binding to the irreversibly injured tissue. The area-at-risk was different for each mouse (planned), although in retrospect it may have been better to aim for a similar area-at-risk between mice.

5.2 Part B: Hexarelin as a cardioprotective agent in ischemic heart disease

5.2.1 Hexarelin treatment preserves myocardial function and reduces cardiac fibrosis in a mouse model of acute myocardial infarction (75)

The results from the following chapter have been published as outlined on page (v)

a. Abstract

Aims: Ischemic heart disease (IHD) is a leading cause of morbidity and mortality worldwide. Growth hormone secretagogues (GHS) have been shown to improve cardiac function in models of IHD. This study aimed to determine whether hexarelin (HEX), a synthetic GHS, preserves cardiac function and morphology in a mouse model of myocardial infarction (MI).

Methods and Results: MI was induced by ligation of the left descending coronary artery in C57BL/6J mice followed by vehicle (VEH; n=16) or HEX (0.3 mg/kg/day; n=16) administration for 21 days. MI-injured and sham mice were subjected to magnetic resonance imaging to measure left ventricular (LV) function, mass and infarct size at 24 hours and 14 days post-MI. MI-HEX mice displayed a significant improvement ($P<0.05$) in LV function compared with MI-VEH mice after 14 days treatment.

A significant decrease in LV mass, interstitial collagen and collagen concentration was demonstrated with chronic HEX treatment, accompanied by a decrease in TGF-β1 expression, myofibroblast differentiation and an increase in collagen-degrading MMP-13 expression levels in MI-HEX mice. Furthermore, heart rate variability analysis demonstrated that HEX treatment shifted the balance of autonomic nervous activity towards a parasympathetic predominance and sympathetic downregulation.

This was combined with a HEX-dependent decrease in troponin-I, IL-1β and TNF-α levels suggestive of amelioration of cardiomyocyte injury.

Conclusion: These results demonstrate that GHS may preserve ventricular function, reduce inflammation and favourably remodel the process of fibrotic healing in a mouse model of MI and hold the potential for translational application to patients suffering from AMI

b. Introduction

Ischemic heart disease (IHD) is a leading cause of morbidity and mortality worldwide (3, 386). A variety of risk factors contribute to the development of heart failure post myocardial infarction (MI) and ultimately cumulate in structural changes within the myocardium leading to left ventricular (LV) dysfunction. A key event in the progression of heart failure is the pathological remodelling of the ventricle secondary to cardiac fibrosis. Cardiac fibrosis has been identified as both a primary and causal driver of disease and has become an important therapeutic target in heart failure patients (12). Stiff fibrotic tissue affects myocardial electrical transmission leading to arrhythmias, contributes to diastolic and systolic dysfunction and can ultimately result in heart failure (12). The mechanisms that underpin the stimulation of cardiac fibrosis are not fully understood and interventions targeting excessive fibrosis as a result of MI are of major therapeutic importance (13, 14).

Growth hormone secretagogues (GHS) have been recently identified as compounds that stimulate growth hormone (GH) release from the pituitary gland through the G protein-coupled receptor (GHS-R) expressed mainly within the pituitary and hypothalamus (25, 387). The endogenous ligand, ghrelin, was originally isolated from the stomach wall in 1999 (26). GHS have many functions other than the control of

GH release. Ghrelin plays a major role in the regulation of systemic metabolism and has been shown to exert a number of central and peripheral actions such as regulation of food intake, control of energy balance, glucose metabolism and insulin release, and stimulation of gastric acid secretion and motility (388, 389). The GHS-R is expressed in many peripheral organs including the stomach, intestine (390), pancreas (391), kidney (392), heart and aorta (393). GHS have been demonstrated to have several cardiovascular effects suggested by the presence of GHS-R on blood vessels and ventricular tissue (149). Hexarelin (HEX), a synthetic hexapeptide belonging to the GHS family has been reported to feature cardiovascular activity and is recognized to be both chemically more stable and functionally more potent than ghrelin (45, 394). The GHS-R appears to mediate the action of HEX (42, 45). The anti-fibrotic effects of GHS have been investigated with promising results in various models of cardiac injury such as doxorubicin cardiotoxicity isoproterenol administration, myocardial infarction and spontaneous or diabetes-associated hypertension (395).

The present study was designed to investigate the therapeutic effects of HEX on myocardial function and cardiac fibrosis using a murine model of MI. Here, we demonstrate a preservation of systolic and diastolic function measured by cardiac magnetic resonance imaging (cMRI) and a HEX-dependent attenuation of cardiac fibrosis . We propose that HEX prevents cardiac fibroblasts from acquiring a pro-inflammatory and fibrogenic phenotype, preventing excessive collagen synthesis and cardiac fibrosis. This may be mediated by HEX's influence on inflammation and the autonomic nervous system evidenced by a reduction in inflammatory cytokines, parasympathetic predominance and sympathetic down-regulation respectively. Thus, the findings of this study indicate that HEX may target fibrotic pathways and preserve LV function in a mouse model of MI.

Animal models of MI:

Ethical approval

All experiments were approved by the Animal Ethics Committee of the University of Queensland and were performed in accordance to national guidelines (Ethics number SBMS/200/13/NHMRC). The investigators understand and comply with the ethical principals of the Journal of Physiology.

MI was induced in 12-14 week old male C57BL/6JArc inbred mice (weight 25-30g) (n=32) (JAX stock number: 000664) by permanent ligation of the left anterior descending coronary artery (LAD). Mice were anaesthetized using a combination of medetomidine (1mg/kg) and ketamine (75mg/kg) administered by intraperitoneal injection, intubated and supported by a small animal ventilator (Harvard Apparatus) with tidal volume and respiratory rate calculated based on body weight (396). Anaesthetic depth was monitored by assessment of the pedal reflex and heart rate by electrocardiographic (ECG) monitoring. A left-sided thoracotomy was performed and the LAD was ligated 2mm below the left auricular appendage using 7-0 Prolene. Successful occlusion was confirmed by visualization of a pallor region in combination with characteristic ECG changes. Sham-operated mice underwent the same procedure excluding ligation of the LAD. The chest was closed using 6-0 polydioxanone and the musculature and cutaneous tissues closed using a 5-0 non-absorbable suture.

After completion of the surgery the mice were administered atipamezole (1mg/kg subcutaneous (SC)), carprofen analgesia (5mg/kg SC) and this was continued once daily for 48 hours post-procedure. A 0.5ml bolus of saline was administered SC on recovery. The mice were recovered in an oxygen- and heat-supplemented environment and then moved to their standard housing consisting of a temperature-

and heat- controlled environment with 12-hour light/dark cycles and provided with free access to food and water *ad libitum* where they remained until the completion of the study.

Hexarelin and vehicle administration:

HEX (0.3 mg/kg/day) or vehicle (VEH) was administered to each mouse SC within the 15-minute period prior to LAD ligation. Similarly, mice undergoing the sham procedure received either VEH or HEX treatment. All mice received their respective treatments once daily throughout the 21-day study period. The HEX dose was chosen based on similar studies by Mao et al (45, 104).

Cardiac Magnetic Resonance Imaging (cMRI):

cMRI was performed at both 24 hours and 14 days post LAD ligation or sham procedure in all animals. Mice were imaged using a 30cm-diameter horizontal bore Bruker Biospec 9.4 Tesla (T) small animal MRI scanner equipped with a BGA 12S HP 660 mT/m gradient set. MRI data was acquired with an 86mm i.d. quadrature transmit coil and a 2x2 phase array receive coil, running Paravision 5.1. (Bruker Biospin, Ettlingen, Germany).

Animal preparation:

Anaesthesia was induced in an induction chamber using 5% isoflurane in 100% medical grade oxygen with a flow rate of 1 L/minute. The mouse was positioned in a purpose-built cradle (Bruker, Germany) and maintained with 1.5-2% isoflurane in 1-2 L/min oxygen via a nose cone. Core temperature was monitored using a rectal probe and maintained with a warm water circulation system incorporated into the animal bed. A SAII Monitoring system (Small Animal Instruments, NY, USA) was used to measure ECG, using a 3-lead system with surface Ag-AgCl electrodes and respiration

was monitored with a pressure-transducer, from which a respiratory gating signal could be derived.

cMRI Protocol:

Gadopententate dimeglumine (Gd-DTPA) (0.3 mmol/kg Magnevist, Bayer, Germany) was administered by intravenous (IV) infusion into the lateral tail vein of the mouse. Following standard pre-scan calibration, 2- and 4-chamber view scout scans were acquired, from which a single mid-cavity short-axis slice was planned. Cine imaging was performed with a retrospectively-triggered (self-gated) INTRAGATE gradient-echo sequence (338), with the following parameters: TR = 5.6 ms, TE = 2.6 ms, flip angle = 10 degrees, number of movie frames = 20, slice thickness = 1mm, matrix =512 x 512, field-of-view (FOV) = 4 x 4 cm^2. This resulted in 78 x 78 um in-plane resolution, with ~5mins acquisition per slice. Seven to nine short-axis slices with no slice gap were acquired to cover the heart from apex to base. Late gadolinium enhancement (LGE) images in the slice locations described above were acquired 10-15 minutes after IV Gd-DTPA and assessed for LGE.

Determination of cardiac functional parameters and LV mass:

MRI images, in DICOM format, were processed with Osirix (340) software. The end-diastolic and end systolic phases were identified on a slice-by-slice basis and both the endocardial and epicardial borders were traced. The LV end systolic volume (ESV), end diastolic volume (EDV), stroke volume (SV) and ejection fraction (EF) were computed from the traced borders and LV mass was obtained by multiplying the volume by the specific gravity of 1.05 g/cm^3 (341).

Determination of infarct volume:

The LGE images were windowed to maximise the signal from the hyperintense region and null that from the non-enhanced region. Manual planimetry was performed on

each slice and the hyperintense region and total LV myocardial area was calculated. Slice hyperintense areas were multiplied by the slice thickness and summed to calculate the infarct volume as a percentage of LV myocardial volume.

Measurement of the chronic infarct: midline length measurement:

In addition to infarct volume, the infarct length was quantified, 14 days post-MI, using an alternative cMRI approach described as a "midline-length measurement". This technique was modified from Takagawa et al (342). Briefly, the *midline infarct length* was determined by measuring the midline length of the infarct that included 50% of the whole thickness of the myocardial wall. The LV myocardial midline was measured as a *midline circumference*. All measurements were taken in diastole. Infarct size was calculated by dividing the sum of midline infarct length from all sections by the sum of the midline circumference from all sections and multiplying by 100.

Post mortem measurement of Infarct size:

At the endpoint of the study mice were euthanized by cervical dislocation. In a subset of mice, the hearts were rapidly excised, trimmed of extracardiac tissue and flushed with saline to remove any remaining blood. Hearts were fixed in OCT compound at -20°C for 15 minutes and transected into 6-8 short axis slices of 1mm thickness using a Zivic Mouse Heart Slicer Matrix (Zivic Instruments). Slices were thawed and immersed in 1% triphenyl tetrazolium chloride (TTC) in PBS at 37°C for 20 minutes whilst being constantly agitated. The slices were fixed in 10% neutral-buffered formalin overnight and each slice photographed on each side with a digital camera mounted on a stereomicroscope (Nikon C51). Manual planimetry of viable and non-viable tissue was performed using ImageJ (397). Specifically, the total LV area and

MI were manually traced for each image and MI size was determined as a percentage of LV mass.

Histology and morphometric analysis:

Serial paraffin-embedded LV sections from each group of mice studied were stained with 0.1% picrosirius red to detect interstitial collagen deposition. Additional serial LV sections from each corresponding group of mice studied were immunohistochemically stained for selected markers associated with collagen turnover; utilizing polyclonal antibodies to transforming growth factor (TGF)-β1 (sc-146; 1:200 dilution; Santa Cruz Biotechnology Inc., Santa Cruz, CA, USA) and matrix metalloproteinase (MMP)-13 (the predominant collagenase in mice; ab75606; 1:100 dilution; Abcam; Redfern, NSW, Australia); or a monoclonal antibody to α-smooth muscle actin (α-SMA; a marker of myofibroblast differentiation; M0851; 1:250 dilution; DAKO Antibodies, Carpinteria, CA, USA). Detection of primary antibody staining was detected using DAKO Envision anti-rabbit or ARK biotinylation kits, respectively, and 3,3-diaminobenzidine. Morphometric analysis of picrosirius red- and immunohistochemically-stained sections was performed using Aperio software (Leica Biosystems, North Ryde, NSW, Australia) on whole tissue sections per mouse. In each case, the percentage staining of each marker analysed per section was derived and expressed as the fold changes relative to the SHAM-VEH group, which was expressed as 1.

Hydroxyproline analysis:

Equivalent frozen portions of LV tissue from each animal studied were lyophilized to dry weight measurements before being hydrolysed in 6M hydrochloric acid for determination of their hydroxyproline content, as described previously (333). Hydroxyproline values were converted to collagen content by multiplying by a factor

of 6.94 (based on hydroxyproline representing approximately 14.4% of the amino acid composition of collagen in most mammalian tissues (334), further expressed as a percentage of the tissue dry weight (to yield collagen concentration), and finally expressed as the relative change, compared to the SHAM-VEH group (which was expressed as 1).

Heart rate variability analysis:

Heart rate variability (HRV) analysis was performed 21 days after MI or sham procedure. ECG signals were recorded using a physiological analysing system (Bio Amp, AD Instruments, CA, USA). Mice were anaesthetized with isoflurane and ECG signals were recorded for a minimum of 20 minutes after heart rate stabilization. Using a technique described in (335); autonomic nervous system function was examined by power spectral analysis of HRV (LabChart Pro 7.0, ADInstruments, Australia). Heart rate was used to generate a power spectral density curve using a fast Fourier transformation. The area under the curve was calculated for the very-low-frequency (VLF: 0-0.15Hz), low-frequency (LF: 0.15-1.5Hz), and high-frequency (HFr: 1.5-5Hz) band, based on previous studies (335). From these, the parameters: LF, HFr, normalized LF power (nLF), normalized HF power (nHFr), and ratio of LF to HFr power (LF/HFr) were calculated as described in (88).

Cytokine and Troponin-I determination:

Blood samples were collected from mice at both 24 hours and 21 days after the procedure. The blood was allowed to clot appropriately and samples were centrifuged for serum removal and stored at -80^0 C until assayed. The serum concentrations of troponin-I (cTnI), interleukin (IL)-1β, IL-6 and tumor necrosis factor (TNF)-α were measured using a MILLIPLEX® map assay according to the manufacturer's instructions (Merck Millipore).

Statistical analysis

Data expressed as the mean +/- SEM or relative mean +/- SEM. Statistical analysis was performed using GraphPad Prism 7. Differences between groups were analysed by one-way ANOVA using either a Bonferroni or Newman Keuls post-hoc test to allow for multiple comparisons between groups. Unpaired *t*-test was applied to comparisons between two groups. $P < 0.05$ was considered statistically significant.

d. Results

cMRI measurement of cardiac function:

LVEF, EDV, ESV:

There was a significant reduction in EF in MI-VEH and MI-HEX mice 24 hours post LAD occlusion. However, a trend towards a preservation of EF was observed in the MI-HEX group compared with the MI-VEH group (Fig. 47A). After 14 days treatment, HEX treatment significantly improved EF compared to MI-VEH mice (HEX: 49.25% +/- SEM 2.3; VEH: 36.96%+/- SEM 3.82) (Fig. 47B).

The MI-VEH group showed a significant increase in EDV 24 hours post-MI. These changes were completely reversed with 14 days of HEX treatment (Fig. 47C). LV ESV was also significantly elevated after 14 days in the MI-VEH group, which again was entirely reversed with HEX treatment (Fig. 47D). These results suggested that HEX treatment may preserve both systolic and diastolic function post-MI.

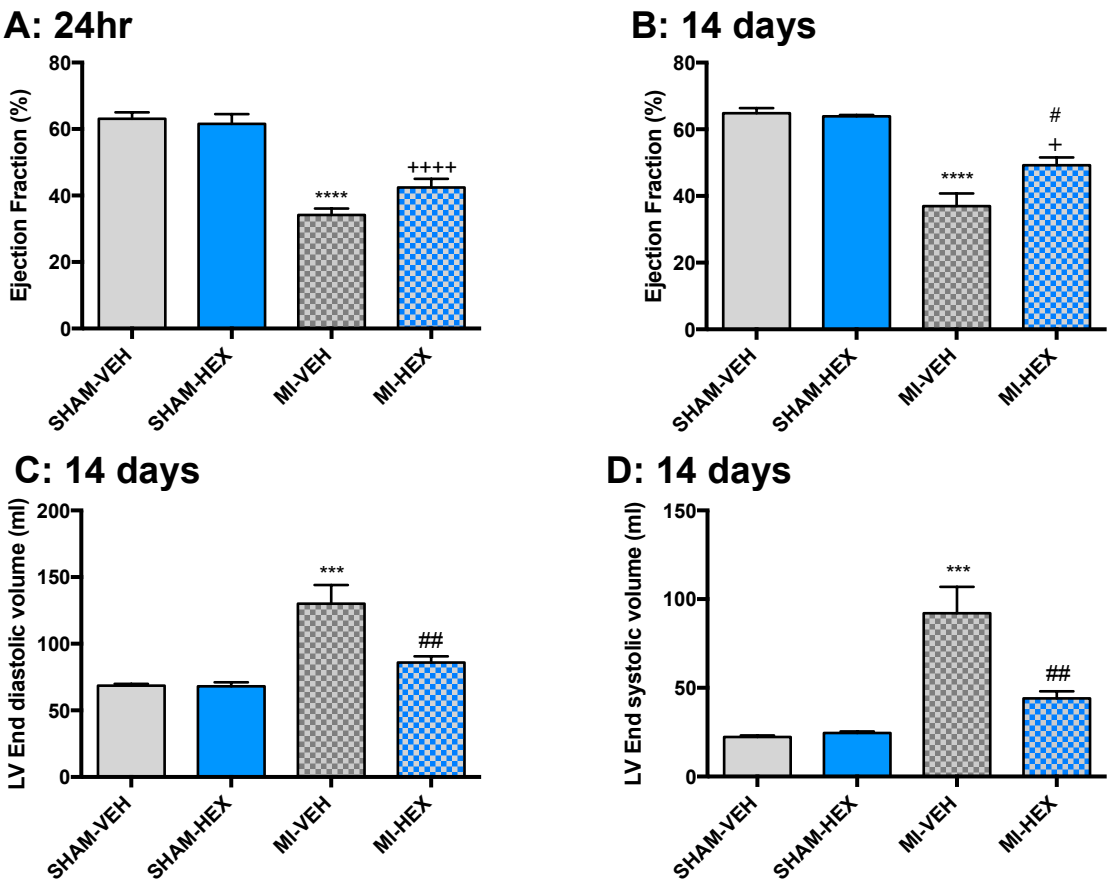

Figure 47: Cardiac functional parameters measured by cMRI:
Ejection fraction (%), LV end-diastolic volume, LV end-systolic volume measured post-MI/sham procedure with or without HEX treatment.
(A). EF 24 hours post-procedure, (SHAM-VEH (n=5), SHAM-HEX (5), MI-VEH (7), MI-HEX (7)); **(B).** EF 14 days post-procedure (n=6/5/10/11); **(C).** LV EDV 14 days post-procedure (n=6/5/10/11); **(D).** LV ESV 14 days post-procedure (n=6/5/10/11).
Data in all figures expressed as mean ± SEM; $^{***}p<0.001$, $^{****}p<0.0001$, versus SHAM-VEH group; $^{\#}p<0.05$, $^{\#\#}p<0.01$, versus MI-VEH group; $^{+}p<0.05$, $^{++++}p<0.0001$, versus SHAM-HEX group.
cMRI, cardiac magnetic resonance imaging; EDV, end diastolic volume; ESV, end systolic volume.

Infarct assessment:

Infarct volume was determined using cMRI and manual planimetry to calculate infarct volume as a percentage of LV myocardial volume (IV%) after 24 hours. Both treatment groups exhibited observable infarction after 24 hours (Fig. 48Aa,b), there was no significant difference in IV% between MI-HEX and MI-VEH treated groups

at this time point (Fig. 48B). This was confirmed by TTC staining in a subset of animals post mortem.

Following 14 days of permanent LAD ligation, VEH and HEX-treated mice exhibited observable myocardial infarction as assessed by LGE. Infarct volume was significantly reduced (3-fold) following HEX treatment (HEX 6.13 +/- 1.11; VEH: 15.21 +/- SEM 2.63) (Fig. 48C). Similarly, when infarct size was assessed using the midline-length measurement approach using cMRI, a significant reduction in infarct midline-length was observed following HEX treatment (Fig. 48D). The midline-length measurement for MI-VEH mice was 2-fold greater than that assessed by the volume approach. In chronic infarcts, the length-based approach has been demonstrated to measure the extent to which the infarct scar radially covers the wall of the LV, without being influenced by thinning of the wall, thus this is likely to explain the different values obtained by the two measurement approaches. The midline-length approach may represent a superior measure to assess chronic infarcts (342).

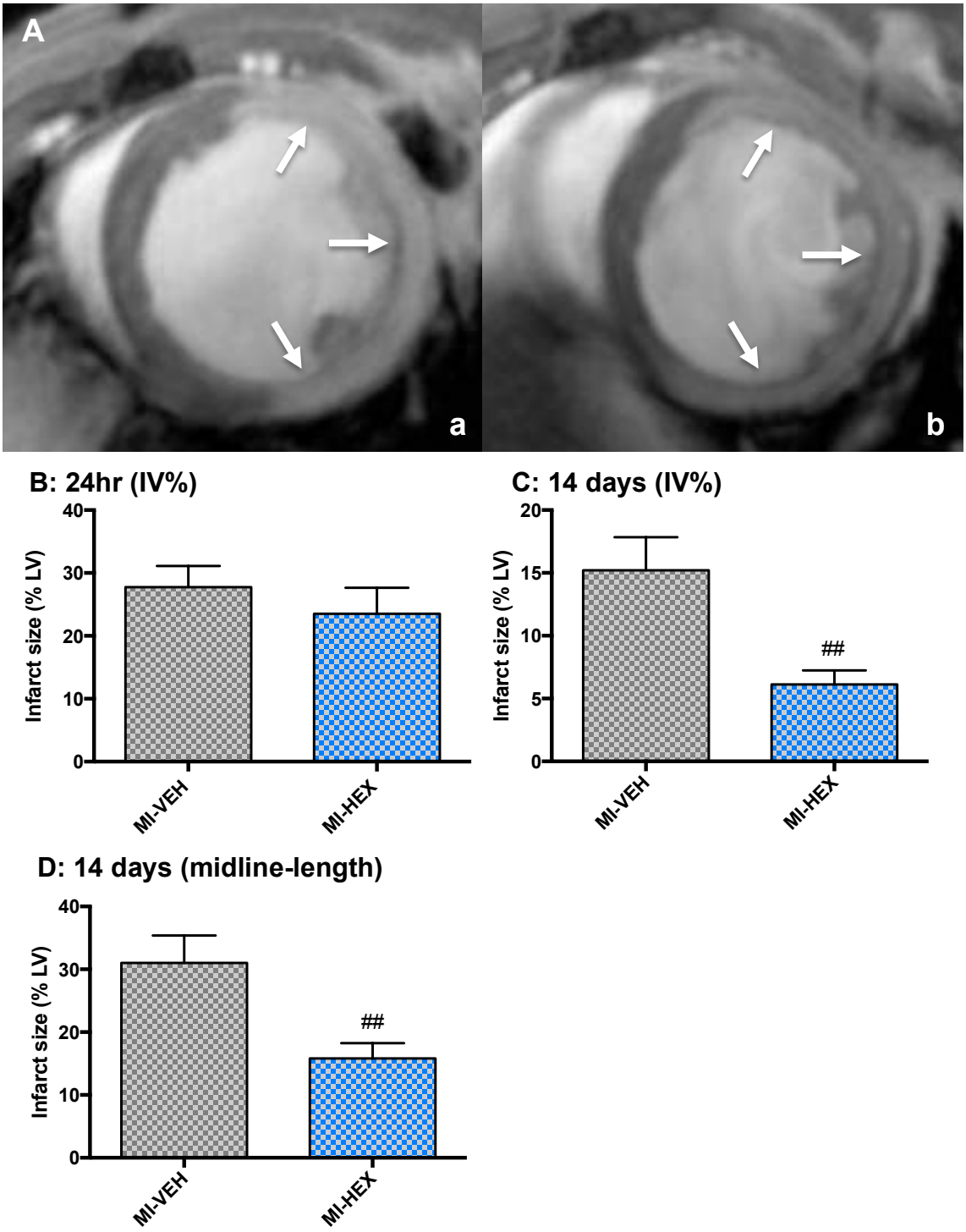

Figure 48: Infarct size measured by cMRI.
(A). Representative LGE images acquired using a T_1-weighted INTRAGATE gradient-echo sequence 24 hours post LAD ligation. The hyperintense region represents the infarcted tissue (indicated by white arrows); **(a).** HEX-treated **(b).** VEH-treated.
(B). Myocardial infarct size assessed 24 hours post-MI (IV%), (n=7/7).
(C). Myocardial infarct size 14 days post-MI, infarct size assessed via IV% approach, or **(D).** via midline-length approach, (n=10/10)
$^{\#\#}P<0.01$ versus MI-VEH group.
IV%, Infarct volume %.

LV size:

LV myocardial mass was determined using cMRI 24 hours and 14 days post-procedure. There was a significant difference in mass between MI-VEH and the respective SHAM-VEH group after 24 hours, while this was not apparent within the MI-HEX group. At this acute time point, there is unlikely to be any significant effect on remodelling but it is thought that these changes may reflect differences in inflammation and/or oedema **(**Fig. 49A). Cardiac mass was significantly elevated after 14 days in the MI-VEH group. This increase was entirely reversed by HEX treatment (Fig. 49B).

To further evaluate cardiac hypertrophy, heart weight (HW) was compared 21 days post-procedure. Tibial length (TL) was used as an adjustment factor as body weight and growth tendencies were found to depend on whether MI or sham operation was performed (45). HW/TL ratios did not differ between the two sham groups. The MI-VEH HW/TL was significantly higher than the SHAM-VEH group. There was a trend towards a decreased HW/TL ratio in the MI-HEX group compared with the MI-VEH group (Fig. 49C). Thus the HW/TL results were consistent with our cMRI myocardial mass data.

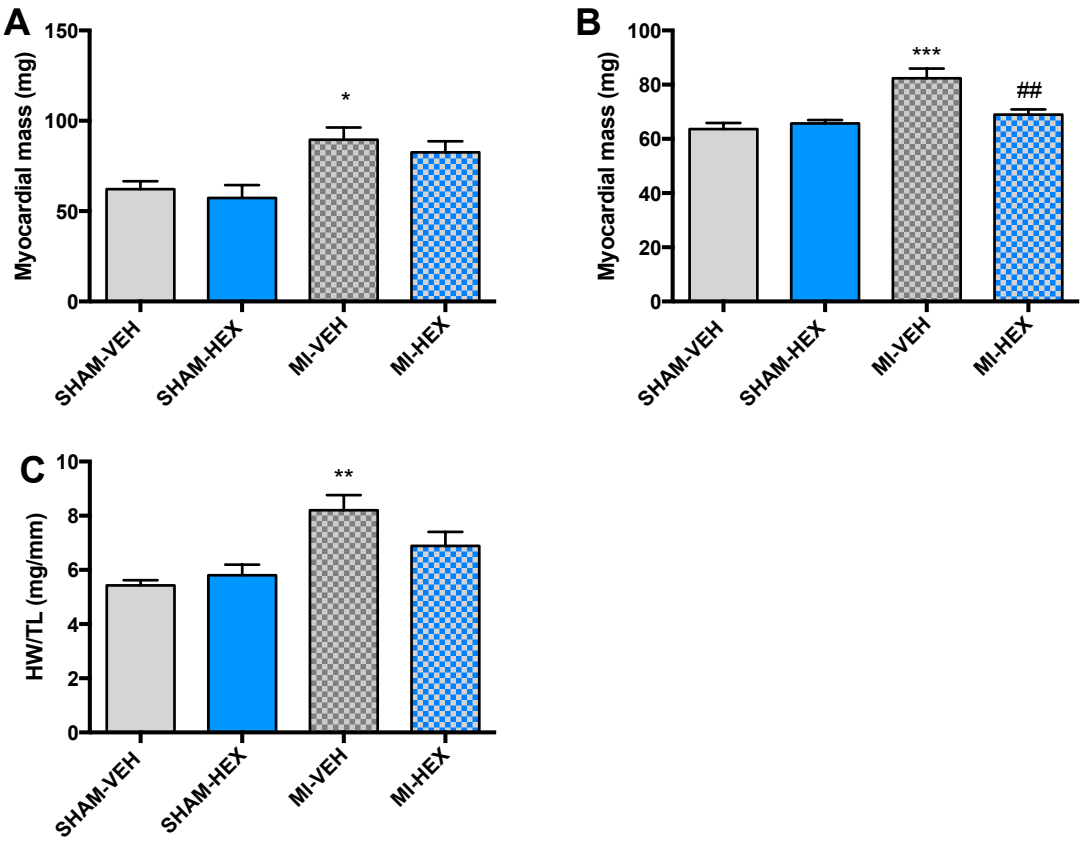

Figure 49: Assessment of LV mass and heart weight.

LV myocardial mass (mg) assessed by cMRI after: **(A).** 24 hours, (SHAM-VEH/HEX (5), MI-VEH/HEX (7)); **(B).** 14 days post-MI/sham procedure with or without HEX treatment, (n=6/5/10/11).
(C). Heart weight compared 21 days post-procedure. Tibial length (TL) was used as an adjustment factor, (n=6/5/5/6).
$^{*}p<0.05$, $^{**}p<0.01$, $^{***}p<0.001$, versus SHAM-VEH group; $^{\#\#}p<0.01$, versus MI-VEH group.
TL, tibial length.

The effect of HEX on MI-induced cardiac remodelling:

To determine the effect of HEX on LV fibrosis in MI, mice were treated with HEX or VEH daily for 21 days.

LV collagen deposition:

Picrosirus red staining of the myocardium was used to detected changes in interstitial collage deposition and was markedly increased in the MI-VEH group compared to that from the SHAM-VEH group. The presence of HEX (MI-HEX) was seen to almost completely reverse the aberrant post-infarct interstitial collagen deposition

measured compared with the MI-VEH group (Fig. 50A). Left ventricular collagen deposition assessed by hydroxyproline analysis was also significantly higher in MI-VEH mice compared to their SHAM-VEH counterparts, while chronic treatment with HEX resulted in almost a 2-fold reduction in LV collagen concentration (Fig. 50B).

TGF-β1, α-SMA, MMP-13:

LV TGF-β1 (Fig. 50C) and α-SMA-associated myofibroblast (Fig. 50D) immunostaining was significantly increased; while LV MMP-13 staining (Fig. 50E) was significantly reduced in MI-VEH mice compared to that measured in SHAM-VEH mice.

HEX (MI-HEX) therapy normalized the aberrant MI-induced increase in TGF-β1 (Fig. 50C) and α-SMA (Fig. 50D) expression, and increased MMP-13 levels to 6-fold of that measured in the MI-VEH group (Fig. 50E). These results suggested that HEX had a regulatory effect on cardiac remodelling and cardiac fibrosis post-MI.

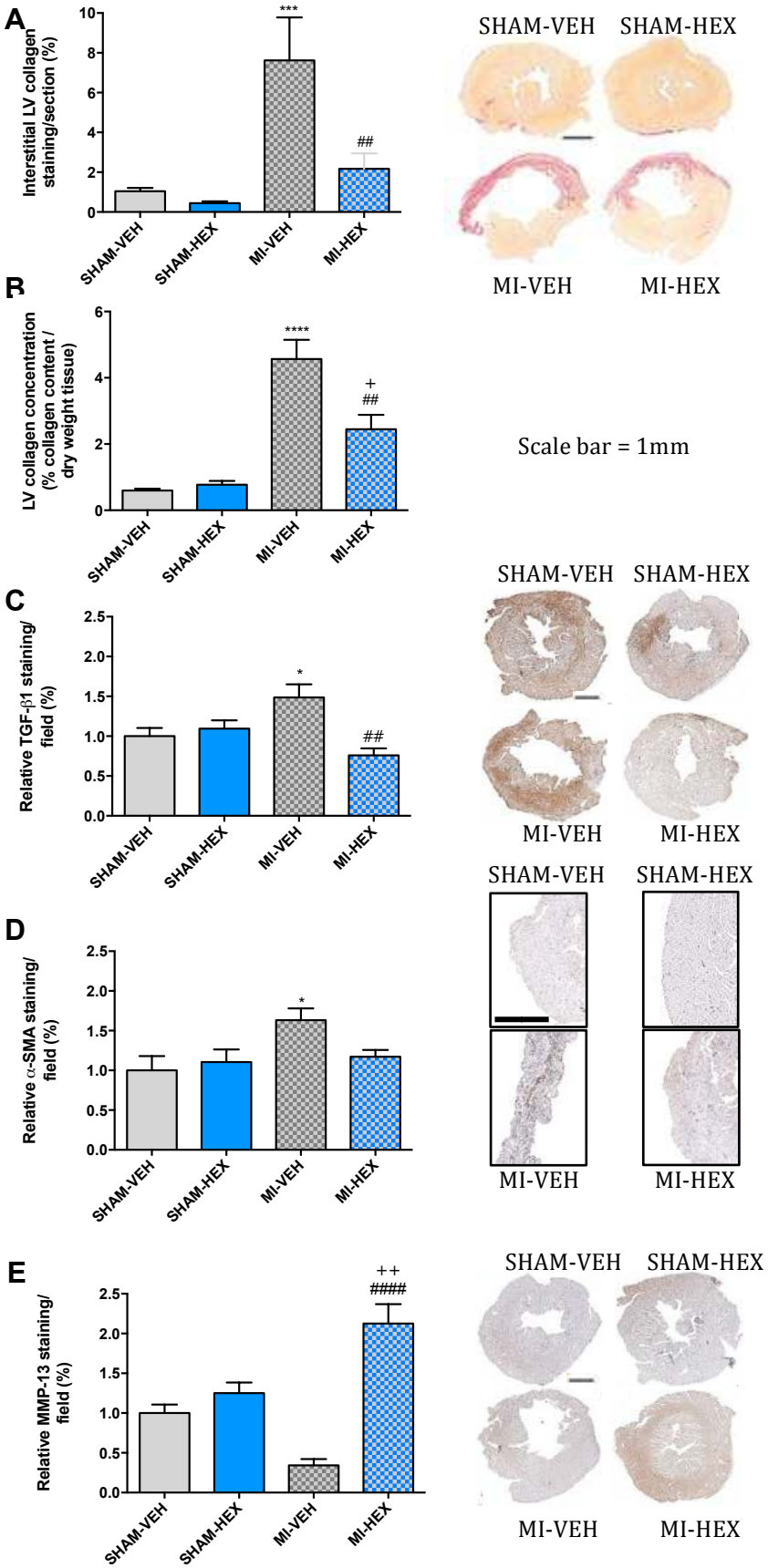
A
Interstitial LV collagen staining/section (%)
10
8
6
4
2
0
***
##
SHAM-VEH
SHAM-HEX
MI-VEH
MI-HEX
SHAM-VEH
SHAM-HEX
MI-VEH
MI-HEX
B
LV collagen concentration (% collagen content / dry weight tissue)
6
4
2
0
****
+
##
SHAM-VEH
SHAM-HEX
MI-VEH
MI-HEX
Scale bar = 1mm
C
Relative TGF-β1 staining/ field (%)
2.5
2.0
1.5
1.0
0.5
0.0
*
##
SHAM-VEH
SHAM-HEX
MI-VEH
MI-HEX
SHAM-VEH
SHAM-HEX
MI-VEH
MI-HEX
D
Relative α-SMA staining/ field (%)
2.5
2.0
1.5
1.0
0.5
0.0
*
SHAM-VEH
SHAM-HEX
MI-VEH
MI-HEX
SHAM-VEH
SHAM-HEX
MI-VEH
MI-HEX
E
Relative MMP-13 staining/ field (%)
2.5
2.0
1.5
1.0
0.5
0.0
++
####
SHAM-VEH
SHAM-HEX
MI-VEH
MI-HEX
SHAM-VEH
SHAM-HEX
MI-VEH
MI-HEX

Figure 50: Histology and morphometric analysis.
(A). Interstitial LV collagen content measured by picrosirus red staining, (n=6/5/6/7); **(B).** LV collagen concentration, measured by hydroxyproline analysis, (n=6/5/4/7); **(C).** TGF-β1 (6/5/5/6), **(D).** α-SMA (5/6/5/7) and **(E).** MMP-13 immunohistochemistry staining (n=6/5/5/6) measured 21 days post-MI/sham procedure with or without HEX treatment.
The right column displays representative sections from each treatment group corresponding to the selected markers and methods described above.
$^{*}p<0.05$, $^{***}p<0.001$, $^{****}p<0.0001$, versus SHAM-VEH group; $^{\#\#}p<0.01$, $^{\#\#\#\#}p<0.0001$, versus MI-VEH group; $^{+}p<0.05$, $^{++}p<0.05$; versus SHAM-HEX group

Troponin-I and Cytokine Measurements:

There was a 3-fold increase in cTn-I after 24 hours in the MI-VEH group compared with the MI-HEX group (VEH 40697pg/ml +/- SEM 7568; HEX 13200pg/ml +/- SEM 7551). HEX treatment was found to significantly prevent the rise in cTnI (Fig. 51A). There was no significant difference in cTnI between the MI-VEH and MI-HEX group after 21 days but a trend towards a reduction in cTnI was maintained in the MI-HEX group.

In MI-VEH mice, serum TNF-α (Fig. 51B) and IL-1β (Fig. 51C) were significantly increased 24 hours post-MI compared to SHAM-VEH counterparts and there was a trend towards increased IL-6 levels (Fig. 51D). The acute MI-induced aberrant increase in TNF-α (VEH 9.94pg/ml +/- SEM 0.38; HEX 4.63pg/ml +/- SEM 1.6) (Fig. 51A) and IL-1β (VEH 9.21pg/ml +/- SEM 2; HEX 4.47pg/ml +/- SEM 0.6) (Fig. 51B) was normalized by HEX (MI-HEX) treatment, while IL-6 levels were unaffected by HEX administration (Fig. 51C). In comparison, there were no differences noted in cytokine levels between MI-HEX and MI-VEH-treatment at the 21-day time point (data not shown).

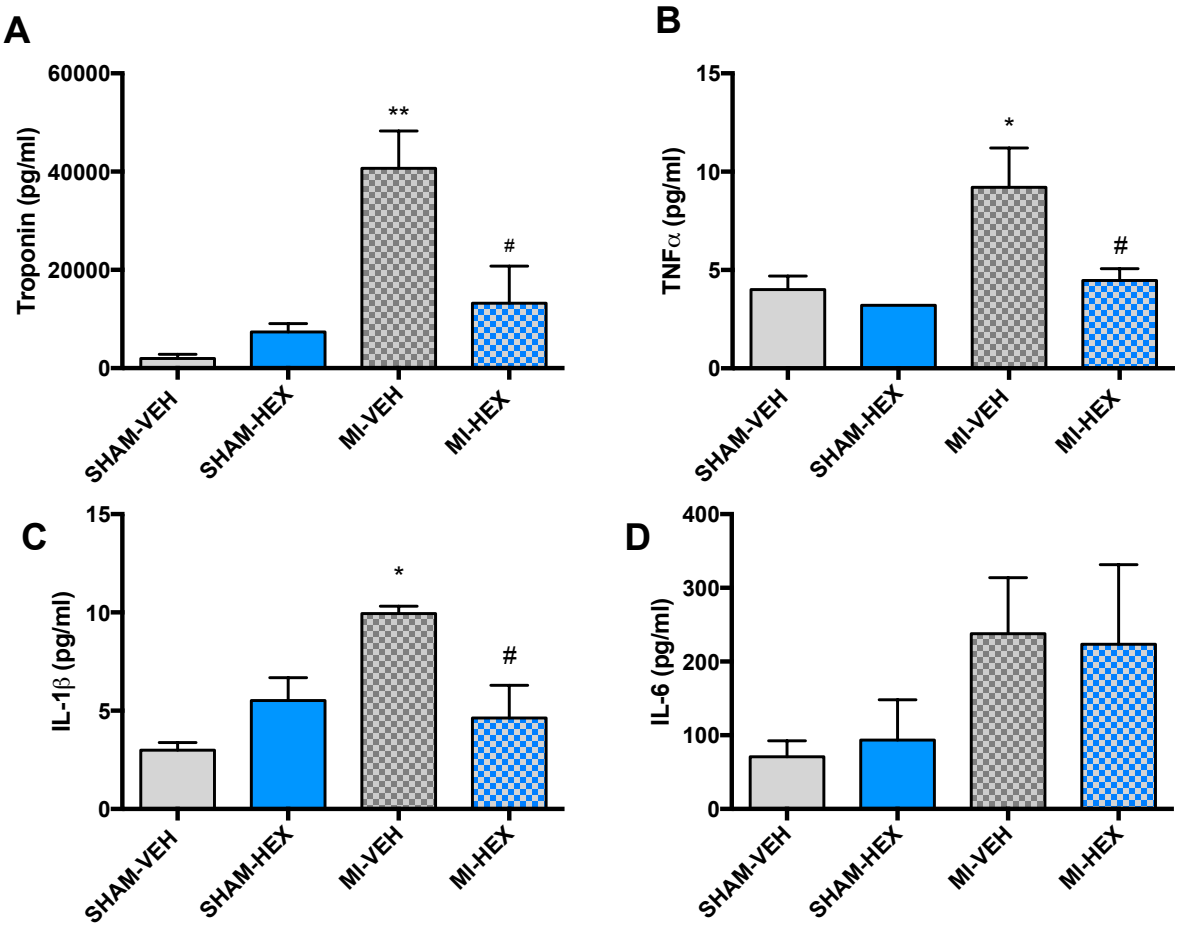

Figure 51: Serum assessment of: **(A).**Troponin-I (pg/ml) (n=4/4/5/5); **(B).** TNF-a (pg/ml) (n=4/4/4/4); **(C).** IL-1b (pg/ml) (n=3/3/4/5); **(D).** IL-6 (pg/ml) (n=4/4/5/4). Serum levels assessed 24 hours post-MI/sham procedure with or without HEX treatment.
$^{*}p<0.05$, $^{**}p<0.01$, versus SHAM-VEH group; $^{\#}p<0.05$, versus MI-VEH group.

Heart rate variability (HRV):

HRV was examined 21 days after sham operation or permanent LAD occlusion. HRV analysis is considered a sensitive, non-invasive, indirect measure of cardiac autonomic tone that has been extensively validated (335, 398). LF/HFr is used to represent cardiac sympathetic nervous activity (SNA), whereas nHFr represents parasympathetic nervous activity (PNA) (335). LF/HFr was markedly increased (Fig. 52A) while nHFr was significantly reduced (Fig. 52B) in MI-VEH mice compared to that measured from their SHAM-VEH counterparts. HEX-treatment (MI-HEX group)

normalized the MI-induced loss of nHFr and increase in LF/HFr (Fig. 52) back to that measured in SHAM-VEH mice, thereby indicating a simultaneous enhancement in PNA and reduction in sympathetic tone.

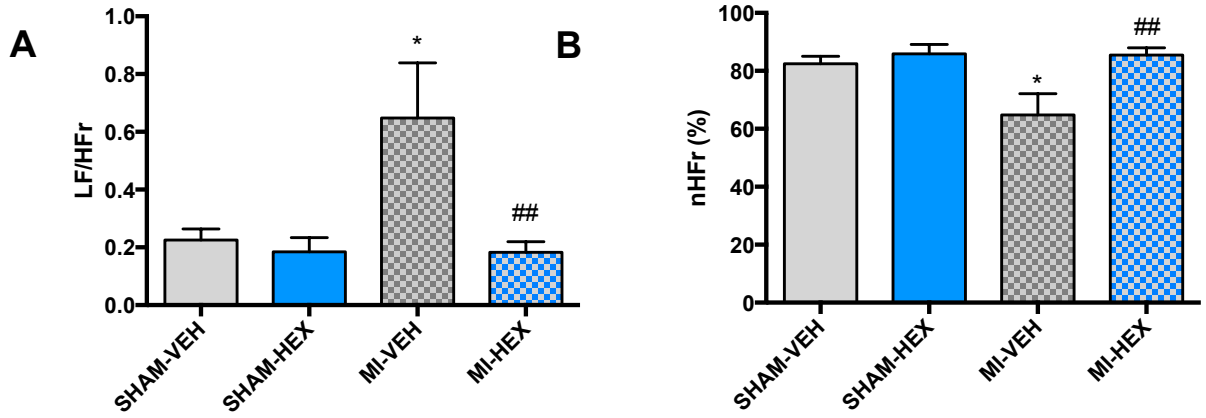

Figure 52: Heart rate variability analysis.
Electrocardiographic data recorded 21 days post-MI/sham procedure with or without HEX treatment. **(A):** Sympathetic nerve activity represented by low-frequency power (LF/HFr), (n=4/5/4/8). **(B):** Parasympathetic nerve activity represented by high-frequency power (nHFr), (n=4/5/4/8).
$^{*}p<0.05$, versus SHAM-VEH group; $^{\#\#}p<0.01$, versus MI-VEH group.
HF, high frequency; LF, low frequency; nHF, normalized high frequency power.

e. Discussion

In this study we have demonstrated that HEX treatment can preserve cardiac function and tissue characteristics in mice after acute MI. This was shown by an improvement in systolic and diastolic function, a lower cardiac mass and HW/TL ratio in MI-injured mice after chronic HEX therapy. One of the major findings of this study was the ability of HEX to significantly reduce measures of cardiac fibrosis after MI. The anti-fibrotic properties of HEX may be associated with an underlying anti-inflammatory mechanism, indicated in this study by a decrease in the proinflammatory cytokines TNF-α and IL-1β and significant reduction in cTnI levels.

Furthermore, this treatment was seen to shift the balance of autonomic nervous system activity towards a parasympathetic predominance as evidenced by a lower LF/HFr ratio and higher nHFr measured by HRV analysis.

HEX administration has been demonstrated to result in marked protection against myocardial stunning with almost complete recovery of LV function post-reperfusion in senescent rats. A simultaneous reduction in creatine kinase concentration suggested HEX-mediated preservation of cardiomyocyte integrity (399). Locatelli et al, concluded that short-term pre-treatment with HEX counteracted ischemic damage in perfused hearts of hypophysectomised rats mediated through cardiac-specific receptors and independent of GH-release (400). The effect of HEX was investigated in normal subjects and in patients with severe GH deficiency with similar conclusions (401). Specifically, a similar increase in LVEF was seen after HEX treatment in: normal subjects, patients with ischemic cardiomyopathy and those with severe GH deficiency, this was independent of GH-release. Interestingly, in this study, acute IV administration of HEX had a positive inotropic effect in patients with ischemic cardiomyopathy-induced severe LV dysfunction but failed to stimulate heart contractility in patients with severe LV dysfunction due to dilated cardiomyopathy (401).

Cardiac fibrosis and remodelling

After myocardial injury, multiple neurohormonal factors and cytokines drive changes in cardiomyocytes and fibroblasts that collectively result in cardiac remodelling (12) (Fig. 53). MI leads to progressive ventricular remodelling, increased myocardial wall stress and ultimately results in heart failure (126). During ventricular remodelling, collagen, the main component of the extracellular matrix (ECM) increases. If sustained increases in wall stress exceed that of the compensatory capacity of the

heart, degradation of the extracellular matrix and alterations of the collagen network progressively result in alterations of LV morphology and function. Continued accumulation of collagen impairs diastolic function and compromises systolic mechanisms (14).

The anti-fibrotic effects of GHS have been investigated in various models of cardiac injury (42, 395). Interventions targeting excessive fibrosis as a result of MI are of major therapeutic importance in the treatment of heart failure (13, 14). HEX treatment may allow normalization of wall stress and preservation of diastolic and systolic function, helping to prevent changes in ventricular wall and chamber dimensions. In this study, HEX therapy blunted changes in LV mass and significantly reduced interstitial LV collagen content and collagen concentration. These findings represent the therapeutic potential of HEX to alleviate degenerative hypertrophic adaptive changes leading to LV dysfunction.

Inflammation and remodelling

HEX has been demonstrated to protect cardiomyocytes against angiotensin (AT)-II-induced apoptosis by inhibiting activation of caspase-3, Bax mRNA expression and increasing the expression of Bcl-2 (402). In addition to inhibition of apoptosis, anti-inflammatory strategies may represent another therapeutic approach to mitigate cardiac fibrosis. Timely activation of the endogenous pathways that inhibit inflammation is important to prevent the catastrophic consequences of uncontrolled inflammation on cardiac geometry and function post myocardial infarction (12). Induction of pro-inflammatory cytokines, such as IL-1 and TNF-α play an important role in acquisition of a pro-inflammatory phenotype by cardiac fibroblasts during the early stages following MI and have been demonstrated to play a role in cardiac

remodelling and progression of heart failure (70). This study demonstrated the ability of HEX to reduce the presence of serum IL-1β and TNF-α in a model of MI (Fig. 51).

Sustained presence of inflammatory cytokines leads to activation of MMPs and results in ventricular dilation through slippage of collagen (73). Our data suggests that HEX may increase the degradation of collagen through increased MMP activity demonstrated by an increase in MMP-13 expression after chronic HEX treatment. Xu et al. also observed similar findings in a study where spontaneously hypertensive rats were treated with HEX (403). In this study, treatment resulted in a significant reduction in cardiac fibrosis, attenuation of LV hypertrophy, diastolic dysfunction and reduced blood pressure. HEX increased MMP-2 and MMP-9 activity and decreased myocardial mRNA expression of TIMP1 suggesting an increased degradation of collagen (403). Thus, we propose that HEX may reverse the mechanisms that lead to progressive LV dysfunction, at least in part, through inhibition of the inflammatory response and regulation of collagen turnover.

Myofibroblast activation

Compared with cardiomyocytes, cardiac fibroblasts are much less vulnerable to oxidant stress following coronary occlusion (404). Given their resistance to ischemic death, location and abundance within the cardiac interstitium, fibroblasts are ideally suited to sense microenvironmental alterations following myocardial injury and initiate the inflammatory response (405). *In vitro*, the response of cardiac fibroblasts to hypoxia is the acquisition of a pro-inflammatory and fibrogenic phenotype characterized by myofibroblast transdifferentiation, enhanced cytokine expression and collagen synthesis (406). It has been suggested that there is direct involvement of fibroblasts in activation of the inflammatory reaction post-infarction (405). TGF-β1

expression is markedly augmented following infarction and has been found to have profound effects on fibroblast phenotype and function, inducing myofibroblast trans-differentiation, upregulating matrix protein synthesis and stimulating the synthesis of protease inhibitors such as TIMP-1 (12, 407). Our study demonstrated a significant reduction in α-SMA expression in HEX-treated mice in combination with a decrease in TGF-β1. This suggests decreased activation of myofibroblasts secondary to a HEX-mediated reduction in TGF-β1 and inflammatory cytokines. Preventing TGF-β1 activation in a myofibroblast-specific manner has promising therapeutic perspectives and HEX may represent a novel pharmacological agent to target this pathway.

Extensive evidence also suggests a crucial role of the renin-angiotensin aldosterone (RAAS) system in activation of infarct myofibroblasts (12). The fibrogenic effects of the RAAS are mediated, at least in part, through activation of growth factors such as TGF-β1 (408). HEX has been shown to suppress ATII and TGF-β1-induced cardiac fibroblast proliferation and collagen synthesis in cultured rat cardiac fibroblasts (409). Our study demonstrated a significant reduction in TGF-β1 expression in HEX-treated mice. Thus suggesting that HEX's ability to influence post-infarct fibrotic healing may involve the ability to suppress the expression and effect of pro-fibrotic factors (such as TGF-β1), that promote fibrogenesis; inhibit myofibroblast differentiation and myofibroblast-induced collagen synthesis; and augment MMP-13-induced collagen breakdown. The combined actions of which favour a net reduction in aberrant collagen content.

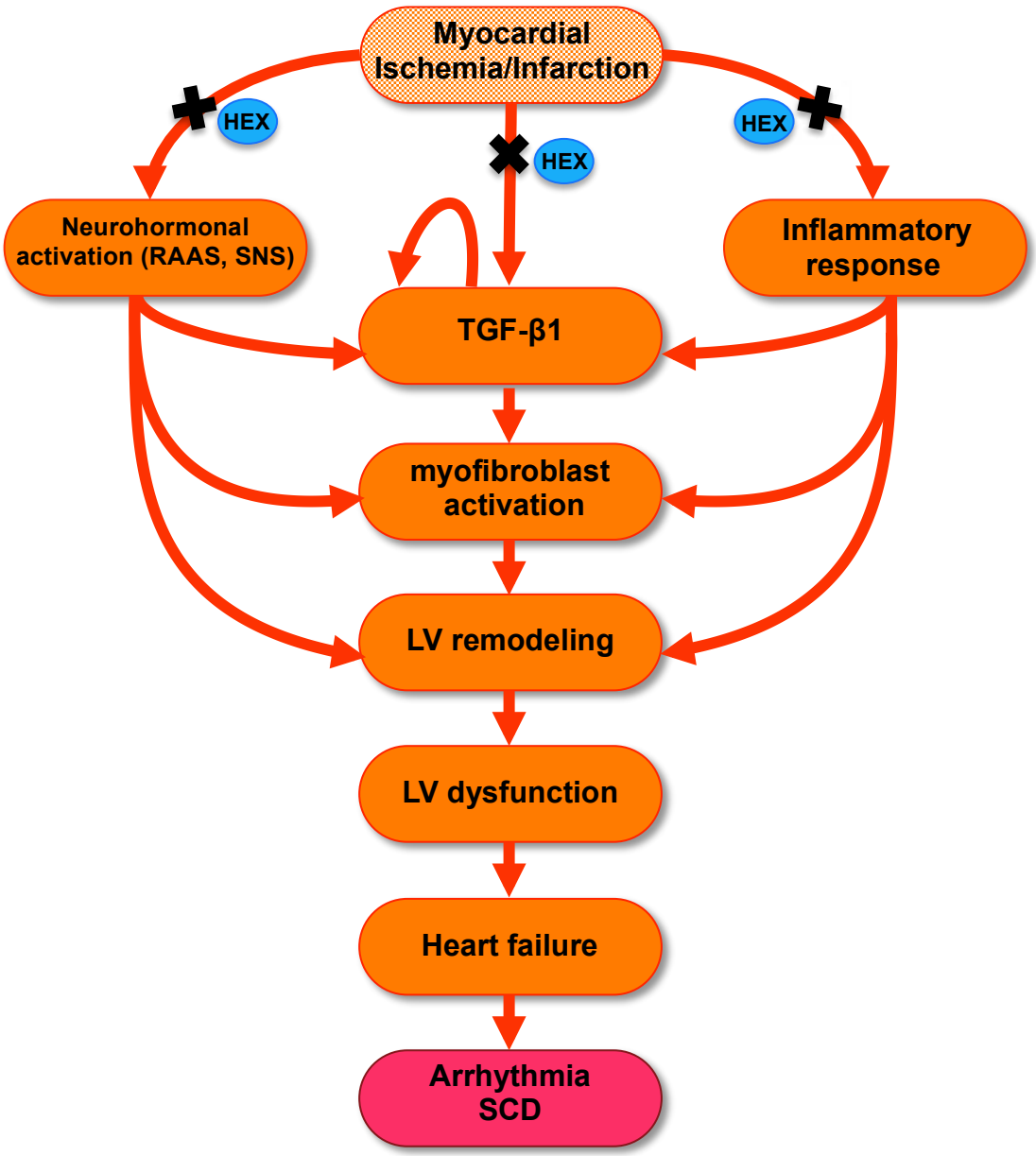

Figure 53: Hexarelin: proposed mechanisms of action (see text):
MI induces dynamic alterations in fibroblast phenotype, initiates an inflammatory response and activates neurohormonal pathways that collectively result in cardiac remodelling, mechanical dysfunction and electrical disturbances in the failing heart, increasing the risk of sudden cardiac death (SCD) (12).
TFG-β1 is markedly augmented following MI and is the most potent profibrotic cytokine known, causing excessive extracellular matrix production, inducing its own secretion and driving myofibroblast activation (12). Inflammatory cytokines exert potent pro-inflammatory actions on cardiac fibroblasts & can negatively affect LV function. Similarly, the RAAS & SNA play a critical role in activation of myofibroblasts and influence LV remodelling & dysfunction (12, 67).
HEX may attenuate and actively reverse cardiac remodelling and myocardial fibrosis by targeting these pathways (indicated by "x") and thus holds promise in returning the failing heart to a functional state.
RAAS, renin angiotensin aldosterone system; SNA, sympathetic nervous activation.

Autonomic nervous system

It is well known that activation of efferent vagal nerve fibres can modulate local and systemic inflammatory responses through activation of the 'cholinergic anti-inflammatory pathway' (165). The vagus is suggested to play a central role in GHS-observed effects and is an important link between the nervous and immune systems. Ghrelin has been shown to have several anti-inflammatory properties involving vagus activation (42, 234, 328). The restoration of parasympathetic tone has emerged as a promising therapeutic approach to normalize autonomic imbalance and inhibit the progression of heart failure (214, 410). Furthermore, SNA in patients with MI has been shown to contribute significantly to disease progression and prognosis (410). Accumulating clinical and experimental evidence indicates that inhibition of cardiac SNA improves survival and mitigates LV remodeling and dysfunction post-MI (11, 90). In the present study, chronic HEX treatment was demonstrated to modulate the autonomic nervous system by blunting SNA and enhancing PSA, and influence the inflammatory response induced by MI.

Limitations

HEX administration immediately prior to ligation represents a potential limitation. Timely reperfusion strategies act to limit infarct development, thus more logically, therapy would be initiated at this point, prior to reperfusion. The effect of reperfusion was not investigated in this study and represents a downfall.

The temporal histopathological and functional infarct changes in mouse models of MI vary when compared to acute myocardial infarction patients, thus representing a limitation of this model.

f. Conclusion

In this study we have demonstrated that HEX treatment has a clear effect on myocardial function, fibrosis and inflammation in a mouse model of MI. Pharmacological strategies targeting fibrogenic growth factors and anti-inflammatory effects may hold promise in prevention of cardiac remodelling and attenuation of diastolic and systolic dysfunction. Modulation of the autonomic nervous system by HEX may offer a novel cardioprotective strategy by acting to modulate the inflammatory reaction and fibrotic pathways.

5.3 Part C: Hexarelin as a cardioprotective agent in reperfused ischemic heart disease

5.3.1 Hexarelin targets inflammation and neural pathways to preserve cardiac function in a reperfused model of myocardial ischemia in mice

The results from the following chapter have been published as outlined on page (vi)

a. Abstract

Acute myocardial ischemia and reperfusion injury (IRI) underly the detrimental effects of coronary heart disease on the myocardium. Despite the ongoing advances in reperfusion therapies, there remains a lack of effective therapeutic strategies for preventing IRI. Growth hormone secretagogues (GHS) have been demonstrated to improve cardiac function, attenuate inflammation and modulate the autonomic nervous system (ANS) in models of cardiovascular disease. Recently, we demonstrated a reduction in infarct size after administration of hexarelin (HEX), in a murine model of myocardial infarction. In the present study we employed a *reperfused* ischemic (IR) model, to determine whether HEX would continue to have a cardioprotective influence in a model of higher clinical relevance

Myocardial ischemia was induced by transient ligation of the left descending coronary artery (tLAD) in C57BL/6J mice followed by HEX (0.3mg/kg/day; n= 20) or vehicle (VEH) (n=18) administration for 21 days, first administered immediately prior-to reperfusion. IR-injured and sham mice were subjected to high-field magnetic resonance imaging to assess left ventricular (LV) function, with HEX-treated mice demonstrating a significant improvement in LV function compared with VEH-treated mice. A significant decrease in interstitial collagen, TGF-β1 expression and

myofibroblast differentiation was also seen in the HEX-treated mice after 21 days. HEX treatment shifted the ANS balance towards a parasympathetic predominance; combined with a significant decrease in cardiac troponin-I and TNF-α levels, these findings were suggestive of an anti-inflammatory action on the myocardium mediated via HEX.

In this model of IR, HEX appeared to rebalance the deregulated ANS and activate vagal anti-inflammatory pathways to prevent adverse remodelling and LV dysfunction. There are limited interventions focusing on IRI that have been successful in improving clinical outcome in acute myocardial infarction (AMI) patients, this study provides compelling evidence towards the translational potential of HEX where all others have largely failed.

b. Introduction

Ischemic heart disease is a major cause of death and disability worldwide (3, 386). Myocardial ischemia occurs when coronary blood flow and oxygen availability are insufficient to meet the requirements of the heart (3). The consequences of this are dependent on the nature and severity of the ischemic episode and the elapsed time to subsequent re-establishment of coronary blood flow (3).

During AMI, occlusion of a coronary artery territory leads to myocyte necrosis. Without reperfusion or collateral blood supply, complete necrosis ensues. In the absence of reperfusion, very few interventions are able to limit infarct development (8, 411). The most effective and well established therapeutic strategy for reducing myocardial ischemic injury and infarct size is timely myocardial reperfusion through thrombolytic therapy or percutaneous coronary intervention (PPCI) (3). Although necessary for tissue salvage, reperfusion may lead to further complications including

diminished cardiac contractile function, arrhythmias and irreversible cell injury leading to necrosis and apoptosis (9). The introduction of early reperfusion therapies have substantially reduced mortality and morbidity amongst AMI patients, however, there remains no effective therapy for the prevention of myocardial IRI and its sequelae (3). Early arrhythmias can often prove fatal and chronic LV remodelling and heart failure continue to be major determinants of prognosis after AMI (11).

Activation of the sympathetic nervous system (SNS) in patients with AMI has been shown to contribute significantly to disease progression and prognosis (410). Autonomic imbalance, characterized by vagal withdrawal and sympathetic predominance has been linked to impaired cardiovascular (CV) function and elevated mortality in patients with heart failure, ventricular arrhythmias, IRI and hypertension (151, 154). Traditionally, the CV function of the vagus nerve (VN) has entailed regulating sinus rhythm and atrioventricular node conduction. However, recent evidence indicates that the VN can have profound effects on CV function, remodelling, arrhythmias, IRI and mortality (155). Reduced vagal tone, characterized by depressed heart rate variability (HRV) and blunted baroreflex sensitivity is closely related to disease progression and poor clinical outcomes in AMI and heart failure patients (156, 412, 413).

Inflammation is an important component of myocardial ischemic injury and heart failure (214). It has been well established that enhancing parasympathetic tone decreases inflammation in various models of physiologic insult, such as cecal ligation and puncture, lipopolysaccharide injection, severe burn injury, traumatic brain injury and myocardial IRI (165, 215, 216, 250). Traditionally, CV drugs have had little influence on cytokines or the inflammatory reflex present in heart failure, thus, modulating the inflammatory response may represent a potential therapeutic strategy

to protect against myocardial IRI and improve recovery of cardiac function (414).

Growth hormone secretagogues (GHS), a class of synthetic peptides stimulating growth hormone release through binding of the G-protein coupled receptor (GHS-R) have been demonstrated to have CV actions (42, 149). A number of studies have demonstrated the protective effects of the synthetic hexapeptide, hexarelin (HEX) in AMI, IR injury and cardiac fibrosis (42, 47, 75, 415). There are accumulating studies that describe the application of GHS in CV disease clinical trials with promising results (53, 393), however there remains a paucity of data detailing the mechanisms underlying these effects. In preclinical disease models, there is evidence supporting the indirect cardioprotective action of GHS through central and peripheral modulation of the ANS (42, 75, 149, 416).

The present study was designed to examine the effects of HEX on LV function and tissue characteristics in a mouse model of myocardial IR. A key event in the progression to heart failure is the pathological remodelling of the LV secondary to cardiac fibrosis (12). In a recent publication we demonstrated the ability of HEX therapy to significantly reduce measures of cardiac fibrosis in myocardial-infarct injured mice using a permanent infarct model (75). Unfortunately, this model is not readily applicable to the human clinical setting, where early reperfusion therapy is paramount to improving outcome in AMI, thus, there is a clear need for studies employing reperfusion techniques at the preclinical level to allow for translational application. This study represents one of the first *in vivo* myocardial IR studies employing chronic HEX therapy.

c. Materials and Methods

All experiments were approved by the Animal Ethics Committee of the University of Queensland and were performed in accordance to national guidelines (Ethics number SBMS/200/13/NHMRC).

IR Surgical protcol

Myocardial IR was induced in 12-14 week old male C57BL/6JArc inbred mice (n=38) (JAX stock number: 000664) by transient ligation of the left anterior descending coronary artery (tLAD). Mice were anesthetized by intraperitoneal injection of medetomidine (1mg/kg) and ketamine (75mg/kg), intubated and supported by a small animal ventilator (Harvard Apparatus) with tidal volume and respiratory rate calculations described previously (396). A left-sided thoracotomy was performed and the LAD was ligated 3mm below the left auricular appendage using a 7-0 Prolene suture threaded through a 2mm piece of sterile PE10 tubing. The tubing was heat-flared at the end in contact with the heart, creating a blunt "foot-print", enabling occlusion of the LAD once tension was applied to the free ends of the suture. Successful occlusion was confirmed by visualization of a pallor region distal to the site of ligation along with characteristic electrocardiography changes. The suture was ligated at the distal end of the tubing for the specified 40-minute ischemic time. Sham-operated mice underwent the same procedure excluding ligation of the LAD.

After 40 minutes of ischemia (or sham procedure) the suture was released and removed with the PE tubing, allowing reperfusion. The chest was closed using 6-0 polydioxanone and the musculature and cutaneous tissues closed using a 5-0 non-absorbable suture.

On recovery, the mice were administered atipamezole (1mg/kg) and a subcutaneous (SC) injection of carprofen (5mg/kg) and 0.5ml saline SC. The mice were recovered

in an oxygen- and heat-supplemented environment and subsequently moved to their standard housing environment where they remained for 21 days whilst the experimental data was collected.

Treatment administration

HEX (0.3mg/kg/day) or VEH was administered SC to each mouse immediately prior to reperfusion. Similarly, mice undergoing the sham procedure also received either VEH or HEX treatment. This dose was chosen based on previous studies demonstrating a cardioprotective effect (45). All mice then received their respective treatments once daily throughout the 21-day study period.

Assessment of myocardial injury, inflammation and remodelling

Cytokine and Cardiac troponin (CnT)-I determination

Blood samples were collected 24 hours and 21 days post tLAD ligation or sham procedure. The blood was allowed to clot and samples were centrifuged. The serum was immediately removed and stored at -80°C until assayed. The serum concentrations of CnT-I, interleukin (IL)-1β, IL-6 and tumor necrosis factor (TNF)-α were measured at 24 hours and 21 days post-operatively using a MILLIPLEX® map Assay according to the manufacturer's instructions (Merck Millipore).

HRV analysis

HRV analysis was performed 21 days post tLAD ligation or sham procedure. ECG signals were recorded using a physiological analyzing system (Bio Amp, AD Instruments, CA, USA). Mice were anaesthetized with isoflurane and ECG signals were recorded for a minimum of 20 minutes once the heart rate (HR) had stabilized.

ANS function was examined by power spectral analysis of HRV (LabChart Pro 7.0, ADInstruments, Australia) where HR was used to generate a power spectral density curve using a fast Fourier transformation (88, 335). The area under the curve was calculated for the very-low-frequency (VLF: 0-0.15Hz), low-frequency (LF: 0.15-1.5Hz), and high-frequency (HF: 1.5-5Hz) bands, with ranges based on previous studies (335). The parameters: LF, HF, normalized LF power (nLF), normalized HF power (nHF), and the ratio of LF to HF power (LF/HF) were calculated as described in (88).

Histology and morphometric analysis

Serial transverse paraffin-embedded LV sections from each group of animals studied were stained with 0.1% picrosirius red to detect interstitial collagen deposition. Additional serial transverse LV sections from each corresponding group of animals studied were immunohistochemically stained for selected markers associated with collagen turnover; utilizing a polyclonal antibodies to transforming growth factor (TGF)-b1 (sc-146; 1:200 dilution; Santa Cruz Biotechnology Inc., Santa Cruz, CA, USA) and matrix metalloproteinase (MMP)-13 (the predominant collagenase in mice; 1:100 dilution; ab75606; Abcam; Redfern, NSW, Australia); or a monoclonal antibody to a-smooth muscle actin (a-SMA; a marker of myofibroblast differentiation; M0851; 1:250 dilution; DAKO Antibodies, Carpinteria, CA, USA). Detection of primary antibody staining was detected using DAKO Envision anti-rabbit or anti-mouse kits, respectively, and 3,3-diaminobenzidine. Morphometric analysis of picrosirius red- and immunohistochemically-stained sections was performed using Aperio software (Leica Biosystems, North Ryde, NSW, Australia) on whole tissue sections (corrected for the area of tissue stained) per animal. In each case, the

percentage staining of each marker analyzed per section was derived and expressed as the fold changes relative to the SHAM-VEH group, which was expressed as 1.

Assessment of myocardial function

High-field cardiac MRI

Mice were imaged using a 30cm-diameter horizontal bore Bruker Biospec 9.4 Tesla (T) small animal MRI scanner equipped with a BGA 12S HP 660 mT/m gradient set. MRI data was acquired with a 86mm i.d. quadrature transmit coil and a 2x2 phase array receive coil, running Paravision 5.1. (Bruker Biospin, Ettlingen, Germany).

Animal preparation

Anesthesia was induced using 5% isoflurane in 100% medical grade oxygen with a flow rate of 1 L/minute into an induction chamber. The mouse was positioned in a purpose-built cradle (Bruker, Germany) and maintained with 1.5-2% isoflurane in 1-2 L/min oxygen via a nose cone. Core temperature was monitored using a rectal probe and maintained with a warm water circulation system incorporated into the animal bed. A SAII Monitoring system (Small Animal Instruments, NY, USA) was used to record the electrocardiogram, using a 3-lead system with surface Ag-AgCl electrodes. Respiration was monitored with a pressure-transducer, from which a respiratory gating signal could be derived.

Protocol

Gadopententate dimeglumine (Gd-DTPA) (0.3 mmol/kg Magnevist, Bayer, Germany) was administered by intravenous (IV) infusion into the lateral tail vein of the mouse.

Following standard pre-scan calibration, 2- and 4-chamber view scout scans were acquired, from which a single mid-cavity short-axis slice was planned. Cine imaging was performed with a retrospectively-triggered (self-gated) INTRAGATE gradient-echo sequence (338), with the following parameters: TR = 5.6 ms, TE = 2.6 ms, flip angle = 10 degrees, number of movie frames = 20, slice thickness = 1mm, matrix =512 x 512, field-of-view (FOV) = 4 x 4 cm^2. This resulted in 78 x 78 um in-plane resolution, with ~5mins acquisition per slice. Seven to nine short-axis slices with no slice gap were acquired to cover the heart from apex to base. Late gadolinium enhancement (LGE) images in the slice locations described above were acquired 10-15 minutes after IV Gd-DTPA (Fig. 54).

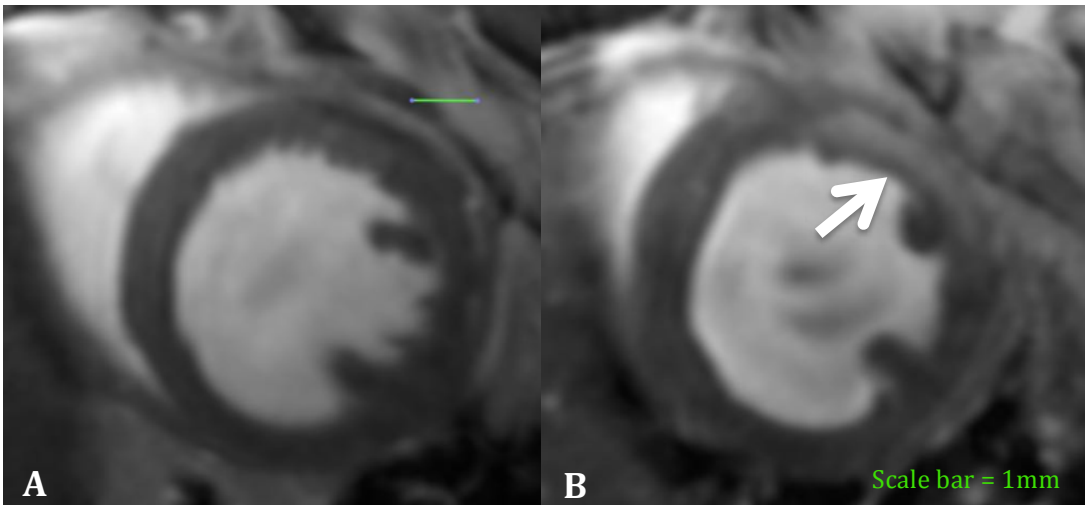

Figure 54: Representative cMRI images with LGE. Representative LGE images acquired using a T_1–weighted INTRAGATE gradient-echo sequence 24 hours post-transient LAD ligation. The hyperintense region represents the infarcted tissue (indicated by arrow). (A). Sham; (B). tLAD.
cMRI, cardiac magnetic resonance imaging; LGE, late gadolinium enhancement; tLAD, transient ligation of the left descending coronary artery.

Functional analysis

cMRI images, in DICOM format, were processed with Osirix (340) software. The end-diastolic and end- systolic phases were identified on a slice-by-slice basis and

both the endocardial and epicardial borders were traced. The LV end systolic volume (ESV), end diastolic volume (EDV), stroke volume (SV) and ejection fraction (EF) were computed from the traced borders and LV mass was obtained by multiplying the volume by the specific gravity of 1.05 g/cm^3 (341).

Statistical analysis

The data was expressed as mean +/- SEM or relative mean +/- SEM. Statistical analysis was performed using GraphPad Prism 7. Differences between groups were analysed by one-way ANOVA using a Newman Keuls post-hoc test to allow for multiple comparisons between groups. Unpaired *t*-test was applied to comparisons between two groups. $P < 0.05$ was considered statistically significant.

d. Results

Assessment of myocardial injury, inflammation and remodelling

CTn-I

In excess of a 4-fold increase in cTn-I was observed 24 hours post tLAD ligation in the IR-VEH compared with the IR-HEX group (Fig. 55A, left column). Thus, by protecting against cardiomyocyte injury after IR, HEX treatment appeared to significantly prevent an acute rise in cTnI. There was no significant difference in cTnI between the IR-VEH and IR-HEX group after 21 days (Fig. 55A, right column).

Cytokines

Serum IL-1β, IL-6 and TNFα levels were determined 24 hours and 21 days post-sham operation or tLAD occlusion.

HEX treatment was found to prevent the significant rise in TNFα seen in the IR-VEH group (Fig. 55B). There were no significant differences noted in IL-6 or IL-1β levels between the groups at either time point, although there was a trend towards reduction in each of the respective inflammatory cytokines' within the IR-HEX group (Fig. 55C/D).

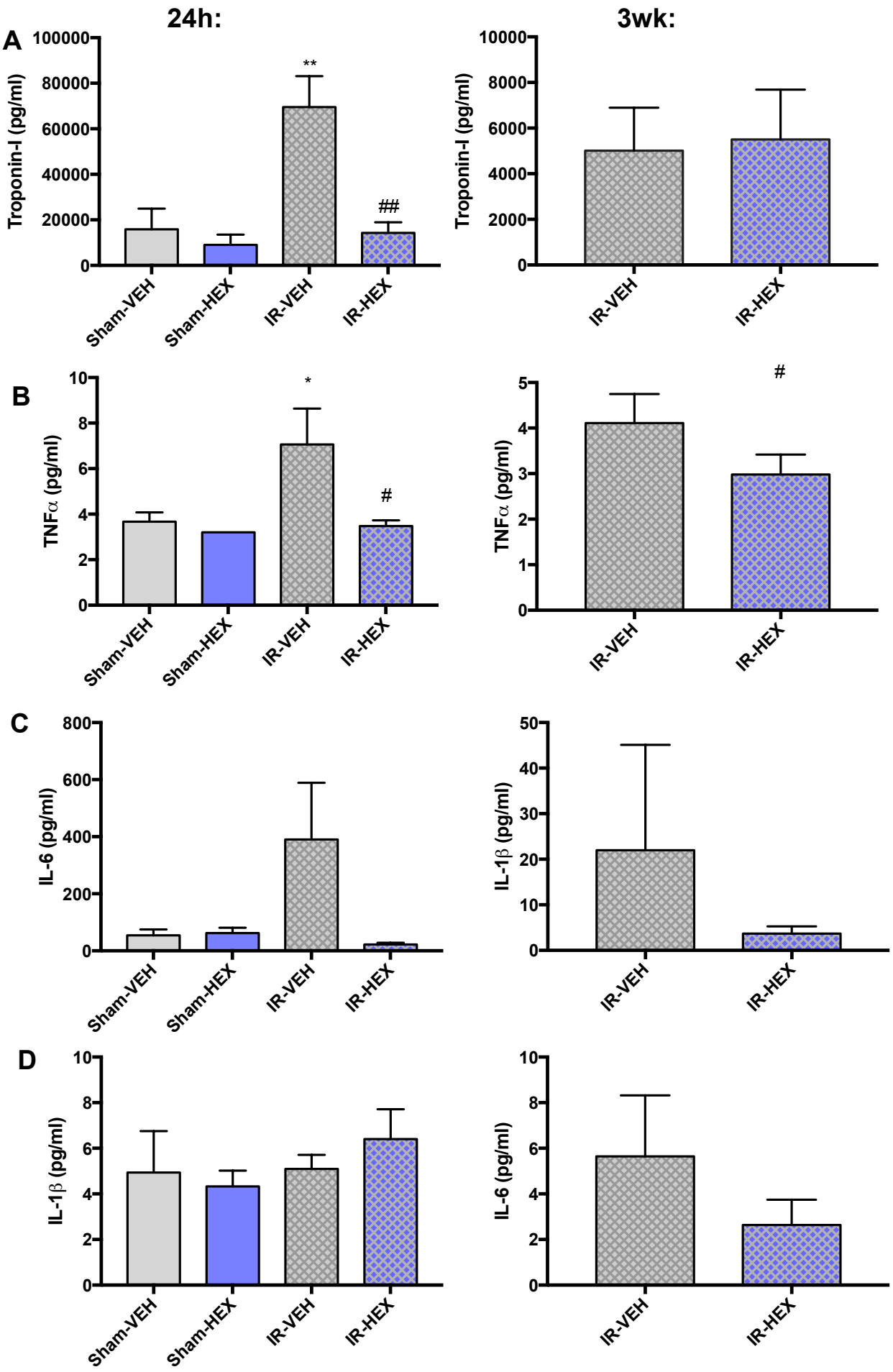
24h:
3wk:
A
Troponin-I (pg/ml)
100000
80000
60000
40000
20000
0
**
##
10000
8000
6000
4000
2000
Sham-VEH
Sham-HEX
IR-VEH
IR-HEX
B
TNFα (pg/ml)
10
8
6
4
2
*
#
5
3
1
C
IL-6 (pg/ml)
800
600
400
200
IL-1β (pg/ml)
50
40
30
20
10
D

Figure 55: Serum assessment of: (A). Troponin-I (pg/ml), (n= Sham-VEH (4), Sham-HEX (4), IR-VEH (4), IR-HEX (5) left & IR-VEH (5), IR-HEX (5) Right); (B). TNF-a (pg/ml), (n=4/4/3/4)/(5/5); (C). IL-6 (pg/ml). (n=4/4/4/4/3)/(4/3); (D). IL-1b (pg/ml), (n=4/4/4/5)/(4/4).
Serum levels assessed 24 hours (left column) and 21 days (right column) post-procedure in sham-injured mice and mice undergoing IR procedure with or without HEX treatment.
Data expressed as mean ± SEM; $^{*}p<0.05$, $^{**}p<0.01$, versus Sham-VEH group; $^{\#}p<0.05$, $^{\#\#}p<0.01$, versus IR-VEH group.
HEX, hexarelin; IR, ischemia reperfusion; LAD, left descending coronary artery; VEH, vehicle.

HRV

HRV was examined in mice 21 days post-procedure. HRV analysis is considered an indirect measure of cardiac autonomic tone (335, 398). LF/HF is used to represent SNS activity, whereas nHF represents parasympathetic nervous activity (335).

The IR-HEX group demonstrated a parasympathetic predominance and sympathetic down-regulation based on a significantly lower LF/HF ratio and higher nHF compared with the IR-VEH group (Fig. 56A, B respectively).

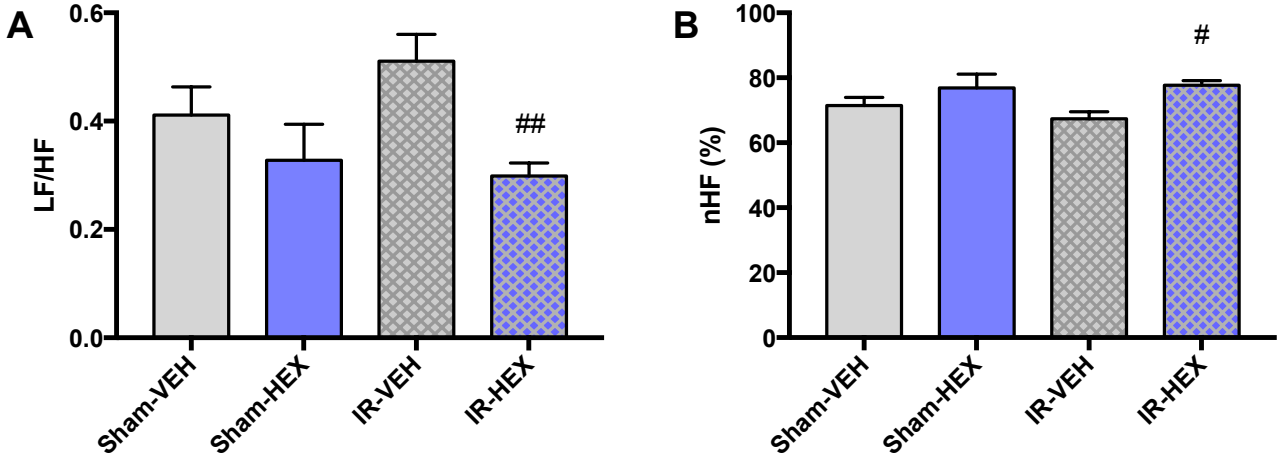

Figure 56: Heart rate variability analysis.
Electrocardiographic data recorded 21 days after sham surgery or transient LAD occlusion with or without HEX treatment. **(A):** Sympathetic nerve activity represented by low-frequency power (LF/HF); **(B):** Parasympathetic nerve activity represented by high-frequency power (nHF), (n=4/5/7/9)
Data expressed as mean ± SEM; $^{\#}p<0.05$, $^{\#\#}p<0.01$, versus IR-VEH group.

HEX, hexarelin; HF, high frequency; IR, ischemia reperfusion; LAD, left descending coronary artery; LF, low frequency; nHF, normalized high frequency power; VEH, vehicle.

LV mass and heart weight (HW)

LV mass was determined using cMRI 24 hours and 21 days post procedure. There were no significant differences in LV mass at either of these time points *(*Fig. 57A/B*)*.

To evaluate cardiac hypertrophy, heart weight was measured 21 days post-procedure. Tibial length (TL) was used as an adjustment factor.

HW/TL ratios did not differ between the groups (Fig. 57C), thus our HW/TL data was reflective of our cMRI-determined LV mass results.

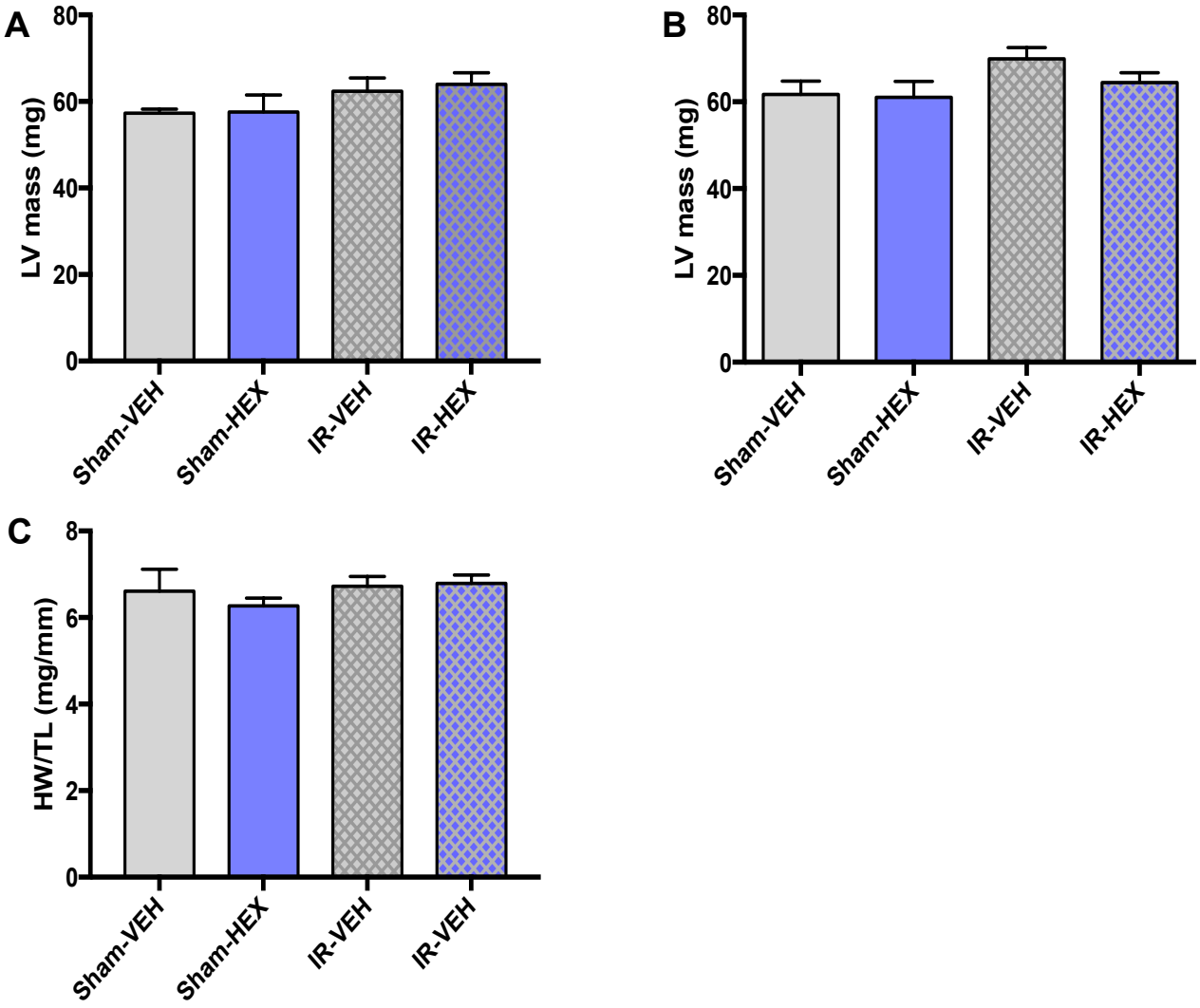

Figure 57: Assessment of myocardial mass and heart weight.
Myocardial mass (mg) assessed by cMRI after: **(A).** 24 hours post tLAD ligation, (n=4/4/8/11); **(B).** 21 days post-procedure (n=5/5/7/8) in sham-injured mice and mice undergoing IR procedure with or without HEX treatment.
Heart weight **(C).** measured post-mortem after 21 days (n=4/4/8/8). Tibial length (TL) was used as an adjustment factor.
The data is expressed as mean +/- SEM. There were no significant differences in myocardial mass or HW/TL ratio between groups.
cMRI, cardiac magnetic resonance imaging; HEX, hexarelin; HW, heart weight; IR, ischemia reperfusion; LAD, left descending coronary artery; LV, left ventricle; TL, tibial length; VEH, vehicle.

Histology and morphometric analysis

Picrosirius red staining of the myocardium was used to detected changes in interstitial collagen (IC) deposition. IC content was significantly increased in the IR-VEH group; the presence of HEX was seen to suppress this aberrant post-IR IC deposition (without affecting basal IC) (Fig. 58A).

TGF-β1 (Fig. 58B) and a-smooth muscle actin (SMA)-associated myofibroblast, arteriole and artery immunostaining (Fig. 58C) was significantly increased in the IR-VEH group compared to that measured in Sham-VEH counterparts. TGF-β1 and a-SMA were both significantly suppressed by HEX-treatment post-IR. There was also a trend towards increased MMP-13 levels in the IR-HEX group compared to that measured in the IR-VEH group (Fig. 58D). These results suggest that HEX had a regulatory effect on cardiac remodelling and fibrosis post-IR.

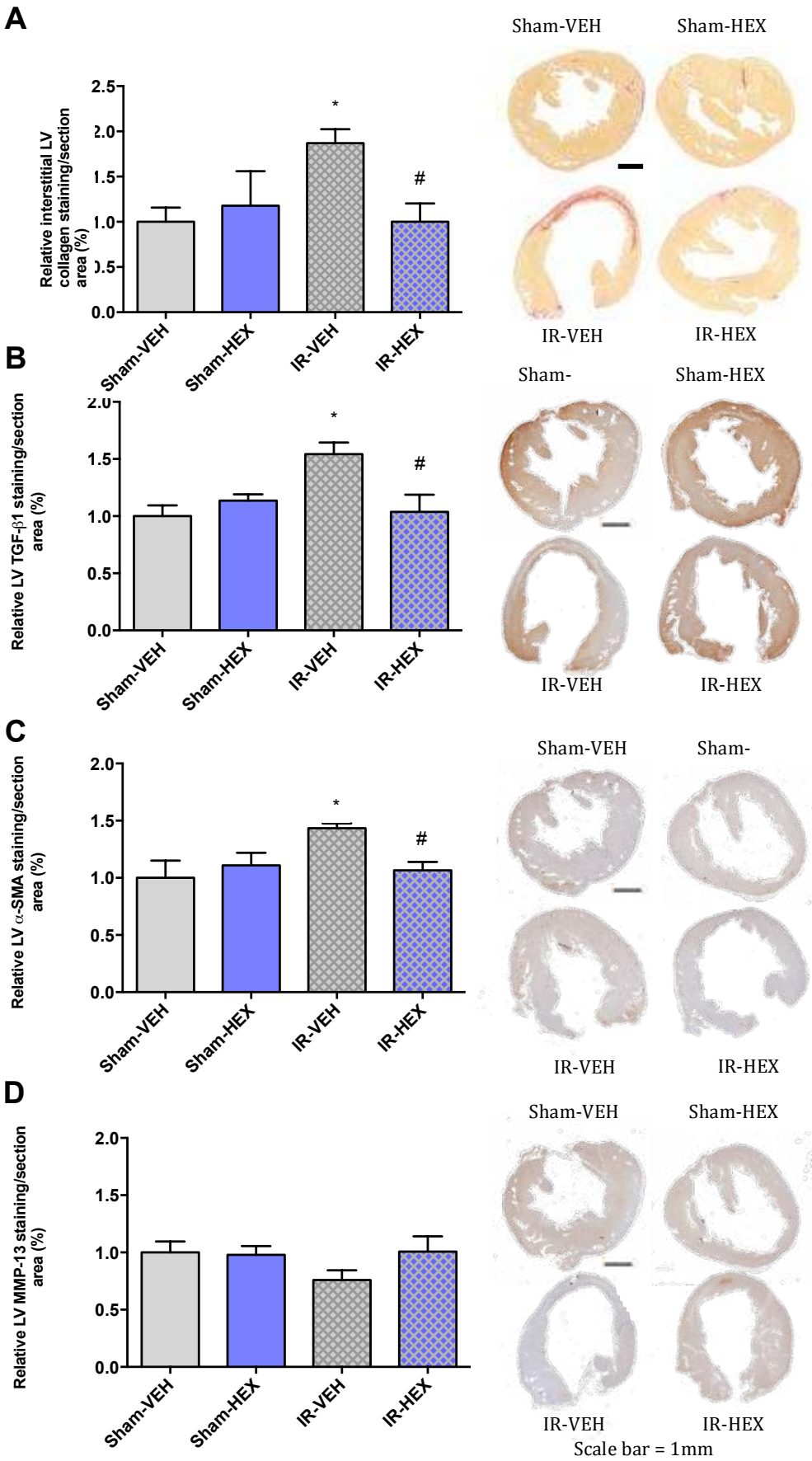
A
Relative interstitial LV collagen staining/section area (%)
2.5
2.0
1.5
1.0
0.5
0.0
*
#
Sham-VEH
Sham-HEX
IR-VEH
IR-HEX
Sham-VEH
Sham-HEX
IR-VEH
IR-HEX
B
Relative LV TGF-β1 staining/section area (%)
2.0
1.5
1.0
0.5
0.0
*
#
Sham-VEH
Sham-HEX
IR-VEH
IR-HEX
Sham-
Sham-HEX
IR-VEH
IR-HEX
C
Relative LV α-SMA staining/section area (%)
2.0
1.5
1.0
0.5
0.0
*
#
Sham-VEH
Sham-HEX
IR-VEH
IR-HEX
Sham-VEH
Sham-
IR-VEH
IR-HEX
D
Relative LV MMP-13 staining/section area (%)
2.0
1.5
1.0
0.5
0.0
Sham-VEH
Sham-HEX
IR-VEH
IR-HEX
Sham-VEH
Sham-HEX
IR-VEH
IR-HEX
Scale bar = 1mm

Figure 58: Histology and morphometric analysis
(A). Interstitial LV collagen content measured by picrosirius red staining (n=4/3/5/4); (B). TGF-β1, (n=3/3/6/5); (C). α-SMA, (n=3/4/4/4); (D). MMP-13 (n=4/4/4/4), immunohistochemistry staining measured in sham-injured mice and mice undergoing IR with or without HEX treatment
The right column displays representative low power photomicrograph sections from each treatment group corresponding to the selected markers and methods described above. Low power (whole mount) sections of heart have been selected to demonstrate the transmural staining with regional differences that would not be as clearly observable at high power.
Data expressed as mean ± SEM; $^{*}p<0.05$, versus Sham-VEH group; $^{\#}p<0.05$, versus IR-VEH group.
HEX, hexarelin; IR, ischemia reperfusion; LV, left ventricle; VEH, vehicle.

Analysis of LV function

Twenty-four hours post IR/sham procedure:

EF (%) was significantly reduced in the IR-VEH compared to the SHAM-VEH group; HEX treatment was seen to completely prevent this reduction. Both IR-VEH and IR-HEX groups showed a significant increase in EDV 24-hours post-IR. The significant elevation in ESV seen within the IR-VEH was limited by HEX treatment (Fig. 59A).

Twenty-one days post procedure:

EF% remained significantly reduced in the IR-VEH group, whereas a normalization of EF% was observed in the IR-HEX group. Similarly, the IR-HEX group displayed a normalization in ESV after the 21 days of HEX therapy. There was no significant difference in LV EDV between the groups at this time point (Fig. 59B).

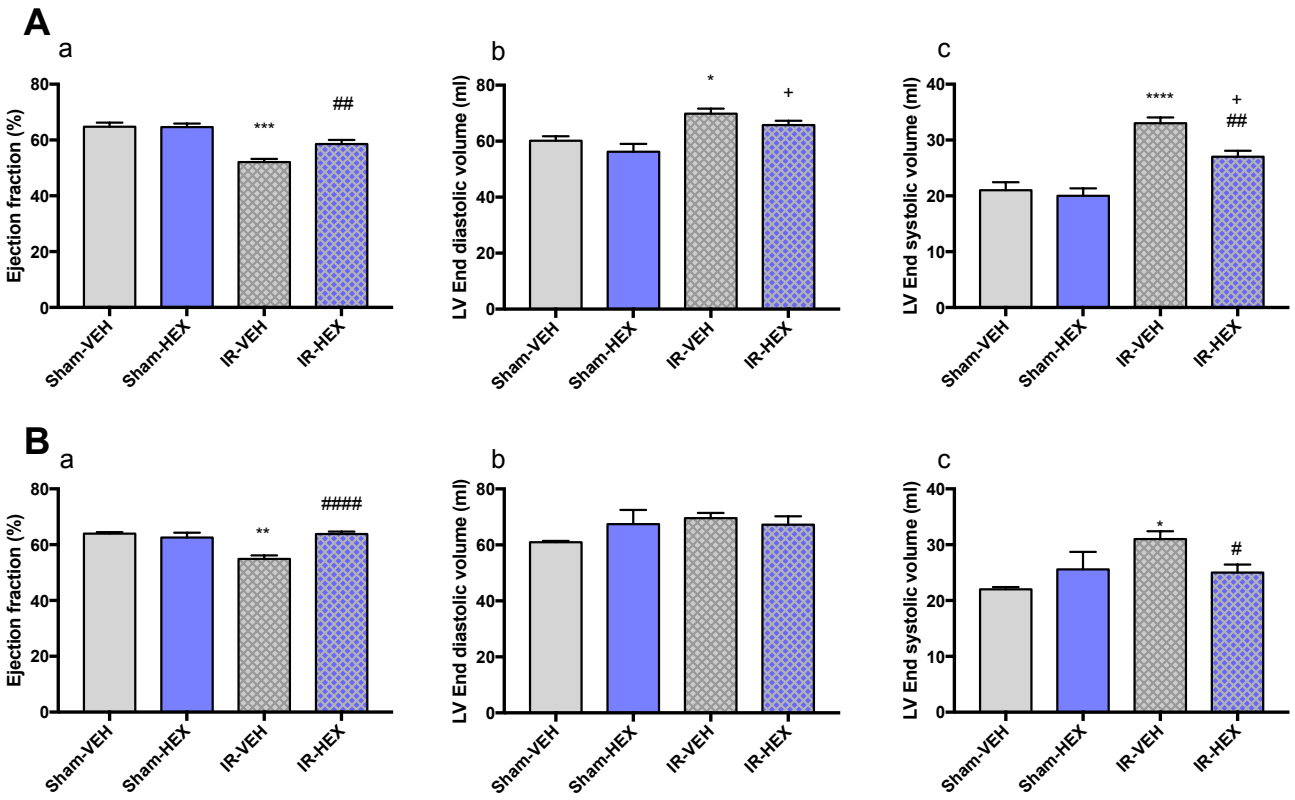

Figure 59: Cardiac functional parameters measured by cMRI.
(a). Ejection fraction (%), (b). LV end-diastolic volume, (c). LV end-systolic volume measured in sham-injured mice and mice undergoing transient LAD occlusion (IR) with or without HEX treatment.
(A). 24 hours post-procedure, (n=4/4/14/13); **(B).** 21 days post-procedure (n=4/5/14/15)
Data expressed as mean ± SEM; $^{*}p<0.05$, $^{**}p<0.01$, $^{***}p<0.001$, $^{****}p<0.0001$, versus Sham-VEH group; $^{\#}p<0.05$, $^{\#\#}p<0.01$, $^{\#\#\#\#}p<0.0001$, versus IR-VEH group; $^{+}p<0.05$, versus Sham-HEX group.
cMRI, cardiac magnetic resonance imaging; HEX, hexarelin; IR, ischemia reperfusion; LAD, left descending coronary artery; LV, left ventricle; VEH, vehicle.

e. Discussion

There is a clear need to determine therapeutic strategies to protect the myocardium from the detrimental effects of IRI. Although improvements in myocardial reperfusion continue to take place with new antiplatelet and thrombolytic agents, there remains to be no effective therapeutic strategy for preventing myocardial IRI (3). In this study we demonstrated that HEX administration reduced serum

inflammatory cytokines profiles and cTn-I, reflecting an overall reduction in cardiomyocyte injury (417). Downstream, the effects of chronic HEX treatment resulted in significantly reduced measures of cardiac fibrosis and an overall preservation in LV function. Additionally, HEX treatment was seen to shift the balance of ANS activity towards a parasympathetic predominance. These findings provide evidence towards the cumulative effects of simultaneous sympathetic down-regulation, vagal enhancement and activation of anti-inflammatory pathways to prevent adverse LV remodelling and dysfunction.

At the hospital, reduction in AMI ischemic injury requires a treatment protocol that minimizes the door-to-PPCI time. Most preclinical studies in this field consist of a surgical protocol involving permanent ligation of the LAD (without allowing reperfusion of the ischemic tissue)(45, 75, 104). Therefore these studies fail to clearly assess the critical interaction of ischemia, reperfusion injury and the subsequent therapeutic intervention. By employing an IR model, the current study closely simulates the critical "door-to-PPCI time" concept; therefore representing a superior model and evidence towards the potential value of HEX in AMI patients.

Relevance of the autonomic nervous system and inflammation

The high mortality in myocardial infarction has been strongly associated with an acute and sustained increase in cardiac SNS activity (11, 88, 410). Although chronic therapeutic interventions have been developed for chronic heart failure, it is the period immediately after AMI, before autonomic modulation of cardiac function becomes irreversibly activated, that appears to be critical for optimizing short and long-term outcome by therapeutic intervention (11). Targeting adverse SNS activation and uncontrolled inflammation immediately post-infarction appears to offer a chronic

cardioprotective advantage by preventing adverse fibroblast activation, ventricular remodelling and dysfunction. There is accumulating clinical and experimental evidence that indicates inhibition of cardiac sympathetic nerve activation improves survival and mitigates LV remodelling and dysfunction post-MI (11, 90).

GHS and the autonomic nervous system

Early treatment with the endogenous GHS ghrelin has been shown to reduce the incidence of ventricular arrhythmias and improve early survival prognosis by preventing the early increase in cardiac sympathetic nervous system activation (CSNA) in rodent models of MI (90). CSNA inhibition was maintained for at least 2 weeks after a single bolus of ghrelin, resulting in attenuation of cardiac dysfunction, remodelling and reduced mortality (11). Comparable findings were demonstrated with chronic ghrelin treatment (91). Similarly, mice that received one oral dose of HEX treatment within 30 minutes of permanent LAD ligation were observed to have a higher ejection fraction 14 days after MI with lowered plasma epinephrine and dopamine levels. These results suggest that early GHS therapy preserves chronic cardiac function after AMI (104).

In a recent study, ghrelin knock-out mice were employed to demonstrate the crucial role of endogenous ghrelin in preventing CSNA, reducing the incidence of arrhythmias and improving survival prognosis post-AMI (145). Catecholamine concentrations were dramatically increased after AMI in ghrelin KO mice, reflective of stronger sympathetic nerve activation in this group. Endogenous ghrelin was demonstrated to prevent adverse ventricular remodelling and preserve myocardial function (145). Interestingly, the beneficial effect of ghrelin was abolished after blockade of the VN (88). Furthermore, it has been suggested that in healthy human

subjects ghrelin may suppress CSNA and stimulate cardiac PS nerve activity, (92) with the sympatho-inhibitory effects of ghrelin not found to be evident in vagotomised humans (86).

The cholinergic anti-inflammatory pathway and GHS

Excessive immune-mediated inflammatory responses in reaction to myocardial injury have been shown to have deleterious effects on post-infarction LV remodelling and dysfunction and can influence progression to heart failure (418). A timely, well-orchestrated inflammatory response is critical to achieve successful infarct healing in patients surviving an AMI (418). It has been well established that increasing parasympathetic tone, through vagal nerve stimulation (VNS) can decrease inflammation in various models of physiologic insult, including myocardial IRI, cecal ligation and puncture, LPS injection, severe burn injury and traumatic brain injury (215-217, 419). Thus, pharmacological stimulation of the VN may offer a novel approach to anti-inflammatory therapy in AMI-patients.

A multitude of studies highlight the importance of the role of the VN in the physiological functions of GHS (328). Ghrelin is known to cross the blood-brain barrier and is produced both centrally and within the periphery (288). The nodose ganglion is a constellation of vagal afferent neurons that synthesize the ghrelin receptor (GHS-R). These receptors are transported to their vagal afferent terminals, such as those located within the digestive tract for regulation of energy metabolism and food intake (148). Studies have also demonstrated the existence of the GHS-R within the infarcted myocardium (91). Co-staining with acetylcholine-esterase suggests that the GHS-R is localized within the VN terminals in the heart and sends afferent projections to the nucleus tractus solitaries (NTS), a major CV control centre

within the brain (147). The ghrelin receptor has also been localized to the dorsal motor nucleus of the vagus (87, 420). It has been demonstrated that GHS-R mediates the action of HEX and HEX is recognized to be both chemically more stable and functionally more potent than ghrelin (44, 421). Peripherally, GHS have been demonstrated to act on the cardiac vagal afferent nerve, resulting in a reflex decrease in sympathetic activity in rats with MI (90, 91).

Furthermore, it has been well described that activation of efferent VN fibres can modulate local and systemic inflammatory responses, through the 'cholinergic anti-inflammatory pathway' (CAP) (165). The CAP is mediated through vagal efferent firing leading to an acetylcholine-dependent interaction with the a-7 nicotinic acetylcholine receptor (a7nAChR) subunit on monocytes and macrophages and ultimately a reduction in inflammatory cytokine production (165). Activation of the CAP is possible via VN stimulation or pharmacologically via administration of selective a7nAChR agonists or inhibitors of acetylcholinesetase (165)**.**

GHS, inflammation and vagal activation

GHS have been shown to have several anti-inflammatory properties involving vagus activation. Intravenous ghrelin administration in septic mice has been shown to decrease levels of pro-inflammatory cytokines mediated through the VN (196). Ghrelin administration has been demonstrated to decrease TNF-α and IL-6, increase cardiac output, organ perfusion and reduce mortality in rat models of endotoxemia and polymicrobial sepsis, again mediated via the VN (196, 219, 422, 423). Vagotomy has been demonstrated to completely prevent these effects (196). Furthermore, ghrelin has been demonstrated to have no direct effect on cytokine release from Kupffer cells or peritoneal macrophages isolated from normal rats, suggesting an indirect anti-

inflammatory mechanism (196).

Inflammation has been demonstrated to play a major role in IRI (214). GHS has been demonstrated to activate the CAP in various IR models, Wu et al demonstrated that administration of ghrelin after gut IR attenuated excessive inflammation and reduced organ injury through the rapid activation of the CAP (231). In a rat model of renal IR, ghrelin administration during reperfusion was found to attenuate both systemic and renal-specific inflammatory responses, also mediated through the VN (232, 424). The absence of endogenous ghrelin has been shown to result in severe cardiac hypertrophy and diastolic dysfunction in a mouse model of pressure-overload cardiac hypertrophy. Inhibition of the CAP was thought to be responsible for these adverse processes and administration of ghrelin was shown to reverse these effects (235).

The cardioprotective actions of HEX in AMI

Myocardial infarction leads to progressive ventricular remodelling, increased myocardial wall stress and possible progression to heart failure (63). Following ischemia, alterations in the collagen network can result in progressive changes in LV morphology and function with an increase in interstitial collagen likely to impair both diastolic and systolic function (14).

Post-infarction repair requires timely suppression of the inflammatory response to prevent catastrophic consequences of uncontrolled inflammation on cardiac geometry and function (63). Studies suggest a direct involvement of fibroblasts in activation of the post-infarction inflammatory reaction. TGF-β1 is markedly augmented following infarction, is a potent pro-fibrotic cytokine and has profound effects on fibroblast phenotype and function, including activation of myofibroblasts. Preventing TGF-β1 activation in a myofibroblast-specific manner holds promise in counteracting cardiac

fibrosis (63).

Our recent work demonstrated a reduction in inflammatory cytokines and improvement in LV function in a mouse model of MI, thought to involve activation of the CAP. In this study, HEX influenced postinfarct fibrotic healing, likely by involving the suppression of profibrotic factors and favouring a net reduction in aberrant collagen content (75). Furthermore, Huang et al. recently demonstrated that HEX protected cardiomyocytes from IR injury partly through modification of the IL-1 signalling pathway *via* activation of the GHS-R (47).

In this current study, we demonstrated a HEX-mediated decrease in TGF-β1 expression and myofibroblast differentiation post-myocardial IR. Several studies have shown that TGF-β1 is a key stimulator of myofibroblast differentiation post-MI (13, 425). MMP-9 and TGF-b1 also both play key roles in the progression of post-MI remodeling (263, 264) and inflammatory cytokines such as IL-1 can regulate fibroblast phenotype. The activation of MMPs may influence changes in extracellular matrix degradation (ECM) and collagen deposition (47, 74, 265).

Thus, *via* vagal enhancement and activation of the cholinergic anti-inflammatory pathway, combined with simultaneous suppression of the acute rise in SNS activation, HEX appears to mitigate adverse inflammation. Furthermore, this anti-inflammatory action appears to downregulate TGF-β1 expression and myofibroblast differentiation as part of its potential therapeutic effects (75) (Fig. 60).

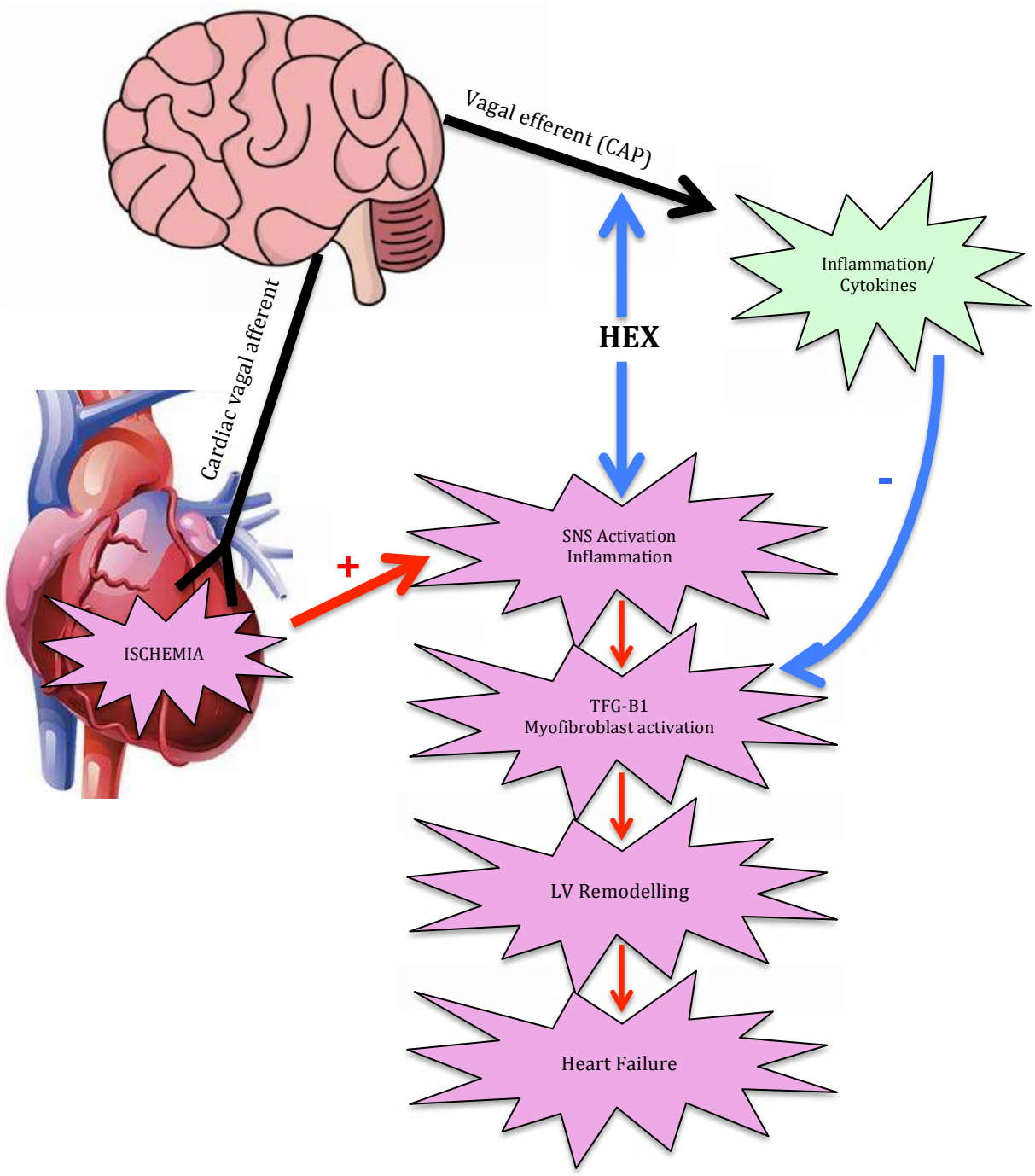

Figure 60: In response to myocardial IR HEX actives endogenous neural pathways to restrain adverse inflammation and plays a role in inhibiting pathways of pathological LV remodelling

Myocardial ischemia initiates SNS activation and an acute inflammatory response; inflammatory cytokines exert pro-inflammatory actions on cardiac fibroblasts and can result in LV dysfunction. TGF-B1, a potent pro-fibrotic cytokine, is increased following MI and can cause excessive ECM production and myofibroblast activation. By suppressing inflammatory pathways and sympathetic activation HEX appears to attenuate these negative effects on cardiac remodelling and dysfunction. Additionally,

pharmacological stimulation of vagal pathways by HEX appears to decrease levels of proinflammatory cytokines through activation of the CAP

f. Conclusion

Targeting autonomic imbalance by augmentation of parasympathetic tone has emerged as a promising therapeutic approach for management of ischemic heart disease and heart failure (214). The VN is suggested to play a central role in GHS-observed effects and acts as an endogenous mechanism to regulate the immune response and inflammation (42). In the present study, HEX treatment was demonstrated to modulate the ANS and influence the inflammatory response induced by myocardial IR. Our results demonstrate that HEX may have an important influence on balancing the sympathetic and parasympathetic nervous system and modulating adverse inflammatory pathways in response to AMI. Pharmacological stimulation of the VN by HEX may offer a novel cardioprotective strategy against IRI by preventing myofibroblast activation and LV remodelling in AMI.

Clinical relevance

The research field of cardio-protection has been plagued by numerous failed attempts to translate promising therapeutic strategies for preventing myocardial ischemic injury discovered in the basic science laboratory into the clinical setting (3). A major factor underlying this failure entails the inappropriate use of experimental animal models. In our previous study we were able to clearly demonstrate the cardioprotective effect of HEX therapy in a mouse model of permanent MI, however, the translational aspect of this model is limited. HEX as an emerging therapeutic agent for prevention of myocardial IRI has shown promise in this study using a clinically relevant model, where HEX was administered prior to myocardial reperfusion (removal of the

coronary ligature), representing a protocol that could be employed in the reperfusion unit. Therefore, this study signifies a noteworthy contribution to the field of cardio-protection.

6. Discussion

6.1 Concluding remarks

The work undertaken throughout this thesis comprises comprehensive longitudinal studies investigating the therapeutic effects of HEX on myocardial function, cardiac inflammation and fibrosis by employing murine models of IHD. Given that HEX is a stable and potent hexapeptide compared with its unstable natural counterpart ghrelin (and can be administered orally) (43), HEX offers potential advantages as a therapeutic agent in IHD. These properties have been clearly demonstrated in Chapter 5.

Throughout this work we have successfully illustrated the ability of HEX to significantly reduce measures of cardiac fibrosis in myocardial-infarct injured mice using models readily applicable to the human clinical setting. Thus, this work satisfies the critical need to employ reperfusion techniques at the preclinical level to allow for more seamless translational application to the Coronary Care Unit. We have also described novel cMRI techniques allowing accurate assessment of myocardial function, the extent of infarction and salvageable tissue. These measures represent important variables for the assessment of therapeutic efficacy and prognosis in the AMI patient. Overall, not only do these findings address the aims of this thesis, but also represent a noteworthy contribution to the field of cardio-protection.

6.2 Inflammation – a link between the brain and heart?

The field of cardioprotection has been fraught with ongoing failed attempts to translate promising therapeutic strategies for AMI from the laboratory to the clinical setting (3). Failure of these therapies has been somewhat attributed to the influence of age, comorbidities and chronic pharmacotherapy in the clinical patient compared to

that of their disease-free preclinical model-counterparts. Therefore, there is a critical need for more detailed and mechanistic preclinical studies that examine cardioprotection in relation to concurrent comorbidities (9).

As discussed throughout this thesis, chronic systemic inflammation has been increasingly recognized as a major risk factor for CVD (426). An adverse inflammatory response has been implicated in the pathophysiology of primary CVD and conversely, inflammation-induced myocardial injury and dysfunction has been seen as a sequalae of various systemic diseases (155, 214). Metabolic diseases such as obesity, diabetes and IBD exhibit strong inflammatory underpinnings and have been associated with increased risk of CVD (426, 427). Thus, it could be speculated that *CVD might be linked with the pro-inflammatory state induced by metabolic disease.*

The development of ventricular dysfunction associated with metabolic disease is likely to be multifactorial, with putative mechanisms including insulin resistance, metabolic disturbances, endothelial dysfunction, myocardial fibrosis, autonomic dysfunction and myocyte damage (428). Proinflammatory cytokines could be viewed as the common denominator here, given their involvement in all of these pathophysiological processes (428, 429) (Fig. 61).

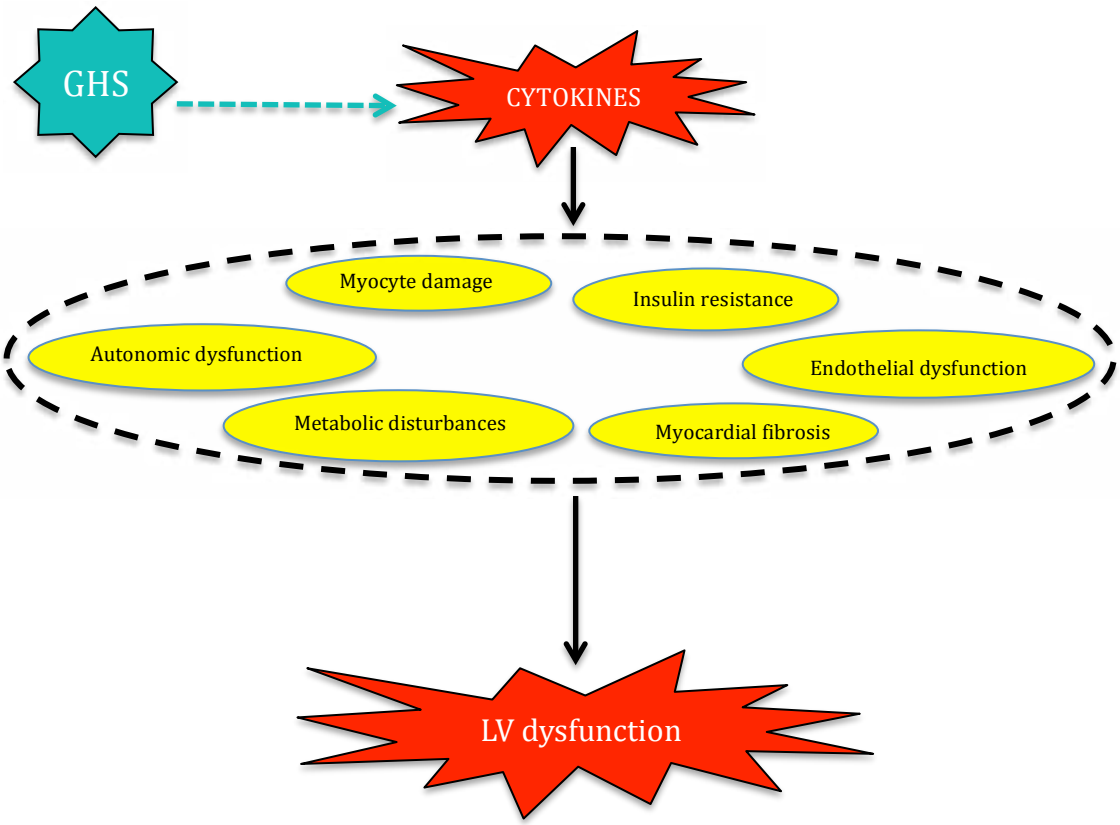

Figure 61: We propose that GHS negatively influence the *proinflammatory state* by modulating inflammatory cytokines (broken arrow). Inflammatory cytokines are likely to represent common link between the pathophysiologial changes culminating in LV dysfunction.

CVD is often associated with systemic diseases such as obesity and type 2 diabetes mellitus (T2DM) (430). GHS-mediated enhancement of cholinergic signaling via the inflammatory reflex may offer a two-fold protective advantage by firstly suppressing obesity-associated inflammation and secondly, the cardiovascular implications linked with this pro-inflammatory state (431) (Fig. 64). *There continues to be a definite need for discovery of new treatments for T2DM, metabolic syndrome and associated disease processes. Ghrelin is an endogenous peptide that may target common steps in the pathogenesis of these diseases. Ghrelin may represent an effective cholinergic modulator, capable of alleviating inflammation and metabolic complications (Fig.*

62). HEX is likely to have similar effects.

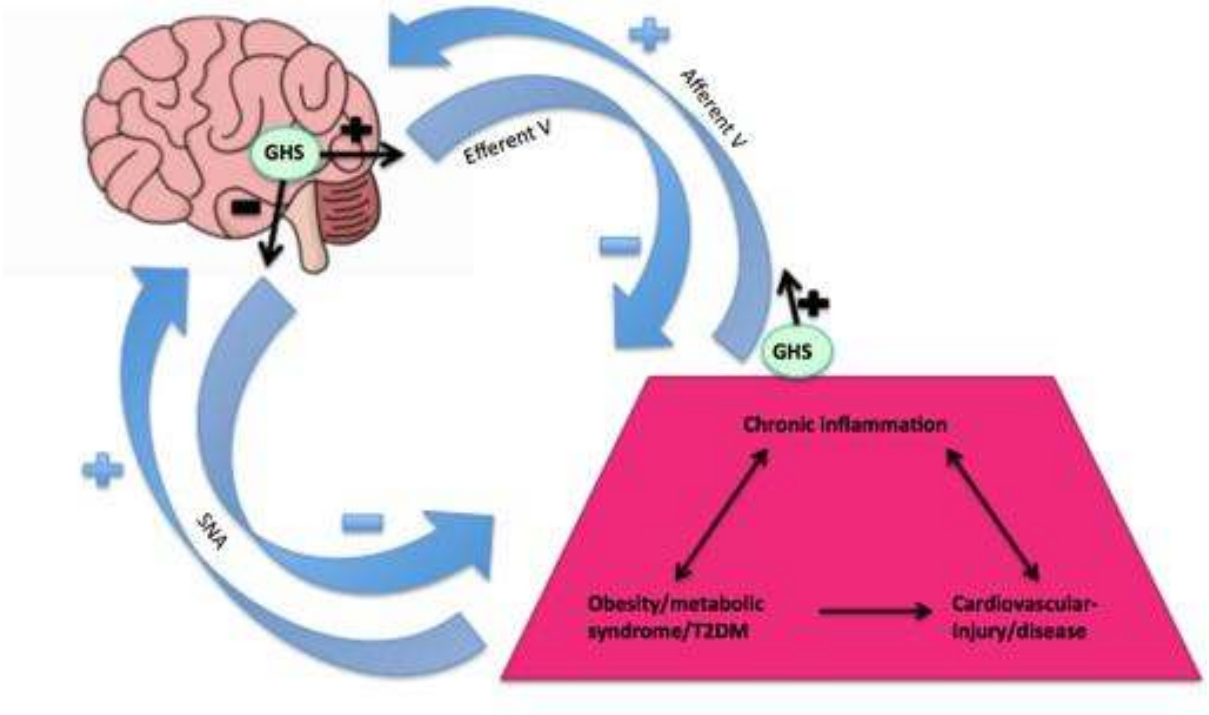

Figure 62: Obesity, metabolic and cardiovascular disease are linked to chronic inflammation. These diseases are associated with a chronic inflammatory state and activation of the sympathetic nervous system. GHS protects against this dysfunction by modulating sympathetic nervous system as well as the afferent and efferent arm of the inflammatory reflex (see text for further detail). Thus, *ghrelin has multifactorial protective influences in both metabolic and CVD.*

Ghrelin is a critical molecule facilitating interactions between the gut, brain and immune system (307). The nodose ganglion synthesizes ghrelin receptors and these receptors are transported to their vagal afferent terminals within the gastrointestinal tract (148). Afferent VN signaling is activated by cytokines or EEC derived peptides, constituting the gut-brain axis (Fig. 63 & 64) (148). It seems likely that the appetite-regulating peptide ghrelin is a crucial factor in the anatomical link mediating this pathway. In a scenario not dissimilar to the gut, the GHS-R has been localized within the VN terminals in the heart and sends afferent projections to the NTS (87, 91, 147).

In a comparable way to the gut, the heart and the brain also appear to communicate bidirectionally through anatomical and humoral pathways mediated by cytokines and neuropeptides (Fig. 63) (288).

Production of immunomodulatory enteroendocrine hormone peptides can regulate our immune system to influence inflammation in metabolic disease (286), however, it also seems likely that these peptides can regulate inflammation in CVD through a similar, if not identical pathway. Thus, we propose the existence of the **"heart-brain axis"** whereby ghrelin (or the synthetic analogue HEX) may act as important mediators to activate the cardiac VN both centrally and peripherally.

GHS appear to represent a crucial link in the gut-brain axis and the similar heart-brain axis whereby they act to modulate inflammation.

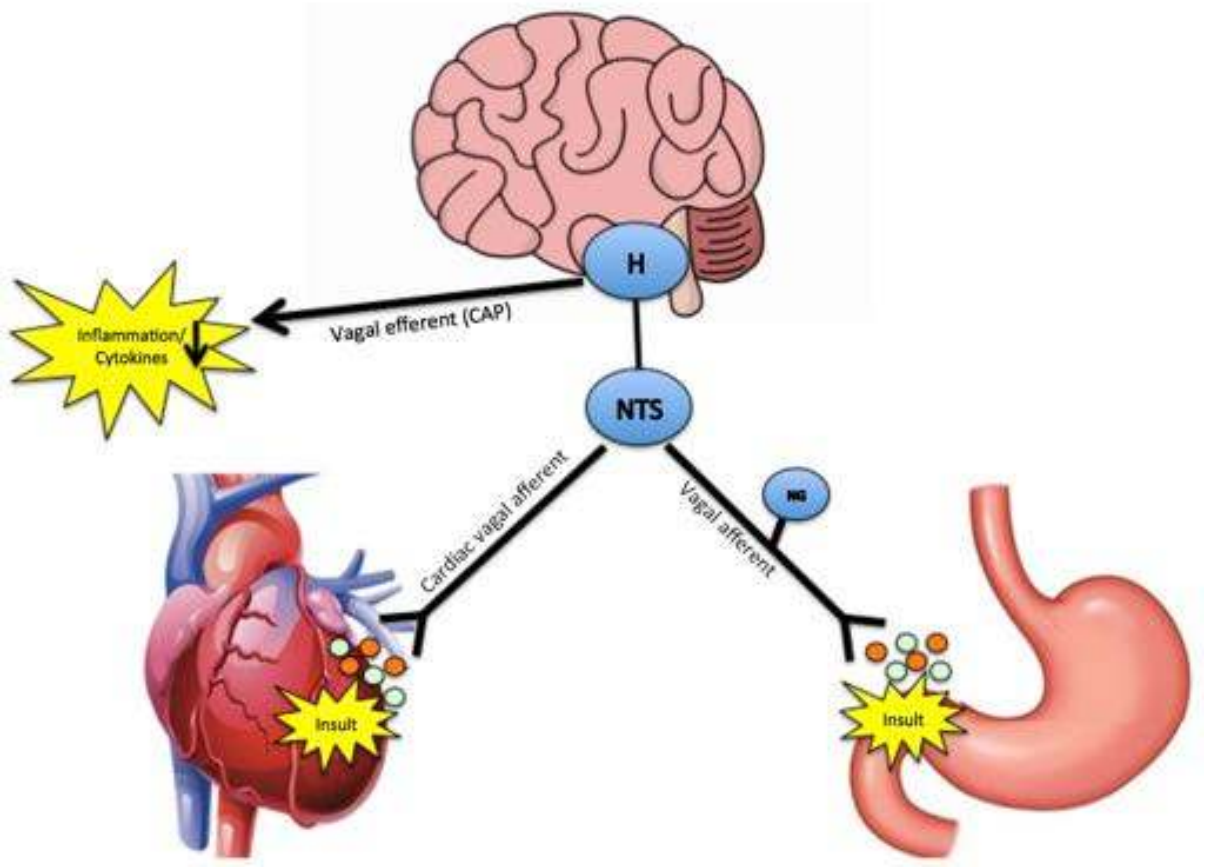

Figure 63: An inflammatory/hypoxic/ischemic insult induces the production of inflammatory cytokines (orange circles). Afferent VN signaling is activated by cytokines or neuroendocrine peptides, such as ghrelin (green circles) by binding to the

GHS-R. The efferent arm of the CAP is activated and suppresses the immune response. Key: CAP, cholinergic anti-inflammatory pathway; H, Hypothalamus; NG, nodose ganglion; NTS nucleus tractus solitaries.

6.2.1 The gut-brain axis and ghrelin

Several lines of evidence indicate that activity of the VN is impaired in obesity (277). Enhancing cholinergic signaling can suppress obesity-associated inflammation and adverse implications, including insulin resistance, hyperglycemia, and CVD (169, 277, 289). Mice fed a high-fat diet have displayed evidence of gastrointestinal inflammation. This inflammation has been seen to spread to the VN ganglion cells and hypothalamus through the vagal afferent pathway distributed along the gastrointestinal tract (148, 432). It is plausible that a similar phenomenon occurs following myocardial injury/ inflammation in CVD and is mediated via the cardiac vagal afferent nerve (Fig. 64 & 65).

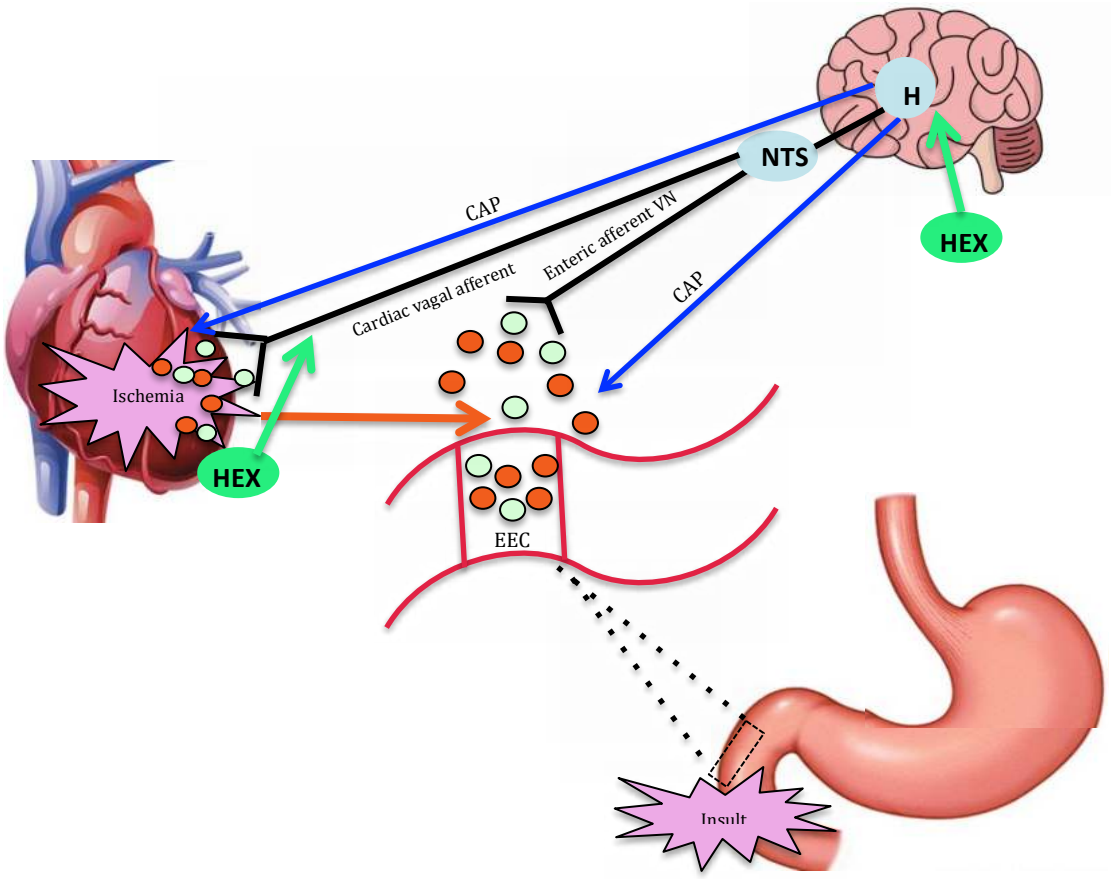

Figure 64: The Gut-brain-Heart Axis and HEX. In the enteric system, an *insult* results in the induction of inflammatory cytokines and liberation of neuroendocrine mediators from enteroendocrine cells that subsequently activate the afferent enteric vagus nerve. Similarly, an ischemic insult in the heart induces inflammatory cytokine release; it is possible that this insult also stimulates release of endogenous ghrelin. GHS can bind to the GHS-R localized in the vagal nerve terminals of the heart and activate the cardiac vagal afferent nerve. Furthermore, IHD, through mechanisms reducing cardiac output (ie, systolic dysfunction, arrhythmias) result in hypoperfusion of the gastrointestinal tract, this "insult" will further liberate inflammatory cytokines and neuroendocrine mediators from the EEC to activate the vagal afferent nerve (orange arrow). This may explain how mediators from the gut can influence cardiac inflammation. Exogenous HEX can peripherally activate the afferent VN and centrally, the CAP. The activated CAP blunts inflammation (blue arrows). Key: CAP, cholinergic anti-inflammatory pathway; EEC, enteroendocrine cells; H, hypothalamus; NTS, nucleus tractus solitarius. Light green circles represent ghrelin, orange circles represent inflammatory cytokines.

Ghrelin plays a crucial role in regulating gastrointestinal inflammation and there is strong evidence supporting its protective influence (307). Ghrelin has been demonstrated to modulate intestinal mucosal immunity directly by acting on immune

cells such as macrophages to suppress pro-inflammatory cytokine production & indirectly via VN stimulation (307). High serum ghrelin levels have been reported in IBD patients and in experimental colitis (307, 308, 316, 433). In contrast, plasma ghrelin is decreased in obesity and negatively correlated with body mass index (306). It is thought that increased ghrelin levels in inflammatory gastrointestinal disease could result as a consequence of tissue injury stimulating the production of endogenous ghrelin in response to intestinal inflammation and damage (307). Thus increased ghrelin expression could be interpreted as a response to counteract the pro-inflammatory response as part of a counterbalance feedback mechanism (307).

Alterations in the VN response towards appetite-regulating peptides have been demonstrated to occur in the obese state (148). High fat diet-induced obese mice showed blunted ghrelin signaling in the nodose ganglion via a mechanism involving in situ activation of inflammation (289). Furthermore, expression of the ghrelin receptor in both the hypothalamus and nodose ganglion was downregulated in high fat diet-fed mice (289). It is thought that ghrelin resistance in the obese state may be caused by dysregulation of ghrelin signaling via the vagal afferent nerve (289). Despite the dysregulation of afferent vagal nerve signaling in obesity, it is likely that exogenous activation of efferent vagal pathways by GHS (ie, pharmacological stimulation of the CAP) will maintain their anti-inflammatory actions. Furthermore, activation of the CAP may ultimately modulate the pro-inflammatory state in the obese patient by resulting in negative feedback inhibition of inflammatory cytokine production in these patients (Fig. 65). This has been largely unexplored.

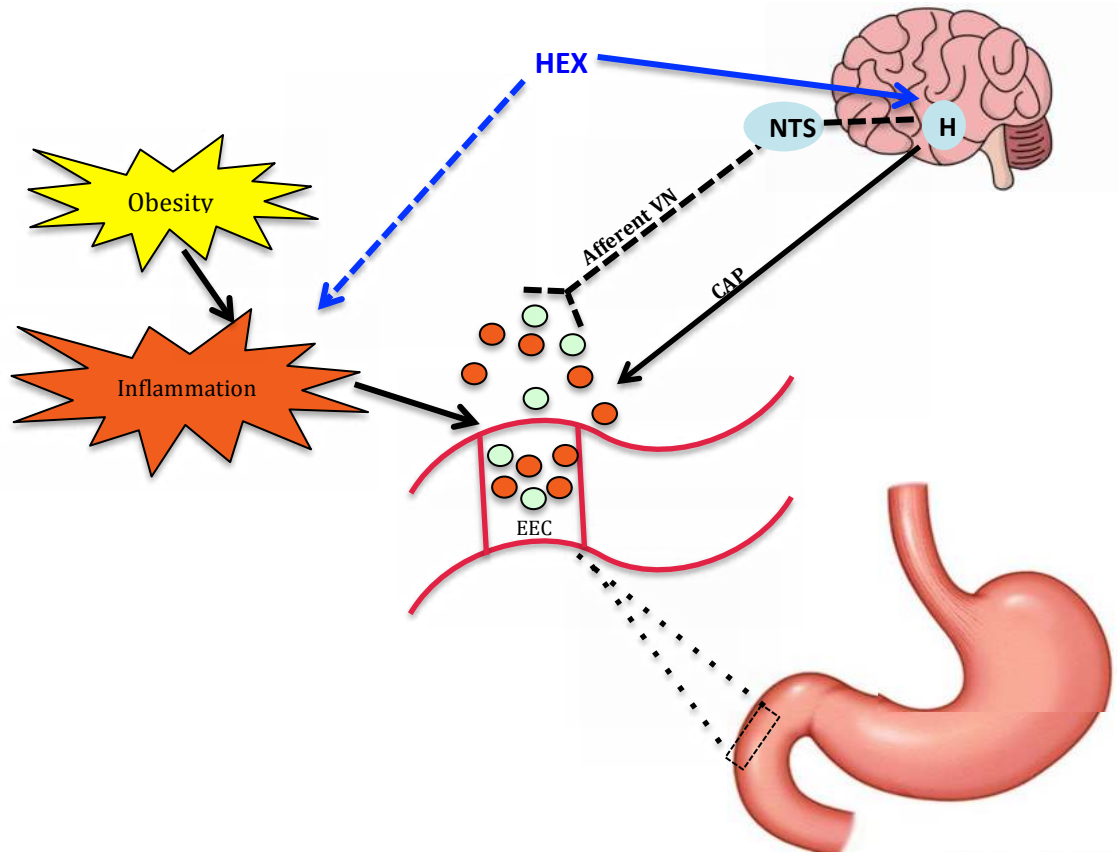

Figure 65: Afferent vagal nerve signaling normally activated by cytokines or neuroendocrine peptides, however this response is blunted in obesity (indicated by dotted line). Never the less, it is likely that pharmacological activation of the CAP by exogenous administration of GHS will suppress the pro-inflammatory cytokines contributing to the pro-inflammatory phenotype of the obese patient, down-regulating inflammation.

6.2.2 The heart-brain axis and ghrelin

The ANS has profound and complex effects on cardiovascular *function, remodelling and mortality (155, 214). GHS appear to modulate outcome and progression of IHD by influencing the ANS and vagal anti-inflammatory pathways.*

Ghrelin activates the VN, the release of ghrelin is similarly promoted by VNS (215). ACH administration and muscarinic receptor agonists also increase ghrelin secretion, whereas muscarinic receptor antagonists decrease secretion (434). Additionally, studies have demonstrated that activation of sympathetic nerves increase ghrelin secretion (435), ghrelin-producing cells also express β1-adrenergic receptors and norepinephrine can stimulate ghrelin release via these receptors directly. Ghrelin

secretion in response to SNA may represent a negative feedback mediator for sympathetic activation (434).

Ghrelin has been implicated as a biomarker and prognostic indicator for patients with chronic heart failure (133). Lower levels of ghrelin have been demonstrated in chronic heart failure patients and correspond to the severity of heart failure diagnosis (133). Similarly, in rat model of MI, decreased levels of plasma and cardiac ghrelin were expressed, however, increased GHS-R expression was observed. Plasma ghrelin was shown to correlate negatively with LV end diastolic pressure (436). Matsumoto et al. reported that serum ghrelin levels were significantly decreased in association with myocardial infarct size and cardiac function in AMI patients (437). With regards to systemic disease, circling levels of ghrelin were significantly decreased in a rat model of sepsis with a marked elevation in GHS-R expression in early sepsis (219, 220, 222, 223).

Interestingly, exercise training has been demonstrated to increase ghrelin levels in patients in the setting of HFpEF. Patients with lower ghrelin levels at baseline were found to experience a more pronounced increase in ghrelin under a training intervention (58). Exercise training has been demonstrated to reduce mortality in MI patients though improving ANS control (438). Chronic benefits of exercise training are thought to be associated with improvement in baroreflex sensitivity with an increase in vagal activity and reduction in sympathetic activity to the heart, reticuloendothelial system and other tissues including the brain, liver, spleen and gastrointestinal tract. It is thought that this autonomic remodeling is directly associated with an improved local and systemic inflammatory profile, thereby reducing cardiovascular risk and enhancing survival post-MI (438). It is interesting to speculate that ghrelin may play a (primary?) role in the protective effects resulting

from exercise training, this is likely through ghrelin-mediated autonomic modulation (Fig. 66).

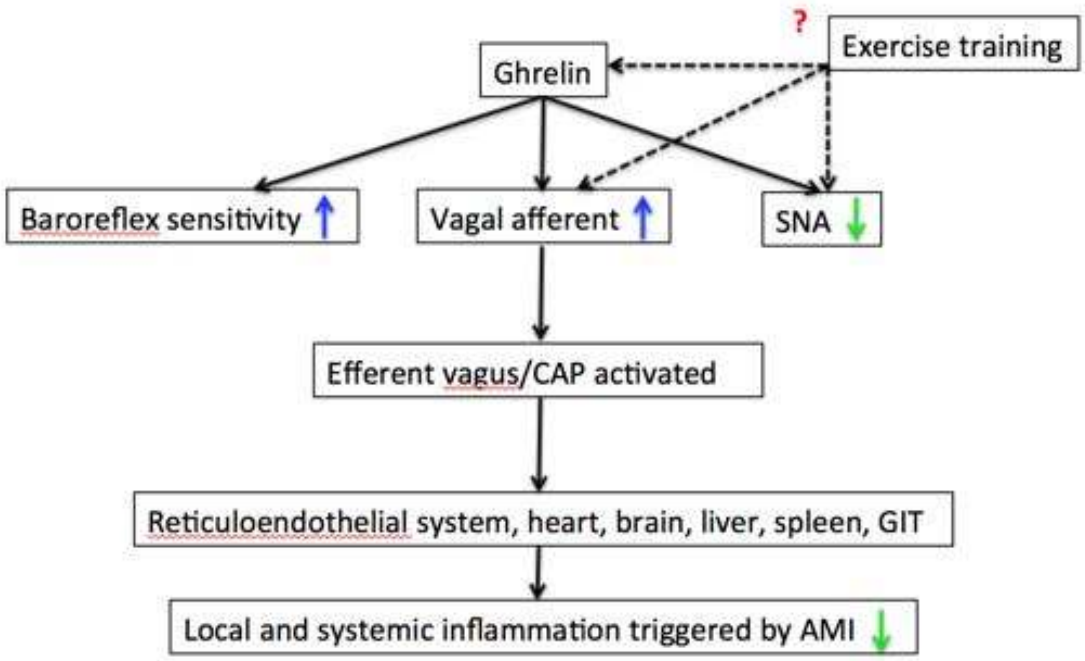

Figure 66: Influence of exercise training on the ANS and inflammation (see text). Green arrows represent down regulation, blue arrows represent enhancement. Exercise training has been shown to increase ghrelin levels in the setting of heart failure, it is unclear whether this is the case in all inflammatory states/diseases.

In patients with end stage chronic heart failure, LV dysfunction and cardiac cachexia are observed. This catabolic state is associated with hormonal changes and cytokine activation (439). Ghrelin has been demonstrated to have an anti-cardiac cachexia effect and is upregulated in cachexic patients with chronic heart failure (57, 440). Considering that ghrelin is closely involved with energy balance, it is possible that altered plasma ghrelin levels in the cachectic chronic heart failure patient may represent a compensatory mechanism for the proinflammatory state (441). Plasma ghrelin levels are seen to increase in association with a decrease in body mass index and an increase in plasma TNF- level in patients with chronic heart failure.

Specifically, plasma ghrelin increased when patients developed cardiac cachexia. Exogenous administration of ghrelin in rats with severe chronic heart failure was seen to attenuate cardiac cachexia and improve cardiac structure and function (57, 439). In conclusion, in the advanced stage of cardiac cachexia, ghrelin may be upregulated to address the catabolic-anabolic energy imbalance and proinflammatory disease state (289, 442, 443).

Overall, there is a complex relationship that exists between plasma and tissue ghrelin, GHS-R expression and energy balance – particularly with the added dimension of cardiac (or metabolic) *disease*. This is demonstrated by the complexity of the "cachexic" CVD patient with upregulated circulating ghrelin versus the "obese" CVD patient with lower circulating ghrelin but upregulation of the GHS-R. There is no doubt that ghrelin plays a significant & multi-modal role in the "metabolic-inflammatory-CVD" patient and it is clear that, detailed investigations are required to clarify the role of ghrelin and energy homeostasis in the context of CVD. None-the-less, there is clearly a therapeutic advantage of exogenous GHS administration in the "CVD-metabolic" patient.

6.2.3 Autonomic modulation

It is interesting to note that the cardioprotective effects of VNS in animal models have not yet been replicated in human clinical studies (274). Importantly, it is worthy to note that patients enrolled in VNS- studies were diagnosed with chronic cardiovascular disease without markers of inflammation (214). Thus, it could be postulated that those with long-standing fibrotic cardiomyopathic diseases may not benefit from the anti-inflammatory action defined by that of VNS. To support this hypothesis, acute IV HEX administration has not been shown to increase LV ejection

fraction in human patients with dilated cardiomyopathy with severe left ventricular dysfunction whereas an increase in ejection fraction has been observed in patients with ischemic cardiomyopathy (401). Those suffering from an acute event, for which there is an initial inflammatory insult (with the potential for cardiac remodelling) may be more likely to have beneficial response to VNS (214, 272). To our knowledge, this has not yet been investigated clinically.

Given that mortality in MI has been strongly associated with an adverse and sustained increase in CSNA initiated acutely post-infarction (11, 88), targeting adverse processes such as SNS activation and uncontrolled inflammation immediately post-infarction may also offer a chronic cardioprotective advantage by ameliorating down-stream pathways culminating in fibroblast activation, ventricular remodelling and dysfunction. Cardioprotective effects have been demonstrated with early ghrelin & HEX administration in models of IHD (42, 104, 444).

Given these findings, it might be reasonable to conclude that GHS therapy may be more effective in the CVD patient characterized by acute, inflammatory insults. Secondly this would also highlight the importance of early therapeutic administration of GHS in IHD patients. None-the-less, ghrelin clearly has effects in chronic CVD and this may also relate to its influence on systemic inflammation, energy balance and metabolic disease, particularly in the multifactorial context that characterizes the typically comorbid CVD patient. These concepts need desperate ongoing investigation in both the preclinical and clinical realms.

Finally, it is critically important that CVD is not seen as an isolated disease entity and needs to be thought of in the context of its comorbidities and risk factors. It is likely that GHS target multiple areas of cardiovascular and metabolic disease and thus may represent a unique therapeutic agent for clinical cardiovascular medicine.

7. Conclusion & future directions

AMI is associated with considerable morbidity and mortality. With more than a million patients hospitalized annually, heart failure continues to be one of the most challenging conditions to prevent and manage (445, 446). To date, there remains a clear lack of effective therapeutic agents available to target the adverse processes involved in the progression of AMI. This work has provided novel insight into the action of HEX in the setting of AMI and has specifically demonstrated that HEX therapy can improve myocardial function, reduce inflammation and infarct size in a mouse models of IHD.

The development of therapeutic approaches to protect the ischemic heart requires preclinical studies that examine cardioprotection specifically in relation to complicating disease states and risk factors (9). Important future directions highlighted from this work include utilizing disease models representative of the target clinical population (i.e, models with metabolic disease, T2DM, obesity, hypertension). Future studies are critical in order to assess the therapeutic response to HEX in models with such comorbidities. Recently, Tan et al generated a mouse model of obesity, hyperglycemia and mild kidney pathology and induced a hypertrophic phenotype by transverse aortic constriction (447), these types of models are critical for advancing investigation assessing the therapeutic efficacy of pharmacological agents in the setting of comorbidities..

Recently, the metabolic pathway involving CD36, a fatty acid transporter and energy substrate supplier to the heart (403) has been identified as a receptor of HEX with the potential to mediate GHS actions in the heart (44). Furthermore, CD36 has been advocated as a potential antifibrotic target in renal proximal tubule fibrosis (448) and

lung fibrosis in mice (449). This pathway is worthy of further investigation in relation to HEX's action in IHD but was beyond the scope of this thesis.

Although animal data indicates that VNS can affect remodelling and survival outcomes in CVD, similar data has not yet translated into the clinical realm. There does, however, appear to be a relationship between VN activation and inflammation in humans (208). To date, there have been no direct clinical studies assessing the application of VNS in AMI patients (450). As a pharmacological activator of the CAP, it would also seem prudent to assess the therapeutic response to HEX in the AMI compared with that of the patient with chronic fibrocardiomyopathic cardiovascular disease.

Finally, once these questions have been answered, there will ultimately be a need to employ clinical trials assessing HEX as a therapeutic agent in the IHD-metabolic patient.

8. References:

1. Robertson J, McElduff P, Pearson S-A, Henry DA, Inder KJ, Attia JR. The health services burden of heart failure: an analysis using linked population health data-sets. *BMC health services research* (2012) 12(1):103.
2. Stewart S, MacIntyre K, Capewell S, McMurray J. Heart failure and the aging population: an increasing burden in the 21st century? *Heart* (2003) 89(1):49-53.
3. Hausenloy DJ, Yellon DM. Myocardial ischemia-reperfusion injury: a neglected therapeutic target. *J Clin Invest* (2013) 123(1):92-100. doi: 10.1172/JCI62874. PubMed PMID: 23281415; PubMed Central PMCID: PMCPMC3533275.
4. Jaswal JS, Keung W, Wang W, Ussher JR, Lopaschuk GD. Targeting fatty acid and carbohydrate oxidation--a novel therapeutic intervention in the ischemic and failing heart. *Biochimica et biophysica acta* (2011) 1813(7):1333-50. doi: 10.1016/j.bbamcr.2011.01.015. PubMed PMID: 21256164.
5. Reimer KA, Lowe JE, Rasmussen MM, Jennings RB. The wavefront phenomenon of ischemic cell death. 1. Myocardial infarct size vs duration of coronary occlusion in dogs. *Circulation* (1977) 56(5):786-94.
6. Jaswal JS, Keung W, Wang W, Ussher JR, Lopaschuk GD. Targeting fatty acid and carbohydrate oxidation—a novel therapeutic intervention in the ischemic and failing heart. *Biochimica et Biophysica Acta (BBA)-Molecular Cell Research* (2011) 1813(7):1333-50.
7. Treibel TA, White SK, Moon JC. Myocardial Tissue Characterization: Histological and Pathophysiological Correlation. *Curr Cardiovasc Imaging Rep* (2014) 7(3):9254. doi: 10.1007/s12410-013-9254-9. PubMed PMID: 25258658; PubMed Central PMCID: PMCPMC4169521.
8. Csonka C, Kupai K, Kocsis GF, Novak G, Fekete V, Bencsik P, et al. Measurement of myocardial infarct size in preclinical studies. *J Pharmacol Toxicol Methods* (2010) 61(2):163-70. doi: 10.1016/j.vascn.2010.02.014. PubMed PMID: 20188845.
9. Ferdinandy P, Schulz R, Baxter GF. Interaction of cardiovascular risk factors with myocardial ischemia/reperfusion injury, preconditioning, and postconditioning. *Pharmacol Rev* (2007) 59(4):418-58. doi: 10.1124/pr.107.06002. PubMed PMID: 18048761.
10. Braunwald E, & Kloner, R. A. . Braunwald, E., & Kloner, R. A. (1985). Myocardial reperfusion: a double-edged sword?. Journal of Clinical Investigation, 76(5), 1713. *Journal of Clinical Investigation* (1985) 76(5):1713.
11. Schwenke DO, Tokudome T, Kishimoto I, Horio T, Cragg PA, Shirai M, et al. One dose of ghrelin prevents the acute and sustained increase in cardiac sympathetic tone after myocardial infarction. *Endocrinology* (2012) 153(5):2436-43. doi: 10.1210/en.2011-2057. PubMed PMID: 22434083.
12. Dixon IM, Cunnington RH, Rattan SG, Wigle JT. Cardiac fibrosis and heart failure—cause or effect? *Cardiac Fibrosis and Heart Failure: Cause or Effect?* : Springer (2015). p. 1-4.
13. Samuel CS, Cendrawan S, Gao XM, Ming Z, Zhao C, Kiriazis H, et al. Relaxin remodels fibrotic healing following myocardial infarction. *Lab Invest* (2011) 91(5):675-90. doi: 10.1038/labinvest.2010.198. PubMed PMID: 21221074.
14. Segura AM, Frazier OH, Buja LM. Fibrosis and heart failure. *Heart Fail Rev* (2014) 19(2):173-85. doi: 10.1007/s10741-012-9365-4. PubMed PMID: 23124941.
15. Pfeffer MA, Braunwald E. Ventricular remodeling after myocardial infarction. Experimental observations and clinical implications. *Circulation* (1990) 81(4):1161-72.
16. Stuckey DJ, Carr CA, Tyler DJ, Clarke K. Cine-MRI versus two-dimensional echocardiography to measure in vivo left ventricular function in rat heart. *NMR in biomedicine* (2008) 21(7):765-72. doi: 10.1002/nbm.1268. PubMed PMID: 18457349.

17. Kim RJ, Fieno DS, Parrish TB, Harris K, Chen E-L, Simonetti O, et al. Relationship of MRI delayed contrast enhancement to irreversible injury, infarct age, and contractile function. *Circulation* (1999) 100(19):1992-2002.
18. Kelle S, Roes SD, Klein C, Kokocinski T, de Roos A, Fleck E, et al. Prognostic value of myocardial infarct size and contractile reserve using magnetic resonance imaging. *Journal of the American College of Cardiology* (2009) 54(19):1770-7.
19. Wu E, Ortiz JT, Tejedor P, Lee DC, Bucciarelli-Ducci C, Kansal P, et al. Infarct size by contrast enhanced cardiac magnetic resonance is a stronger predictor of outcomes than left ventricular ejection fraction or end-systolic volume index: prospective cohort study. *Heart* (2008) 94(6):730-6.
20. Roes SD, Kelle S, Kaandorp TA, Kokocinski T, Poldermans D, Lamb HJ, et al. Comparison of myocardial infarct size assessed with contrast-enhanced magnetic resonance imaging and left ventricular function and volumes to predict mortality in patients with healed myocardial infarction. *The American journal of cardiology* (2007) 100(6):930-6.
21. Eitel I, Friedrich MG. T2-weighted cardiovascular magnetic resonance in acute cardiac disease. *Journal of cardiovascular magnetic resonance : official journal of the Society for Cardiovascular Magnetic Resonance* (2011) 13:13. doi: 10.1186/1532-429X-13-13. PubMed PMID: 21332972; PubMed Central PMCID: PMC3060149.
22. Stork A, Muellerleile K, Bansmann PM, Graessner J, Kaul M, Kemper J, et al. Value of T2-weighted, first-pass and delayed enhancement, and cine CMR to differentiate between acute and chronic myocardial infarction. *European radiology* (2007) 17(3):610-7. doi: 10.1007/s00330-006-0460-6. PubMed PMID: 17149626.
23. Akki A, Gupta A, Weiss RG. Magnetic resonance imaging and spectroscopy of the murine cardiovascular system. *American journal of physiology Heart and circulatory physiology* (2013) 304(5):H633-48. doi: 10.1152/ajpheart.00771.2011. PubMed PMID: 23292717; PubMed Central PMCID: PMC3602757.
24. Howard AD, Feighner SD, Cully DF, Arena JP, Liberator PA, Rosenblum CI, et al. A receptor in pituitary and hypothalamus that functions in growth hormone release. *Science* (1996) 273(5277):974-7.
25. Kojima M, Kangawa K. Ghrelin: structure and function. *Physiological reviews* (2005) 85(2):495-522.
26. Kojima M, Hosoda H, Date Y, Nakazato M, Matsuo H, Kangawa K. Ghrelin is a growth-hormone-releasing acylated peptide from stomach. *Nature* (1999) 402(6762):656-60.
27. Hosoda H, Kojima M, Matsuo H, Kangawa K. Ghrelin and des-acyl ghrelin: two major forms of rat ghrelin peptide in gastrointestinal tissue. *Biochemical and biophysical research communications* (2000) 279(3):909-13.
28. Chen CY, Asakawa A, Fujimiya M, Lee SD, Inui A. Ghrelin gene products and the regulation of food intake and gut motility. *Pharmacol Rev* (2009) 61(4):430-81. doi: 10.1124/pr.109.001958. PubMed PMID: 20038570.
29. Baldanzi G, Filigheddu N, Cutrupi S, Catapano F, Bonissoni S, Fubini A, et al. Ghrelin and des-acyl ghrelin inhibit cell death in cardiomyocytes and endothelial cells through ERK1/2 and PI 3-kinase/AKT. *The Journal of cell biology* (2002) 159(6):1029-37. doi: 10.1083/jcb.200207165. PubMed PMID: 12486113; PubMed Central PMCID: PMC2173981.
30. Broglio F, Prodam F, Riganti F, Muccioli G, Ghigo E. Ghrelin: from somatotrope secretion to new perspectives in the regulation of peripheral metabolic functions. *Pituitary Today: Molecular, Physiological and Clinical Aspects*. 35. Karger Publishers (2006). p. 102-14.
31. Stengel A, Taché Y. Ghrelin–a pleiotropic hormone secreted from endocrine X/A-like cells of the stomach. *Frontiers in neuroscience* (2012) 6:24.
32. Date Y, Kojima M, Hosoda H, Sawaguchi A, Mondal MS, Suganuma T, et al. Ghrelin, a novel growth hormone-releasing acylated peptide, is synthesized in a distinct endocrine cell

type in the gastrointestinal tracts of rats and humans. *Endocrinology* (2000) 141(11):4255-61. doi: 10.1210/endo.141.11.7757. PubMed PMID: 11089560.
33. Guan XM, Yu H, Palyha OC, McKee KK, Feighner SD, Sirinathsinghji DJ, et al. Distribution of mRNA encoding the growth hormone secretagogue receptor in brain and peripheral tissues. *Brain research Molecular brain research* (1997) 48(1):23-9. PubMed PMID: 9379845.
34. Mori K, Yoshimoto A, Takaya K, Hosoda K, Ariyasu H, Yahata K, et al. Kidney produces a novel acylated peptide, ghrelin. *FEBS letters* (2000) 486(3):213-6. PubMed PMID: 11119706.
35. Marleau S, Mulumba M, Lamontagne D, Ong H. Cardiac and peripheral actions of growth hormone and its releasing peptides: relevance for the treatment of cardiomyopathies. *Cardiovascular research* (2006) 69(1):26-35.
36. Dezaki K. Ghrelin function in insulin release and glucose metabolism. *The Ghrelin System*. 25. Karger Publishers (2013). p. 135-43.
37. Briggs DI, Andrews ZB. Metabolic status regulates ghrelin function on energy homeostasis. *Neuroendocrinology* (2011) 93(1):48-57.
38. Sangiao-Alvarellos S, Cordido F. Effect of ghrelin on glucose-insulin homeostasis: therapeutic implications. *International Journal of Peptides* (2010) 2010.
39. Cheng K-C, Li Y-X, Asakawa A, Inui A. The role of ghrelin in energy homeostasis and its potential clinical relevance. *International journal of molecular medicine* (2010) 26(6):771-8.
40. Granata R, Isgaard J, Alloatti G, Ghigo E. Cardiovascular actions of the ghrelin gene-derived peptides and growth hormone-releasing hormone. *Experimental Biology and Medicine* (2011) 236(5):505-14.
41. Bisi G, Podio V, Valetto M, Broglio F, Bertuccio G, Del Rio G, et al. Acute cardiovascular and hormonal effects of GH and hexarelin, a synthetic GH-releasing peptide, in humans. *Journal of endocrinological investigation* (1999) 22(4):266-72.
42. Mao Y, Tokudome T, Kishimoto I. The cardiovascular action of hexarelin. *J Geriatr Cardiol* (2014) 11(3):253-8. doi: 10.11909/j.issn.1671-5411.2014.03.007. PubMed PMID: 25278975; PubMed Central PMCID: PMCPMC4178518.
43. Deghenghi R, Cananzi MM, Torsello A, Battisti C, Muller EE, Locatelli V. GH-releasing activity of hexarelin, a new growth hormone releasing peptide, in infant and adult rats. *Life sciences* (1994) 54(18):1321-8.
44. Bodart V, Febbraio M, Demers A, McNicoll N, Pohankova P, Perreault A, et al. CD36 mediates the cardiovascular action of growth hormone-releasing peptides in the heart. *Circulation research* (2002) 90(8):844-9.
45. Mao Y, Tokudome T, Kishimoto I, Otani K, Hosoda H, Nagai C, et al. Hexarelin treatment in male ghrelin knockout mice after myocardial infarction. *Endocrinology* (2013) 154(10):3847-54. doi: 10.1210/en.2013-1291. PubMed PMID: 23861368.
46. McDonald H, Peart J, Kurniawan N, Galloway G, Royce S, Samuel C, et al. Hexarelin targets neuroinflammatory pathways to preserve cardiac morphology and function in a mouse model of myocardial ischemia-reperfusion. *Biomedicine & Pharmacotherapy* (2020) 127:110165.
47. Huang J, Li Y, Zhang J, Liu Y, Lu Q. The Growth Hormone Secretagogue Hexarelin Protects Rat Cardiomyocytes From in vivo Ischemia/Reperfusion Injury Through Interleukin-1 Signaling Pathway. *International Heart Journal* (2017) 58(2):257-63.
48. Torsello A, Bresciani E, Rossoni G, Avallone R, Tulipano G, Cocchi D, et al. Ghrelin plays a minor role in the physiological control of cardiac function in the rat. *Endocrinology* (2003) 144(5):1787-92.

49. Falls HD, Dayton BD, Fry DG, Ogiela CA, Schaefer VG, Brodjian S, et al. Characterization of ghrelin receptor activity in a rat pituitary cell line RC-4B/C. *Journal of molecular endocrinology* (2006) 37(1):51-62.
50. Ma Y, Zhang L, Edwards JN, Launikonis BS, Chen C. Growth hormone secretagogues protect mouse cardiomyocytes from in vitro ischemia/reperfusion injury through regulation of intracellular calcium. *PLoS One* (2012) 7(4):e35265. doi: 10.1371/journal.pone.0035265. PubMed PMID: 22493744; PubMed Central PMCID: PMCPMC3320867.
51. Ma Y, Zhang L, Launikonis BS, Chen C. Growth hormone secretagogues preserve the electrophysiological properties of mouse cardiomyocytes isolated from in vitro ischemia/reperfusion heart. *Endocrinology* (2012) 153(11):5480-90. doi: 10.1210/en.2012-1404. PubMed PMID: 22948211.
52. Sun Q, Ma Y, Zhang L, Zhao YF, Zang WJ, Chen C. Effects of GH secretagogues on contractility and Ca2+ homeostasis of isolated adult rat ventricular myocytes. *Endocrinology* (2010) 151(9):4446-54. doi: 10.1210/en.2009-1432. PubMed PMID: 20610573.
53. Nagaya N, Moriya J, Yasumura Y, Uematsu M, Ono F, Shimizu W, et al. Effects of ghrelin administration on left ventricular function, exercise capacity, and muscle wasting in patients with chronic heart failure. *Circulation* (2004) 110(24):3674-9. doi: 10.1161/01.CIR.0000149746.62908.BB. PubMed PMID: 15569841.
54. Nagaya N, Miyatake, K., Uematsu, M., Oya, H., Shimizu, W., Hosoda, H., ... & Kangawa, K. Hemodynamic, Renal, and Hormonal Effects of Ghrelin Infusion in Patients with Chronic Heart Failure. *The Journal of Clinical Endocrinology & Metabolism* (2001) 86(12):5854-9.
55. Vestergaard ET, Andersen NH, Hansen TK, Rasmussen LM, Moller N, Sorensen KE, et al. Cardiovascular effects of intravenous ghrelin infusion in healthy young men. *Am J Physiol Heart Circ Physiol* (2007) 293(5):H3020-6. doi: 10.1152/ajpheart.00496.2007. PubMed PMID: 17873022.
56. Nagaya N, Kojima, M., Uematsu, M., Yamagishi, M., Hosoda, H., Oya, H., ... & Kangawa, K. Hemodynamic and hormonal effects of human ghrelin in healthy volunteers. *American Journal of Physiology-Regulatory, Integrative and Comparative Physiology* (2001) 280(5):R1483-R7.
57. Nagaya N, Uematsu M, Kojima M, Ikeda Y, Yoshihara F, Shimizu W, et al. Chronic administration of ghrelin improves left ventricular dysfunction and attenuates development of cardiac cachexia in rats with heart failure. *Circulation* (2001) 104(12):1430-5.
58. Trippel TD, Holzendorf V, Halle M, Gelbrich G, Nolte K, Duvinage A, et al. Ghrelin and hormonal markers under exercise training in patients with heart failure with preserved ejection fraction: results from the Ex-DHF pilot study. *ESC Heart Failure* (2016). doi: 10.1002/ehf2.12109.
59. Beiras-Fernandez A, Kreth S, Weis F, Ledderose C, Pöttinger T, Dieguez C, et al. Altered myocardial expression of ghrelin and its receptor (GHSR-1a) in patients with severe heart failure. *Peptides* (2010) 31(12):2222-8.
60. Sullivan R, Randhawa V, Stokes A, Wu D, Lalonde T, Kiaii B, et al. The Growth Hormone Secretagogue Receptor, Ghrelin and Biochemical Signaling Molecules in Human Heart Failure. *bioRxiv* (2018):362525.
61. Sullivan R, McGirr R, Hu S, Tan A, Wu D, Charron C, et al. Changes in the cardiac GHSR1a-ghrelin system correlate with myocardial dysfunction in diabetic cardiomyopathy in mice. *Journal of the Endocrine Society* (2017) 2(2):178-89.
62. McKelvie R, Benedict C, Yusuf S. Prevention of congestive heart failure and management of asymptomatic left ventricular dysfunction. *Bmj* (1999) 318(7195):1400-2.
63. Dixon IM, et al. . *Cardiac fibrosis and heart failure- Cause or effect* (2015).
64. Leask A. TGFβ, cardiac fibroblasts, and the fibrotic response. *Cardiovascular research* (2007) 74(2):207-12.

65. Sun Y, Weber KT. Angiotensin converting enzyme and myofibroblasts during tissue repair in the rat heart. *Journal of molecular and cellular cardiology* (1996) 28(5):851-8.
66. Vracko R, Thorning D. Contractile cells in rat myocardial scar tissue. *Laboratory investigation; a journal of technical methods and pathology* (1991) 65(2):214-27.
67. Sun Y, Weber KT. Infarct scar: a dynamic tissue. *Cardiovascular research* (2000) 46(2):250-6.
68. Porter KE, Turner NA. Cardiac fibroblasts: at the heart of myocardial remodeling. *Pharmacol Ther* (2009) 123(2):255-78. doi: 10.1016/j.pharmthera.2009.05.002. PubMed PMID: 19460403.
69. Nian M, Lee P, Khaper N, Liu P. Inflammatory cytokines and postmyocardial infarction remodeling. *Circ Res* (2004) 94(12):1543-53. doi: 10.1161/01.RES.0000130526.20854.fa. PubMed PMID: 15217919.
70. Saxena A, Chen W, Su Y, Rai V, Uche OU, Li N, et al. IL-1 induces proinflammatory leukocyte infiltration and regulates fibroblast phenotype in the infarcted myocardium. *J Immunol* (2013) 191(9):4838-48. doi: 10.4049/jimmunol.1300725. PubMed PMID: 24078695; PubMed Central PMCID: PMCPMC3822582.
71. Turner NA, Das A, Warburton P, O'Regan DJ, Ball SG, Porter KE. Interleukin-1α stimulates proinflammatory cytokine expression in human cardiac myofibroblasts. *American Journal of Physiology-Heart and Circulatory Physiology* (2009) 297(3):H1117-H27.
72. Zymek P, Nah D-Y, Bujak M, Ren G, Koerting A, Leucker T, et al. Interleukin-10 is not a critical regulator of infarct healing and left ventricular remodeling. *Cardiovascular research* (2007) 74(2):313-22.
73. Deschamps AM, Spinale FG. Pathways of matrix metalloproteinase induction in heart failure: bioactive molecules and transcriptional regulation. *Cardiovascular Research* (2006) 69(3):666-76.
74. Siwik DA, Chang DL-F, Colucci WS. Interleukin-1β and tumor necrosis factor-α decrease collagen synthesis and increase matrix metalloproteinase activity in cardiac fibroblasts in vitro. *Circulation research* (2000) 86(12):1259-65.
75. McDonald H, Peart J, Kurniawan N, Galloway G, Royce S, Samuel CS, et al. Hexarelin treatment preserves myocardial function and reduces cardiac fibrosis in a mouse model of acute myocardial infarction. *Physiol Rep* (2018) 6(9):e13699. doi: 10.14814/phy2.13699. PubMed PMID: 29756411; PubMed Central PMCID: PMCPMC5949285.
76. Cao J-M, Chen LS, KenKnight BH, Ohara T, Lee M-H, Tsai J, et al. Nerve sprouting and sudden cardiac death. *Circulation research* (2000) 86(7):816-21.
77. Cao J-M, Fishbein MC, Han JB, Lai WW, Lai AC, Wu T-J, et al. Relationship between regional cardiac hyperinnervation and ventricular arrhythmia. *Circulation* (2000) 101(16):1960-9.
78. Swissa M, Zhou S, Chang C-M, Lai AC, Cates A, Fishbein MC, et al. Induction of cardiac nerve sprouting and sympathetic hyperinnervation by subthreshold electrical stimulation of the left stellate ganglion in dogs. *Journal of the American College of Cardiology* (2002) 39:81.
79. Zhou S, CAO JM, Tebb ZD, Ohara T, HUANG HLA, Omichi C, et al. Modulation of QT interval by cardiac sympathetic nerve sprouting and the mechanisms of ventricular arrhythmia in a canine model of sudden cardiac death. *Journal of cardiovascular electrophysiology* (2001) 12(9):1068-73.
80. Chen P-S, Chen LS, Cao J-M, Sharifi B, Karagueuzian HS, Fishbein MC. Sympathetic nerve sprouting, electrical remodeling and the mechanisms of sudden cardiac death. *Cardiovascular research* (2001) 50(2):409-16.
81. Vanoli E, De Ferrari GM, Stramba-Badiale M, Hull S, Foreman RD, Schwartz PJ. Vagal stimulation and prevention of sudden death in conscious dogs with a healed myocardial infarction. *Circulation research* (1991) 68(5):1471-81.

82. La Rovere MT, Bigger JT, Marcus FI, Mortara A, Schwartz PJ, Investigators A. Baroreflex sensitivity and heart-rate variability in prediction of total cardiac mortality after myocardial infarction. *The Lancet* (1998) 351(9101):478-84.
83. Shivkumar K, Ajijola OA, Anand I, Armour JA, Chen PS, Esler M, et al. Clinical neurocardiology defining the value of neuroscience-based cardiovascular therapeutics. *J Physiol* (2016) 594(14):3911-54. doi: 10.1113/JP271870. PubMed PMID: 27114333; PubMed Central PMCID: PMCPMC4945719.
84. Vaseghi M, Shivkumar K. The role of the autonomic nervous system in sudden cardiac death. *Progress in cardiovascular diseases* (2008) 50(6):404.
85. Schwartz PJ. Cardiac sympathetic denervation to prevent life-threatening arrhythmias. *Nature reviews Cardiology* (2014) 11(6):346.
86. Huda MS, Mani H, Dovey T, Halford JC, Boyland E, Daousi C, et al. Ghrelin inhibits autonomic function in healthy controls, but has no effect on obese and vagotomized subjects. *Clin Endocrinol (Oxf)* (2010) 73(5):678-85. doi: 10.1111/j.1365-2265.2010.03865.x. PubMed PMID: 20738316.
87. Lin Y, Matsumura K, Fukuhara M, Kagiyama S, Fujii K, Iida M. Ghrelin acts at the nucleus of the solitary tract to decrease arterial pressure in rats. *Hypertension* (2004) 43(5):977-82. doi: 10.1161/01.HYP.0000122803.91559.55. PubMed PMID: 14993197.
88. Mao Y, Tokudome T, Otani K, Kishimoto I, Nakanishi M, Hosoda H, et al. Ghrelin prevents incidence of malignant arrhythmia after acute myocardial infarction through vagal afferent nerves. *Endocrinology* (2012) 153(7):3426-34. doi: 10.1210/en.2012-1065. PubMed PMID: 22535766.
89. Matsumura K, Tsuchihashi T, Fujii K, Abe I, Iida M. Central Ghrelin Modulates Sympathetic Activity in Conscious Rabbits. *Hypertension* (2002) 40(5):694-9. doi: 10.1161/01.hyp.0000035395.51441.10.
90. Schwenke DO, Tokudome T, Kishimoto I, Horio T, Shirai M, Cragg PA, et al. Early ghrelin treatment after myocardial infarction prevents an increase in cardiac sympathetic tone and reduces mortality. *Endocrinology* (2008) 149(10):5172-6. doi: 10.1210/en.2008-0472. PubMed PMID: 18599547.
91. Soeki T, Kishimoto I, Schwenke DO, Tokudome T, Horio T, Yoshida M, et al. Ghrelin suppresses cardiac sympathetic activity and prevents early left ventricular remodeling in rats with myocardial infarction. *Am J Physiol Heart Circ Physiol* (2008) 294(1):H426-32. doi: 10.1152/ajpheart.00643.2007. PubMed PMID: 18024547.
92. Soeki T, Koshiba K, Niki T, Kusunose K, Yamaguchi K, Yamada H, et al. Effect of ghrelin on autonomic activity in healthy volunteers. *Peptides* (2014) 62:1-5. doi: 10.1016/j.peptides.2014.09.015. PubMed PMID: 25265271.
93. Yasuda T, Masaki T, Kakuma T, Yoshimatsu H. Centrally administered ghrelin suppresses sympathetic nerve activity in brown adipose tissue of rats. *Neuroscience Letters* (2003) 349(2):75-8. doi: 10.1016/s0304-3940(03)00789-4.
94. Yuan MJ, Huang H, Tang YH, Wu G, Gu YW, Chen YJ, et al. Effects of ghrelin on Cx43 regulation and electrical remodeling after myocardial infarction in rats. *Peptides* (2011) 32(11):2357-61. doi: 10.1016/j.peptides.2011.10.004. PubMed PMID: 22008733.
95. Severs NJ, Bruce AF, Dupont E, Rothery S. Remodelling of gap junctions and connexin expression in diseased myocardium. *Cardiovasc Res* (2008) 80(1):9-19. doi: 10.1093/cvr/cvn133. PubMed PMID: 18519446; PubMed Central PMCID: PMCPMC2533424.
96. Roell W, Lewalter T, Sasse P, Tallini YN, Choi B-R, Breitbach M, et al. Engraftment of connexin 43-expressing cells prevents post-infarct arrhythmia. *Nature* (2007) 450(7171):819-24.
97. Yao J-A, Gutstein DE, Liu F, Fishman GI, Wit AL. Cell coupling between ventricular myocyte pairs from connexin43-deficient murine hearts. *Circulation research* (2003) 93(8):736-43.

98. Gutstein DE, Morley GE, Tamaddon H, Vaidya D, Schneider MD, Chen J, et al. Conduction slowing and sudden arrhythmic death in mice with cardiac-restricted inactivation of connexin43. *Circulation research* (2001) 88(3):333-9.
99. Beardslee MA, Lerner DL, Tadros PN, Laing JG, Beyer EC, Yamada KA, et al. Dephosphorylation and intracellular redistribution of ventricular connexin43 during electrical uncoupling induced by ischemia. *Circulation research* (2000) 87(8):656-62.
100. Lerner DL, Yamada KA, Schuessler RB, Saffitz JE. Accelerated onset and increased incidence of ventricular arrhythmias induced by ischemia in Cx43-deficient mice. *Circulation* (2000) 101(5):547-52.
101. Jiang H, Hu X, Lu Z, Wen H, Zhao D, Tang Q, et al. Effects of sympathetic nerve stimulation on ischemia-induced ventricular arrhythmias by modulating connexin43 in rats. *Arch Med Res* (2008) 39(7):647-54. doi: 10.1016/j.arcmed.2008.07.005. PubMed PMID: 18760192.
102. Ando M, Katare RG, Kakinuma Y, Zhang D, Yamasaki F, Muramoto K, et al. Efferent vagal nerve stimulation protects heart against ischemia-induced arrhythmias by preserving connexin43 protein. *Circulation* (2005) 112(2):164-70. doi: 10.1161/CIRCULATIONAHA.104.525493. PubMed PMID: 15998674.
103. Soeki T, Niki T, Uematsu E, Bando S, Matsuura T, Kusunose K, et al. Ghrelin protects the heart against ischemia-induced arrhythmias by preserving connexin-43 protein. *Heart Vessels* (2013) 28(6):795-801. doi: 10.1007/s00380-013-0333-2. PubMed PMID: 23494606.
104. Mao Y, Tokudome T, Kishimoto I, Otani K, Miyazato M, Kangawa K. One dose of oral hexarelin protects chronic cardiac function after myocardial infarction. *Peptides* (2014) 56:156-62. doi: 10.1016/j.peptides.2014.04.004. PubMed PMID: 24747279.
105. Govoni S, Pascale A, Amadio M, Calvillo L, D'Elia E, Cereda C, et al. NGF and heart: Is there a role in heart disease? *Pharmacological research* (2011) 63(4):266-77.
106. Korsching S. The neurotrophic factor concept: a reexamination. *The Journal of neuroscience* (1993) 13(7):2739-48.
107. Zhou S, Chen LS, Miyauchi Y, Miyauchi M, Kar S, Kangavari S, et al. Mechanisms of cardiac nerve sprouting after myocardial infarction in dogs. *Circulation research* (2004) 95(1):76-83.
108. Hasan W, Jama A, Donohue T, Wernli G, Onyszchuk G, Al-Hafez B, et al. Sympathetic hyperinnervation and inflammatory cell NGF synthesis following myocardial infarction in rats. *Brain research* (2006) 1124(1):142-54.
109. Baeuerle PA, Henkel T. Function and activation of NF-kappaB in the immune system. *Annual review of immunology* (1994) 12(1):141-79.
110. Reichardt LF. Neurotrophin-regulated signalling pathways. *Philosophical Transactions of the Royal Society of London B: Biological Sciences* (2006) 361(1473):1545-64.
111. Ieda M, Fukuda K, Hisaka Y, Kimura K, Kawaguchi H, Fujita J, et al. Endothelin-1 regulates cardiac sympathetic innervation in the rodent heart by controlling nerve growth factor expression. *The Journal of clinical investigation* (2004) 113(6):876-84.
112. Yuan MJ, Huang CX, Tang YH, Wang X, Huang H, Chen YJ, et al. A novel peptide ghrelin inhibits neural remodeling after myocardial infarction in rats. *Eur J Pharmacol* (2009) 618(1-3):52-7. doi: 10.1016/j.ejphar.2009.07.015. PubMed PMID: 19616538.
113. Guarda E, Katwa LC, Myers PR, Tyagi SC, Weber KT. Effects of endothelins on collagen turnover in cardiac fibroblasts. *Cardiovascular research* (1993) 27(12):2130-4.
114. Mansoor AM, Honda M, Saida K, Ishinaga Y, Kuramochi T, Maeda A, et al. Endothelin-induced collagen remodeling in experimental pulmonary hypertension. *Biochemical and biophysical research communications* (1995) 215(3):981-6.
115. Rizvi MA, Katwa L, Spadone DP, Myers PR. The effects of endothelin-1 on collagen type I and type III synthesis in cultured porcine coronary artery vascular smooth muscle cells. *Journal of molecular and cellular cardiology* (1996) 28(2):243-52.

116. Lagares D, Busnadiego O, García‐Fernández RA, Kapoor M, Liu S, Carter DE, et al. Inhibition of focal adhesion kinase prevents experimental lung fibrosis and myofibroblast formation. *Arthritis & Rheumatism* (2012) 64(5):1653-64.
117. Lagares D, Busnadiego O, García-Fernández RA, Lamas S, Rodríguez-Pascual F. Adenoviral gene transfer of endothelin-1 in the lung induces pulmonary fibrosis through the activation of focal adhesion kinase. *American journal of respiratory cell and molecular biology* (2012) 47(6):834-42.
118. Lagares D, García‐Fernández RA, Jiménez CL, Magán‐Marchal N, Busnadiego O, Lamas S, et al. Endothelin 1 contributes to the effect of transforming growth factor β1 on wound repair and skin fibrosis. *Arthritis & Rheumatism* (2010) 62(3):878-89.
119. Fligny C, Duffield JS. Activation of pericytes: recent insights into kidney fibrosis and microvascular rarefaction. *Current opinion in rheumatology* (2013) 25(1):78-86.
120. Simonson MS, Ismail-Beigi F. Endothelin-1 increases collagen accumulation in renal mesangial cells by stimulating a chemokine and cytokine autocrine signaling loop. *Journal of Biological Chemistry* (2011) 286(13):11003-8.
121. Jain R, Shaul PW, Borok Z, Willis BC. Endothelin-1 induces alveolar epithelial–mesenchymal transition through endothelin type A receptor–mediated production of TGF-β1. *American journal of respiratory cell and molecular biology* (2007) 37(1):38-47.
122. Piera-Velazquez S, Li Z, Jimenez SA. Role of endothelial-mesenchymal transition (EndoMT) in the pathogenesis of fibrotic disorders. *The American journal of pathology* (2011) 179(3):1074-80.
123. Sun G, Stacey MA, Bellini A, Marini M, Mattoli S. Endothelin-1 induces bronchial myofibroblast differentiation. *Peptides* (1997) 18(9):1449-51.
124. Mueller EE, Momen A, Masse S, Zhou YQ, Liu J, Backx PH, et al. Electrical remodelling precedes heart failure in an endothelin-1-induced model of cardiomyopathy. *Cardiovasc Res* (2011) 89(3):623-33. doi: 10.1093/cvr/cvq351. PubMed PMID: 21062919.
125. Spinella F, Rosanò L, Di Castro V, Nicotra MR, Natali PG, Bagnato A. Endothelin-1 decreases gap junctional intercellular communication by inducing phosphorylation of connexin 43 in human ovarian carcinoma cells. *Journal of Biological Chemistry* (2003) 278(42):41294-301.
126. Huang CX, Yuan MJ, Huang H, Wu G, Liu Y, Yu SB, et al. Ghrelin inhibits post-infarct myocardial remodeling and improves cardiac function through anti-inflammation effect. *Peptides* (2009) 30(12):2286-91. doi: 10.1016/j.peptides.2009.09.004. PubMed PMID: 19747956.
127. Rosker C, Salvarani N, Schmutz S, Grand T, Rohr S. Abolishing myofibroblast arrhythmogeneicity by pharmacological ablation of alpha-smooth muscle actin containing stress fibers. *Circ Res* (2011) 109(10):1120-31. doi: 10.1161/CIRCRESAHA.111.244798. PubMed PMID: 21921266.
128. Cohn JN LT, Olivari MT, Garberg V, Lura D, Francis GS, Simon AB, Rector T. Plasma norepinephrine as a guide to prognosis in patients with chronic congestive heart failure. *New England journal of medicine* (1984) 311(13):819-23.
129. Malliani A, & Pagani, M. The role of the sympathetic nervous system in congestive heart failure. *European heart journal* (1983) 4(suppl_A):49-54.
130. Kaye DM LJ, Jennings GL, Bergin P, Broughton A, Esler MD. Adverse consequences of high sympathetic nervous activity in the failing human heart. *Journal of the American College of Cardiology* (1995) 26(5):1257-63.
131. Swedberg K EP, Kjekshus J, Wilhelmsen L. Hormones regulating cardiovascular function in patients with severe congestive heart failure and their relation to mortality. CONSENSUS Trial Study Group. *Circulation* (1990) 82(5):1730-6.
132. Zhang Y, Popovic ZB, Bibevski S, Fakhry I, Sica DA, Van Wagoner DR, et al. Chronic vagus nerve stimulation improves autonomic control and attenuates systemic inflammation

and heart failure progression in a canine high-rate pacing model. *Circ Heart Fail* (2009) 2(6):692-9. doi: 10.1161/CIRCHEARTFAILURE.109.873968. PubMed PMID: 19919995.
133. Chen Y, Ji XW, Zhang AY, Lv JC, Zhang JG, Zhao CH. Prognostic value of plasma ghrelin in predicting the outcome of patients with chronic heart failure. *Arch Med Res* (2014) 45(3):263-9. doi: 10.1016/j.arcmed.2014.01.004. PubMed PMID: 24508287.
134. Jardine D, Charles C, Ashton R, Bennett S, Whitehead M, Frampton C, et al. Increased cardiac sympathetic nerve activity following acute myocardial infarction in a sheep model. *The Journal of physiology* (2005) 565(1):325-33.
135. Sutton MGSJ, Sharpe N. Left ventricular remodeling after myocardial infarction: pathophysiology and therapy. *Circulation* (2000) 101(25):2981-8.
136. Nishiue T, Tsuji H, Tarumi N, Tokunaga S, Tamura K, Masaki M, et al. Heart rate variability and left ventricular dilatation early after myocardial infarction. *Journal of electrocardiology* (1999) 32(3):263-8.
137. Packer M, Bristow MR, Cohn JN, Colucci WS, Fowler MB, Gilbert EM, et al. The effect of carvedilol on morbidity and mortality in patients with chronic heart failure. *New England Journal of Medicine* (1996) 334(21):1349-55.
138. Hjalmarson Å, Goldstein S, Fagerberg B, Wedel H, Waagstein F, Kjekshus J, et al. Effects of controlled-release metoprolol on total mortality, hospitalizations, and well-being in patients with heart failure: the Metoprolol CR/XL Randomized Intervention Trial in congestive heart failure (MERIT-HF). *Jama* (2000) 283(10):1295-302.
139. Olshansky B, Sullivan RM, Colucci WS, Sabbah HN. The Parasympathetic Nervous System and Heart Failure: Pathophysiology and Potential Therapeutic Modalities for Heart Failure. (2015):107-28. doi: 10.1007/978-3-319-15961-4_6.
140. Lechat P, Brunhuber K, Hofmann R, Kuhn P, Nesser H, Slany J, et al. The cardiac insufficiency bisoprolol study II (CIBIS-II): a randomised trial. *Lancet* (1999) 353(9146):9-13.
141. Lymperopoulos A, Rengo G, Gao E, Ebert SN, Dorn GW, Koch WJ. Reduction of sympathetic activity via adrenal-targeted GRK2 gene deletion attenuates heart failure progression and improves cardiac function after myocardial infarction. *Journal of Biological Chemistry* (2010) 285(21):16378-86.
142. Ismahil MA, Hamid T, Bansal SS, Patel B, Kingery JR, Prabhu SD. Remodeling of the mononuclear phagocyte network underlies chronic inflammation and disease progression in heart failure: critical importance of the cardiosplenic axis. *Circulation research* (2014) 114(2):266-82.
143. Huston JM, Gallowitsch-Puerta M, Ochani M, Ochani K, Yuan R, Rosas-Ballina M, et al. Transcutaneous vagus nerve stimulation reduces serum high mobility group box 1 levels and improves survival in murine sepsis. *Read Online: Critical Care Medicine| Society of Critical Care Medicine* (2007) 35(12):2762-8.
144. Emami H, Singh P, MacNabb M, Vucic E, Lavender Z, Rudd JH, et al. Splenic metabolic activity predicts risk of future cardiovascular events: demonstration of a cardiosplenic axis in humans. *JACC: Cardiovascular Imaging* (2015) 8(2):121-30.
145. Mao Y, Tokudome T, Otani K, Kishimoto I, Miyazato M, Kangawa K. Excessive sympathoactivation and deteriorated heart function after myocardial infarction in male ghrelin knockout mice. *Endocrinology* (2013) 154(5):1854-63. doi: 10.1210/en.2012-2132. PubMed PMID: 23515286.
146. Chang L, Ren Y, Liu X, Li WG, Yang J, Geng B, et al. Protective effects of ghrelin on ischemia/reperfusion injury in the isolated rat heart. *Journal of cardiovascular pharmacology* (2004) 43(2):165-70.
147. Shimizu S, Akiyama T, Kawada T, Sonobe T, Kamiya A, Shishido T, et al. Centrally administered ghrelin activates cardiac vagal nerve in anesthetized rabbits. *Auton Neurosci* (2011) 162(1-2):60-5. doi: 10.1016/j.autneu.2011.04.001. PubMed PMID: 21543266.

148. Ueno H, Nakazato M. Mechanistic relationship between the vagal afferent pathway, central nervous system and peripheral organs in appetite regulation. *Journal of diabetes investigation* (2016) 7(6):812-8.
149. Kishimoto I, Tokudome T, Schwenke DO, Takeshi S, Hosoda H, Nagaya N, et al. Therapeutic potential of ghrelin in cardiac diseases. *Expert Review of Endocrinology & Metabolism* (2009) 4(3):283-9.
150. Date Y, Nakazato M, Murakami N, Kojima M, Kangawa K, Matsukura S. Ghrelin acts in the central nervous system to stimulate gastric acid secretion. *Biochemical and biophysical research communications* (2001) 280(3):904-7.
151. Bibevski S, Dunlap ME. Evidence for impaired vagus nerve activity in heart failure. *Heart Fail Rev* (2011) 16(2):129-35. doi: 10.1007/s10741-010-9190-6. PubMed PMID: 20820912.
152. Porter TR, Eckberg, D. L., Fritsch, J. M., Rea, R. F., Beightol, L. A., Schmedtje Jr, J. F., & Mohanty, P. K. Autonomic Pathophysiology in Heart Failure Patients Sympathetic-Cholinergic Interrelations. *Journal of Clinical Investigation* (1990) 85(5):1362.
153. Azevedo ER, & Parker, J. D. Parasympathetic Control of Cardiac Sympathetic Activity Normal Ventricular Function Versus Congestive Heart Failure. *Circulation* (1999) 100(3):274-9.
154. Abboud FM, Harwani SC, Chapleau MW. Autonomic neural regulation of the immune system: implications for hypertension and cardiovascular disease. *Hypertension* (2012) 59(4):755-62. doi: 10.1161/HYPERTENSIONAHA.111.186833. PubMed PMID: 22331383; PubMed Central PMCID: PMCPMC3313828.
155. Olshansky B, Sabbah HN, Hauptman PJ, Colucci WS. Parasympathetic nervous system and heart failure: pathophysiology and potential implications for therapy. *Circulation* (2008) 118(8):863-71. doi: 10.1161/CIRCULATIONAHA.107.760405. PubMed PMID: 18711023.
156. Wu L, Jiang Z, Li C, Shu M. Prediction of heart rate variability on cardiac sudden death in heart failure patients: a systematic review. *Int J Cardiol* (2014) 174(3):857-60. doi: 10.1016/j.ijcard.2014.04.176. PubMed PMID: 24804906; PubMed Central PMCID: PMCPMC4318838.
157. La Rovere MT, Pinna GD, Maestri R, Sleight P. Clinical value of baroreflex sensitivity. *Netherlands heart journal : monthly journal of the Netherlands Society of Cardiology and the Netherlands Heart Foundation* (2013) 21(2):61-3. doi: 10.1007/s12471-012-0349-8. PubMed PMID: 23184601; PubMed Central PMCID: PMC3547421.
158. Schwartz PJ. Vagal stimulation for heart diseases: from animals to men. An example of translational cardiology. *Netherlands heart journal : monthly journal of the Netherlands Society of Cardiology and the Netherlands Heart Foundation* (2013) 21(2):82-4. doi: 10.1007/s12471-012-0368-5. PubMed PMID: 23250848; PubMed Central PMCID: PMC3547428.
159. He X, Zhao M, Bi X, Sun L, Yu X, Zhao M, et al. Novel strategies and underlying protective mechanisms of modulation of vagal activity in cardiovascular diseases. *British journal of pharmacology* (2014). doi: 10.1111/bph.13010. PubMed PMID: 25378088.
160. De Ferrari GM, Tuinenburg AE, Ruble S, Brugada J, Klein H, Butter C, et al. Rationale and study design of the NEuroCardiac TherApy foR Heart Failure Study: NECTAR-HF. *European journal of heart failure* (2014) 16(6):692-9. doi: 10.1002/ejhf.80. PubMed PMID: 24846173; PubMed Central PMCID: PMC4288987.
161. Masuda Y, Tanaka T, Inomata N, Ohnuma N, Tanaka S, Itoh Z, et al. Ghrelin stimulates gastric acid secretion and motility in rats. *Biochem Biophys Res Commun* (2000) 276(3):905-8. doi: 10.1006/bbrc.2000.3568. PubMed PMID: 11027567.

162. Date Y, Nakazato M, Murakami N, Kojima M, Kangawa K, Matsukura S. Ghrelin acts in the central nervous system to stimulate gastric acid secretion. *Biochem Biophys Res Commun* (2001) 280(3):904-7. doi: 10.1006/bbrc.2000.4212. PubMed PMID: 11162609.
163. Habara H, Hayashi Y, Inomata N, Niijima A, Kangawa K. Organ-specific activation of the gastric branch of the efferent vagus nerve by ghrelin in urethane-anesthetized rats. *Journal of pharmacological sciences* (2014) 124(1):31-9.
164. Shimizu S, Akiyama T, Kawada T, Shishido T, Yamazaki T, Kamiya A, et al. In vivo direct monitoring of vagal acetylcholine release to the sinoatrial node. *Autonomic neuroscience : basic & clinical* (2009) 148(1-2):44-9. doi: 10.1016/j.autneu.2009.02.006. PubMed PMID: 19278905.
165. Tracey KJ. Physiology and immunology of the cholinergic antiinflammatory pathway. *J Clin Invest* (2007) 117(2):289-96. doi: 10.1172/JCI30555. PubMed PMID: 17273548; PubMed Central PMCID: PMCPMC1783813.
166. Floto RA, Smith KGC. The vagus nerve, macrophages, and nicotine. *The Lancet* (2003) 361(9363):1069-70. doi: 10.1016/s0140-6736(03)12902-9.
167. Pavlov VA, Wang, H., Czura, C. J., Friedman, S. G., & Tracey, K. J. . The cholinergic anti-inflammatory pathway: a missing link in neuroimmunomodulation. *Molecular medicine* (2003) 9(5-8):125.
168. Johnston GR, Webster NR. Cytokines and the immunomodulatory function of the vagus nerve. *Br J Anaesth* (2009) 102(4):453-62. doi: 10.1093/bja/aep037. PubMed PMID: 19258380.
169. Huston JM, Tracey KJ. The pulse of inflammation: heart rate variability, the cholinergic anti-inflammatory pathway and implications for therapy. *J Intern Med* (2011) 269(1):45-53. doi: 10.1111/j.1365-2796.2010.02321.x. PubMed PMID: 21158977; PubMed Central PMCID: PMCPMC4527046.
170. Rosas-Ballina M, Tracey KJ. Cholinergic control of inflammation. *J Intern Med* (2009) 265(6):663-79. doi: 10.1111/j.1365-2796.2009.02098.x. PubMed PMID: 19493060; PubMed Central PMCID: PMCPMC4540232.
171. Pavlov VA, Tracey KJ. The cholinergic anti-inflammatory pathway. *Brain, behavior, and immunity* (2005) 19(6):493-9. doi: 10.1016/j.bbi.2005.03.015. PubMed PMID: 15922555.
172. Bernik TR, Friedman, S. G., Ochani, M., DiRaimo, R., Ulloa, L., Yang, H., ... & Tracey, K. J. Pharmacological Stimulation of the Cholinergic Antiinflammatory Pathway. *The Journal of experimental medicine* (2002) 195(6):781-8.
173. Sternberg EM. Neural-immune Interactions in Health and Disease. *100(11)* (1997):2641.
174. Parrish WR, Rosas-Ballina M, Gallowitsch-Puerta M, Ochani M, Ochani K, Yang LH, et al. Modulation of TNF release by choline requires alpha7 subunit nicotinic acetylcholine receptor-mediated signaling. *Mol Med* (2008) 14(9-10):567-74. doi: 10.2119/2008-00079.Parrish. PubMed PMID: 18584048; PubMed Central PMCID: PMCPMC2435495.
175. Wang H, Yu M, Ochani M, Amella C, Tanovic M, Susarla S, et al. Nicotinic acetylcholine receptor alpha7 subunit is an essential regulator of inflammation Nature 2003 421. *N* 6921:384-8.
176. Pavlov VA. Cholinergic modulation of inflammation. *International journal of clinical and experimental medicine* (2008) 1(3):203.
177. Pavlov VA, Ochani M, Yang LH, Gallowitsch-Puerta M, Ochani K, Lin X, et al. Selective alpha7-nicotinic acetylcholine receptor agonist GTS-21 improves survival in murine endotoxemia and severe sepsis. *Critical care medicine* (2007) 35(4):1139-44. doi: 10.1097/01.CCM.0000259381.56526.96. PubMed PMID: 17334244.
178. Hofer S, Eisenbach C, Lukic IK, Schneider L, Bode K, Brueckmann M, et al. Pharmacologic cholinesterase inhibition improves survival in experimental sepsis. *Critical care medicine* (2008) 36(2):404-8.

179. Yeboah MM, Xue X, Javdan M, Susin M, Metz CN. Nicotinic acetylcholine receptor expression and regulation in the rat kidney after ischemia-reperfusion injury. *American journal of physiology Renal physiology* (2008) 295(3):F654-61. doi: 10.1152/ajprenal.90255.2008. PubMed PMID: 18614620; PubMed Central PMCID: PMC2536882.
180. Huston JM. The vagus nerve and the inflammatory reflex: wandering on a new treatment paradigm for systemic inflammation and sepsis. *Surgical infections* (2012) 13(4):187-93. doi: 10.1089/sur.2012.126. PubMed PMID: 22913335.
181. Boland C, Collet V, Laterre E, Lecuivre C, Wittebole X, Laterre P-F. Electrical vagus nerve stimulation and nicotine effects in peritonitis-induced acute lung injury in rats. *Inflammation* (2011) 34(1):29-35.
182. Su X, Matthay MA, Malik AB. Requisite Role of the Cholinergic α7 nAChR Pathway in Suppressing Gram-Negative Sepsis-Induced Acute Lung Inflammatory Injury. *The Journal of Immunology* (2009).
183. van Maanen MA, Lebre MC, van der Poll T, LaRosa GJ, Elbaum D, Vervoordeldonk MJ, et al. Stimulation of nicotinic acetylcholine receptors attenuates collagen‐induced arthritis in mice. *Arthritis & Rheumatism* (2009) 60(1):114-22.
184. Song X-M, Li J-G, Wang Y-L, Liang H, Huang Y, Yuan X, et al. Effect of vagus nerve stimulation on thermal injury in rats. *Burns* (2010) 36(1):75-81.
185. Costantini TW, Bansal V, Peterson CY, Loomis WH, Putnam JG, Rankin F, et al. Efferent vagal nerve stimulation attenuates gut barrier injury after burn: modulation of intestinal occludin expression. *The Journal of trauma* (2010) 68(6):1349.
186. Ay I, Lu J, Ay H, Sorensen AG. Vagus nerve stimulation reduces infarct size in rat focal cerebral ischemia. *Neuroscience letters* (2009) 459(3):147-51.
187. Meregnani J, Clarençon D, Vivier M, Peinnequin A, Mouret C, Sinniger V, et al. Anti-inflammatory effect of vagus nerve stimulation in a rat model of inflammatory bowel disease. *Autonomic Neuroscience* (2011) 160(1-2):82-9.
188. Nizri E, Irony-Tur-Sinai M, Lory O, Orr-Urtreger A, Lavi E, Brenner T. Activation of the cholinergic anti-inflammatory system by nicotine attenuates neuroinflammation via suppression of Th1 and Th17 responses. *The Journal of Immunology* (2009) 183(10):6681-8.
189. Guarini S, Cainazzo MM, Giuliani D, Mioni C, Altavilla D, Marini H, et al. Adrenocorticotropin reverses hemorrhagic shock in anesthetized rats through the rapid activation of a vagal anti-inflammatory pathway. *Cardiovascular research* (2004) 63(2):357-65.
190. Guarini S, Altavilla D, Cainazzo M-M, Giuliani D, Bigiani A, Marini H, et al. Efferent vagal fibre stimulation blunts nuclear factor-κB activation and protects against hypovolemic hemorrhagic shock. *Circulation* (2003) 107(8):1189-94.
191. Lee S-T, Chu K, Jung K-H, Kang K-M, Kim J-H, Bahn J-J, et al. Cholinergic anti-inflammatory pathway in intracerebral hemorrhage. *Brain research* (2010) 1309:164-71.
192. Mioni C, Bazzani C, Giuliani D, Altavilla D, Leone S, Ferrari A, et al. Activation of an efferent cholinergic pathway produces strong protection against myocardial ischemia/reperfusion injury in rats. *Critical care medicine* (2005) 33(11):2621-8.
193. Yeboah M, Xue X, Duan B, Ochani M, Tracey K, Susin M, et al. Cholinergic agonists attenuate renal ischemia–reperfusion injury in rats. *Kidney international* (2008) 74(1):62-9.
194. Altavilla D, Guarini S, Bitto A, Mioni C, Giuliani D, Bigiani A, et al. Activation of the cholinergic anti-inflammatory pathway reduces NF-κB activation, blunts TNF-α production, and protects againts splanchic artery occlusion shock. *Shock* (2006) 25(5):500-6.
195. Van Westerloo DJ, Giebelen IA, Florquin S, Bruno MJ, LaRosa GJ, Ulloa L, et al. The vagus nerve and nicotinic receptors modulate experimental pancreatitis severity in mice. *Gastroenterology* (2006) 130(6):1822-30.

196. Wu R, Dong W, Cui X, Zhou M, Simms HH, Ravikumar TS, et al. Ghrelin down-regulates proinflammatory cytokines in sepsis through activation of the vagus nerve. *Ann Surg* (2007) 245(3):480-6. doi: 10.1097/01.sla.0000251614.42290.ed. PubMed PMID: 17435556; PubMed Central PMCID: PMCPMC1877017.
197. Song X-M, Li J-G, Wang Y-L, Hu Z-F, Zhou Q, Du Z-H, et al. The protective effect of the cholinergic anti-inflammatory pathway against septic shock in rats. *Shock* (2008) 30(4):468-72.
198. Van Westerloo DJ, Giebelen IA, Florquin S, Daalhuisen J, Bruno MJ, de Vos AF, et al. The cholinergic anti-inflammatory pathway regulates the host response during septic peritonitis. *Journal of Infectious Diseases* (2005) 191(12):2138-48.
199. The FO, Boeckxstaens GE, Snoek SA, Cash JL, Bennink R, LaRosa GJ, et al. Activation of the cholinergic anti-inflammatory pathway ameliorates postoperative ileus in mice. *Gastroenterology* (2007) 133(4):1219-28.
200. Kim YS, Kim, J. S., Kwon, J. S., Jeong, M. H., Cho, J. G., Park, J. C., ... & Ahn, Y. BAY 11-7082, a Nuclear Factor-κB Inhibitor, Reduces Inflammation and Apoptosis in a Rat Cardiac Ischemia-Reperfusion Injury Model. *International heart journal* (2010) 51(5)(348-353).
201. Chappell D, Dorfler N, Jacob M, Rehm M, Welsch U, Conzen P, et al. Glycocalyx protection reduces leukocyte adhesion after ischemia/reperfusion. *Shock* (2010) 34(2):133-9. doi: 10.1097/SHK.0b013e3181cdc363. PubMed PMID: 20634656.
202. Bonaz B, Sinniger V, Pellissier S. Anti-inflammatory properties of the vagus nerve: potential therapeutic implications of vagus nerve stimulation. *J Physiol* (2016) 594(20):5781-90. doi: 10.1113/JP271539. PubMed PMID: 27059884; PubMed Central PMCID: PMCPMC5063949.
203. Huston JM, Ochani M, Rosas-Ballina M, Liao H, Ochani K, Pavlov VA, et al. Splenectomy inactivates the cholinergic antiinflammatory pathway during lethal endotoxemia and polymicrobial sepsis. *The Journal of experimental medicine* (2006) 203(7):1623-8. doi: 10.1084/jem.20052362. PubMed PMID: 16785311; PubMed Central PMCID: PMC2118357.
204. Wang H, Yu, M., Ochani, M., Amella, C. A., Tanovic, M., Susarla, S., ... & Tracey, K. J. Nicotinic acetylcholine receptor alpha7 subunit is an essential regulator of inflammation. *Nature* (2003) N421, 6921:384-8.
205. de Jonge WJ, Ulloa L. The alpha7 nicotinic acetylcholine receptor as a pharmacological target for inflammation. *British journal of pharmacology* (2007) 151(7):915-29. doi: 10.1038/sj.bjp.0707264. PubMed PMID: 17502850; PubMed Central PMCID: PMC2042938.
206. de Jonge WJ, van der Zanden EP, The FO, Bijlsma MF, van Westerloo DJ, Bennink RJ, et al. Stimulation of the vagus nerve attenuates macrophage activation by activating the Jak2-STAT3 signaling pathway. *Nature immunology* (2005) 6(8):844-51. doi: 10.1038/ni1229. PubMed PMID: 16025117.
207. Rosas-Ballina M, Ochani M, Parrish WR, Ochani K, Harris YT, Huston JM, et al. Splenic nerve is required for cholinergic antiinflammatory pathway control of TNF in endotoxemia. *Proceedings of the National Academy of Sciences of the United States of America* (2008) 105(31):11008-13. doi: 10.1073/pnas.0803237105. PubMed PMID: 18669662; PubMed Central PMCID: PMC2504833.
208. Olshansky B. Vagus nerve modulation of inflammation: Cardiovascular Implications. *Trends in cardiovascular medicine* (2015). doi: 10.1016/j.tcm.2015.03.016.
209. Tracey KJ. The inflammatory reflex. *Nature* (2002) 420(6917):853-9.
210. Nathan C. Points of control in inflammation. *Nature* (2002) 420(6917):846-52.
211. Orr-Urtreger A, Göldner, F. M., Saeki, M., Lorenzo, I., Goldberg, L., De Biasi, M., ... & Beaudet, A. L. . Mice Deficient in the a7 Neuronal Nicotinic Acetylcholine Receptor Lack a-

Bungarotoxin Binding Sites and Hippocampal Fast Nicotinic currents. *The Journal of neuroscience* (1997) 17(23),:9165-71.
212. Wang H, Liao H, Ochani M, Justiniani M, Lin X, Yang L, et al. Cholinergic agonists inhibit HMGB1 release and improve survival in experimental sepsis. *Nature medicine* (2004) 10(11):1216-21.
213. Borovikova LV, Ivanova, S., Zhang, M., Yang, H., Botchkina, G. I., Watkins, L. R., ... & Tracey, K. J. Vagus nerve stimulation attenuates the systemic inflammatory response to endotoxin. *Nature* (2000) 405(6785):458-62.
214. Olshansky B. Vagus nerve modulation of inflammation: Cardiovascular implications. *Trends Cardiovasc Med* (2015). doi: 10.1016/j.tcm.2015.03.016. PubMed PMID: 25939778.
215. Bansal V, Costantini T, Ryu SY, Peterson C, Loomis W, Putnam J, et al. Stimulating the central nervous system to prevent intestinal dysfunction after traumatic brain injury. *J Trauma* (2010) 68(5):1059-64. doi: 10.1097/TA.0b013e3181d87373. PubMed PMID: 20453760; PubMed Central PMCID: PMCPMC4251579.
216. Costantini TW, Bansal V, Peterson CY, Loomis WH, Putnam JG, Rankin F, et al. Efferent vagal nerve stimulation attenuates gut barrier injury after burn: modulation of intestinal occludin expression. *J Trauma* (2010) 68(6):1349-54; discussion 54-6. doi: 10.1097/TA.0b013e3181dccea0. PubMed PMID: 20539179; PubMed Central PMCID: PMCPMC4251593.
217. Pavlov VA, Ochani M, Yang L-H, Gallowitsch-Puerta M, Ochani K, Lin X, et al. Selective α7-nicotinic acetylcholine receptor agonist GTS-21 improves survival in murine endotoxemia and severe sepsis. *Critical care medicine* (2007) 35(4):1139-44.
218. Li Y. Sensory Signal Transduction in the Vagal Primary Afferent Neurons. *Current medicinal chemistry* (2007) 14(24):2554-63.
219. Chang L, Zhao J, Yang J, Zhang Z, Du J, Tang C. Therapeutic effects of ghrelin on endotoxic shock in rats. *European journal of pharmacology* (2003) 473(2):171-6.
220. Li WG, Gavrila D, Liu X, Wang L, Gunnlaugsson S, Stoll LL, et al. Ghrelin inhibits proinflammatory responses and nuclear factor-kappaB activation in human endothelial cells. *Circulation* (2004) 109(18):2221-6. doi: 10.1161/01.CIR.0000127956.43874.F2. PubMed PMID: 15117840.
221. Wu R, Zhou M, Das P, Dong W, Ji Y, Yang D, et al. Ghrelin inhibits sympathetic nervous activity in sepsis. *American journal of physiology Endocrinology and metabolism* (2007) 293(6):E1697-702. doi: 10.1152/ajpendo.00098.2007. PubMed PMID: 17911350.
222. Basa NR, Wang L, Arteaga JR, Heber D, Livingston EH, Taché Y. Bacterial lipopolysaccharide shifts fasted plasma ghrelin to postprandial levels in rats. *Neuroscience Letters* (2003) 343(1):25-8. doi: 10.1016/s0304-3940(03)00312-4.
223. Wu R, Zhou, M., Cui, X., Simms, H. H., & Wang, P. . Upregulation of cardiovascular ghrelin receptor occurs in the hyperdynamic phase of sepsis. *American Journal of Physiology-Heart and Circulatory Physiology* (2004) 287(3):H1296-H302.
224. Cheyuo C, Jacob A, Wang P. Ghrelin-mediated sympathoinhibition and suppression of inflammation in sepsis. *American journal of physiology Endocrinology and metabolism* (2012) 302(3):E265-72. doi: 10.1152/ajpendo.00508.2011. PubMed PMID: 22068604; PubMed Central PMCID: PMC3287362.
225. Yang S, Koo, D. J., Zhou, M., Chaudry, I. H., & Wang, P. Gut-derived norepinephrine plays a critical role in producing hepatocellular dysfunction during early sepsis. *American Journal of Physiology-Gastrointestinal and Liver Physiology* (2000) 279(6):G1274-G81.
226. Eisenhofer GRAEME, Aneman, A. N. D. E. R. S., Hooper, D. O. U. G. L. A. S., Holmes, C. O. U. R. T. N. E. Y., Goldstein, D. S., & Friberg, P. E. T. E. R. . Production and metabolism of dopamine and norepinephrine in mesenteric organs and liver of swine

. *American Journal of Physiology-Gastrointestinal and Liver Physiology* (1995) 268(4):G641-G9.

227. Eisenhofer G, Åneman, A., Hooper, D., Rundqvist, B., & Friberg, P. . Mesenteric Organ Production, Hepatic Metabolism, and Renal Elimination of Norepinephrine and Its Metabolites in Humans. *Journal of neurochemistry* (1996) 66(4):1565-73.
228. Kim YS, Kim JS, Kwon JS, Jeong MH, Cho JG, Park JC, et al. BAY 11-7082, a Nuclear Factor-. KAPPA. B Inhibitor, Reduces Inflammation and Apoptosis in a Rat Cardiac Ischemia-Reperfusion Injury Model. *International heart journal* (2010) 51(5):348-53.
229. Chappell D, Dörfler N, Jacob M, Rehm M, Welsch U, Conzen P, et al. Glycocalyx protection reduces leukocyte adhesion after ischemia/reperfusion. *Shock* (2010) 34(2):133-9.
230. Raghay K, Akki R, Bensaid D, Errami M. Ghrelin as an anti-inflammatory and protective agent in ischemia/reperfusion injury. *Peptides* (2020) 124:170226.
231. Wu R, Dong W, Ji Y, Zhou M, Marini CP, Ravikumar TS, et al. Orexigenic hormone ghrelin attenuates local and remote organ injury after intestinal ischemia-reperfusion. *PloS one* (2008) 3(4):e2026. doi: 10.1371/journal.pone.0002026. PubMed PMID: 18431503; PubMed Central PMCID: PMC2295264.
232. Rajan D, Wu R, Shah KG, Jacob A, Coppa GF, Wang P. Human ghrelin protects animals from renal ischemia-reperfusion injury through the vagus nerve. *Surgery* (2012) 151(1):37-47.
233. Nojiri T, Hosoda H, Kimura T, Tokudome T, Miura K, Takabatake H, et al. Protective effects of ghrelin on cisplatin-induced nephrotoxicity in mice. *Peptides* (2016) 82:85-91. doi: 10.1016/j.peptides.2016.06.003. PubMed PMID: 27298204.
234. Khowailed A, Younan SM, Ashour H, Kamel AE, Sharawy N. Effects of ghrelin on sepsis-induced acute kidney injury: one step forward. *Clinical and experimental nephrology* (2015) 19(3):419-26.
235. Mao Y, Tokudome T, Kishimoto I, Otani K, Nishimura H, Yamaguchi O, et al. Endogenous ghrelin attenuates pressure overload-induced cardiac hypertrophy via a cholinergic anti-inflammatory pathway. *Hypertension* (2015) 65(6):1238-44. doi: 10.1161/HYPERTENSIONAHA.114.04864. PubMed PMID: 25870195.
236. Mann DL, McMurray JJ, Packer M, Swedberg K, Borer JS, Colucci WS, et al. Targeted anticytokine therapy in patients with chronic heart failure: results of the Randomized Etanercept Worldwide Evaluation (RENEWAL). *Circulation* (2004) 109(13):1594-602. doi: 10.1161/01.CIR.0000124490.27666.B2. PubMed PMID: 15023878.
237. Metra M, Eichhorn E, Abraham WT, Linseman J, Bohm M, Corbalan R, et al. Effects of low-dose oral enoximone administration on mortality, morbidity, and exercise capacity in patients with advanced heart failure: the randomized, double-blind, placebo-controlled, parallel group ESSENTIAL trials. *European heart journal* (2009) 30(24):3015-26. doi: 10.1093/eurheartj/ehp338. PubMed PMID: 19700774; PubMed Central PMCID: PMC2792716.
238. Sabbah HN, Ilsar I, Zaretsky A, Rastogi S, Wang M, Gupta RC. Vagus nerve stimulation in experimental heart failure. *Heart Fail Rev* (2011) 16(2):171-8. doi: 10.1007/s10741-010-9209-z. PubMed PMID: 21128115; PubMed Central PMCID: PMCPMC3784341.
239. Li M, Zheng C, Sato T, Kawada T, Sugimachi M, Sunagawa K. Vagal nerve stimulation markedly improves long-term survival after chronic heart failure in rats. *Circulation* (2004) 109(1):120-4. doi: 10.1161/01.CIR.0000105721.71640.DA. PubMed PMID: 14662714.
240. Zheng C, Meihua Li, Masashi Inagaki, Toru Kawada, Kenji Sunagawa, and Masaru Sugimachi. Vagal stimulation markedly suppresses arrhythmias in conscious rats with chronic heart failure after myocardial infarction. *In 2005 IEEE Engineering in Medicine and Biology 27th Annual Conference* (2006) (IEEE):7072-5.
241. Sun J, Yanmei Lu, Yan Huang, and Najina Wugeti. Unilateral vagus nerve stimulation improves ventricular autonomic nerve distribution and functional

imbalance in a canine heart failure model. *International journal of clinical and experimental medicine* (2015) 8(6):9334.
242. Shen MJ, Shinohara T, Park HW, Frick K, Ice DS, Choi EK, et al. Continuous low-level vagus nerve stimulation reduces stellate ganglion nerve activity and paroxysmal atrial tachyarrhythmias in ambulatory canines. *Circulation* (2011) 123(20):2204-12. doi: 10.1161/CIRCULATIONAHA.111.018028. PubMed PMID: 21555706; PubMed Central PMCID: PMCPMC3101282.
243. De Ferrari GM, Crijns HJ, Borggrefe M, Milasinovic G, Smid J, Zabel M, et al. Chronic vagus nerve stimulation: a new and promising therapeutic approach for chronic heart failure. *Eur Heart J* (2011) 32(7):847-55. doi: 10.1093/eurheartj/ehq391. PubMed PMID: 21030409.
244. Aukrust P, Ueland T, Lien E, Bendtzen K, Müller F, Andreassen AK, et al. Cytokine network in congestive heart failure secondary to ischemic or idiopathic dilated cardiomyopathy. *The American journal of cardiology* (1999) 83(3):376-82.
245. Yan AT, Yan RT, Cushman M, Redheuil A, Tracy RP, Arnett DK, et al. Relationship of interleukin-6 with regional and global left-ventricular function in asymptomatic individuals without clinical cardiovascular disease: insights from the Multi-Ethnic Study of Atherosclerosis. *European heart journal* (2010) 31(7):875-82.
246. Deswal A, Petersen NJ, Feldman AM, Young JB, White BG, Mann DL. Cytokines and cytokine receptors in advanced heart failure: an analysis of the cytokine database from the Vesnarinone trial (VEST). *Circulation* (2001) 103(16):2055-9.
247. Aukrust P, Gullestad L, Ueland T, Damås JK, Yndestad A. Inflammatory and anti‐inflammatory cytokines in chronic heart failure: Potential therapeutic implications. *Annals of medicine* (2005) 37(2):74-85.
248. Li W, Olshansky B. Inflammatory cytokines and nitric oxide in heart failure and potential modulation by vagus nerve stimulation. *Heart Fail Rev* (2011) 16(2):137-45. doi: 10.1007/s10741-010-9184-4. PubMed PMID: 20658318.
249. Borovikova LV, Svetlana Ivanova, Minghuang Zhang, Huan Yang, Galina I. Botchkina, Linda R. Watkins, Haichao Wang, Naji Abumrad, John W. Eaton, and Kevin J. Tracey. Vagus nerve stimulation attenuates the systemic inflammatory response to endotoxin. *Nature* (2000) 405(6785):458.
250. Calvillo L, Vanoli E, Andreoli E, Besana A, Omodeo E, Gnecchi M, et al. Vagal stimulation, through its nicotinic action, limits infarct size and the inflammatory response to myocardial ischemia and reperfusion. *Journal of cardiovascular pharmacology* (2011) 58(5):500-7.
251. Bernik TR, Friedman SG, Ochani M, DiRaimo R, Susarla S, Czura CJ, et al. Cholinergic antiinflammatory pathway inhibition of tumor necrosis factor during ischemia reperfusion. *Journal of vascular surgery* (2002) 36(6):1231-6.
252. Kong SS, Liu JJ, Hwang TC, Yu XJ, Lu Y, Zang WJ. Tumour necrosis factor-alpha and its receptors in the beneficial effects of vagal stimulation after myocardial infarction in rats. *Clinical and experimental pharmacology & physiology* (2011) 38(5):300-6. doi: 10.1111/j.1440-1681.2011.05505.x. PubMed PMID: 21362018.
253. Katare RG, Ando M, Kakinuma Y, Arikawa M, Handa T, Yamasaki F, et al. Vagal nerve stimulation prevents reperfusion injury through inhibition of opening of mitochondrial permeability transition pore independent of the bradycardiac effect. *The Journal of thoracic and cardiovascular surgery* (2009) 137(1):223-31. doi: 10.1016/j.jtcvs.2008.08.020. PubMed PMID: 19154929.
254. Uemura K, Zheng C, Li M, Kawada T, Sugimachi M. Early short-term vagal nerve stimulation attenuates cardiac remodeling after reperfused myocardial infarction. *Journal of cardiac failure* (2010) 16(8):689-99. doi: 10.1016/j.cardfail.2010.03.001. PubMed PMID: 20670848.

255. Shinlapawittayatorn K, Chinda K, Palee S, Surinkaew S, Kumfu S, Kumphune S, et al. Vagus nerve stimulation initiated late during ischemia, but not reperfusion, exerts cardioprotection via amelioration of cardiac mitochondrial dysfunction. *Heart rhythm : the official journal of the Heart Rhythm Society* (2014) 11(12):2278-87. doi: 10.1016/j.hrthm.2014.08.001. PubMed PMID: 25093803.
256. Shinlapawittayatorn K, Chinda K, Palee S, Surinkaew S, Thunsiri K, Weerateerangkul P, et al. Low-amplitude, left vagus nerve stimulation significantly attenuates ventricular dysfunction and infarct size through prevention of mitochondrial dysfunction during acute ischemia-reperfusion injury. *Heart rhythm : the official journal of the Heart Rhythm Society* (2013) 10(11):1700-7. doi: 10.1016/j.hrthm.2013.08.009. PubMed PMID: 23933295.
257. Hamann JJ, Ruble SB, Stolen C, Wang M, Gupta RC, Rastogi S, et al. Vagus nerve stimulation improves left ventricular function in a canine model of chronic heart failure. *Eur J Heart Fail* (2013) 15(12):1319-26. doi: 10.1093/eurjhf/hft118. PubMed PMID: 23883651; PubMed Central PMCID: PMCPMC3895958.
258. Vanoli E, De Ferrari, G. M., Stramba-Badiale, M., Hull, S. S., Foreman, R. D., & Schwartz, P. J. Vagal Stimulation and Prevention of Sudden DeathinConsciousDogsWitha Healed Myocardial Infarction. *Circulation Research* (1991) 68(5):1471-81.
259. Zhang L, Lu Y, Sun J, Zhou X, Tang B. Subthreshold vagal stimulation suppresses ventricular arrhythmia and inflammatory response in a canine model of acute cardiac ischemia and reperfusion. *Exp Physiol* (2015). doi: 10.1113/EP085518. PubMed PMID: 26553757.
260. McKelvie RS, Benedict, C.R. and Yusuf, S. Prevention of congestive heart failure and management of asymptomatic left ventricular dysfunction. *Bmj* (1999) 318(7195):1400-2.
261. Uemura K, Li M, Tsutsumi T, Yamazaki T, Kawada T, Kamiya A, et al. Efferent vagal nerve stimulation induces tissue inhibitor of metalloproteinase-1 in myocardial ischemia-reperfusion injury in rabbit. *American Journal of Physiology-Heart and Circulatory Physiology* (2007) 293(4):H2254-H61.
262. Wang Z, Yu L, Huang B, Wang S, Liao K, Saren G, et al. Low-level transcutaneous electrical stimulation of the auricular branch of vagus nerve ameliorates left ventricular remodeling and dysfunction by downregulation of matrix metalloproteinase 9 and transforming growth factor β1. *Journal of cardiovascular pharmacology* (2015) 65(4):342-8.
263. Yokota T TH, Mori Y, Kudo T, Hiraga H, Suto N, Higuma T, Abe N, Hanada H, Osanai T, Okumura K. Imidapril and enalapril similarly inhibit plasma matrix metalloproteinase activities and attenuate left ventricular remodeling in patients with acute myocardial infarction. *Journal of cardiovascular pharmacology* (2014) 63(6):528-32.
264. Lu Y, Liu, J.J., Bi, X.Y., Yu, X.J., Kong, S.S., Qin, F.F., Zhou, J. and Zang, W.J. Pyridostigmine ameliorates cardiac remodeling induced by myocardial infarction via inhibition of the transforming growth factor-β1/TGF-β1–activated kinase pathway. *Journal of cardiovascular pharmacology* (2014) 63(5):412-20.
265. Bujak M, Dobaczewski M, Chatila K, Mendoza LH, Li N, Reddy A, et al. Interleukin-1 receptor type I signaling critically regulates infarct healing and cardiac remodeling. *The American journal of pathology* (2008) 173(1):57-67.
266. Yu L, Benjamin J. Scherlag, Shaolong Li, Youqi Fan, John Dyer, Shailesh Male, Vandana Varma, Yong Sha, Stavros Stavrakis, and Sunny S. Po. Low-level transcutaneous electrical stimulation of the auricular branch of the vagus nerve: a noninvasive approach to treat the initial phase of atrial fibrillation. *Heart rhythm* (2013) 10(3):428-35.
267. Wang Z, Yu L, Chen M, Wang S, Jiang H. Transcutaneous electrical stimulation of auricular branch of vagus nerve: a noninvasive therapeutic approach for post-ischemic heart failure. *Int J Cardiol* (2014) 177(2):676-7. doi: 10.1016/j.ijcard.2014.09.165. PubMed PMID: 25449481.

268. Sloan RP, McCreath H, Tracey KJ, Sidney S, Liu K, Seeman T. RR interval variability is inversely related to inflammatory markers: the CARDIA study. *Mol Med* (2007) 13(3-4):178-84. doi: 10.2119/2006-00112.Sloan. PubMed PMID: 17592552; PubMed Central PMCID: PMCPMC1892756.
269. Beekwilder JP, & Beems, T. Overview of the Clinical Applications of Vagus Nerve Stimulation. *Journal of Clinical Neurophysiology* (2010) 27(2),:130-8.
270. Schwartz PJ, De Ferrari GM, Sanzo A, Landolina M, Rordorf R, Raineri C, et al. Long term vagal stimulation in patients with advanced heart failure: first experience in man. *Eur J Heart Fail* (2008) 10(9):884-91. doi: 10.1016/j.ejheart.2008.07.016. PubMed PMID: 18760668.
271. Premchand RK, Sharma K, Mittal S, Monteiro R, Dixit S, Libbus I, et al. Autonomic regulation therapy via left or right cervical vagus nerve stimulation in patients with chronic heart failure: results of the ANTHEM-HF trial. *J Card Fail* (2014) 20(11):808-16. doi: 10.1016/j.cardfail.2014.08.009. PubMed PMID: 25187002.
272. Zannad F, De Ferrari GM, Tuinenburg AE, Wright D, Brugada J, Butter C, et al. Chronic vagal stimulation for the treatment of low ejection fraction heart failure: results of the NEural Cardiac TherApy foR Heart Failure (NECTAR-HF) randomized controlled trial. *Eur Heart J* (2015) 36(7):425-33. doi: 10.1093/eurheartj/ehu345. PubMed PMID: 25176942; PubMed Central PMCID: PMCPMC4328197.
273. Hauptman PJ, Schwartz PJ, Gold MR, Borggrefe M, Van Veldhuisen DJ, Starling RC, et al. Rationale and study design of the increase of vagal tone in heart failure study: INOVATE-HF. *American heart journal* (2012) 163(6):954-62 e1. doi: 10.1016/j.ahj.2012.03.021. PubMed PMID: 22709747.
274. Gold MR, Van Veldhuisen DJ, Hauptman PJ, Borggrefe M, Kubo SH, Lieberman RA, et al. Vagus Nerve Stimulation for the Treatment of Heart Failure: The INOVATE-HF Trial. *J Am Coll Cardiol* (2016) 68(2):149-58. doi: 10.1016/j.jacc.2016.03.525. PubMed PMID: 27058909.
275. Zhao M, Sun L, Liu JJ, Wang H, Miao Y, Zang WJ. Vagal nerve modulation: a promising new therapeutic approach for cardiovascular diseases. *Clinical and experimental pharmacology & physiology* (2012) 39(8):701-5. doi: 10.1111/j.1440-1681.2011.05644.x. PubMed PMID: 22077771.
276. Zietek T, Rath E. Inflammation Meets Metabolic Disease: Gut Feeling Mediated by GLP-1. *Front Immunol* (2016) 7:154. doi: 10.3389/fimmu.2016.00154. PubMed PMID: 27148273; PubMed Central PMCID: PMCPMC4840214.
277. Pavlov VA, Tracey KJ. The vagus nerve and the inflammatory reflex—linking immunity and metabolism. *Nature Reviews Endocrinology* (2012) 8(12):743-54.
278. Bastard J-P, Maachi M, Lagathu C, Kim MJ, Caron M, Vidal H, et al. Recent advances in the relationship between obesity, inflammation, and insulin resistance. *European cytokine network* (2006) 17(1):4-12.
279. Shoelson SE, Herrero L, Naaz A. Obesity, inflammation, and insulin resistance. *Gastroenterology* (2007) 132(6):2169-80.
280. Aukrust P, Ueland T, Müller F, Andreassen AK, Nordøy I, Aas H, et al. Elevated circulating levels of CC chemokines in patients with congestive heart failure. *Circulation* (1998) 97(12):1136-43.
281. Kubota T, McTiernan CF, Frye CS, Slawson SE, Lemster BH, Koretsky AP, et al. Dilated cardiomyopathy in transgenic mice with cardiac-specific overexpression of tumor necrosis factor-α. *Circulation research* (1997) 81(4):627-35.
282. Mann DL, McMurray JJ, Packer M, Swedberg K, Borer JS, Colucci WS, et al. Targeted anticytokine therapy in patients with chronic heart failure. *Circulation* (2004) 109(13):1594-602.

283. Powell N, Marjorie M. Walker, and Nicholas J. Talley. The mucosal immune system: master regulator of bidirectional gut–brain communications. *Nature Reviews Gastroenterology & Hepatology* (2017) 14(3):143. doi: 10.1038/nrgastro.2016.191.
284. Berthoud Hr. Vagal and hormonal gut–brain communication: from satiation to satisfaction. *Neurogastroenterology & Motility* (2008) 20:64-72.
285. Harrison E, Lal S, McLaughlin JT. Enteroendocrine cells in gastrointestinal pathophysiology. *Current opinion in pharmacology* (2013) 13(6):941-5.
286. Worthington JJ. The intestinal immunoendocrine axis: novel cross-talk between enteroendocrine cells and the immune system during infection and inflammatory disease. *Biochem Soc Trans* (2015) 43(4):727-33. doi: 10.1042/BST20150090. PubMed PMID: 26551720; PubMed Central PMCID: PMCPMC4613519.
287. Genton L, Kudsk KA. Interactions between the enteric nervous system and the immune system: role of neuropeptides and nutrition. *The American journal of surgery* (2003) 186(3):253-8.
288. González-Arancibia C, Escobar-Luna J, Barrera-Bugueño C, Díaz-Zepeda C, González-Toro MP, Olavarría-Ramírez L, et al. What goes around comes around: novel pharmacological targets in the gut–brain axis. *Therapeutic advances in gastroenterology* (2016) 9(3):339-53.
289. Naznin F, Toshinai K, Waise TM, NamKoong C, Md Moin AS, Sakoda H, et al. Diet-induced obesity causes peripheral and central ghrelin resistance by promoting inflammation. *J Endocrinol* (2015) 226(1):81-92. doi: 10.1530/JOE-15-0139. PubMed PMID: 26016745; PubMed Central PMCID: PMCPMC4485401.
290. Zhuo H, Ichikawa H, Helke C. Neurochemistry of the nodose ganglion. *Progress in neurobiology* (1997) 52(2):79-107.
291. Konturek S, Konturek P, Pawlik T, Brzozowski T. Brain-gut axis and its role in the control of food intake. *Journal of physiology and pharmacology* (2004) 55(2):137-54.
292. Tong J, Mannea E, Aimé P, Pfluger PT, Yi C-X, Castaneda TR, et al. Ghrelin enhances olfactory sensitivity and exploratory sniffing in rodents and humans. *Journal of Neuroscience* (2011) 31(15):5841-6.
293. Mousseaux D, Le Gallic L, Ryan J, Oiry C, Gagne D, Fehrentz JA, et al. Regulation of ERK1/2 activity by ghrelin‐activated growth hormone secretagogue receptor 1A involves a PLC/PKCε pathway. *British journal of pharmacology* (2006) 148(3):350-65.
294. Gutkind JS. Regulation of mitogen-activated protein kinase signaling networks by G protein-coupled receptors. *Sci Stke* (2000) 2000(40):re1-re.
295. Fung TC, Christine A. Olson, and Elaine Y. Hsiao. Interactions between the microbiota, immune and nervous systems in health and disease. *Nature neuroscience* (2017) 20(2):145. doi: 10.1038/nn.4476.
296. Houlden A, Goldrick M, Brough D, Vizi ES, Lénárt N, Martinecz B, et al. Brain injury induces specific changes in the caecal microbiota of mice via altered autonomic activity and mucoprotein production. *Brain, behavior, and immunity* (2016) 57:10-20.
297. Powell N, Walker MM, Talley NJ. The mucosal immune system: master regulator of bidirectional gut–brain communications. *Nature Reviews Gastroenterology & Hepatology* (2017) 14(3):143.
298. Furness JB. The enteric nervous system and neurogastroenterology. *Nature reviews Gastroenterology & hepatology* (2012) 9(5):286.
299. Rouach V, Bloch M, Rosenberg N, Gilad S, Limor R, Stern N, et al. The acute ghrelin response to a psychological stress challenge does not predict the post-stress urge to eat. *Psychoneuroendocrinology* (2007) 32(6):693-702.
300. Kristenssson E, Sundqvist M, Astin M, Kjerling M, Mattsson H, de la Cour CD, et al. Acute psychological stress raises plasma ghrelin in the rat. *Regulatory peptides* (2006) 134(2-3):114-7.

301. Lutter M, Sakata I, Osborne-Lawrence S, Rovinsky SA, Anderson JG, Jung S, et al. The orexigenic hormone ghrelin defends against depressive symptoms of chronic stress. *Nature neuroscience* (2008) 11(7):752.
302. Hotamisligil GS. Inflammation and metabolic disorders. *Nature* (2006) 444(7121):860.
303. Nielsen ST, Janum S, Krogh-Madsen R, Solomon TP, Møller K. The incretin effect in critically ill patients: a case–control study. *Critical Care* (2015) 19(1):402.
304. Steven S, Hausding M, Kröller-Schön S, Mader M, Mikhed Y, Stamm P, et al. Gliptin and GLP‐1 analog treatment improves survival and vascular inflammation/dysfunction in animals with lipopolysaccharide‐induced endotoxemia. *Basic research in cardiology* (2015) 110(2):6.
305. Tschöp M, Weyer C, Tataranni PA, Devanarayan V, Ravussin E, Heiman ML. Circulating ghrelin levels are decreased in human obesity. *Diabetes* (2001) 50(4):707-9.
306. Shiiya T, Nakazato M, Mizuta M, Date Y, Mondal MS, Tanaka M, et al. Plasma ghrelin levels in lean and obese humans and the effect of glucose on ghrelin secretion. *The Journal of Clinical Endocrinology & Metabolism* (2002) 87(1):240-4.
307. Eissa N, Ghia J. Immunomodulatory effect of ghrelin in the intestinal mucosa. *Neurogastroenterology & Motility* (2015) 27(11):1519-27.
308. Karmiris K, Koutroubakis IE, Xidakis C, Polychronaki M, Voudouri T, Kouroumalis EA. Circulating levels of leptin, adiponectin, resistin, and ghrelin in inflammatory bowel disease. *Inflammatory bowel diseases* (2006) 12(2):100-5.
309. Pellissier S, Dantzer C, Mondillon L, Trocme C, Gauchez A-S, Ducros V, et al. Relationship between vagal tone, cortisol, TNF-alpha, epinephrine and negative affects in Crohn's disease and irritable bowel syndrome. *PloS one* (2014) 9(9):e105328.
310. Ates Y, Degertekin B, Erdil A, Yaman H, Dagalp K. Serum ghrelin levels in inflammatory bowel disease with relation to disease activity and nutritional status. *Digestive diseases and sciences* (2008) 53(8):2215-21.
311. Xu Y, Li Z, Yin Y, Lan H, Wang J, Zhao J, et al. Ghrelin inhibits the differentiation of T helper 17 cells through mTOR/STAT3 signaling pathway. *PLoS One* (2015) 10(2):e0117081.
312. Zhang H, Cui Z, Luo G, Zhang J, Ma T, Hu N, et al. Ghrelin attenuates intestinal ischemia/reperfusion injury in mice by activating the mTOR signaling pathway. *International journal of molecular medicine* (2013) 32(4):851-9.
313. Taub DD, Murphy WJ, Longo DL. Rejuvenation of the aging thymus: growth hormone-mediated and ghrelin-mediated signaling pathways. *Current opinion in pharmacology* (2010) 10(4):408-24.
314. Hattori N, Saito T, Yagyu T, Jiang B-H, Kitagawa K, Inagaki C. GH, GH receptor, GH secretagogue receptor, and ghrelin expression in human T cells, B cells, and neutrophils. *The Journal of Clinical Endocrinology & Metabolism* (2001) 86(9):4284-91.
315. Di Giovangiulio M, Stakenborg N, Bosmans G, Meroni E, Farro G, Gomez‐Pinilla PJ, et al. Ghrelin receptor modulates T helper cells during intestinal inflammation. *Neurogastroenterology & Motility* (2015) 27(11):1542-52.
316. Karmiris K, Koutroubakis IE, Kouroumalis EA. Leptin, adiponectin, resistin, and ghrelin–implications for inflammatory bowel disease. *Molecular nutrition & food research* (2008) 52(8):855-66.
317. Zhao D, Zhan Y, Zeng H, Moyer MP, Mantzoros CS, Pothoulakis C. Ghrelin stimulates interleukin‐8 gene expression through protein kinase C‐mediated NF‐κB pathway in human colonic epithelial cells. *Journal of cellular biochemistry* (2006) 97(6):1317-27.
318. Cailotto C, Gomez-Pinilla PJ, Costes LM, van der Vliet J, Di Giovangiulio M, Némethova A, et al. Neuro-anatomical evidence indicating indirect modulation of macrophages by vagal efferents in the intestine but not in the spleen. *PLoS One* (2014) 9(1):e87785.

319. Clancy JA, Deuchars SA, Deuchars J. The wonders of the Wanderer. *Experimental physiology* (2013) 98(1):38-45.
320. Parker AP, Polkey CE, Binnie CD, Madigan C, Ferrie CD, Robinson RO. Vagal nerve stimulation in epileptic encephalopathies. *Pediatrics* (1999) 103(4):778-82.
321. Yi C-X, La Fleur SE, Fliers E, Kalsbeek A. The role of the autonomic nervous liver innervation in the control of energy metabolism. *Biochimica et Biophysica Acta (BBA)-Molecular Basis of Disease* (2010) 1802(4):416-31.
322. Richter W, Geiss H, Aleksic S, Schwandt P. Cardiac autonomic nerve function and insulin sensitivity in obese subjects. *International journal of obesity and related metabolic disorders: journal of the International Association for the Study of Obesity* (1996) 20(10):966-9.
323. Karason K, Mølgaard H, Wikstrand J, Sjöström L. Heart rate variability in obesity and the effect of weight loss. *The American journal of cardiology* (1999) 83(8):1242-7.
324. Ziegler D, Zentai C, Perz S, Rathmann W, Haastert B, Meisinger C, et al. Selective contribution of diabetes and other cardiovascular risk factors to cardiac autonomic dysfunction in the general population. *Experimental and clinical endocrinology & diabetes* (2006) 114(04):153-9.
325. Bonaz B, Bazin T, Pellissier S. The vagus nerve at the interface of the microbiota-gut-brain axis. *Frontiers in neuroscience* (2018) 12:49.
326. Browning KN, Verheijden S, Boeckxstaens GE. The vagus nerve in appetite regulation, mood, and intestinal inflammation. *Gastroenterology* (2017) 152(4):730-44.
327. Bansal V, Ryu SY, Lopez N, Allexan S, Krzyzaniak M, Eliceiri B, et al. Vagal stimulation modulates inflammation through a ghrelin mediated mechanism in traumatic brain injury. *Inflammation* (2012) 35(1):214-20. doi: 10.1007/s10753-011-9307-7. PubMed PMID: 21360048; PubMed Central PMCID: PMCPMC3282000.
328. Date Y, Murakami N, Toshinai K, Matsukura S, Niijima A, Matsuo H, et al. The role of the gastric afferent vagal nerve in ghrelin-induced feeding and growth hormone secretion in rats. *Gastroenterology* (2002) 123(4):1120-8.
329. Tarnavski O, McMullen JR, Schinke M, Nie Q, Kong S, Izumo S. Mouse cardiac surgery: comprehensive techniques for the generation of mouse models of human diseases and their application for genomic studies. *Physiological genomics* (2004) 16(3):349-60. doi: 10.1152/physiolgenomics.00041.2003. PubMed PMID: 14679301.
330. Redel A, Jazbutyte V, Smul TM, Lange M, Eckle T, Eltzschig H, et al. Impact of ischemia and reperfusion times on myocardial infarct size in mice in vivo. *Experimental biology and medicine* (2008) 233(1):84-93. doi: 10.3181/0612-RM-308. PubMed PMID: 18156310.
331. Michael LH, Entman ML, Hartley CJ, Youker KA, Zhu J, Hall SR, et al. Myocardial ischemia and reperfusion: a murine model. *American Journal of Physiology-Heart and Circulatory Physiology* (1995) 269(6):H2147-H54.
332. Nossuli T, Lakshminarayanan V, Baumgarten G, Taffet G, Ballantyne C, Michael L, et al. A chronic mouse model of myocardial ischemia-reperfusion: essential in cytokine studies. *American Journal of Physiology-Heart and Circulatory Physiology* (2000) 278(4):H1049-H55.
333. Samuel CS. Determination of collagen content, concentration, and sub-types in kidney tissue. *Kidney Research: Experimental Protocols* (2009):223-35.
334. Gallop PM, Paz MA. Posttranslational protein modifications, with special attention to collagen and elastin. *Physiological reviews* (1975) 55(3):418-87.
335. Thireau J, Zhang BL, Poisson D, Babuty D. Heart rate variability in mice: a theoretical and practical guide. *Exp Physiol* (2008) 93(1):83-94. doi: 10.1113/expphysiol.2007.040733. PubMed PMID: 17911354.
336. Camm A, Malik M, Bigger J, Breithardt G, Cerutti S, Cohen R, et al. Heart rate variability: standards of measurement, physiological interpretation and clinical use. Task

Force of the European Society of Cardiology and the North American Society of Pacing and Electrophysiology. *Circulation* (1996) 93(5):1043-65.
337. Lang RM, Bierig M, Devereux RB, Flachskampf FA, Foster E, Pellikka PA, et al. Recommendations for chamber quantification. *European journal of echocardiography* (2006) 7(2):79-108.
338. Bovens SM, Boekhorst B, den Ouden K, van de Kolk KWA, Nauerth A, Nederhoff MGJ, et al. Evaluation of infarcted murine heart function: comparison of prospectively triggered with self-gated MRI. *Nmr in Biomedicine* (2011) 24(3):307-15. doi: 10.1002/nbm.1593. PubMed PMID: WOS:000288400500011.
339. Kober F, Troalen T, Bernard M. Recent Developments in Small Animal Cardiovascular MRI. *Current Cardiovascular Imaging Reports* (2014) 7(2). doi: 10.1007/s12410-013-9249-6.
340. Rosset A, Spadola L, Ratib O. OsiriX: An Open-Source Software for Navigating in Multidimensional DICOM Images. *Journal of Digital Imaging* (2004) 17(3):205-16. doi: 10.1007/s10278-004-1014-6.
341. Bohl S, Lygate CA, Barnes H, Medway D, Stork LA, Schulz-Menger J, et al. Advanced methods for quantification of infarct size in mice using three-dimensional high-field late gadolinium enhancement MRI. *Am J Physiol Heart Circ Physiol* (2009) 296(4):H1200-8. doi: 10.1152/ajpheart.01294.2008. PubMed PMID: 19218501; PubMed Central PMCID: PMCPMC2670705.
342. Takagawa J, Zhang Y, Wong ML, Sievers RE, Kapasi NK, Wang Y, et al. Myocardial infarct size measurement in the mouse chronic infarction model: comparison of area- and length-based approaches. *J Appl Physiol (1985)* (2007) 102(6):2104-11. doi: 10.1152/japplphysiol.00033.2007. PubMed PMID: 17347379; PubMed Central PMCID: PMCPMC2675697.
343. Chapon C, Herlihy AH, Bhakoo KK. Assessment of myocardial infarction in mice by late gadolinium enhancement MR imaging using an inversion recovery pulse sequence at 9.4T. *Journal of cardiovascular magnetic resonance : official journal of the Society for Cardiovascular Magnetic Resonance* (2008) 10:6. doi: 10.1186/1532-429X-10-6. PubMed PMID: 18272007; PubMed Central PMCID: PMC2244610.
344. Weinsaft JW, Klem I, Judd RM. MRI for the assessment of myocardial viability. *Magnetic resonance imaging clinics of North America* (2007) 15(4):505-25.
345. Schelbert EB, Hsu LY, Anderson SA, Mohanty BD, Karim SM, Kellman P, et al. Late gadolinium-enhancement cardiac magnetic resonance identifies postinfarction myocardial fibrosis and the border zone at the near cellular level in ex vivo rat heart. *Circulation Cardiovascular imaging* (2010) 3(6):743-52. doi: 10.1161/CIRCIMAGING.108.835793. PubMed PMID: 20847191; PubMed Central PMCID: PMC3398602.
346. Ugander M, Bagi PS, Oki AJ, Chen B, Hsu LY, Aletras AH, et al. Myocardial edema as detected by pre-contrast T1 and T2 CMR delineates area at risk associated with acute myocardial infarction. *JACC Cardiovascular imaging* (2012) 5(6):596-603. doi: 10.1016/j.jcmg.2012.01.016. PubMed PMID: 22698528; PubMed Central PMCID: PMC3769169.
347. Grieve SM, Mazhar J, Callaghan F, Kok CY, Tandy S, Bhindi R, et al. Automated quantification of myocardial salvage in a rat model of ischemia-reperfusion injury using 3D high-resolution magnetic resonance imaging (MRI). *Journal of the American Heart Association* (2014) 3(4). doi: 10.1161/JAHA.114.000956. PubMed PMID: 25146703; PubMed Central PMCID: PMC4310382.
348. Carpenter J-P, He T, Kirk P, Roughton M, Anderson LJ, de Noronha SV, et al. On T2* magnetic resonance and cardiac iron. *Circulation* (2011) 123(14):1519-28.
349. Arai AE. Magnetic resonance imaging for area at risk, myocardial infarction, and myocardial salvage. *Journal of cardiovascular pharmacology and therapeutics* (2011) 16(3-4):313-20. doi: 10.1177/1074248411412378. PubMed PMID: 21821534.

350. Aletras AH, Tilak GS, Natanzon A, Hsu L-Y, Gonzalez FM, Hoyt RF, et al. Retrospective determination of the area at risk for reperfused acute myocardial infarction with T2-weighted cardiac magnetic resonance imaging. *Circulation* (2006) 113(15):1865-70.
351. Friedrich MG, Abdel-Aty H, Taylor A, Schulz-Menger J, Messroghli D, Dietz R. The salvaged area at risk in reperfused acute myocardial infarction as visualized by cardiovascular magnetic resonance. *Journal of the American College of Cardiology* (2008) 51(16):1581-7.
352. de Jong S, Zwanenburg JJ, Visser F, van der Nagel R, van Rijen HV, Vos MA, et al. Direct detection of myocardial fibrosis by MRI. *Journal of molecular and cellular cardiology* (2011) 51(6):974-9.
353. Coelho-Filho OR, Mongeon FP, Mitchell R, Moreno H, Jr., Nadruz W, Jr., Kwong R, et al. Role of transcytolemmal water-exchange in magnetic resonance measurements of diffuse myocardial fibrosis in hypertensive heart disease. *Circulation Cardiovascular imaging* (2013) 6(1):134-41. doi: 10.1161/CIRCIMAGING.112.979815. PubMed PMID: 23159497; PubMed Central PMCID: PMC3587170.
354. Coelho-Filho OR, Shah RV, Mitchell R, Neilan TG, Moreno H, Jr., Simonson B, et al. Quantification of cardiomyocyte hypertrophy by cardiac magnetic resonance: implications for early cardiac remodeling. *Circulation* (2013) 128(11):1225-33. doi: 10.1161/CIRCULATIONAHA.112.000438. PubMed PMID: 23912910.
355. Nakamori S, Dohi K, Ishida M, Goto Y, Imanaka-Yoshida K, Omori T, et al. Native T1 mapping and extracellular volume mapping for the assessment of diffuse myocardial fibrosis in dilated cardiomyopathy. *JACC: Cardiovascular Imaging* (2018) 11(1):48-59.
356. Iles L, Pfluger H, Phrommintikul A, Cherayath J, Aksit P, Gupta SN, et al. Evaluation of diffuse myocardial fibrosis in heart failure with cardiac magnetic resonance contrast-enhanced T1 mapping. *Journal of the American College of Cardiology* (2008) 52(19):1574-80. doi: 10.1016/j.jacc.2008.06.049. PubMed PMID: 19007595.
357. Luetkens JA, Klein S, Träber F, Schmeel FC, Sprinkart AM, Kuetting DL, et al. Quantification of liver fibrosis at T1 and T2 mapping with extracellular volume fraction MRI: preclinical results. *Radiology* (2018) 288(3):748-54.
358. Loganathan R, Bilgen M, Al-Hafez B, Smirnova IV. Characterization of alterations in diabetic myocardial tissue using high resolution MRI. *The international journal of cardiovascular imaging* (2006) 22(1):81-90. doi: 10.1007/s10554-005-5386-6. PubMed PMID: 16362172.
359. Jivraj N, Phinikaridou A, Shah AM, Botnar RM. Molecular imaging of myocardial infarction. *Basic research in cardiology* (2014) 109(1):397. doi: 10.1007/s00395-013-0397-2. PubMed PMID: 24322905.
360. Mavrogeni S, Apostolou D, Argyriou P, Velitsista S, Papa L, Efentakis S, et al. T1 and T2 mapping in cardiology:“mapping the obscure object of desire”. *Cardiology* (2017) 138(4):207-17.
361. Messroghli DR, Moon JC, Ferreira VM, Grosse-Wortmann L, He T, Kellman P, et al. Clinical recommendations for cardiovascular magnetic resonance mapping of T1, T2, T2* and extracellular volume: a consensus statement by the Society for Cardiovascular Magnetic Resonance (SCMR) endorsed by the European Association for Cardiovascular Imaging (EACVI). *Journal of Cardiovascular Magnetic Resonance* (2017) 19(1):1-24.
362. Ghugre NR, Ramanan V, Pop M, Yang Y, Barry J, Qiang B, et al. Quantitative tracking of edema, hemorrhage, and microvascular obstruction in subacute myocardial infarction in a porcine model by MRI. *Magnetic resonance in medicine : official journal of the Society of Magnetic Resonance in Medicine / Society of Magnetic Resonance in Medicine* (2011) 66(4):1129-41. doi: 10.1002/mrm.22855. PubMed PMID: 21337425.

363. Saraste A, Nekolla S, Schwaiger M. Contrast-enhanced magnetic resonance imaging in the assessment of myocardial infarction and viability. *Journal of Nuclear Cardiology* (2007). doi: 10.1016/j.nuclcard.2007.11.002.
364. Protti A, Sirker A, Shah AM, Botnar R. Late gadolinium enhancement of acute myocardial infarction in mice at 7T: Cine‐FLASH versus inversion recovery. *Journal of Magnetic Resonance Imaging* (2010) 32(4):878-86.
365. van Nierop BJ, Bax NA, Nelissen JL, Arslan F, Motaal AG, de Graaf L, et al. Assessment of myocardial fibrosis in mice using a T2*-weighted 3D radial magnetic resonance imaging sequence. *PloS one* (2015) 10(6):e0129899.
366. Aguor EN, Arslan F, van de Kolk CW, Nederhoff MG, Doevendans PA, van Echteld CJ, et al. Quantitative T 2* assessment of acute and chronic myocardial ischemia/reperfusion injury in mice. *Magma* (2012) 25(5):369-79. doi: 10.1007/s10334-012-0304-0. PubMed PMID: 22327962; PubMed Central PMCID: PMC3458196.
367. Kim RJ, Shah DJ, Judd RM. How We Perform Delayed Enhancement Imaging. *Journal of Cardiovascular Magnetic Resonance* (2003) 5(3):505-14. doi: 10.1081/jcmr-120022267.
368. Nahrendorf M, Hiller K-H, Hu K, Ertl G, Haase A, Bauer WR. Cardiac magnetic resonance imaging in small animal models of human heart failure. *Medical image analysis* (2003) 7(3):369-75.
369. Nahrendorf M, Wiesmann F, Hiller K-H, Han H, Hu K, Waller C, et al. In vivo assessment of cardiac remodeling after myocardial infarction in rats by cine–magnetic resonance imaging. *Journal of Cardiovascular Magnetic Resonance* (2000) 2(3):171-80.
370. Ibrahim T, Nekolla SG, Hornke M, Bulow HP, Dirschinger J, Schomig A, et al. Quantitative measurement of infarct size by contrast-enhanced magnetic resonance imaging early after acute myocardial infarction: comparison with single-photon emission tomography using Tc99m-sestamibi. *Journal of the American College of Cardiology* (2005) 45(4):544-52. doi: 10.1016/j.jacc.2004.10.058. PubMed PMID: 15708702.
371. Ojha N, Roy S, Radtke J, Simonetti O, Gnyawali S, Zweier JL, et al. Characterization of the structural and functional changes in the myocardium following focal ischemia-reperfusion injury. *American journal of physiology Heart and circulatory physiology* (2008) 294(6):H2435-43. doi: 10.1152/ajpheart.01190.2007. PubMed PMID: 18375718.
372. Simonetti OP, Kim, R. J., Fieno, D. S., Hillenbrand, H. B., Wu, E., Bundy, J. M., ... & Judd, R. M. . An Improved MR Imaging Technique for the Visualization of Myocardial Infarction. *Radiology* (2001) 218(1):215-23.
373. Yang Z, Berr SS, Gilson WD, Toufektsian MC, French BA. Simultaneous evaluation of infarct size and cardiac function in intact mice by contrast-enhanced cardiac magnetic resonance imaging reveals contractile dysfunction in noninfarcted regions early after myocardial infarction. *Circulation* (2004) 109(9):1161-7. doi: 10.1161/01.CIR.0000118495.88442.32. PubMed PMID: 14967719.
374. Chapon C, Lemaire L, Franconi F, Marescaux L, Legras P, Denizot B, et al. Assessment of myocardial viability in rats: Evaluation of a new method using superparamagnetic iron oxide nanoparticles and Gd-DOTA at high magnetic field. *Magnetic resonance in medicine : official journal of the Society of Magnetic Resonance in Medicine / Society of Magnetic Resonance in Medicine* (2004) 52(4):932-6. doi: 10.1002/mrm.20210. PubMed PMID: 15389960.
375. Redfors B, Shao Y, Omerovic E. Myocardial infarct size and area at risk assessment in mice. *Experimental & Clinical Cardiology* (2012) 17(4):268.
376. Friedrich MG, Abdel-Aty H, Taylor A, Schulz-Menger J, Messroghli D, Dietz R. The salvaged area at risk in reperfused acute myocardial infarction as visualized by cardiovascular magnetic resonance. *Journal of the American College of Cardiology* (2008) 51(16):1581-7. doi: 10.1016/j.jacc.2008.01.019. PubMed PMID: 18420102.

377. Rehwald WG, Fieno DS, Chen E-L, Kim RJ, Judd RM. Myocardial magnetic resonance imaging contrast agent concentrations after reversible and irreversible ischemic injury. *Circulation* (2002) 105(2):224-9.
378. Tilak GS, Hsu L-Y, Hoyt Jr RF, Arai AE, Aletras AH. In vivo T2-weighted magnetic resonance imaging can accurately determine the ischemic area at risk for 2-day-old nonreperfused myocardial infarction. *Investigative radiology* (2008) 43(1):7-15.
379. Beyers RJ, Smith RS, Xu Y, Piras BA, Salerno M, Berr SS, et al. T(2) -weighted MRI of post-infarct myocardial edema in mice. *Magnetic resonance in medicine : official journal of the Society of Magnetic Resonance in Medicine / Society of Magnetic Resonance in Medicine* (2012) 67(1):201-9. doi: 10.1002/mrm.22975. PubMed PMID: 21630350; PubMed Central PMCID: PMC3188362.
380. Fishbein MC, Meerbaum S, Rit J, Lando U, Kanmatsuse K, Mercier JC, et al. Early phase acute myocardial infarct size quantification: validation of the triphenyl tetrazolium chloride tissue enzyme staining technique. *American heart journal* (1981) 101(5):593-600.
381. Ojha N, Roy S, Radtke J, Simonetti O, Gnyawali S, Zweier JL, et al. Characterization of the structural and functional changes in the myocardium following focal ischemia-reperfusion injury. *American Journal of Physiology-Heart and Circulatory Physiology* (2008) 294(6):H2435-H43.
382. Luo D, Yao Y-Y, Li Y-F, Sheng Z-L, Tang Y, Fang F, et al. Myocardial infarction quantification with late gadolinium-enhanced magnetic resonance imaging in rats using a 7-T scanner. *Cardiovascular Pathology* (2012) 21(2):112-9.
383. Bohl S, Medway DJ, Schulz-Menger J, Schneider JE, Neubauer S, Lygate CA. Refined approach for quantification of in vivo ischemia-reperfusion injury in the mouse heart. *American journal of physiology Heart and circulatory physiology* (2009) 297(6):H2054-8. doi: 10.1152/ajpheart.00836.2009. PubMed PMID: 19820193; PubMed Central PMCID: PMC2793132.
384. Mewton N, Rapacchi S, Augeul L, Ferrera R, Loufouat J, Boussel L, et al. Determination of the myocardial area at risk with pre-versus post-reperfusion imaging techniques in the pig model. *Basic research in cardiology* (2011) 106(6):1247-57.
385. Eitel I, Friedrich MG. T2-weighted cardiovascular magnetic resonance in acute cardiac disease. *Journal of Cardiovascular Magnetic Resonance* (2011) 13(1):13.
386. Suvarna S. *Cardiac pathology: a guide to current practice*: Springer Science & Business Media (2012).
387. Baldanzi G, Filigheddu N, Cutrupi S, Catapano F, Bonissoni S, Fubini A, et al. Ghrelin and des-acyl ghrelin inhibit cell death in cardiomyocytes and endothelial cells through ERK1/2 and PI 3-kinase/AKT. *The Journal of cell biology* (2002) 159(6):1029-37.
388. Inui. The role of ghrelin in energy homeostasis and its potential clinical relevance (Review). *International Journal of Molecular Medicine* (2010) 26(6). doi: 10.3892/ijmm_00000524.
389. Kojima M, Kangawa K. Ghrelin: structure and function. *Physiological reviews* (2005) 85(2):495-522. doi: 10.1152/physrev.00012.2004. PubMed PMID: 15788704.
390. Date Y, Kojima M, Hosoda H, Sawaguchi A, Mondal MS, Suganuma T, et al. Ghrelin, a novel growth hormone-releasing acylated peptide, is synthesized in a distinct endocrine cell type in the gastrointestinal tracts of rats and humans 1. *Endocrinology* (2000) 141(11):4255-61.
391. Guan X-M, Yu H, Palyha OC, McKee KK, Feighner SD, Sirinathsinghji DJ, et al. Distribution of mRNA encoding the growth hormone secretagogue receptor in brain and peripheral tissues. *Molecular brain research* (1997) 48(1):23-9.
392. Mori K, Yoshimoto A, Takaya K, Hosoda K, Ariyasu H, Yahata K, et al. Kidney produces a novel acylated peptide, ghrelin. *FEBS letters* (2000) 486(3):213-6.

393. Nagaya N, Kojima M, Uematsu M, Yamagishi M, Hosoda H, Oya H, et al. Hemodynamic and hormonal effects of human ghrelin in healthy volunteers. *American Journal of Physiology-Regulatory, Integrative and Comparative Physiology* (2001) 280(5):R1483-R7.
394. Deghenghi R. Synthetic peptides and their non-peptidyl mimetics in endocrinology: From synthesis to clinical perspectives. *Journal of endocrinological investigation* (1998) 21(11):787-93.
395. Angelino E, Reano S, Ferrara M, Agosti E, Graziani A, Filigheddu N. Antifibrotic activity of acylated and unacylated ghrelin. *Int J Endocrinol* (2015) 2015:385682. doi: 10.1155/2015/385682. PubMed PMID: 25960743; PubMed Central PMCID: PMCPMC4415458.
396. Tarnavski O, McMullen JR, Schinke M, Nie Q, Kong S, Izumo S. Mouse cardiac surgery: comprehensive techniques for the generation of mouse models of human diseases and their application for genomic studies. *Physiological genomics* (2004) 16(3):349-60.
397. Schneider CA, Rasband WS, Eliceiri KW. NIH Image to ImageJ: 25 years of image analysis. *Nat Meth* (2012) 9(7):671-5.
398. Cardiology TFotESo. Heart rate variability standards of measurement, physiological interpretation, and clinical use. *Eur Heart J* (1996) 17:354-81.
399. Rossoni G, Colonna VDG, Bernareggi M, Polvani GL, Müller EE, Berti F. Protectant activity of hexarelin or growth hormone against postischemic ventricular dysfunction in hearts from aged rats. *Journal of cardiovascular pharmacology* (1998) 32(2):260-5.
400. Locatelli V, Rossoni G, Schweiger F, Torsello A, De Gennaro Colonna V, Bernareggi M, et al. Growth hormone-independent cardioprotective effects of hexarelin in the rat. *Endocrinology* (1999) 140(9):4024-31.
401. Imazio M, Bobbio M, Broglio F, Benso A, Podio V, Valetto M, et al. GH‐independent cardiotropic activities of hexarelin in patients with severe left ventricular dysfunction due to dilated and ischemic cardiomyopathy. *European journal of heart failure* (2002) 4(2):185-91.
402. Pang J-J, Xu R-K, Xu X-B, Cao J-M, Ni C, Zhu W-L, et al. Hexarelin protects rat cardiomyocytes from angiotensin II-induced apoptosis in vitro. *American Journal of Physiology-Heart and Circulatory Physiology* (2004) 286(3):H1063-H9.
403. Xu X, Ding F, Pang J, Gao X, Xu RK, Hao W, et al. Chronic administration of hexarelin attenuates cardiac fibrosis in the spontaneously hypertensive rat. *Am J Physiol Heart Circ Physiol* (2012) 303(6):H703-11. doi: 10.1152/ajpheart.00257.2011. PubMed PMID: 22842067.
404. Zhang X, Azhar G, Nagano K, Wei JY. Differential vulnerability to oxidative stress in rat cardiac myocytes versus fibroblasts. *Journal of the American College of Cardiology* (2001) 38(7):2055-62.
405. Chen W, Frangogiannis NG. Fibroblasts in post-infarction inflammation and cardiac repair. *Biochim Biophys Acta* (2013) 1833(4):945-53. doi: 10.1016/j.bbamcr.2012.08.023. PubMed PMID: 22982064; PubMed Central PMCID: PMCPMC3541439.
406. Shivakumar K, Sollott SJ, Sangeetha M, Sapna S, Ziman B, Wang S, et al. Paracrine effects of hypoxic fibroblast-derived factors on the MPT-ROS threshold and viability of adult rat cardiac myocytes. *American Journal of Physiology-Heart and Circulatory Physiology* (2008) 294(6):H2653-H8.
407. Willems I, Havenith MG, De Mey J, Daemen M. The alpha-smooth muscle actin-positive cells in healing human myocardial scars. *The American journal of pathology* (1994) 145(4):868.
408. Detillieux KA, Sheikh F, Kardami E, Cattini PA. Biological activities of fibroblast growth factor-2 in the adult myocardium. *Cardiovascular research* (2003) 57(1):8-19.

409. Xu X, Pang J, Yin H, Li M, Hao W, Chen C, et al. Hexarelin suppresses cardiac fibroblast proliferation and collagen synthesis in rat. *Am J Physiol Heart Circ Physiol* (2007) 293(5):H2952-8. doi: 10.1152/ajpheart.00004.2007. PubMed PMID: 17766487.
410. Kaye DM, Lefkovits J, Jennings GL, Bergin P, Broughton A, Esler MD. Adverse consequences of high sympathetic nervous activity in the failing human heart. *Journal of the American College of Cardiology* (1995) 26(5):1257-63.
411. Braunwald E, Kloner RA. Myocardial reperfusion: a double-edged sword? *Journal of Clinical Investigation* (1985) 76(5):1713.
412. La Rovere M, Pinna G, Maestri R, Sleight P. Clinical value of baroreflex sensitivity. *Netherlands Heart Journal* (2013) 21(2):61-3.
413. Schwartz P. Vagal stimulation for heart diseases: from animals to men. An example of translational cardiology. *Netherlands Heart Journal* (2013) 21(2):82-4.
414. Xiong J, Yuan Y, Xue F, Wang Q, Li S, Liao X, et al. Combined postconditioning with ischemia and α7nAChR agonist produces an enhanced protection against rat myocardial ischemia reperfusion injury. *Chinese medical journal* (2012) 125(2):326-31.
415. Berlanga-Acosta J, Abreu-Cruz A, García-del Barco Herrera D, Mendoza-Marí Y, Rodríguez-Ulloa A, García-Ojalvo A, et al. Synthetic Growth Hormone-Releasing Peptides (GHRPs): A Historical Appraisal of the Evidences Supporting Their Cytoprotective Effects. *Clinical Medicine Insights Cardiology* (2017) 11.
416. Shirai M, Joe N, Tsuchimochi H, Sonobe T, Schwenke DO. Ghrelin Supresses Sympathetic Hyperexcitation in Acute Heart Failure in Male Rats: Assessing Centrally and Peripherally Mediated Pathways. *Endocrinology* (2015) 156(9):3309-16. doi: 10.1210/EN.2015-1333. PubMed PMID: 26121343.
417. Frobert A, Valentin J, Magnin J-L, Riedo E, Cook S, Giraud M-N. Prognostic value of troponin I for infarct size to improve preclinical myocardial infarction small animal models. *Frontiers in physiology* (2015) 6:353.
418. Latet SC, Hoymans VY, Van Herck PL, Vrints CJ. The cellular immune system in the post-myocardial infarction repair process. *International journal of cardiology* (2015) 179:240-7.
419. Mioni C, Bazzani C, Giuliani D, Altavilla D, Leone S, Ferrari A, et al. Activation of an efferent cholinergic pathway produces strong protection against myocardial ischemia/reperfusion injury in rats*. *Critical Care Medicine* (2005) 33(11):2621-8. doi: 10.1097/01.ccm.0000186762.05301.13.
420. Zhang W, Lin TR, Hu Y, Fan Y, Zhao L, Stuenkel EL, et al. Ghrelin stimulates neurogenesis in the dorsal motor nucleus of the vagus. *J Physiol* (2004) 559(Pt 3):729-37. doi: 10.1113/jphysiol.2004.064121. PubMed PMID: 15272046; PubMed Central PMCID: PMCPMC1665175.
421. Sun Q, Zang W-J, Chen C. Growth hormone secretagogues reduce transient outward K+ current via phospholipase C/protein kinase C signaling pathway in rat ventricular myocytes. *Endocrinology* (2010) 151(3):1228-35.
422. Wu R, Dong W, Zhou M, Zhang F, Marini CP, Ravikumar TS, et al. Ghrelin attenuates sepsis-induced acute lung injury and mortality in rats. *American journal of respiratory and critical care medicine* (2007) 176(8):805-13.
423. Wu R, Zhou M, Das P, Dong W, Ji Y, Yang D, et al. Ghrelin inhibits sympathetic nervous activity in sepsis. *American Journal of Physiology-Endocrinology and Metabolism* (2007) 293(6):E1697-E702.
424. Chen C-Y, Asakawa A, Fujimiya M, Lee S-D, Inui A. Ghrelin gene products and the regulation of food intake and gut motility. *Pharmacological Reviews* (2009) 61(4):430-81.
425. Shinde AV, Humeres C, Frangogiannis NG. The role of α-smooth muscle actin in fibroblast-mediated matrix contraction and remodeling. *Biochimica et Biophysica Acta (BBA)-Molecular Basis of Disease* (2017) 1863(1):298-309.

426. Singh S, Singh H, Loftus EV, Jr., Pardi DS. Risk of cerebrovascular accidents and ischemic heart disease in patients with inflammatory bowel disease: a systematic review and meta-analysis. *Clin Gastroenterol Hepatol* (2014) 12(3):382-93 e1: quiz e22. doi: 10.1016/j.cgh.2013.08.023. PubMed PMID: 23978350.
427. Singh GM, Danaei G, Farzadfar F, Stevens GA, Woodward M, Wormser D, et al. The age-specific quantitative effects of metabolic risk factors on cardiovascular diseases and diabetes: a pooled analysis. *PloS one* (2013) 8(7):e65174.
428. Dinh W, Futh R, Nickl W, Krahn T, Ellinghaus P, Scheffold T, et al. Elevated plasma levels of TNF-alpha and interleukin-6 in patients with diastolic dysfunction and glucose metabolism disorders. *Cardiovasc Diabetol* (2009) 8:58. doi: 10.1186/1475-2840-8-58. PubMed PMID: 19909503; PubMed Central PMCID: PMCPMC2778641.
429. Ing DJ, Zang J, Dzau VJ, Webster KA, Bishopric NH. Modulation of cytokine-induced cardiac myocyte apoptosis by nitric oxide, Bak, and Bcl-x. *Circulation Research* (1999) 84(1):21-33.
430. Lorber D. Importance of cardiovascular disease risk management in patients with type 2 diabetes mellitus. *Diabetes, metabolic syndrome and obesity: targets and therapy* (2014) 7:169.
431. Xu X-B, Pang J-J, Cao J-M, Ni C, Xu R-K, Peng X-Z, et al. GH-releasing peptides improve cardiac dysfunction and cachexia and suppress stress-related hormones and cardiomyocyte apoptosis in rats with heart failure. *American Journal of Physiology-Heart and Circulatory Physiology* (2005) 289(4):H1643-H51.
432. Naznin F, Toshinai K, Waise TZ, NamKoong C, Moin ASM, Sakoda H, et al. Diet-induced obesity causes peripheral and central ghrelin resistance by promoting inflammation. *Journal of Endocrinology* (2015):JOE-15-0139.
433. Tiaka EK, Manolakis AC, Kapsoritakis AN, Potamianos SP. Unraveling the link between leptin, ghrelin and different types of colitis. *Annals of Gastroenterology: Quarterly Publication of the Hellenic Society of Gastroenterology* (2011) 24(1):20.
434. Mao Y, Tokudome T, Kishimoto I. Ghrelin and Blood Pressure Regulation. *Curr Hypertens Rep* (2016) 18(2):15. doi: 10.1007/s11906-015-0622-5. PubMed PMID: 26781255.
435. Mundinger TO, Cummings DE, Taborsky Jr GJ. Direct stimulation of ghrelin secretion by sympathetic nerves. *Endocrinology* (2006) 147(6):2893-901.
436. Yuan MJ, Huang H, Quan L, Tang YH, Wang X, Jiang H, et al. Expression of ghrelin and its receptor in rats after coronary artery ligation. *Regul Pept* (2014) 192-193:1-5. doi: 10.1016/j.regpep.2014.07.001. PubMed PMID: 25058156.
437. Matsumoto M, Yasuda S, Miyazaki S, Kataoka Y, Hosoda H, Nagaya N, et al. Decreased serum ghrelin levels in patients with acute myocardial infarction. *The Tohoku journal of experimental medicine* (2013) 231(3):235-42.
438. Rodrigues B, Lira FS, Consolim-Colombo FM, Rocha JA, Caperuto EC, De Angelis K, et al. Role of exercise training on autonomic changes and inflammatory profile induced by myocardial infarction. *Mediators Inflamm* (2014) 2014:702473. doi: 10.1155/2014/702473. PubMed PMID: 25045212; PubMed Central PMCID: PMCPMC4090432.
439. Nagaya N, Kangawa K. Ghrelin improves left ventricular dysfunction and cardiac cachexia in heart failure. *Current opinion in pharmacology* (2003) 3(2):146-51.
440. Akamizu T, Kangawa K. Emerging results of anticatabolic therapy with ghrelin. *Current Opinion in Clinical Nutrition & Metabolic Care* (2007) 10(3):278-83.
441. Nagaya N, Uematsu M, Kojima M, Date Y, Nakazato M, Okumura H, et al. Elevated circulating level of ghrelin in cachexia associated with chronic heart failure: relationships between ghrelin and anabolic/catabolic factors. *Circulation* (2001) 104(17):2034-8.
442. Andrews ZB, Erion DM, Beiler R, Choi CS, Shulman GI, Horvath TL. Uncoupling protein-2 decreases the lipogenic actions of ghrelin. *Endocrinology* (2010) 151(5):2078-86.

443. McFarlane MR, Brown MS, Goldstein JL, Zhao T-J. Induced ablation of ghrelin cells in adult mice does not decrease food intake, body weight, or response to high-fat diet. *Cell metabolism* (2014) 20(1):54-60.
444. Tokudome T, Otani K, Miyazato M, Kangawa K. Ghrelin and the heart. *Peptides* (2018). doi: 10.1016/j.peptides.2018.05.006.
445. Khatib MN, Shankar A, Kirubakaran R, Agho K, Simkhada P, Gaidhane S, et al. Effect of ghrelin on mortality and cardiovascular outcomes in experimental rat and mice models of heart failure: a systematic review and meta-analysis. *PLoS One* (2015) 10(5):e0126697. doi: 10.1371/journal.pone.0126697. PubMed PMID: 26016489; PubMed Central PMCID: PMCPMC4446297.
446. Ponikowski P, Anker SD, AlHabib KF, Cowie MR, Force TL, Hu S, et al. Heart failure: preventing disease and death worldwide. *ESC heart failure* (2014) 1(1):4-25.
447. Tan WS, Mullins TP, Flint M, Walton SL, Bielefeldt-Ohmann H, Carter DA, et al. Modeling heart failure risk in diabetes and kidney disease: limitations and potential applications of transverse aortic constriction in high-fat-fed mice. *American Journal of Physiology-Regulatory, Integrative and Comparative Physiology* (2018) 314(6):R858-R69. doi: 10.1152/ajpregu.00357.2017.
448. Yang YL, Lin SH, Chuang LY, Guh JY, Liao TN, Lee TC, et al. CD36 is a novel and potential anti‐fibrogenic target in albumin‐induced renal proximal tubule fibrosis. *Journal of cellular biochemistry* (2007) 101(3):735-44.
449. Wang X, Lv L, Chen Y, Chen J. A CD36 synthetic peptide inhibits silica-induced lung fibrosis in the mice. *Toxicology and industrial health* (2010) 26(1):47-53.
450. Chen M, Li X, Yang H, Tang J, Zhou S. Hype or hope: Vagus nerve stimulation against acute myocardial ischemia-reperfusion injury. *Trends in Cardiovascular Medicine* (2019).

9. Appendix:

9.1 Ethical Approval Certificate

UQ Research and Innovation
Director, Research Management Office
Nicole Thompson

Animal Ethics Approval Certificate

28-Aug-2015

Please check all details below and inform the Animal Welfare Unit within 10 working days if anything is incorrect.

Activity Details

Chief Investigator:	Professor Chen Chen, Biomedical Sciences
Title:	Protective effect of growth hormone releasing peptide on heart function after ischemia/reperfusion
AEC Approval Number:	SBMS/200/13/NHMRC
Previous AEC Number:	SBMS/055/13/NHMRC
Approval Duration:	10-Oct-2013 to 10-Oct-2016
Funding Body:	Internal Funds - UQ, NHMRC
Group:	Anatomical Biosciences
Other Staff/Students:	Frederik Steyn, Xinli Zhang, Karine Mardon, Tamara Paravicini, Katrina Geary, Nyoman Kurniawan, Gary Cowin, Hayley McDonald, Zoe Schoefield, Lili Huang
Location(s):	St Lucia Bldg 76 - Chemistry (SCMB) St Lucia Bldg 81 - Otto Hirschfeld St Lucia Bldg 57 - Centre of Advanced Imaging

Summary

Subspecies	Strain	Class	Gender	Source	Approved	Remaining
Mice - genetically modified	MKR	Adults	Mix	Institutional Breeding Colony	144	144
Mice - non genetically modified	C57BL/6	Adults	Male	Institutional Breeding Colony	422	319

Permits

Provisos

This approval is subject to a pilot study in experiment one. The Committee determined that work beyond the pilot study is subject to Committee approval of the pilot study report.

Approval Details

Description		Amount	Balance
Mice - genetically modified (MKR, Mix, Adults, Institutional Breeding Colony)			
10 Jun 2015	Mod #11	144	144
Mice - non genetically modified (C57BL/6, Male, Adults, Institutional Breeding Colony)			
11 Sep 2013	Initial approval - pilot study	12	12
31 Dec 2013	Use in 2013 (from 2014 MAR)	0	12
11 Jun 2014	Initial approval - post pilot study	240	252
14 Aug 2014	Mod #7	30	282
29 Aug 2014	Mod #6	30	312

Animal Welfare Unit
UQ Research and Innovation
The University of Queensland

Cumbrae-Stewart Building
Research Road
Brisbane Qld 4072 Australia

+61 7 336 52925 (Enquiries)
+61 7 334 68710 (Enquiries)
+61 7 336 52713 (Coordinator)

animalwelfare@research.uq.edu.au
uq.edu.au/research

10 Dec 2014	Mod #8	30	342
31 Dec 2014	Use in 2014 (from 2015 MAR)	-103	239
8 Apr 2015	Mod #10	80	319

Please note the animal numbers supplied on this certificate are the total allocated for the approval duration

Please use this Approval Number:

1. When ordering animals from Animal Breeding Houses
2. For labelling of all animal cages or holding areas. In addition please include on the label, Chief Investigator's name and contact phone number.
3. When you need to communicate with this office about the project.

It is a condition of this approval that all project animal details be made available to Animal House OIC.
(UAEC Ruling 14/12/2001)

The Chief Investigator takes responsibility for ensuring all legislative, regulatory and compliance objectives are satisfied for this project.

This certificate supercedes all preceeding certificates for this project (i.e. those certificates dated before 28-Aug-2015)